NASA CONTRACTOR REPORT

NASA CR-

NASA CR-2604

HIGH REYNOLDS NUMBER TESTS OF A C-141A AIRCRAFT SEMISPAN MODEL TO INVESTIGATE SHOCK-INDUCED SEPARATION

W. T. Blackerby and J. F. Cahill

Prepared by
LOCKHEED-GEORGIA COMPANY
Marietta, Ga.
for Ames Research Center

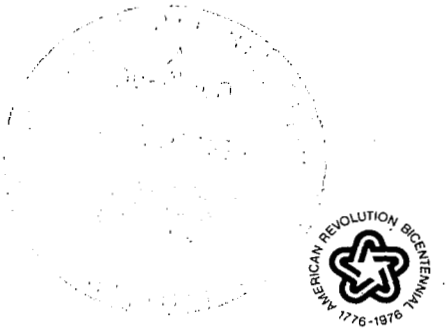

NATIONAL AERONAUTICS AND SPACE ADMINISTRATION • WASHINGTON, D. C. • OCTOBER 1975

1. Report No.	2. Government Accession No.	3. Rec
NASA CR-2604		

4. Title and Subtitle	5. Report Date
"High Reynolds Number Tests of a C-141A Aircraft Semispan Model to Investigate Shock-Induced Separation"	October 1975
	6. Performing Organization Code
7. Author(s)	8. Performing Organization Report No.
W. T. Blackerby and J. F. Cahill	
	10. Work Unit No.
9. Performing Organization Name and Address	11. Contract or Grant No.
Lockheed-Georgia Company Marietta, Georgia	NAS 2-8269
	13. Type of Report and Period Covered
12. Sponsoring Agency Name and Address	Contractor Report
National Aeronautics & Space Administration Washington, D.C. 20546	14. Sponsoring Agency Code

15. Supplementary Notes

16. Abstract

Results from a high Reynolds number transonic wind tunnel investigation on a semispan model of the C-141A airplane are presented. Wing chordwise pressure distributions were measured over a matrix of Mach numbers and angles-of-attack for which shock-induced separations are known to exist. The range of Reynolds number covered by these data nearly spanned the gap between previously available wind tunnel and flight test data. The results are compared with both flight and low Reynolds number data.

17. Key Words (Suggested by Author(s))	18. Distribution Statement
Transonic Aircraft C141A Wing-Shock Location Pressure Distribution Wind Tunnel Data	UNCLASSIFIED-UNLIMITED STAR Category 05

19. Security Classif. (of this report)	20. Security Classif. (of this page)	21. No. of Pages	22. Price*
UNCLASSIFIED	UNCLASSIFIED	192	$7.00

*For sale by the National Technical Information Service, Springfield, Virginia 22161

HIGH REYNOLDS NUMBER TESTS OF A C-141A AIRCRAFT SEMISPAN MODEL TO INVESTIGATE SHOCK-INDUCED SEPARATION

By
W. T. Blackerby and J. F. Cahill

SUMMARY

Tests of a semispan model of the USAF/Lockheed C-141 aircraft have been conducted in the Lockheed-Georgia high Reynolds number transonic wind tunnel (Compressible Flow Facility). Wing chordwise pressure distributions were measured over a matrix of Mach numbers and angles of attack for which shock-induced separations are known to exist. The range of Reynolds numbers covered by these tests nearly spanned the gap between previously available wind-tunnel and flight-test data.

Results showed that use of the semispan test technique produced good correlation with the prior data at both ends of the Reynolds number range, but indicated strong sensitivity to details of the test setup. The severity of flow separation at low Reynolds numbers is shown to increase with spanwise distance from the centerline. The scale effect on that separation also increases with spanwise distance, resulting in a more uniform distribution of trailing-edge pressure recovery at high Reynolds numbers. The rate of change of shock location and trailing-edge pressure recovery with Reynolds number increases with increasing Reynolds number at outboard locations on the wing. The trends of these variations in severity of separation are interpreted as an indication of spanwise contamination resulting from outboard flows in the boundary layer behind the shock. These data show that for the C-141 configuration no Reynolds number less than the full-scale value produces a satisfactory simulation of the flight test results.

INTRODUCTION

This report presents the results of tests of a semispan model of the USAF/Lockheed C-141 aircraft in the Lockheed-Georgia 20 X 28-inch high Reynolds number transonic wind tunnel (CFF). Wing pressure distributions were measured at three spanwise stations over a Reynolds number range from approximately 3 million to slightly over 20 million at Mach numbers from 0.75 to 0.85.

The primary objective of this program is to develop data on the occurrence and the effects of shock-induced separation in the range of Reynolds numbers between those achievable in existing large transonic wind tunnels (AEDC 16-Foot Test TF-139, reference 2) and those experienced by the aircraft in flight (reference 1). Secondary objectives include a demonstration of the validity of semispan testing to obtain data of this type at high Reynolds numbers, an evaluation of whether a minimum Reynolds number can be identified as adequate for duplication of flight characteristics, and a correlation of data measured in this program with those from previous flight and wind tunnel tests.

Several previous studies have been conducted on the shock-induced separation characteristics of the C-141 aircraft wing because a significant amount of data on sensitivity to scale effects was measured during the initial development of this aircraft. Results of those studies, presented in references 1 through 6, have confirmed the intimate relationship between trailing-edge separation and shock location in these scale effects, the large influence of transition location, and a strong dependence on wing planform geometry (as distinguished from airfoil section effects). These facts are apparent in figure 1, which summarizes results from a large-scale panel model and from the complete aircraft configuration (reference 5). Tests of the panel model covered a range of Reynolds number from approximately 4 million to 28 million; but for the complete aircraft configuration, a gap was present in Reynolds number between the highest wind tunnel value of 8-1/2 million and the lowest flight value of 35 to 40 million.

The Lockheed-Georgia CFF is designed to permit tests at Reynolds numbers up to approximately 164 million per meter (55 million per foot). A large semispan model of the C-141 aircraft designed for the CFF test section, 71.2 X 183 cm (20 X 28 in.), has a mean chord of 12.7 cm (5 in.) and, therefore, enables the acquisition of data at chord Reynolds numbers somewhat greater than 20 million. This program was undertaken to exploit the semispan model technique and the capabilities of the CFF to expand current understanding of these transonic scaling phenomena.

SYMBOLS

b	wing span, cm (in.)
C_P	pressure coefficient
$C_{P_{.3}}$	pressure coefficient at 30 percent chord
C_{P_L}	lower-surface pressure coefficient
$C_{P_{TE}}$	trailing-edge pressure coefficient
C_{P_u}	upper-surface pressure coefficient
M	freestream Mach number
MAC	mean aerodynamic chord, cm (in.)
M_{LN}	local Mach number normal to the local element line of the wing
p	static pressure, N/m^2 (lb/ft^2)
p/H	ratio of static pressure to total pressure
R_e	Reynolds number
S	wing area, m^2 (ft^2)
X/C	nondimensional chordwise station
$(X/C)_{SH}$	shock location along the chord
α	angle of attack, deg
α_{CFF}	geometric angle of attack for the semispan model in the Lockheed-Georgia Compressible Flow Facility
γ	ratio of specific heats
η	nondimensional spanwise station
Λ_e	sweep angle of an element line on the wing

APPARATUS AND PROCEDURES

Model

The C-141 wing-fuselage semispan model used in this investigation was designed at the Lockheed-Georgia Company under contract NAS2-7081. This 0.0188-scale semispan model is shown installed in the 50.8 cm (20 in.) X 71.2 cm (28 in.) working section of the Lockheed Compressible Flow Facility in figure 2. Model size is based on a good compromise between high Reynolds number requirements and consideration of model/wall interference and solid blockage. The model consists of a left wing, half fuselage, and gear fairing attached to a 0.51 cm (0.2 in.) thick plate as shown in the sketch of figure 3. The model plane of symmetry was displaced 3.8 cm (1.5 in.) from the tunnel floor to allow for the floor boundary layer, and the plate attached to the base provides reflection plane characteristics. The model span is 45.72 cm (18 in.), and the effective semispan/tunnel height ratio is 0.696 with the 0.51 cm (1.5 in.) displacement. The solid blockage is estimated to be 2.5 percent.

Surface pressure orifices were installed on the wing at semispan stations of 0.193, 0.389 and 0.637 b/2. Orifices were provided on both upper and lower surfaces, and additional orifices were located at intermediate stations to monitor spanwise effects. Orifice locations are detailed in table 1. Spacing of the orifices was limited to 2.5 percent chord over most of the rear half of the airfoil at each of the three semispan stations. This ensures sufficient pressure data to accurately determine shock locations and local conditions in the vicinity of the shock.

Instrumentation

Measurements of the static pressures on the model surfaces were made using electronically actuated pressure scanning valves. The full-scale range of the quarter-percent accuracy Statham transducers in the valves was selected to provide maximum accuracy for the wind tunnel conditions tested at model pressures of $\pm$ 34 dynes/cm^2 (50 psi). CEC force balance pressure transducers were used in conjunction with CEC servo amplifiers to provide a precise measurement of the atmospheric pressure, stagnation pressure, and test section static pressure to 0.05 percent of the 172 dynes/cm^2 (250 psi) capacity. These transducers allow determination of the test section Mach number to an accuracy of $\pm$ 0.002 at the highest stagnation pressure.

Angle of attack was measured with a calibrated potentiometer operated by the angle of attack drive mechanism.

Raw pressure data were recorded on magnetic tape using the CFF high-speed data acquisition system. The data acquisition system consists of a Lockheed Electronics Company MAC-16 computer and associated peripheral equipment. The raw data were reduced to coefficient form with a CDC 1700 computer.

Test Facility

The general arrangement of the Lockheed Compressible Flow Facility (CFF) is shown in figure 4. The tunnel is of the blow-down type, exhausting directly to the atmosphere. The air storage capability is 368 m^3 (13,000 ft^3) at 413 dynes/cm^2 (600 psia). A sleeve-type control valve accurately maintains the settling chamber stagnation pressure at selected pressure less than or equal to the 172 dynes/cm^2 (250 psia) maximum and at mass flow rates less than 1089 kg/sec (240 lb/sec). The test section is 50.8 cm (20.0 in.) wide X 71.2 cm (28.0 in.) high X 183 cm (72.0 in.) long, and it is enclosed in a 3.7 m (12.0 ft) diameter plenum chamber. Two model support systems are available: a two-dimensional (side wall to side wall) system, and a three-dimensional wing or half-model system (bottom wall). The bottom-wall model mount system, used for semispan testing, has three variable-porosity walls and one fixed-porosity wall (bottom wall). Porosity is variable from zero to ten percent in the side and top walls by sliding two parallel plates with 0.635 cm (0.25 in.) diameter holes slanted 60 degrees from the vertical. The fixed-porosity floor has the same porosity pattern as that of the variable porosity walls, and the porosity can be reduced by manually sealing the holes. A more detailed description of facility is presented in reference 7.

TESTS

General Test Conditions

Unit Reynolds number for the test ranged from a low of about 19.7 million per meter (6 million per foot) to a maximum of about 190 million per meter (58 million per foot). This corresponds to a variation in model Reynolds numbers from about 2.5 million to 24 million/MAC. The Reynolds numbers were selected to provide wing shock/boundary layer characteristics which close the gap between model and full-scale results. Reynolds numbers for previous wind tunnel tests on the complete model were limited to 8.5 million/MAC and flight test Reynolds numbers range from 35 to 70 million/MAC. Mach numbers for the current program were 0.75, 0.8, 0.825, and 0.85; these were selected, together with model geometric angles of attack of 1°, 2°, 3°, and 4°, to correspond to those flight conditions where scale effects on wing shock characteristics are prominent. A summary of the current test program is given in table 2.

The model was tested smooth and with transition strips of Ballotini glass beads. The Ballotini strips were placed on upper and lower wing surfaces and on the fuselage nose. A particle height of 0.0069 cm (0.0027 in.) was determined for the low-Reynolds-number test condition, according to the criteria of reference 8, and was used throughout the fixed transition portion of the test. The roughness strips were placed 0.76 cm (0.3 in.) aft of the wing leading edge and 1.9 cm (0.75 in.) aft of the fuselage nose to simulate the location used in reference 2. The Ballotini strips were 0.13 cm (0.05 in.) wide and were set with Eastman 910 adhesive.

Angle-of-Attack Correlation

Difficulties in measuring angle of attack accurately during maneuvers in flight tests, differences in aeroelastic twist of the various models considered and of the flight test aircraft, differences in model configurations, and the lack of a precise method for calculating wall-induced flow angles in perforated wall transonic wind tunnels combine to produce a requirement for definition of an effective angle of attack which will assure that data from all available sources are being compared for equivalent flow conditions. The basis for the concept used in this study is illustrated by the data from another test program shown in figure 5. This figure shows a comparison of data at one test condition from a wind tunnel test at 7.4×10^6 Reynolds number with data from flight tests at a Reynolds number of 82×10^6. Because of the difference in Reynolds number, a significant difference in the degree of trailing-edge separation occurs, and the shock location changes by nine percent of the wing chord. In spite of these differences in shock location and in local velocities over the after portion of the wing, the remainder of the pressure distribution is in nearly exact agreement. On the other hand, variations in angle of attack (as shown by plots in the Appendix) cause large differences in the entire level of the velocity distribution. The concept used in defining the effective angle of attack, therefore, depends on the following assumptions, which are well supported by data from this and several

prior studies:

1. At a given Mach number, only angle of attack causes a change in pressure distribution forward of the shock. With fully developed transonic flow, changes in circulation due to trailing-edge separation cause no significant changes in pressure distribution except in the subsonic flow behind the shock.
2. Since the shape of the pressure distribution remains constant at any fixed Mach number and angle of attack, specification of pressure coefficient at any single point on the wing upper surface defines an angle of attack.

The method of implementing this concept is illustrated by figure 6. In the upper part of this figure, the value of the pressure coefficient at 30 percent chord, $C_{P_{.3}}$, is plotted against angle of attack for a Mach number of 0.825. In the lower portion of the figure, shock locations from previous wind tunnel and flight tests are plotted against their accompanying values of $C_{P_{.3}}$. Values of shock location selected from these plots at values of $C_{P_{.3}}$ corresponding to the angle of attack for the CFF tests then enables a proper comparison of data from these other sources with data from the CFF. This determination of equivalent angle of attack was accomplished for each spanwise station individually and, therefore, compensated for differences in aeroelastic twist among the several data sources.

Model and Tunnel Configuration

Prior to the start of the basic test program, a series of preparatory test runs were made to verify the proper model and tunnel configuration. The rationale for selection of the final test configuration was based on subjective judgments made after comparing current semispan test data with previous complete model results. A good match of pressure data from AEDC Test TF-139 (reference 2) on the wing upper surface back to the shock was the basic criterion used to define an equivalent geometric angle of attack. Consideration was then given to matching shock location at the equivalent conditions. Since correlation of the lower surface pressures is somewhat limited by configuration differences, no significance can be attached to either local lower surface pressures or lift coefficients for this analysis. A brief discussion of these differences is given in the next section.

The initial tunnel/model configuration was as follows:

- Model and model support tang as shown in figure 3. The model support between the boundary layer diverter and the tunnel floor having a simple rectangular cross-section.

- CFF floor porosity of six percent, other walls having a porosity of four percent.

The floor porosity was selected as a starting point on the assumption that it represented a reasonable compromise between a 100 percent reflection plane with a thick boundary layer and a partial (but adequate) reflection plane from which a substantial portion of the boundary layer bleeds through the partial porosity. A four-percent porosity on the other three walls was selected based on experience gained from recent testing of two-dimensional airfoils in the CFF (reference 9). The rectangular cross-section of the model support tang was assumed to

be satisfactory because of shielding provided by the boundary layer diverter. Results obtained for this initial configuration indicated that the partial floor porosity was undesirable, and a quick check was obtained by testing with tape placed over the floor holes. The floor was then sealed firmly by filling all the holes with epoxy, and the balance of the testing was accomplished with the floor sealed in this manner.

Figure 7 shows preliminary wall porosity effects obtained after sealing the floor. Semispan data at two degrees geometric angle are compared with complete model data from AEDC TF-139 at zero degree geometric angle. This two degree difference was selected to approximately match the flow condition on the two models and is probably due to the difference in wall-induced angularity between the two tests discussed previously. These data indicate expected increases in local velocities over the airfoils accompanied by rearward shock movement as the wall porosity is gradually decreased. At the extremely low porosity of one percent, noticeable velocity increases have occurred, and the trailing-edge pressure recovery has deteriorated substantially, especially on the two outboard stations. The aft shock movement with lower porosity improves the agreement of semispan and full-span pressure distributions and implies use of a rather low porosity for the test. At this point in the preliminary testing, a value of two percent was chosen while further checks on the overall tunnel/model configuration were being made.

Figure 8 summarizes the effects on the chordwise pressure distributions for the major steps taken to finalize the configuration. Comparisons of CFF results at two percent porosity are made against data from AEDC TF-139, again at equivalent angle of attack. Agreement of data for the initial configuration with full-span results is confined to the most forward portion for the two inboard stations with some improvement outboard. Shock locations for the initial configuration are six to ten percent forward of the full-span case. The substantial improvement in the correlation gained by sealing the floor can be clearly seen in these comparisons. A smaller improvement was obtained by adding a fairing to the model support tang below the diverter plate. This fairing changed the cross-section of the tang from rectangular to that of an airfoil shape and significantly increased its fineness ratio. Because of the improvements due to these two changes, the test configuration was updated to include both the sealed floor and the support tang fairing.

Before concluding the preparatory testing, a final check on porosity was made with this test configuration using values of four, three, and two percent for wall porosity. The results are shown in Figure 9. In this case, a porosity of two percent produced the substantial loss in trailing-edge pressure recovery seen previously at one percent. The reason for this cannot be substantiated but is associated with large reductions in the drag of the overall model/support configuration due to the addition of the tang fairings. Based on these data, selection of three percent as the correct porosity was made, and the main program was run using this value. The tang fairing used for these test runs and all subsequent testing was slightly thicker than that for the data discussed in the previous paragraph and produced slightly different test results.

Correlation of Pressure Distribution with Full-Span Data

As mentioned previously, lower surface pressures measured on the semispan model do not correlate with data measured on the complete model in AEDC TF-139. This difference, together with other observations regarding correlation of the CFF pressure data, will be discussed here.

Figure 10 shows an overall comparison of pressure results from three sources: current CFF semispan test, AEDC TF-139 test, and flight test. These data have approximately the same pressure coefficient at 30 percent chord on the inboard part of the wing. This assures an equivalent angle of attack inboard. Any spanwise variation in local angle of attack will result in further discrepancies outboard. Figure 10 reveals that this does, in fact, happen. The data for the outboard station indicates that this section on the aircraft is obviously at an effective lower angle of attack than the same section on the AEDC and CFF models. This is due purely to differences in aeroelastic twist on the wind tunnel model wing compared with the full-scale aircraft wing. Typical values of aeroelastic twist calculated for conditions encountered in the flight test program are 1-1/2 to 2 degrees at the wing tip.

Two significant differences in the wind tunnel models can be identified which at least partially explain the kind of flow differences seen on the inboard lower surfaces in figure 10:

- The model used in AEDC TF-139 consisted of a C-141 wing mounted on a C-5 model fuselage.
- The semispan model did not include pylons and nacelles.

The exchange of a C-5 fuselage and wheel pod fairing for those of a C-141 could produce noticeable flow changes on the inboard lower surface of the wing. The differences in pressure distribution on the lower surface of the inboard station, aft of 30 percent chord, between the flight data and AEDC TF-139 test data indicate the effect of the fuselage/wheel pod exchange. The peak pressure for the flight case is shifted further aft with respect to the AEDC data, and the aft loading is increased. The semispan data, where the C-141 fuselage/wheel pod is also used, tends to follow the pattern of the flight data. The large discrepancy forward on the section is obviously not being caused by the fuselage/wheel pod exchange. Some of this difference can be attributed to the absence of pylons and nacelles on the semispan model. Previously measured data on a similar configuration indicate that approximately half of the increment between the complete and semispan model results could be due to pylon and nacelles.

RESULTS

The basic test results are shown in Appendix A in the form of computer-generated pressure distribution plots. Generally, each figure presents pressure distributions for a series of angles of attack at fixed values of Mach number, Reynolds number, and spanwise location. Typical developments of flow separation as the angle of attack or Mach number increase can

be observed in a gross sense simply by comparing these pressure distribution plots. For example, Appendix figures 52A to 54A, showing data measured at a Reynolds number of 15 X 10^6 and a Mach number of 0.825, indicate a progressive deterioration of trailing-edge pressure recovery as the angle of attack is increased, with an accompanying forward movement of shock location. These effects increase in severity with increasing spanwise distance from the centerline. Figures 25A to 27A, for a Mach number of 0.80, show substantially smaller separation effects; and figures 76A to 78A, for a Mach number of 0.85, indicate somewhat greater separation. Details of the scale effects displayed by these data will be presented in the body of the report.

Definition of Shock Location

Figure 11 illustrates the definition of shock location used in this report. The abrupt pressure rise through the shock is fitted with a straight line which is extrapolated, if necessary, to a pressure coefficient corresponding to a local Mach number of 1.0 considered normal to local element lines of the wing. This pressure coefficient is defined from the following equation:

$$C_p = \frac{2}{\gamma M^2}\left[\left(\frac{1 + \frac{\gamma-1}{2}M^2 \cos^2 \Lambda_e}{1 + \frac{\gamma-1}{2}M_{LN}^2}\right)^{\frac{\gamma}{\gamma-1}} - 1\right]$$

where Λ_e is the sweep angle of each element line on the wing (constant percent chord), M_{LN} is the Mach number corresponding to the local velocity on the wing surface normal to the element line (set equal to 1.0 for this purpose). (Other terms have their conventional meanings and are defined in the Symbols Section.) The chordwise location of the intersection of the extrapolated shock line with the local Mach number 1.0 line is defined as the shock location, X/C_{SH}. This concept of considering Mach numbers normal to local element lines is used at this point only as a convention for defining shock location and is completely valid for this purpose when applied in a consistent manner. If Mach numbers normal to isobars were used instead, a foundation would exist also for a quantitative prediction of shock characteristics. In the absence of sufficient data to define isobar sweep, the sweep of element lines is frequently used as a reasonable approximation for those quantitative purposes.

Basic Scale Effects

Using the angle-of-attack correlation concept described previously, data from previous investigations have been combined with those from the present tests to show scale effects on shock location and trailing-edge pressure coefficient over the full range of available data. These data are presented in figures 12, 13, and 14 for each of the Mach number/angle-of-attack combinations for which strong shocks were observed. Because of the unsteady nature of the separated flows which are being investigated, a modest amount of scatter appears in all of the data shown. However, this scatter is not so large as to obscure the trends of the data, and good correlation generally exists among the data from the three sources available. In several instances (spanwise station .637, figure 12(a) is a good example), two distinct variations in shock location are shown for low Reynolds numbers with the transition fixed. It is believed that the differences shown can be attributed to the fact that, in some of the test runs, the boundary layer transition occurred at the grit strip, while

in others, the transition point moved farther forward. The curves drawn on these plots are faired through the points showing the more forward shock locations, since the higher Reynolds number results (where the natural-transition and the fixed-transition data agree) should experience the more forward transition location. A similar variation is shown by drag data presented in reference 9. A systematic disparity between the shock locations observed in flight and those which would be expected from the semispan results is shown for the two inboard stations at low angles of attack for a Mach number of 0.8. The source of this apparent discrepancy has not been identified. At a Mach number of 0.85, where flight data were measured at Reynolds numbers of 45 and 60 million, the trailing-edge pressure recovery is poorer, and the shock location is farther forward at the higher of these Reynolds numbers. Since this trend is in opposition to logical expectations, the curves are faired between the two values.

Low Reynolds number data from tests with natural transition indicate a tendency, shown in several previous studies (references 3 and 10),to provide a better simulation of the flight results than do those with the transition artificially fixed. This tendency is demonstrated also by the data shown in figures 12 to 14 (except figure 12a where the flight shock locations appear suspiciously far forward). The difference between the fixed transition and the natural transition data is significantly less pronounced for the most inboard wing station, where the flow can be contaminated by boundary layer flow from the fuselage. In the absence of sufficiently high Reynolds number test facilities, testing at low Reynolds numbers with natural transition still appears to provide a useful means to improve the accuracy of full-scale simulation. Unfortunately, quantitative methods to provide a precise simulation of a specific high Reynolds number condition have not yet been demonstrated.

As discussed previously, the model used in the present tests did not include pylons and nacelles, while all data available from previous testing were obtained with the pylons and nacelles installed. The good correlation shown at both high and low Reynolds number in figures 12 to 14 indicates that the absence of the pylons and nacelles has little, if any, influence on upper surface flows in spite of the obvious effects on lower surface pressure distribution. An initial criterion in C-141 development specified that the pylon leading edge should intersect the wing surface aft of the attachment line. Therefore, it is logical that the upper surface boundary layer is not disturbed by the pylons.

Evidence of Spanwise Contamination

It was previously pointed out that the trailing-edge separation increases as the measurement station moves outboard. This fact is strongly reflected by the much more forward shock location for outboard stations at low Reynolds numbers in figures 12 through 14. These figures also show a more pronounced scale effect on separation and shock location for the outboard stations. Therefore, the spanwise variation in shock location is very much smaller at high Reynolds numbers.

In a number of instances, especially at the outboard stations, the data in figures 12 through 14 show an increasing slope in the scale effect on shock location at Reynolds numbers above 15 to 20 million. Figures 15 and 16 combine data from several of those figures to show how this slope increase develops with increasing Mach number or angle of attack.

Figure 15 shows data for several angles of attack at a Mach number of 0.825. At one degree angle of attack, the scale effect curves have a nearly constant slope for station .637, culminating in essentially unseparated flow at the highest Reynolds number. For the two more inboard stations, the pressure recovery reaches typical unseparated values at lower Reynolds numbers, and the shock locations show a plateau for Reynolds numbers of approximately 30 to 60 million.

At two degrees angle of attack, the pressure recovery still shows attached flow at station .637 and 40 million Reynolds number; but the separation increases rapidly as the Reynolds number is decreased, causing the shock location to move rapidly forward for Reynolds numbers down to approximately 10 million. The shock location curve shows evidence of approaching a plateau at station .389, and a distinct plateau still exists at station .193.

At higher angles of attack, no flight data are available for station .637, but the data for station .389 indicate increasing slopes of the aft movement of shock location for Reynolds numbers above approximately 15 million. A plateau is still apparent at station .193 for high Reynolds numbers, even for the highest angle of attack.

Figure 16 shows scale effect data at an angle of attack of two degrees for several Mach numbers. At station .637, essentially attached flow is indicated for the highest Reynolds number and for all Mach numbers. The separation again increases rapidly at .825 and .85 Mach numbers as the Reynolds number decreases, resulting in an abrupt variation in shock location with Reynolds number. At station .389, the separation for the highest Reynolds numbers is more severe than at station .637, and no abrupt movement in shock location occurs. At station .193, the separation is never very severe, and a normal aft movement of shock location with increase in Mach number is shown for the highest Reynolds number.

These variations would seem to indicate the presence of spanwise contamination effects, causing separations to develop more rapidly than anticipated at outboard stations because of outboard flows along the trailing edge. At inboard stations, the separation is primarily a function of the local section and planform properties. At outboard stations, those normal separation tendencies are amplified by additional influences contributed by the spanwise flow. For the highest Reynolds numbers, of course, the spanwise contamination effects are minimal because no strong separations are present on the inboard portions of the wing.

Shock locations and trailing-edge pressure coefficients for two degree angle of attack at .825 Mach number are shown cross-plotted against spanwise station in figure 17(a). At a Reynolds number of 10 million, the trailing-edge pressure recovery deteriorates rapidly from inboard to outboard stations, and the shock location moves forward approximately 20 percent of the chord. At 40 million Reynolds number, the trailing-edge pressure coefficient is near 0.2 at all spanwise stations, and the shock location changes by only three percent chord. The pressure recovery is slightly worse at station .389 than at either the more inboard or the more outboard station in this case, possibly as a result of the break in

the trailing-edge sweep angle which is quite near this station.

In figure 17(b), similar data are shown for a Mach number of 0.85. Again, a rapid increase in separation and forward shock movement occur for increasing outboard location at 10 million Reynolds number. At higher Reynolds numbers, the separation is obviously most severe at station .389, with significant improvement at the most outboard station. This fact does not contradict previous statements regarding spanwise contamination, since the effects of increased Reynolds number in improving the resistance to local separation tendencies can overpower the effects of spanwise flow.

Figure 18 shows the pattern of surface flows on a large-chord panel model having no taper and no spanwise variation in airfoil section or twist. The airfoil section of this model was the same as that at wing station .389 on the C-141A wing, and three-dimensional streamline-shaped plates were attached to the root and tip of the model to eliminate end effects. Near the root, the flow is smooth and continuous through the shock (indicated by the abrupt change in flow direction at approximately 0.75 chord). A strong spanwise flow appears in the boundary layer behind the shock. At more outboard spanwise stations, the shock moves forward on the chord, and a distinct discontinuity appears in the boundary layer flow at the shock. Although not conclusive, this would appear to offer additional evidence of the influence of spanwise flows on the severity of trailing-edge separations and, therefore, on shock location.

Correlation of Shock Location and Trailing Edge Separation

Previous references have been made to the direct correlation of trailing-edge separation with shock location, and this is illustrated by the similarity in the shape of scale-effect curves for these two parameters. In figure 19, shock location is plotted against trailing-edge pressure coefficient using data from the various sources available and showing that, in a quantitative sense, this correlation is quite rigorous. These data lend additional weight to the argument that the kind of scale effects considered here are predominantly a function of trailing-edge separation effects rather than discrete shock-boundary layer interaction phenomena in the immediate vicinity of the shock. In other instances (with less severe aft pressure gradients, for example), the effects at the shock might be dominant, but no data from the present study indicate that kind of phenomenon.

The data shown in figure 20 show further substantiation of the strong dependence of shock location on trailing-edge separation phenomena and illustrate the mechanism by which the shock is caused to move. In figure 20(a), data are shown from reference 2 with, and without, vortex generators at 70 percent chord on a C-141 wing model. With no vortex generators, a small region of separated flow is apparent aft of 85 or 90 percent chord. Adding vortex generators aft of the shock eliminated that separation and caused the shock to move rearward. The direct cause of the shock movement is the change in the pressure distribution from the foot of the shock aft resulting from elimination of the trailing-edge separation. The shock acts to produce the change in local Mach number from supersonic to sub-

sonic. Since the pressure rise through the shock is a function of the supersonic Mach number at which it occurs, it must position itself in such a way that its pressure rise is compatible with both the upstream local supersonic Mach number and the downstream pressure distribution. Any change which causes the downstream pressures to be more negative, as shown here due to eliminating the trailing-edge separation, requires the shock to occur at a higher local Mach number and, therefore, to move aft.

In figure 20(b), a similar change in shock location is shown to be caused by changes in downstream pressures resulting from aileron deflection. Upward (negative) deflections of the aileron cause the pressure on the rear of the wing to be more positive and, therefore, require the shock to move forward. The fact that the downstream pressures comprise the driving factor and that shock location is the result (rather than the inverse) is demonstrated by the fact that the downstream pressures are predicted quite well by a Karman-Tsien transformation of pressures measured for the same aileron deflections at low Mach numbers for which no shock was present.

In the case of the scale effects under consideration here, no change in airfoil geometry is involved; as the pressure changes downstream of the shock are uniquely controlled by trailing-edge separation, it is possible to correlate shock location against trailing-edge pressure recovery.

Comparison with Panel Model Data

Pressure distribution data measured at station .389 at a Reynolds number of 20 million are compared in figure 21 with data measured at three stations near the mid-semispan of the panel model of reference 5. Excellent agreement of the pressure distributions is shown over most of the chord. Immediately forward of the shock, a rather rapid increase in velocity is shown in the data from the present investigation. The velocity variation in this small region is accurately simulated by the panel data at station 40. At the other two panel model stations, this small area of increased velocity is less noticeable.

Figure 22 shows scale effects on shock location from the present tests and from the panel model test for two angles of attack at $M = .825$. At the highest Reynolds number, or at the lowest Reynolds number with natural transition, the shock locations from these two sources agree very well. However, at lower Reynolds numbers with the transition fixed, the separation is more severe in the complete configuration data, and the scale effect curves are, therefore, significantly steeper.

This failure of the panel model data to simulate scale effects on the complete configuration, when viewed in conjunction with other previously discussed effects, would appear to result from its inadequate simulation of the complete configuration geometry (either inadequate span for matching spanwise contamination or the absence of the local disturbance produced by the break in trailing-edge sweep angle). The surface flow pattern shown in figure 18 indicates that, if measurements were available at more outboard stations on the

panel, they would show more pronounced separations and certainly more forward shock locations. Caution is obviously required in attempting to predict complete wing scale effects on the basis of data from simplified models such as this panel or airfoil sections.

CONCLUSIONS

1. Good correlation of data from several sources indicates that these semispan tests produced a good simulation of flow conditions existing on the complete configuration. However, preparatory testing to establish the final model/tunnel configuration showed a strong sensitivity to configuration details and indicated that a large boundary layer diverter plate cannot be relied upon to shield the model from inboard disturbances.

2. Results from this program provide a good bridge between previously available low-scale wind tunnel data and full-scale flight data. Abrupt increases in the rate of variation of shock location with Reynolds number are shown for high Reynolds numbers, especially on outboard portions of the wing span.

3. At low Reynolds numbers, the severity of trailing-edge separation increases with increase in spanwise distance from the centerline, apparently as a result of spanwise flows in the region behind the shock. At higher Reynolds numbers, this spanwise contamination is significantly reduced.

4. For the C141 configuration, no Reynolds number less than the full-scale flight value provides a satisfactory simulation of the full-scale flows. Furthermore, the abrupt increase in the rate of variation of shock location with Reynolds number increases the difficulty of reliable extrapolation of low-scale measurements.

5. Because of the spanwise contamination effects suggested by the data from these tests, data from simplified models such as constant-chord panels or two-dimensional models cannot be relied upon to produce an accurate indication of scale effects involving shock-induced separation.

REFERENCES

1. Cahill, J. F.; and Cooper, B. L.: Flight Test Investigation of Transonic Shock-Boundary Layer Phenomena. AFFDL-TR 68-84, July 1968.

2. Wright, J. M.: Development of Testing Technique Required to Duplicate Full Scale Wing Shock Location on a Wind Tunnel Model. Lockheed-Georgia Company Report LGIT6-1-16, May 1966.

3. Loving, D. L.: Wind Tunnel-Flight Correlation of Shock-Induced Separated Flow. NASA TN D-3580, 1966.

4. Cahill, J. F.; and Stanewsky, E.: Wind Tunnel Tests of a Large-Chord, Swept-Panel Model to Investigate Shock Induced Separation Phenomena. AFFDL-TR-69-78, October 1969.

5. Cahill, Jones F.; Treon, S. L.; and Hofstetter, W. R.: Feasibility of Testing a Large-Chord, Swept-Panel Model to Determine Wing Shock Location at Flight Reynolds Number. AGARD Conference Proceedings No. 83, April 1971.

6. Cahill, Jones F.: Simulation of Full-Scale Flight Aerodynamic Characteristics by Tests in Existing Transonic Wind Tunnels. AGARD Conference Proceedings No. 83, April 1971.

7. Pounds, G. A.; and Stanewsky, E.: The Research Compressible Flow Facility. Lockheed-Georgia Company ER-9219, 1967.

8. Braslow, A. L.; Hicks, R. M.; and Harris, R. V., Jr.: Use of Grit-Type Boundary-Layer-Transition Trips on Wind Tunnel Models. NASA TN D-3579, 1966.

9. Burdges, Kenneth P.; Blackwell, James A., Jr.; and Pounds, Gerald A.: High Reynolds Number Test of a NACA 65_1-213, $a = 0.5$ Airfoil at Transonic Speeds. Lockheed-Georgia Company LG74ER0072; NASA CR 2499.

10. Blackwell, J. A.: Effect of Reynolds Number and Boundary-Layer Transition Location on Shock-Induced Separation. AGARD Conference Proceedings No. 35, 1968.

11. Bolen, G. C.: Investigation of Static Pressure Distributions at High Mach and Reynolds Numbers of a 0.040 Scale Model in the AEDC 16-Foot Wind Tunnel. Lockheed-Georgia Company Report LGIT6-1-18, September 1966.

TABLE 1

ORIFICE LOCATIONS

STATION X/C	.193		.298	.343	.389		.422	.488	.637	
	UPPER	LOWER	UPPER	UPPER	UPPER	LOWER	UPPER	UPPER	UPPER	LOWER
0	o	o			o	o			o	o
.025	o	o			o	o			o	o
.05	o	o			o	o			o	o
.075	o	o			o	o			o	o
.1	o	o			o	o			o	o
.125	o				o				o	
.15	o	o			o	o			o	o
.175	o				o				o	
.2	o	o			o	o			o	o
.25	o				o				o	
.3	o	o			o	o			o	o
.35	o				o				o	
.4	o	o			o	o			o	o
.45	o				o				o	
.475	o				o				o	
.5	o	o			o				o	o
.525	o				o				o	
.55	o				o				o	
.575	o				o				o	
.6	o	o			o	o			o	o
.625	o				o				o	
.65					o				o	
.675	o				o				o	
.7	o	o	o	o	o	o	o	o	o	o
.725	o				o				o	
.75	o				o				o	
.775	o				o				o	
.8	o	o	o	o	o	o	o	o	o	o
.85	o				o				o	
.9	o	o	o	o	o	o	o	o	o	o
.95	o				o				o	
1.0	o	o			o	o			o	o

TABLE 2. PROGRAM SUMMARY

WING GRIT	R_e X 10^6/ MAC	MACH NO.	RUN NUMBER @ INDICATED ANGLE OF ATTACK 1°	2°	3°	4°	REMARKS
FREE	2.7	.75	394, 392*, 393	396, 395*	397	398	
		.8	386	387	389, 388*	391, 390*	
		.825	412(409-411)*	414, 413*	415	416	
		.85	380	381	427, 426*	385, 384*	
	4.4	.825	374	375	376	378, 377*	
		.85	417	418	419	420	
	6.0	.75	201	202	203	224, 222* 223*	(α=0°, RUN 200)
		.8	205	206	207	208	(α=0°, RUN 204)
		.825	211, 209, 210* 401, 399*, 400*	212, 402 425	213, 403	214, 404	
		.85	216, 215* 405	217 406	218 407	221, 219* 220*, 408	
	8.2	.75	226, 225*	227	228	229	
		.8	230	231	232	233	
		.825	234, 421	235, 422	236, 423	237, 424	
		.85	240, 238*, 239*	242	243	244	
	15	.75	246, 245*	247	248	249	
		.8	250	251	252	253	
		.825	254	255	256	258	
		.85	259	261	262	263	
	20	.75	265, 264*	266	267	268	
		.8	273	274	275	276	
		.825	269	270	271	272	
		.85	277	278	279	280	
	24	.825		281			
FIXED	2.7	.8	444	445	446	447	
		.825	432(429-431)*	433, 323	434	436, 435*	
		.85	440(437-439)*	441	442	443	
	6	.75	334	336, 335*	337	338	
		.8	340, 339* 449	341 450	342 451	343 452	GRIT ERODED ON RUNS 339-343
		.825	330	331, 325 324*	332	333	
		.85	344 453	345 455, 454*	346 456	347 457	GRIT ERODED ON RUNS 344-347
	8.2	.75	352	353	354	355	
		.8	357, 356*	358	359	360	
		.825	348	349, 327 326*	350	351	
		.85	362	363	364	365	
	15	.825	366	367, 328	368	369	
		.85	370	371	372	373	
	20	.825		428, 329		458	

NOTE: ASTERISKS DENOTE ADDITIONAL MACH NUMBER RUNS.

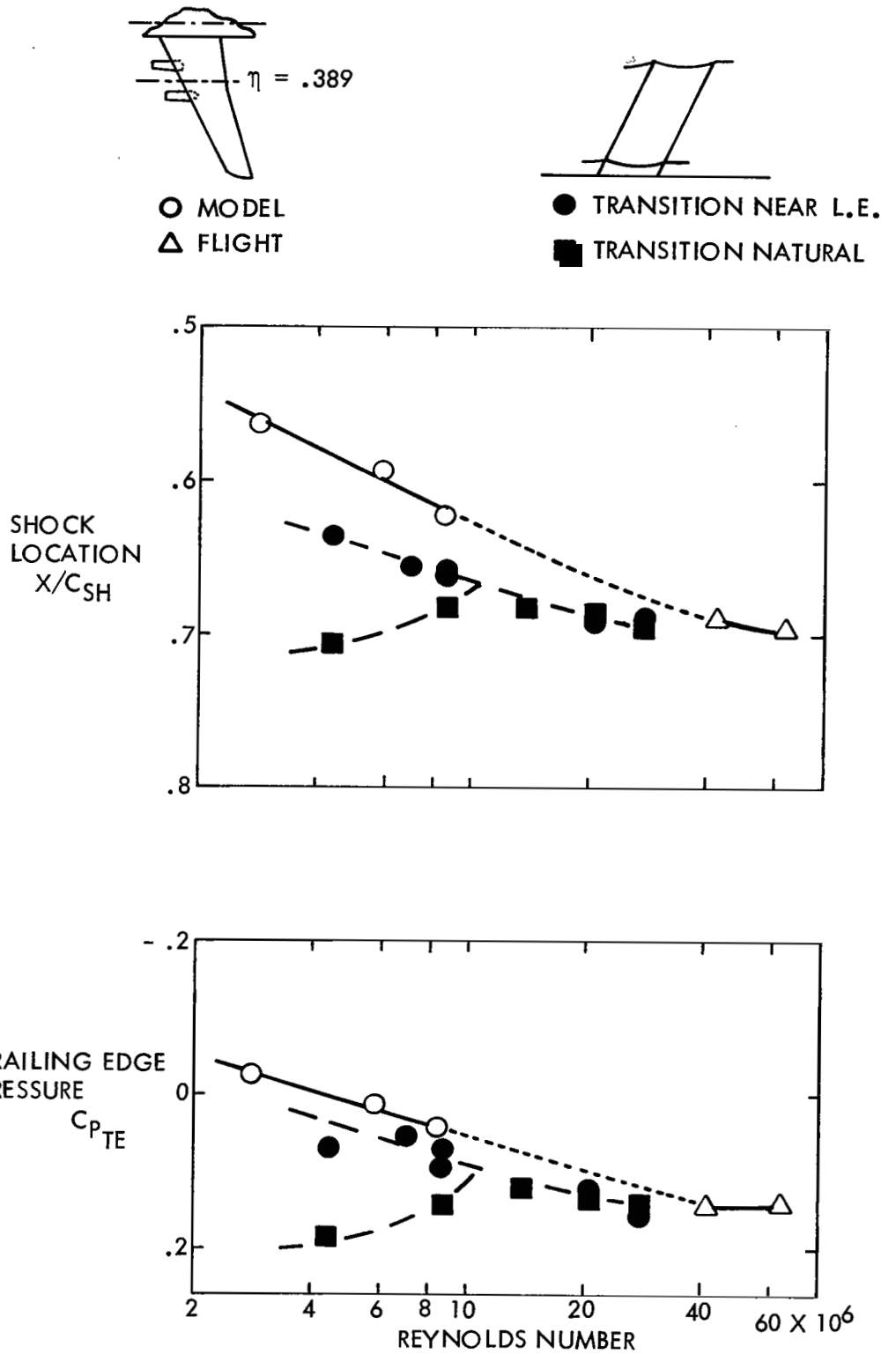

Figure 1. Typical Scale Effects from Previous C-141 Testing

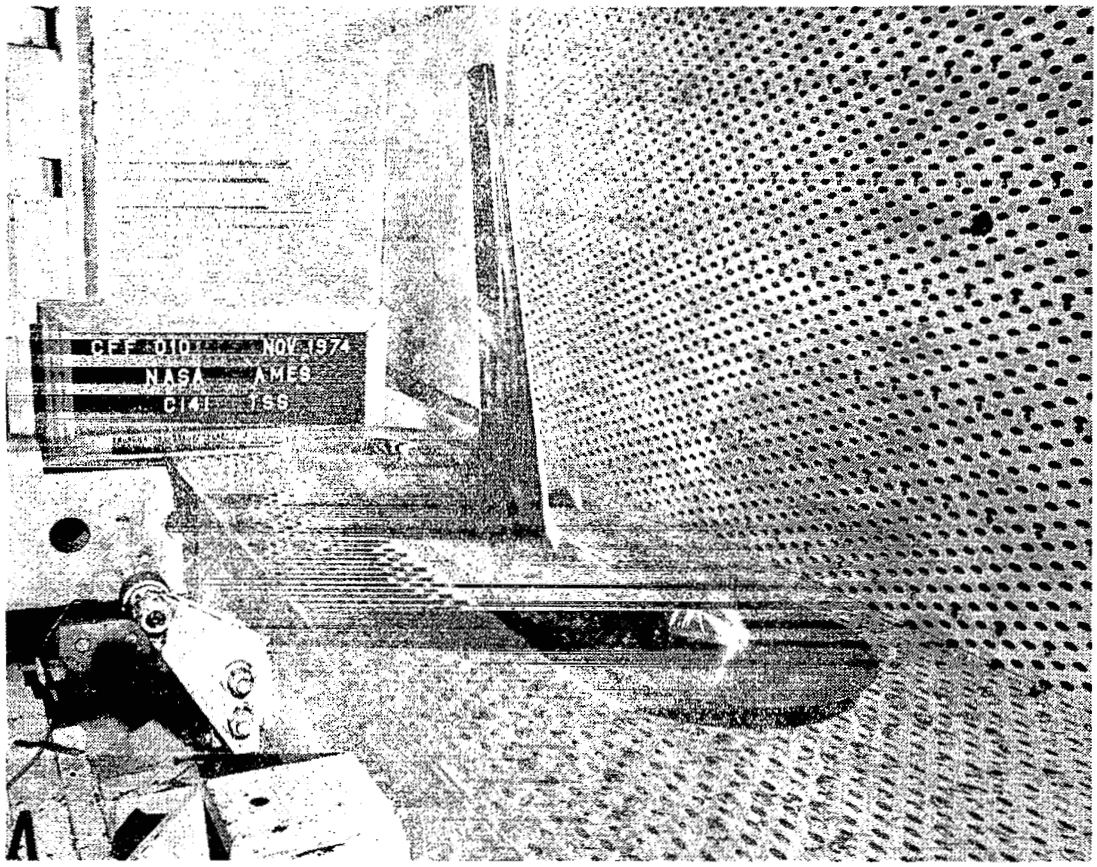

Figure 2. Photograph of Model Installed in the CFF Wind Tunnel. (One Sidewall Removed.)

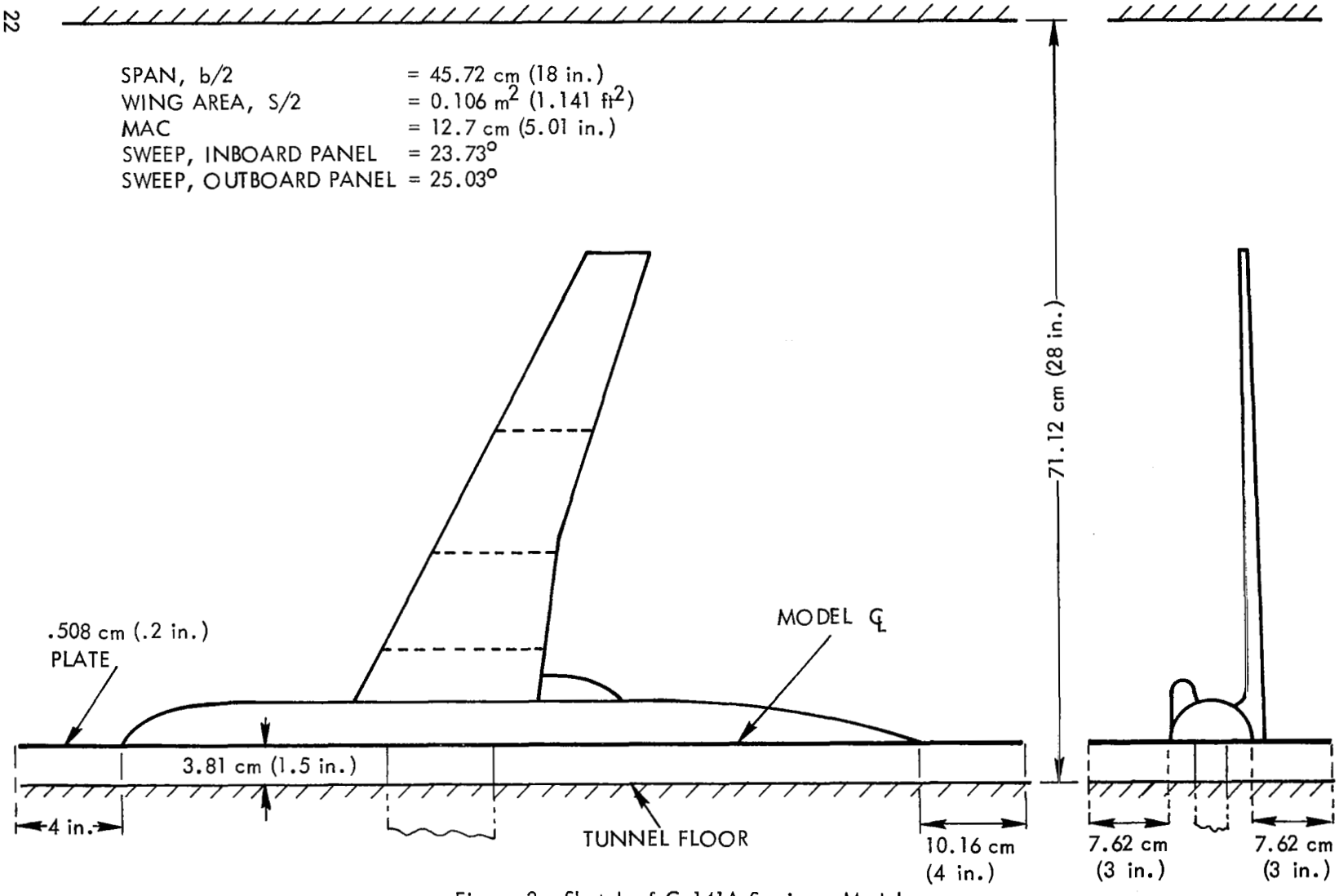

Figure 3. Sketch of C-141A Semispan Model

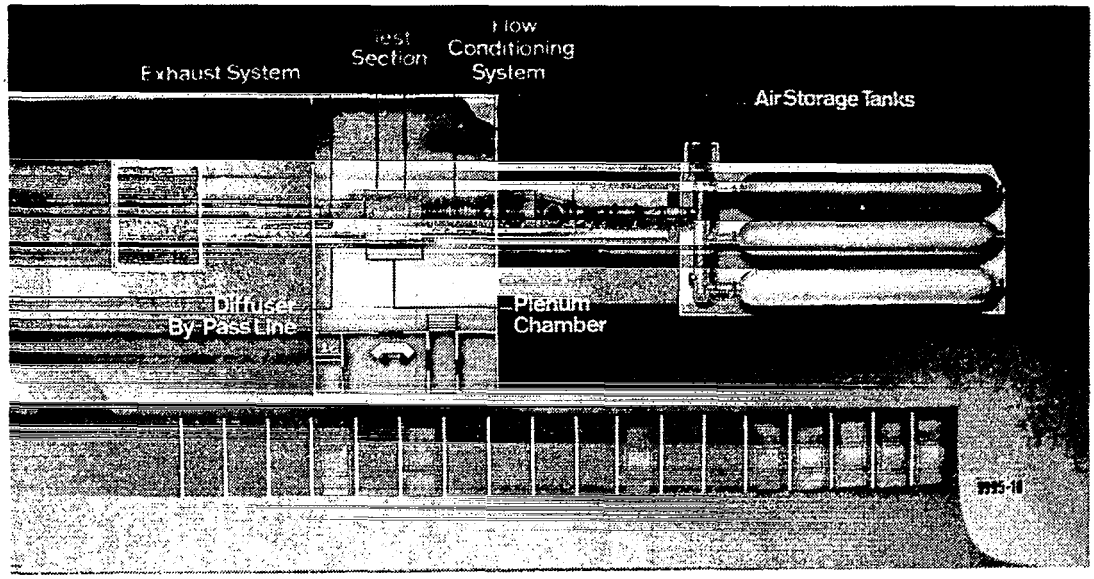

Figure 4. Lockheed-Georgia Compressible Flow Facility

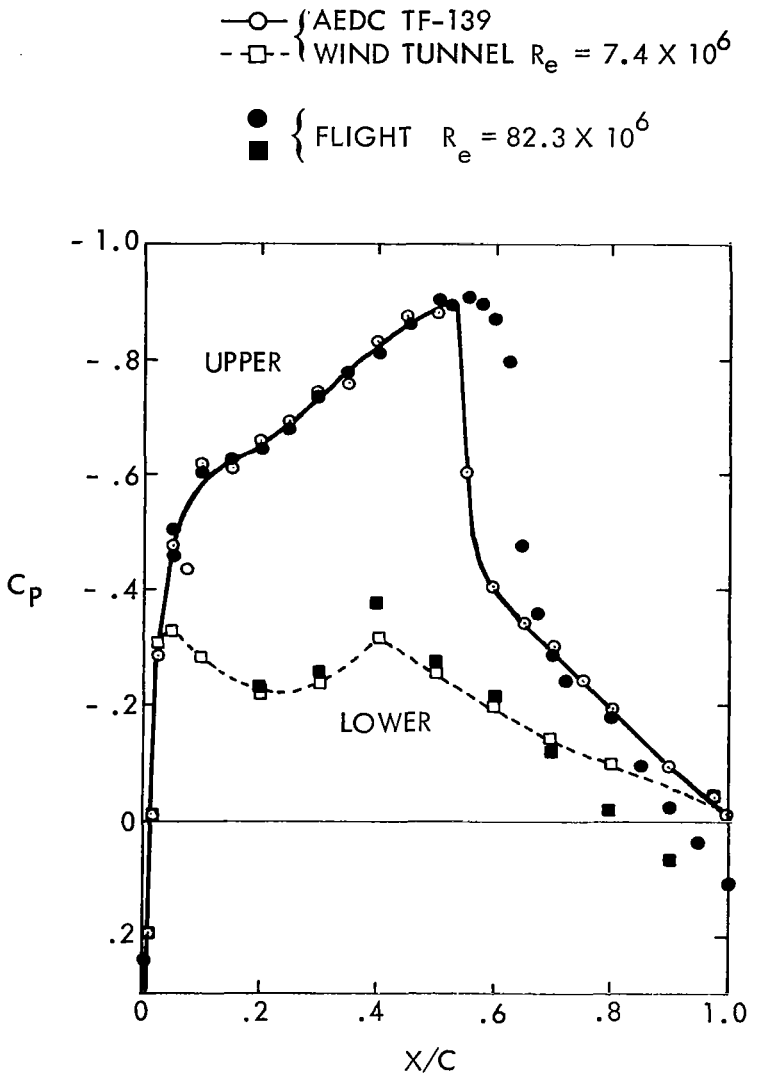

Figure 5. Comparison of Wind Tunnel and Flight Test Pressure Distributions Using the Angle of Attack Correlations. C-5 Wing, η = .70, M = .86, $\alpha = 0^o$

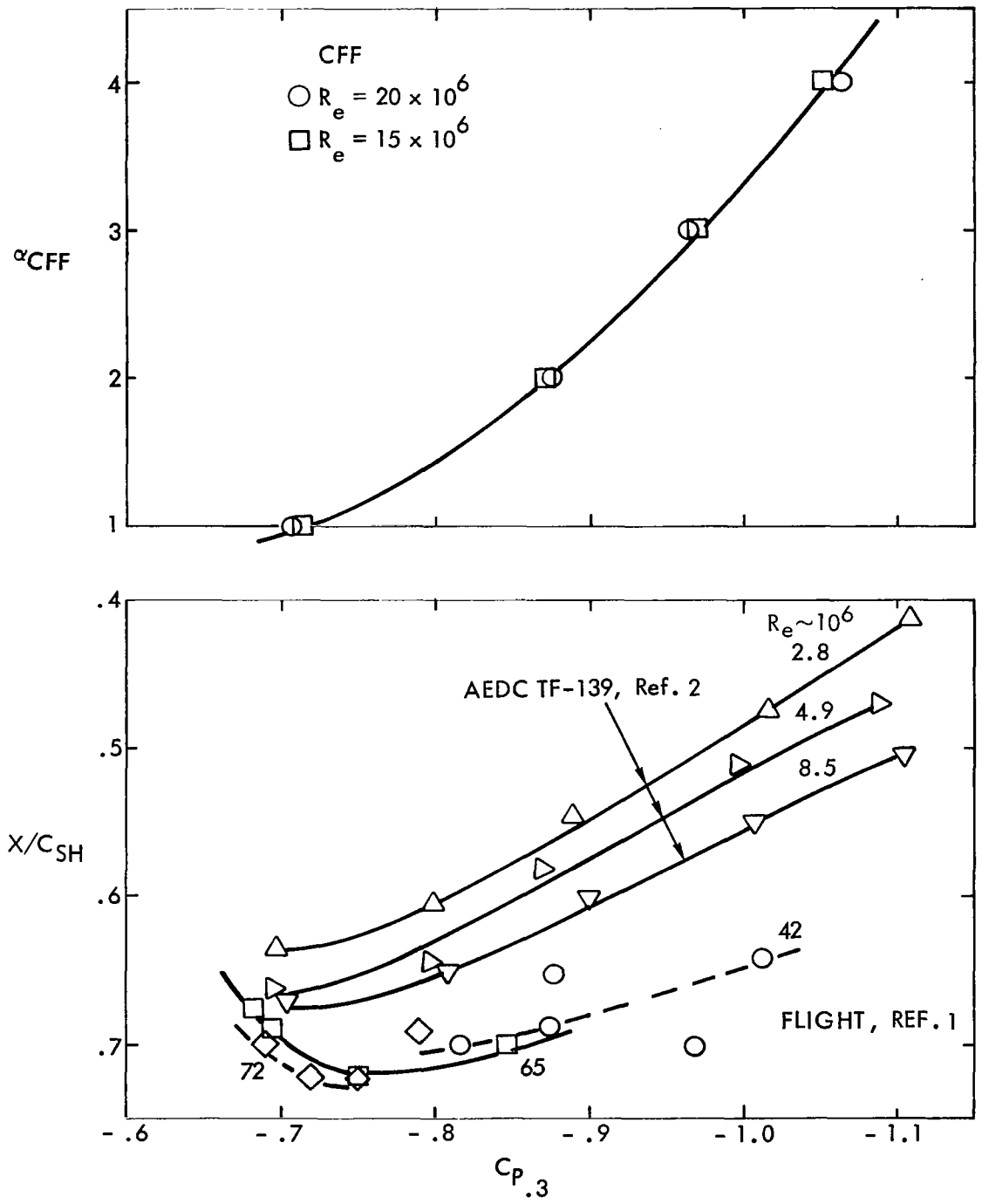

Figure 6. Concept for Shock Location Correlation
M = .825 η = .389

DATA	REYNOLDS NO.	MACH NO.	ALPHA	POROSITY
○ CFF	7.5 X 10^6/MAC	0.8	2°	6%
□ CFF	7.5 X 10^6/MAC	0.8	2°	4%
◇ CFF	7.5 X 10^6/MAC	0.8	2°	2%
⌂ CFF	7.5 X 10^6/MAC	0.8	2°	1%
— TF-139	8.5 X 10^6/MAC	0.8	0°	

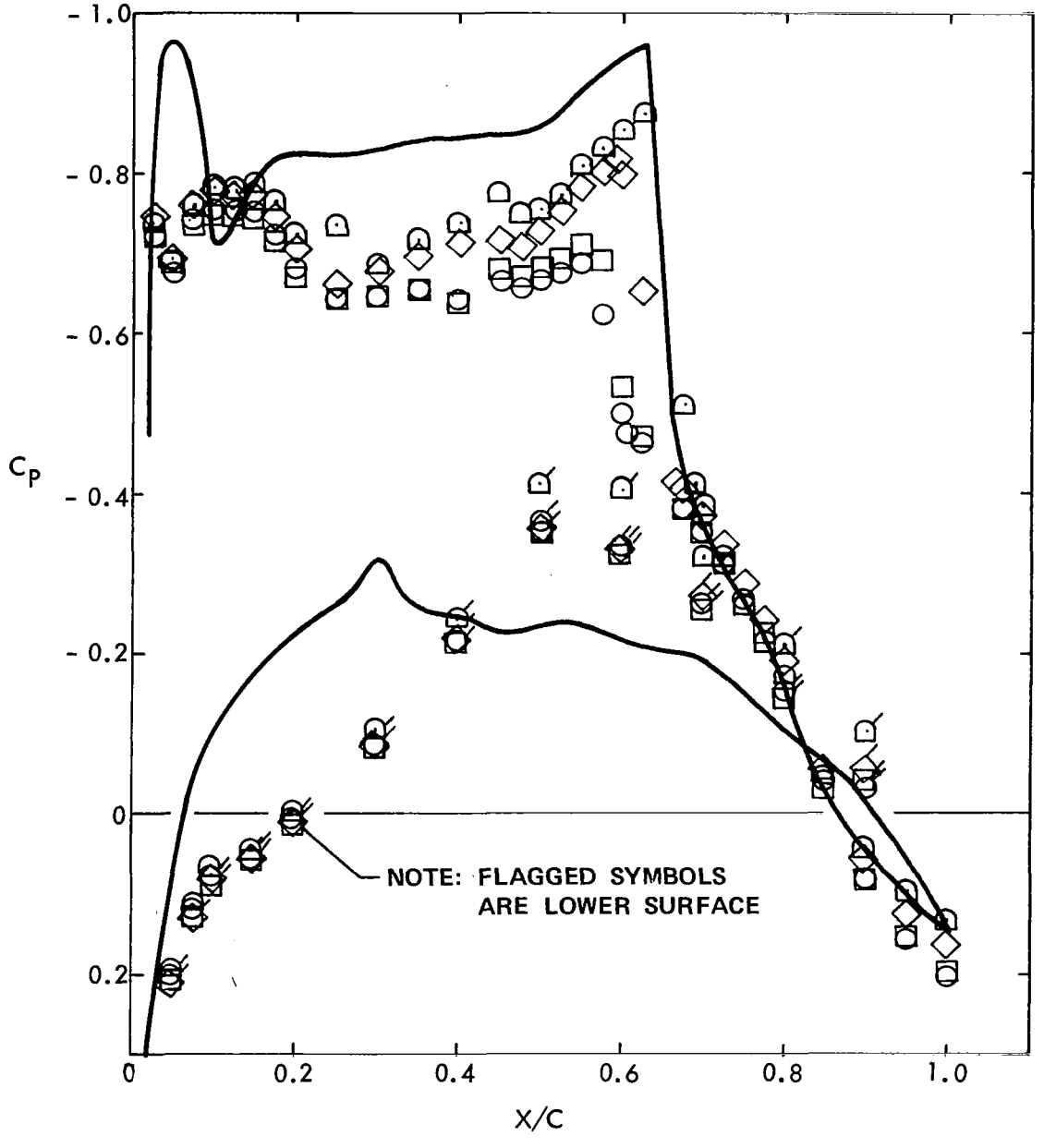

Figure 7. Porosity Effects, Floor Sealed
(a) η = .193

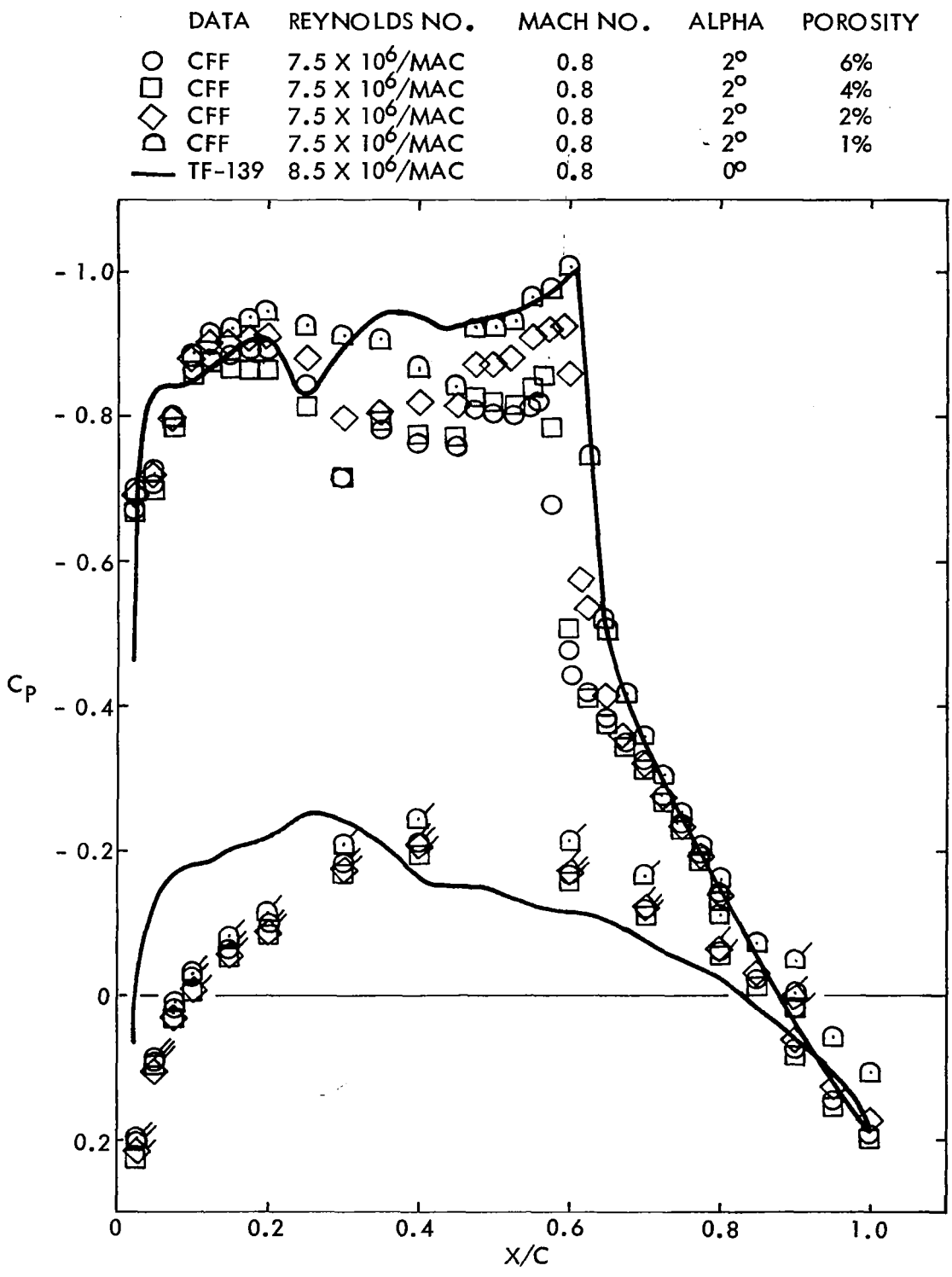

Figure 7. Continued (b) η = .389

DATA	REYNOLDS NO.	MACH NO.	ALPHA	POROSITY
○ CFF	7.5 X 10^6/MAC	0.8	2°	6%
□ CFF	7.5 X 10^6/MAC	0.8	2°	4%
◇ CFF	7.5 X 10^6/MAC	0.8	2°	2%
⌓ CFF	7.5 X 10^6/MAC	0.8	2°	1%
— TF-139	8.5 X 10^6/MAC	0.8	0°	

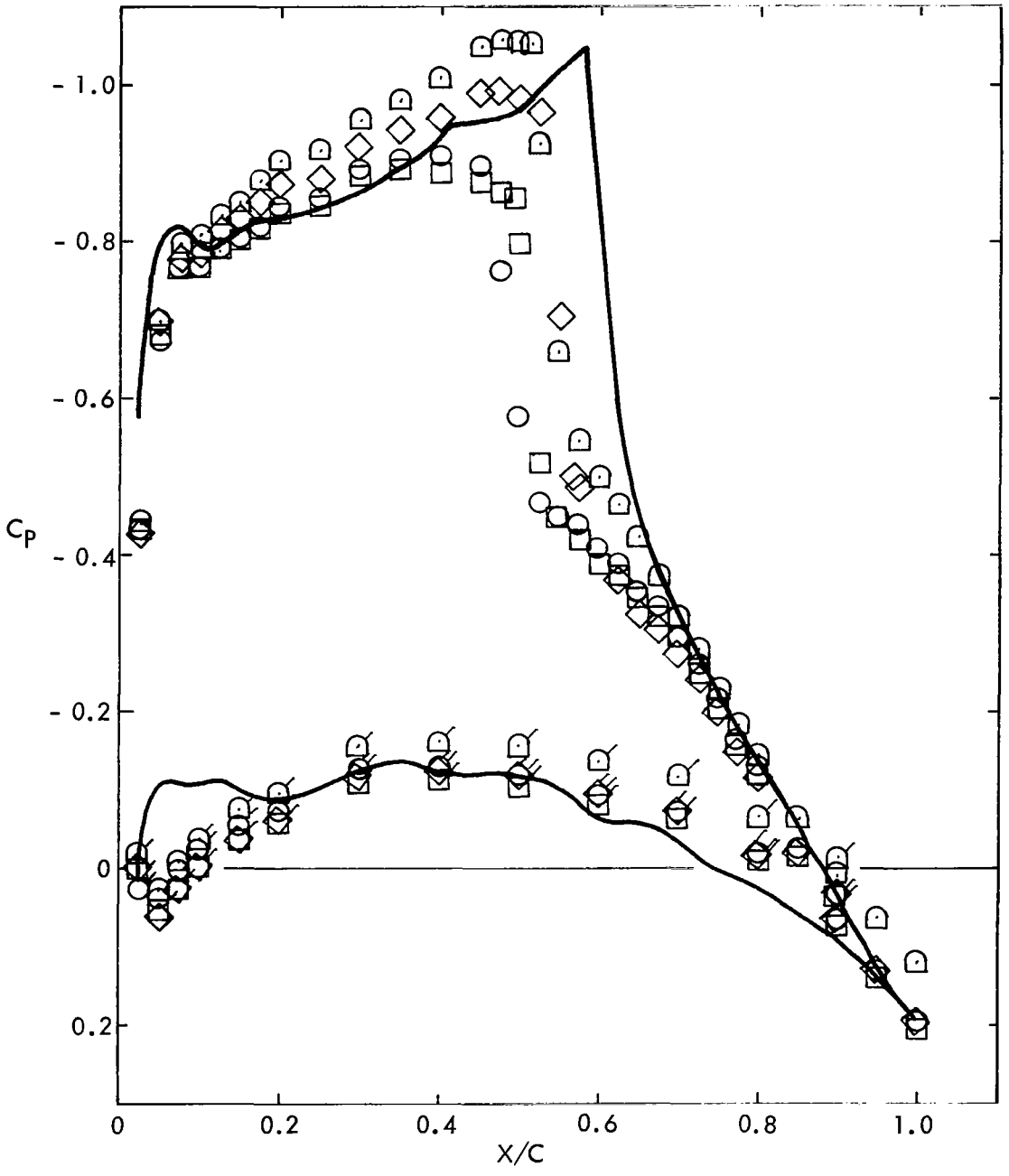

Figure 7. Concluded (c) η = .637

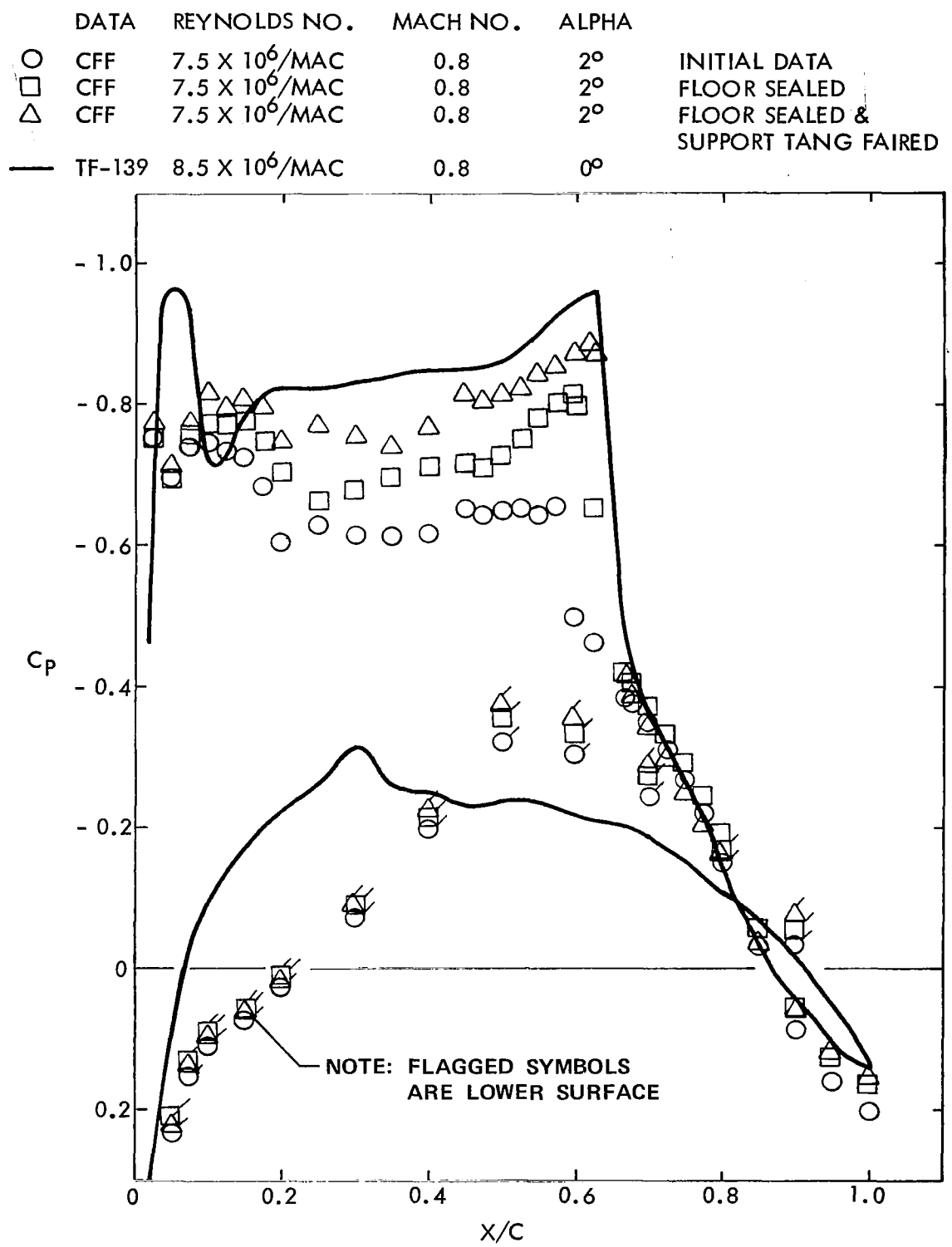

Figure 8. Model/Tunnel Configuration Effects
(a) η = .193

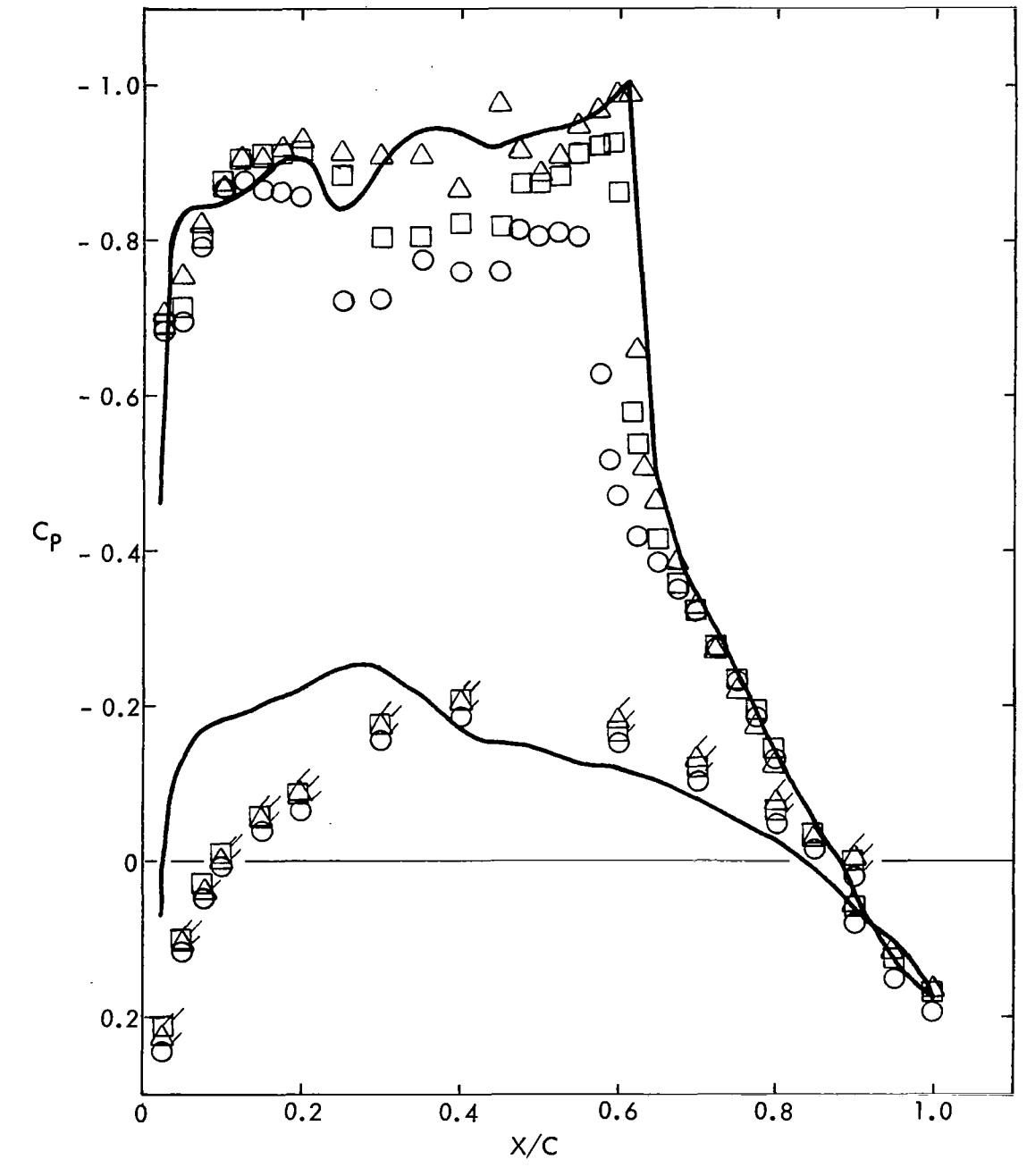

Figure 8. Continued (b) η = .389

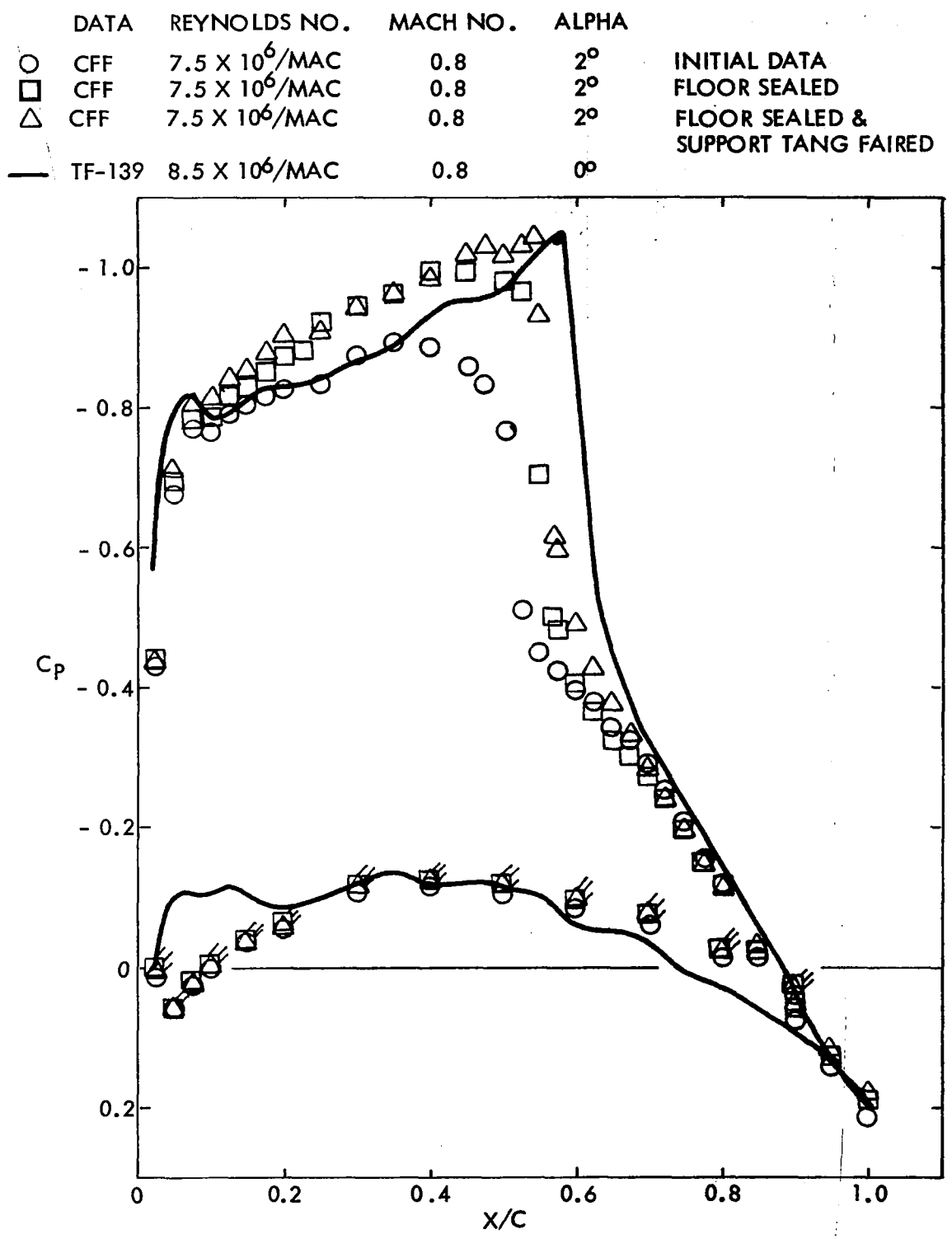

Figure 8. Concluded (c) $\eta = .637$

DATA	REYNOLDS NO.	MACH NO.	ALPHA	POROSITY
○ CFF	7.5 X 10^6/MAC	0.8	2°	4%
□ CFF	7.5 X 10^6/MAC	0.8	2°	3%
△ CFF	7.5 X 10^6/MAC	0.8	2°	2%
— TF-139	8.5 X 10^6/MAC	0.8	0°	

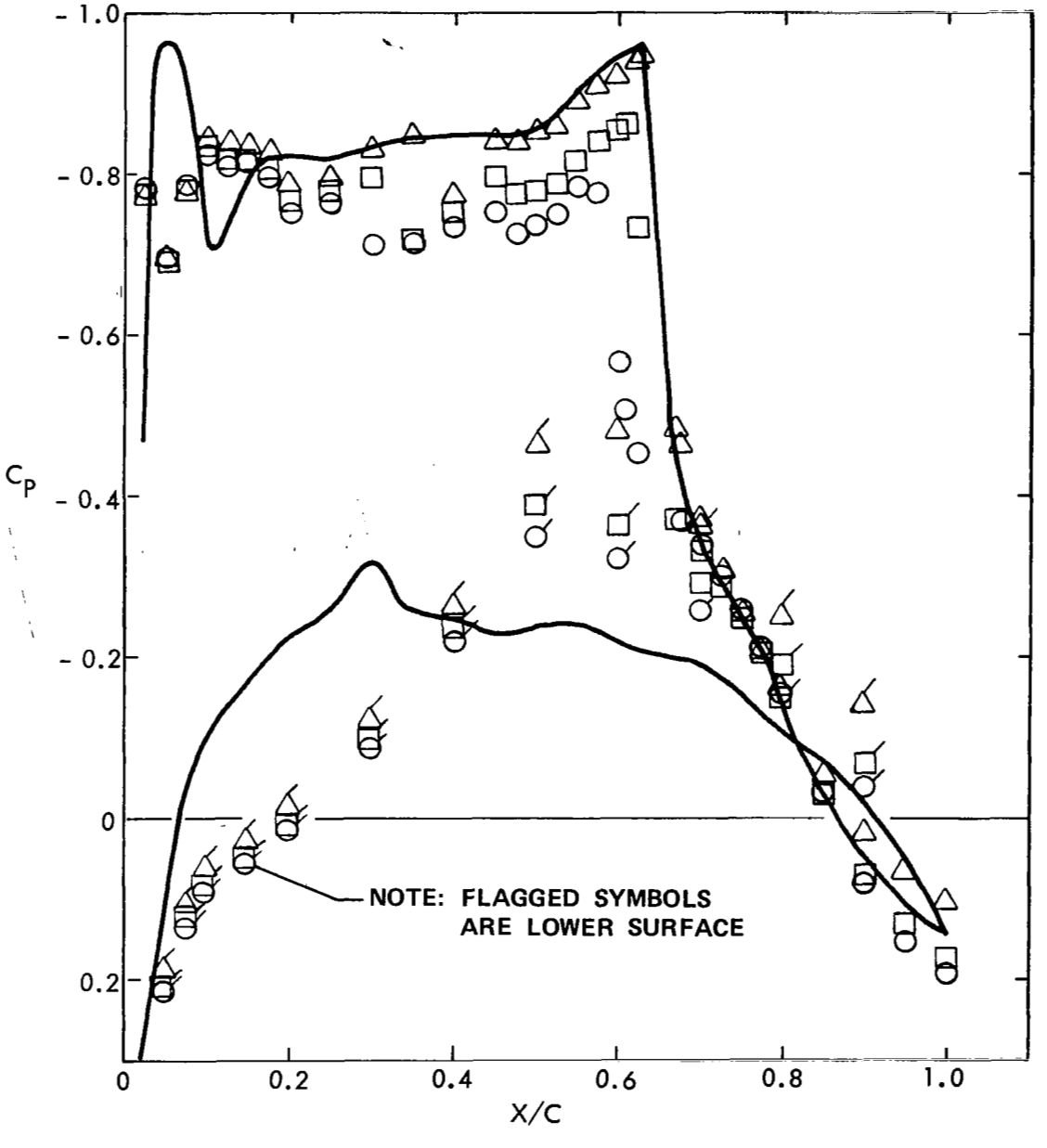

Figure 9. Porosity Effects, Floor Sealed and Support Tang Faired
(a) η = .193

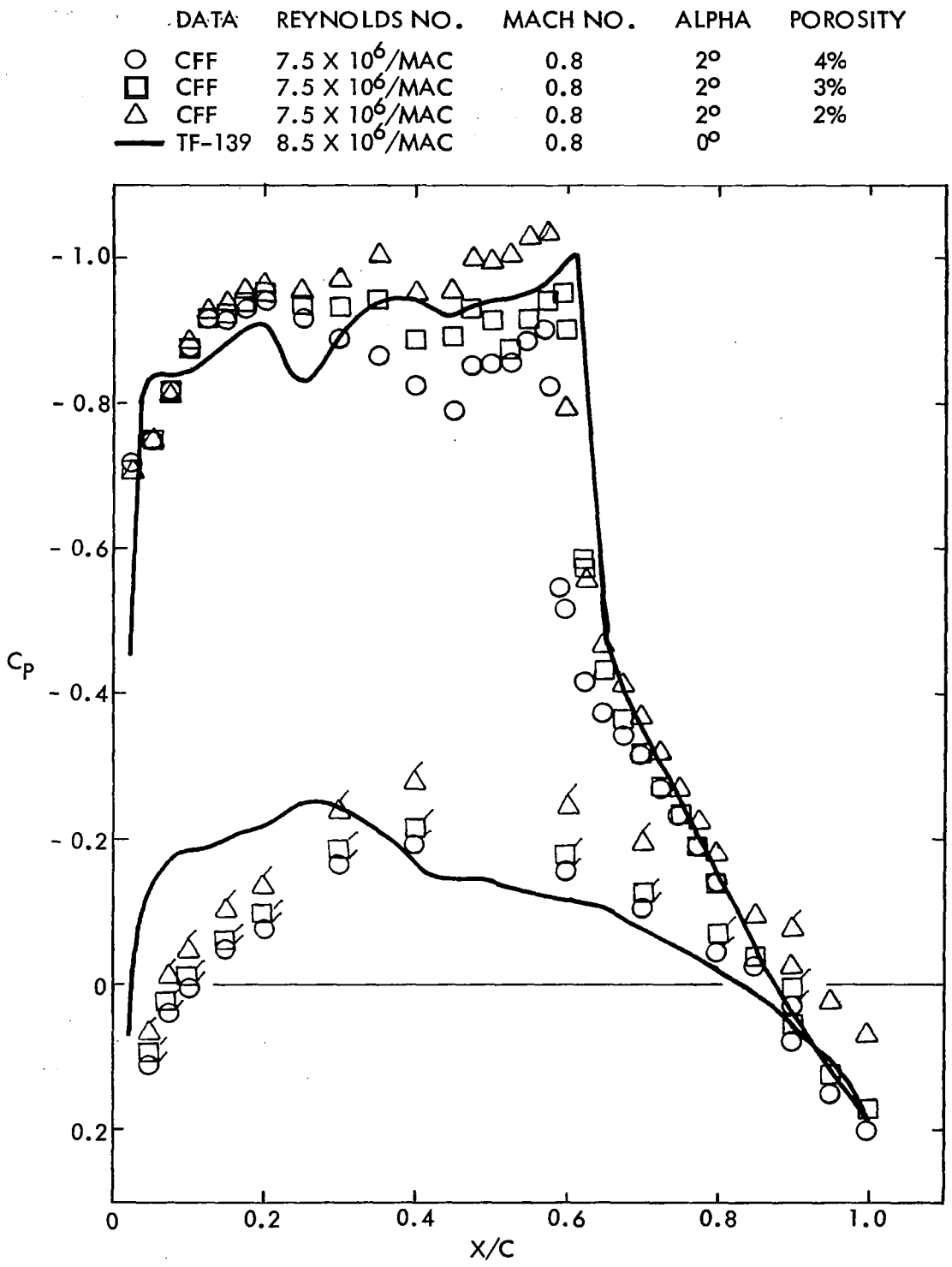

Figure 9. Continued (b) η = .389

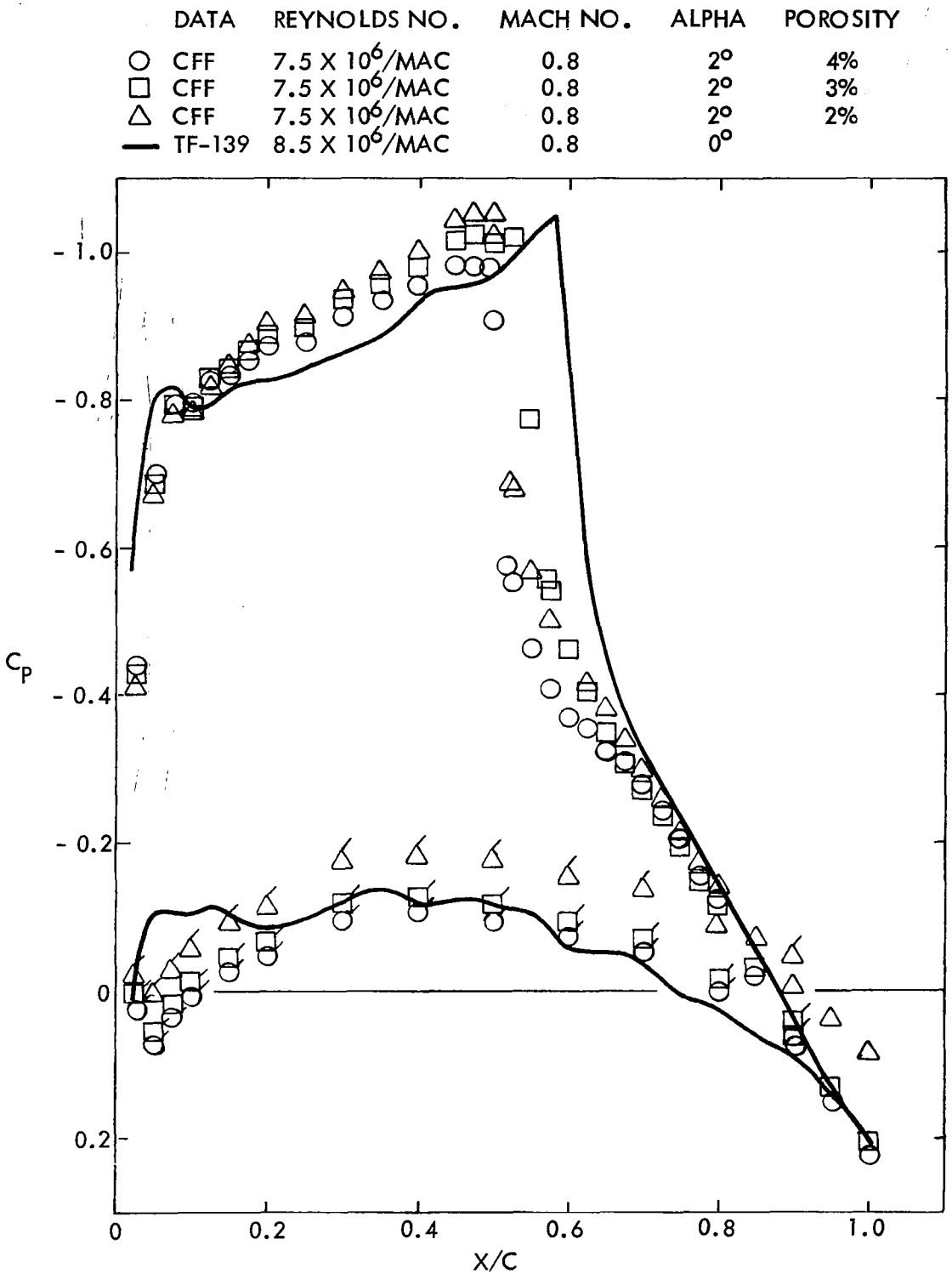

Figure 9. Concluded (c) η = .637

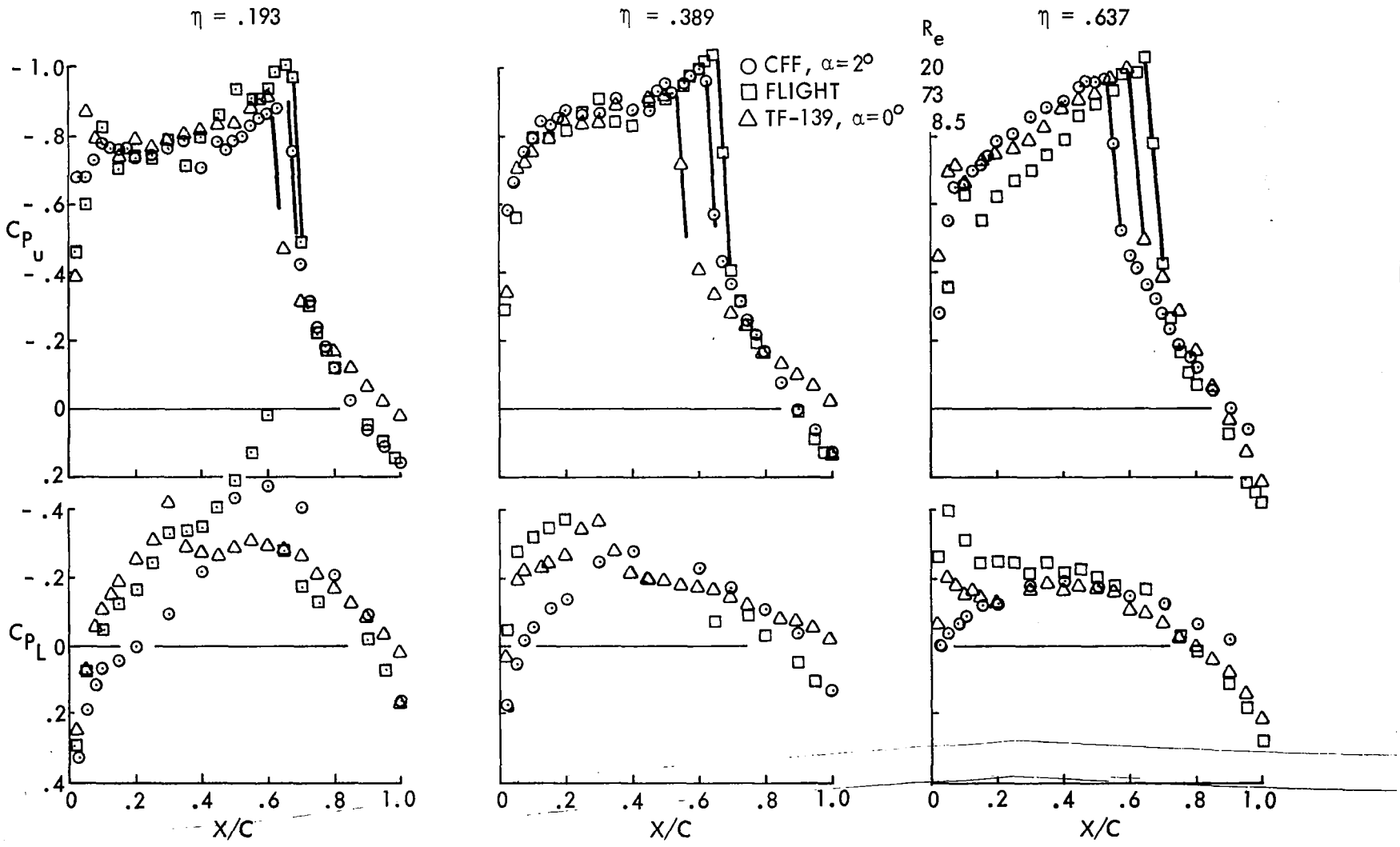

Figure 10. Correlation of Pressure Data with Full Span Data, M = 0.825

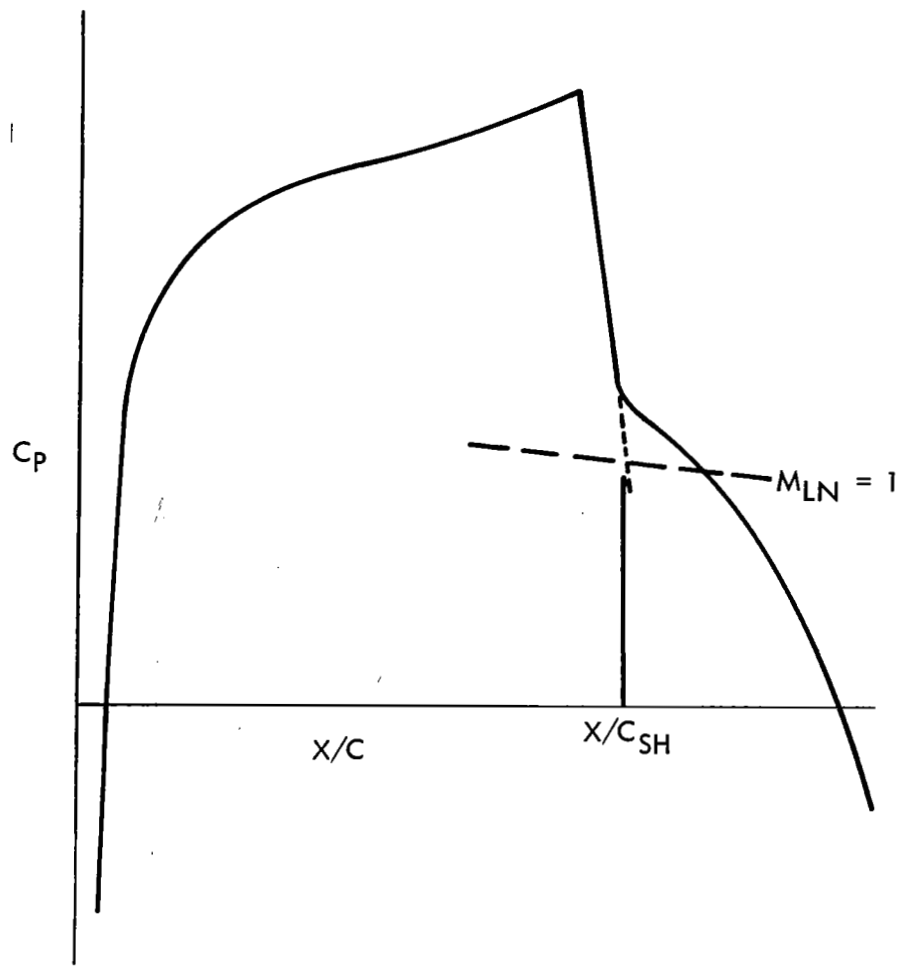

Figure 11. Definition of Shock Location

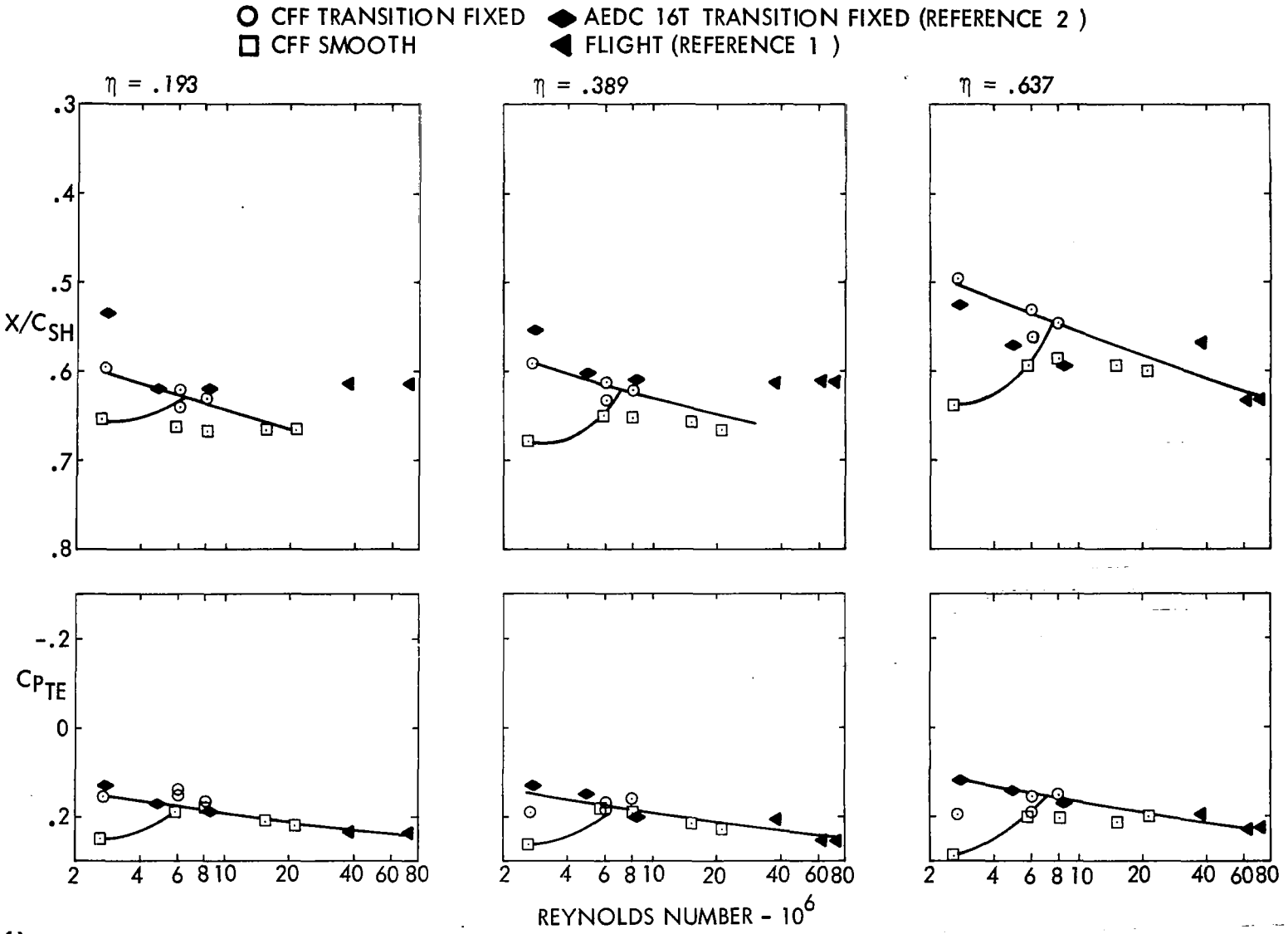

Figure 12. Scale Effect on Shock Location and Trailing Edge Pressure Recovery
M = .80 (a) α_{CFF} = 1°

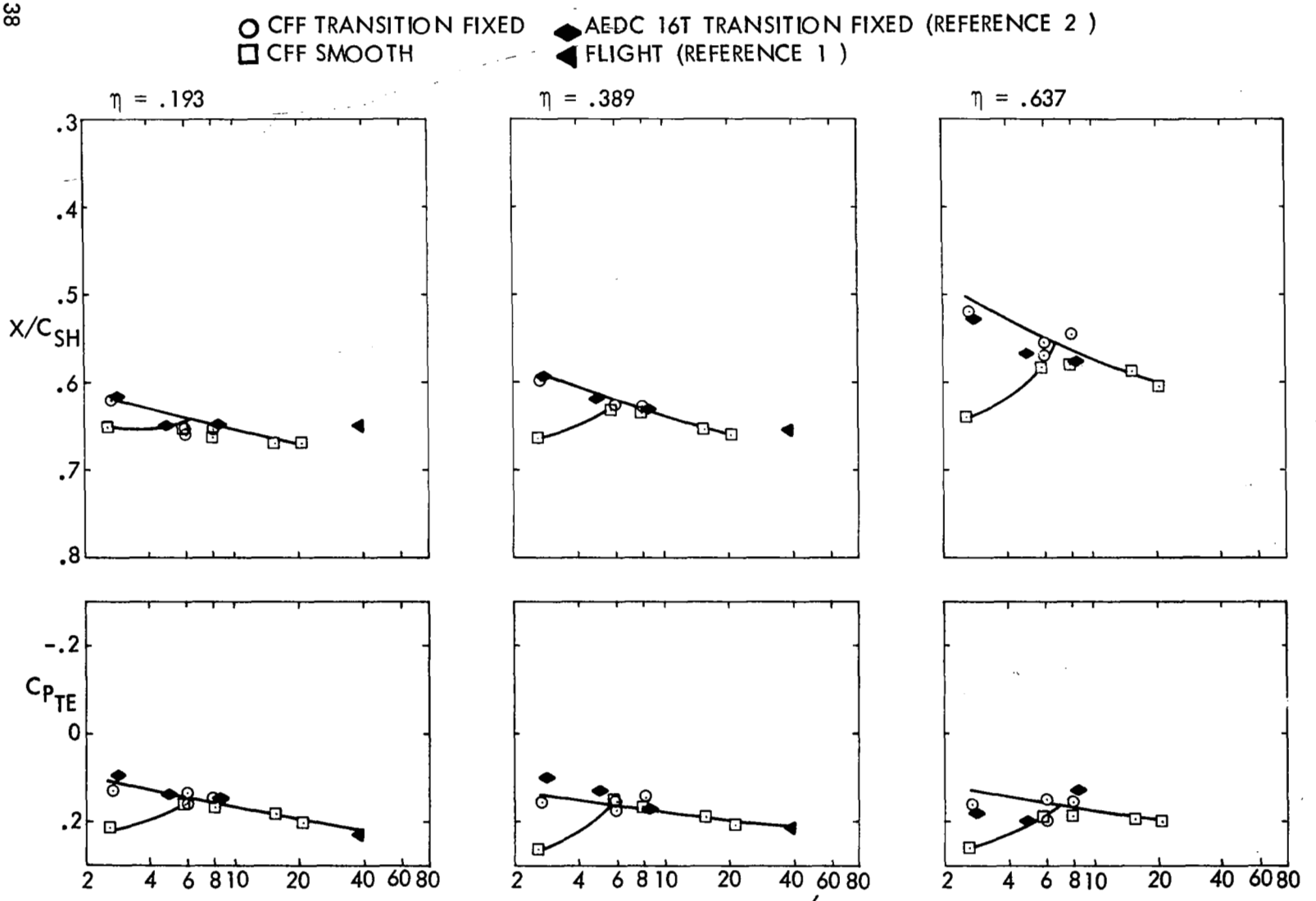

Figure 12 . Continued
(b) $\alpha_{CFF} = 2^{o}$

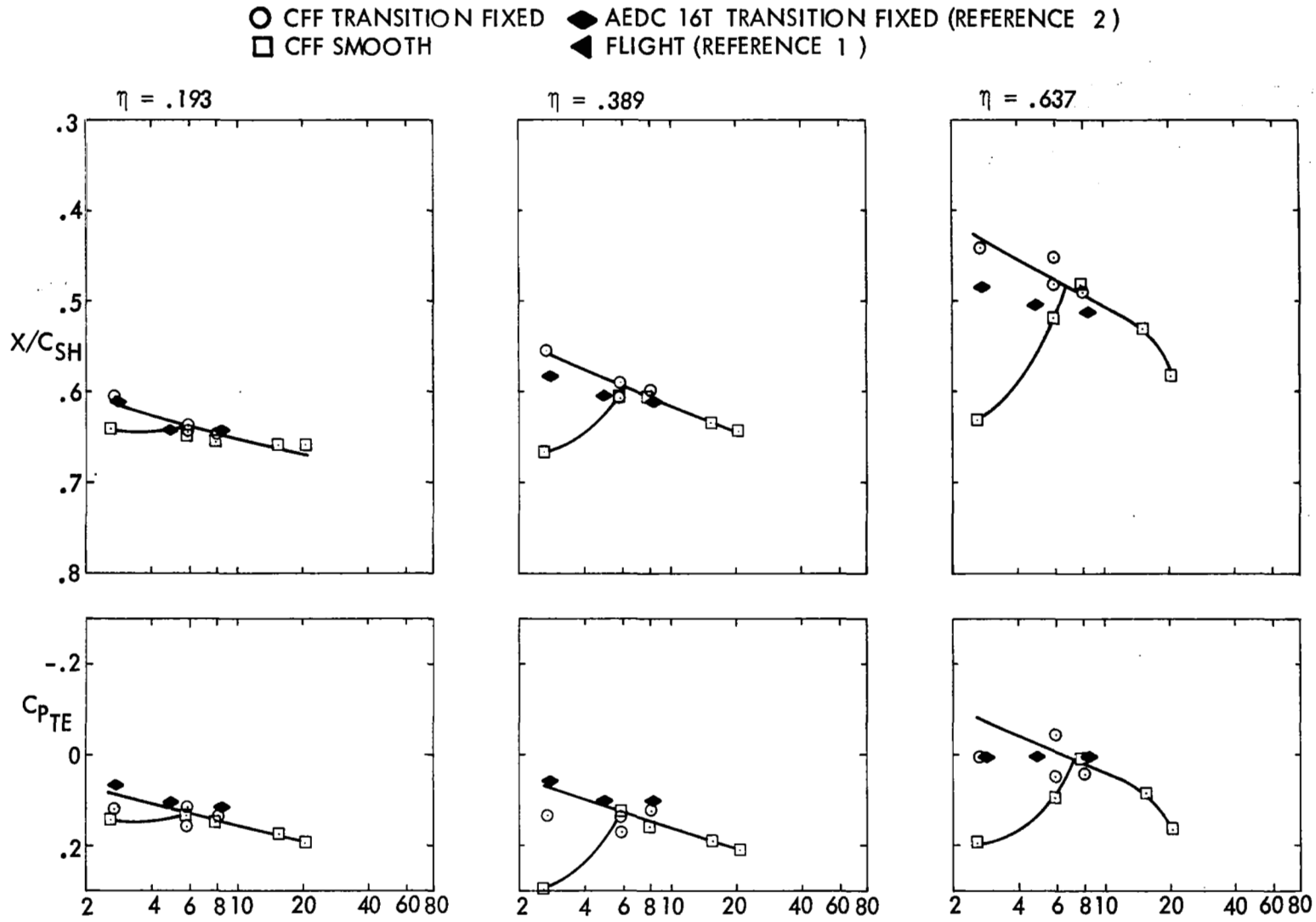

Figure 12. Continued

(c) $\alpha_{CFF} = 3^{o}$

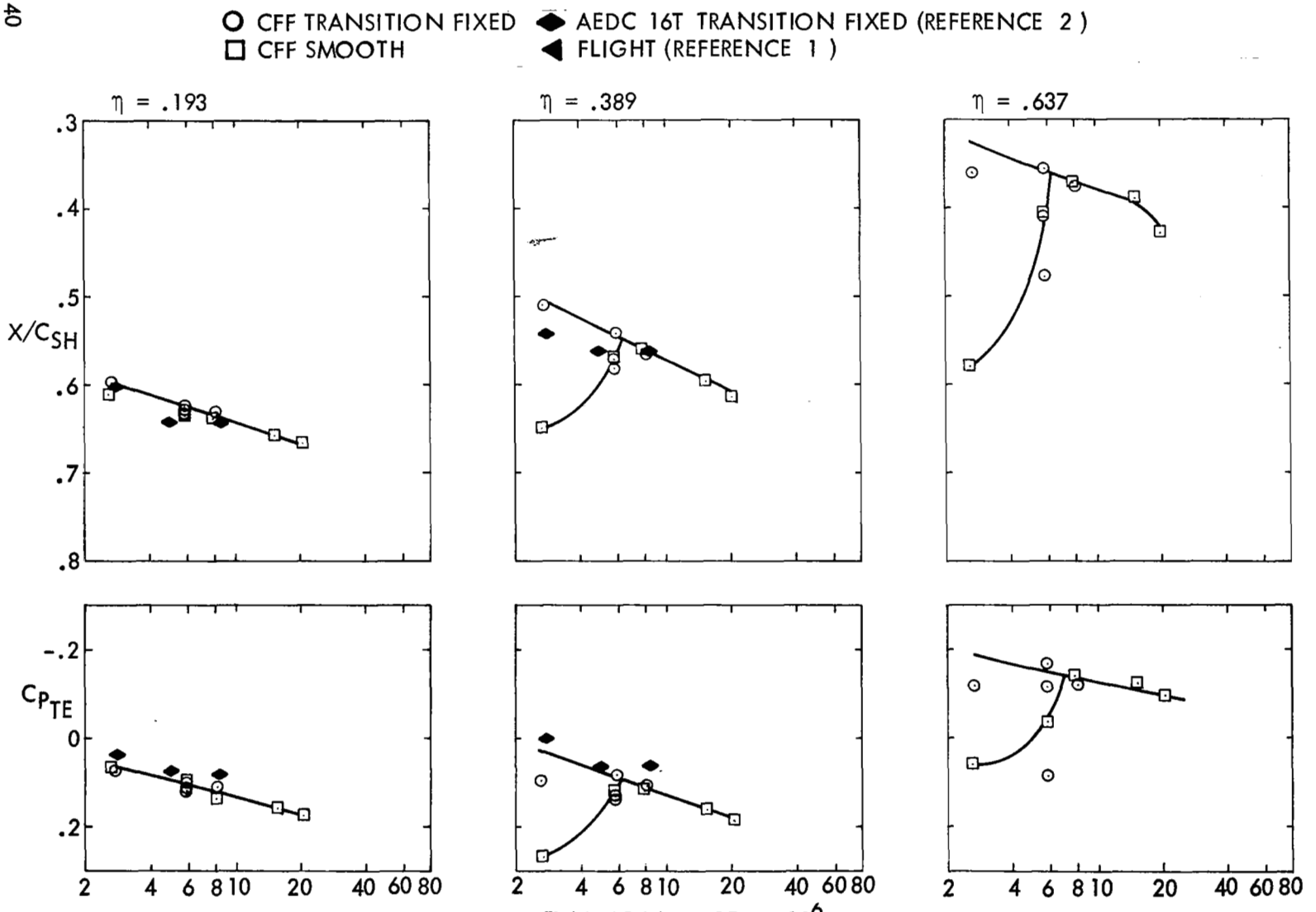

Figure 12. Concluded

(d) $\alpha_{CFF} = 4^{o}$

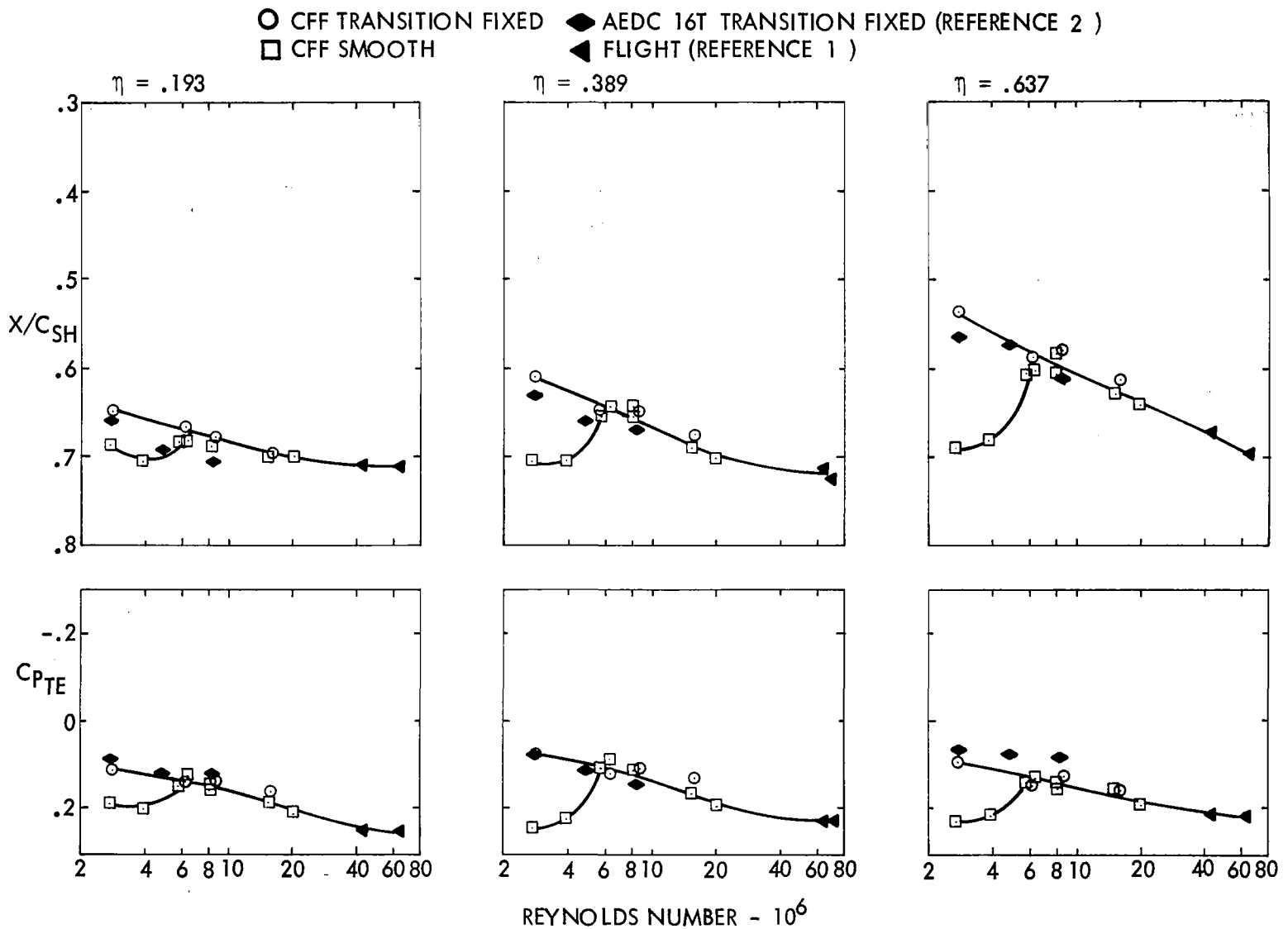

Figure 13. Scale Effect on Shock Location and Trailing Edge Pressure Recovery
M = .825 (a) α_{CFF} = 1°

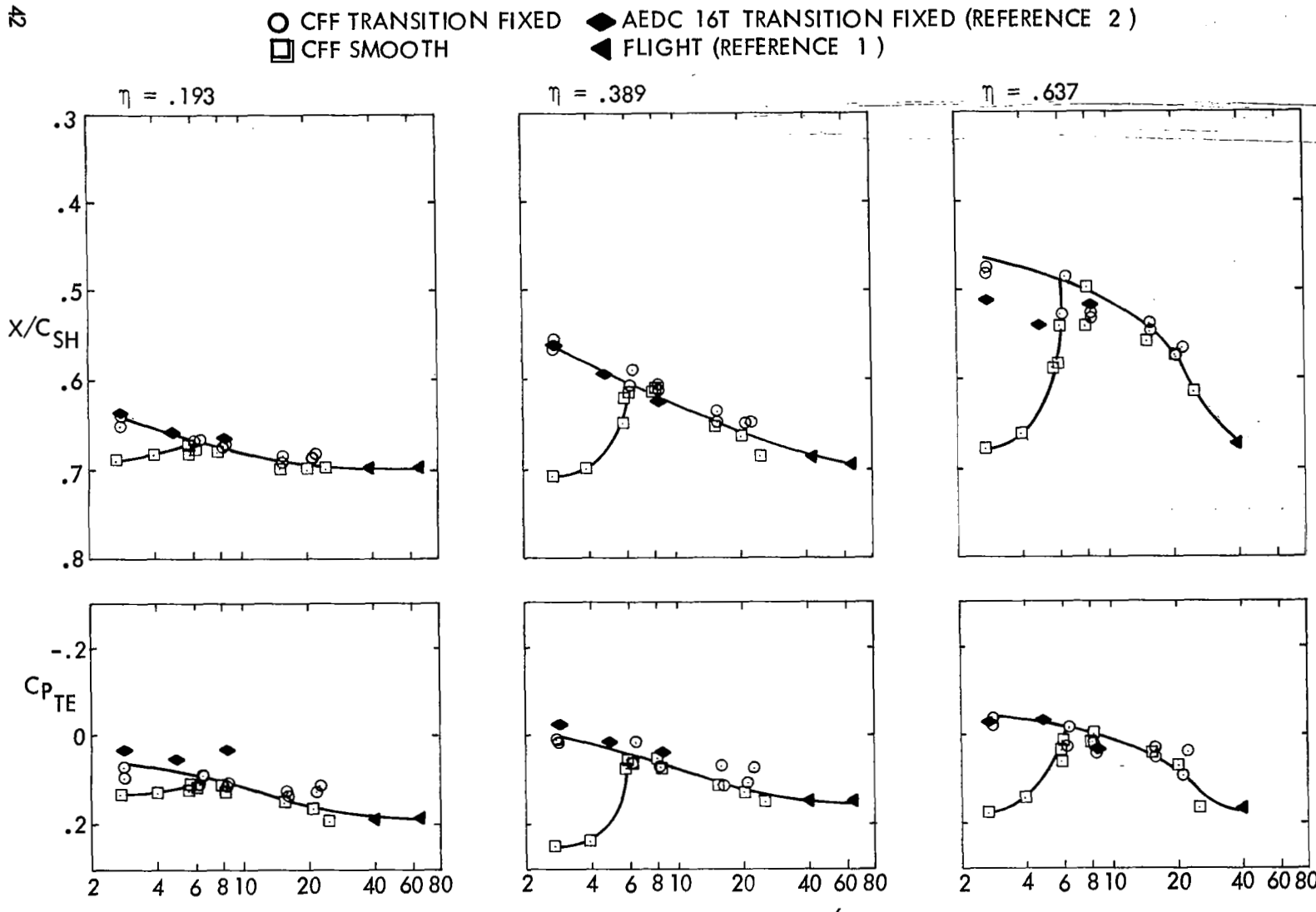

Figure 13. Continued
(b) $\alpha_{CFF} = 2^{o}$

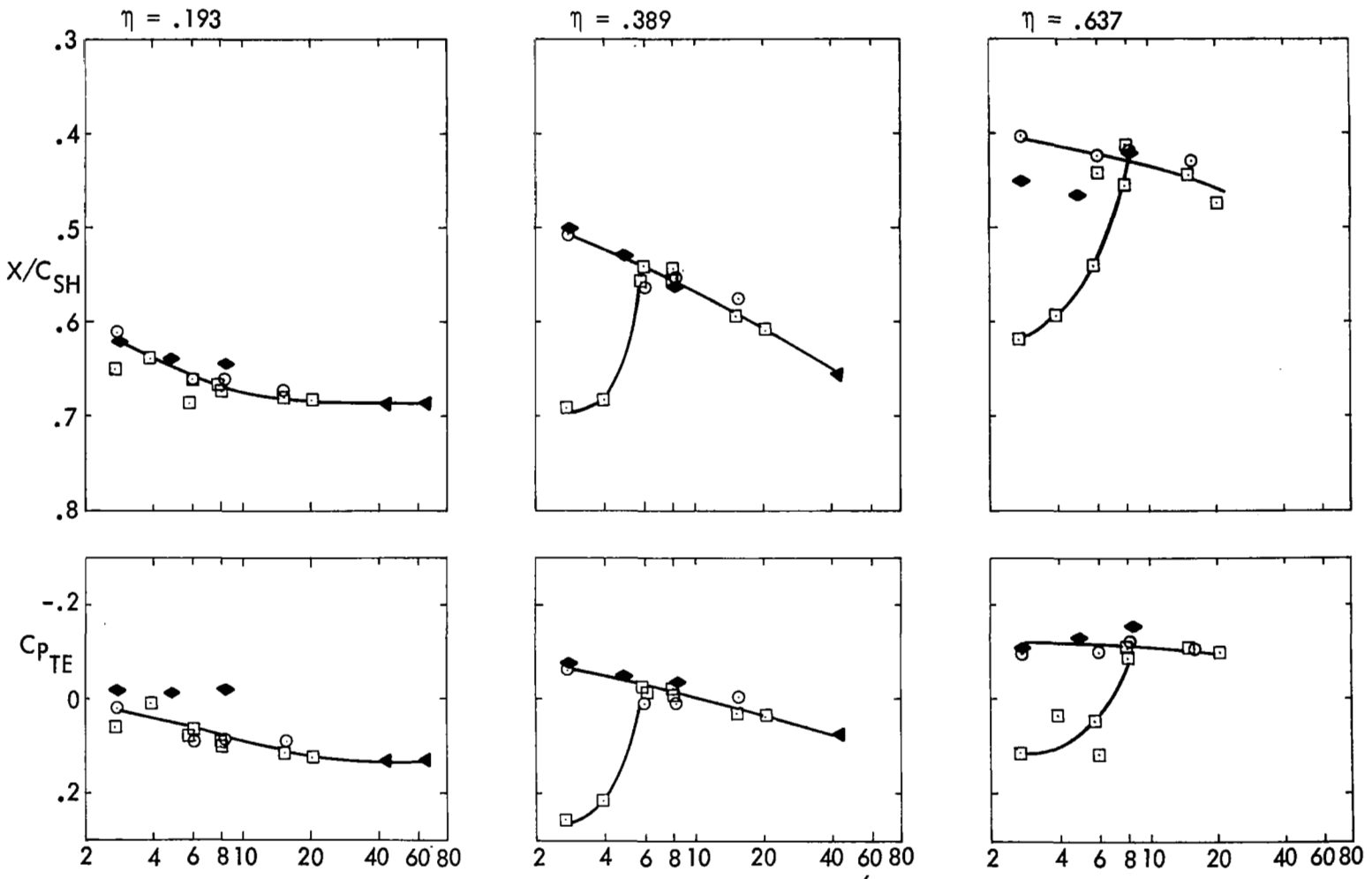

Figure 13. Continued

(c) $\alpha_{CFF} = 3^{o}$

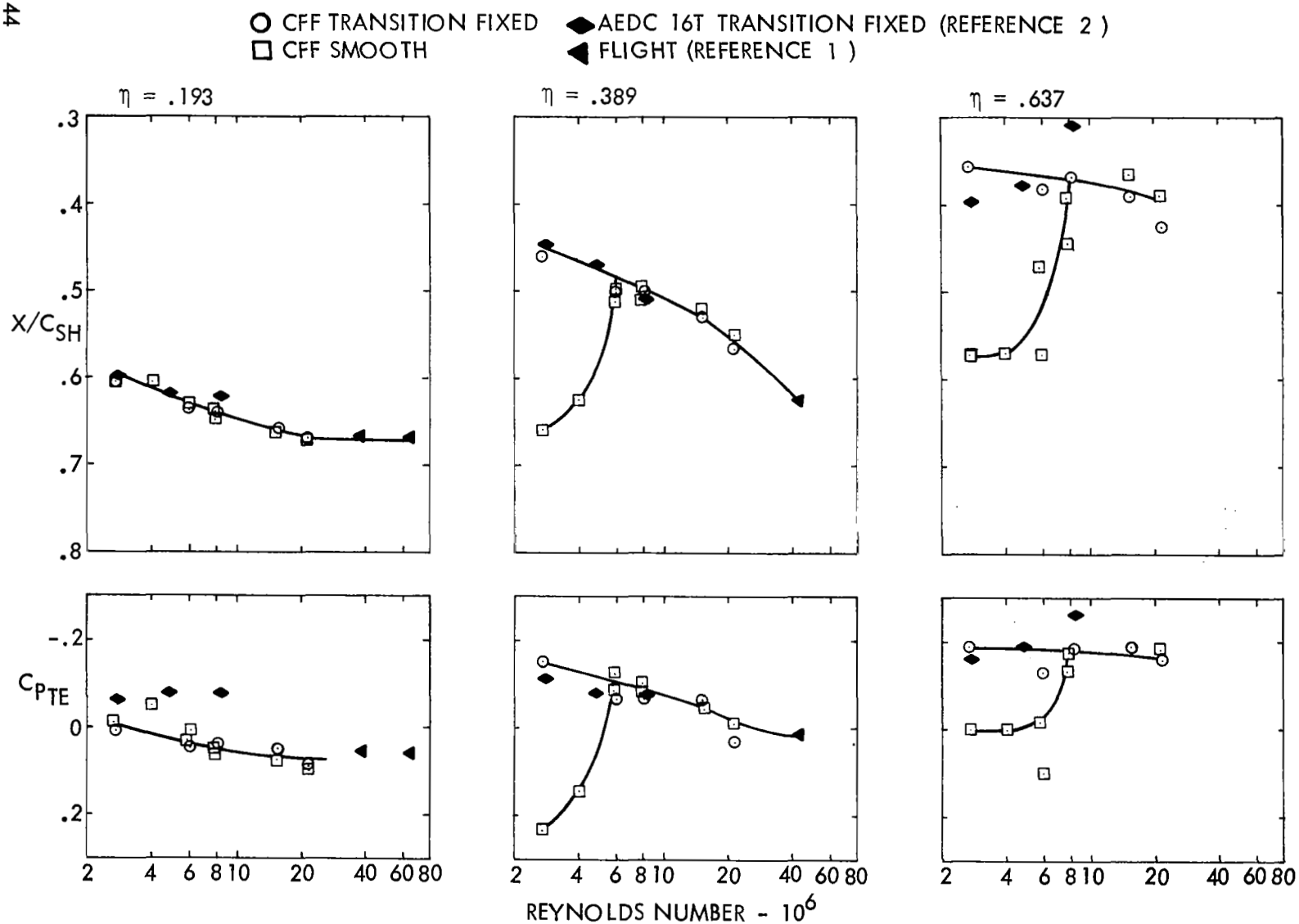

Figure 13. Concluded

(d) $\alpha_{CFF} = 4^{o}$

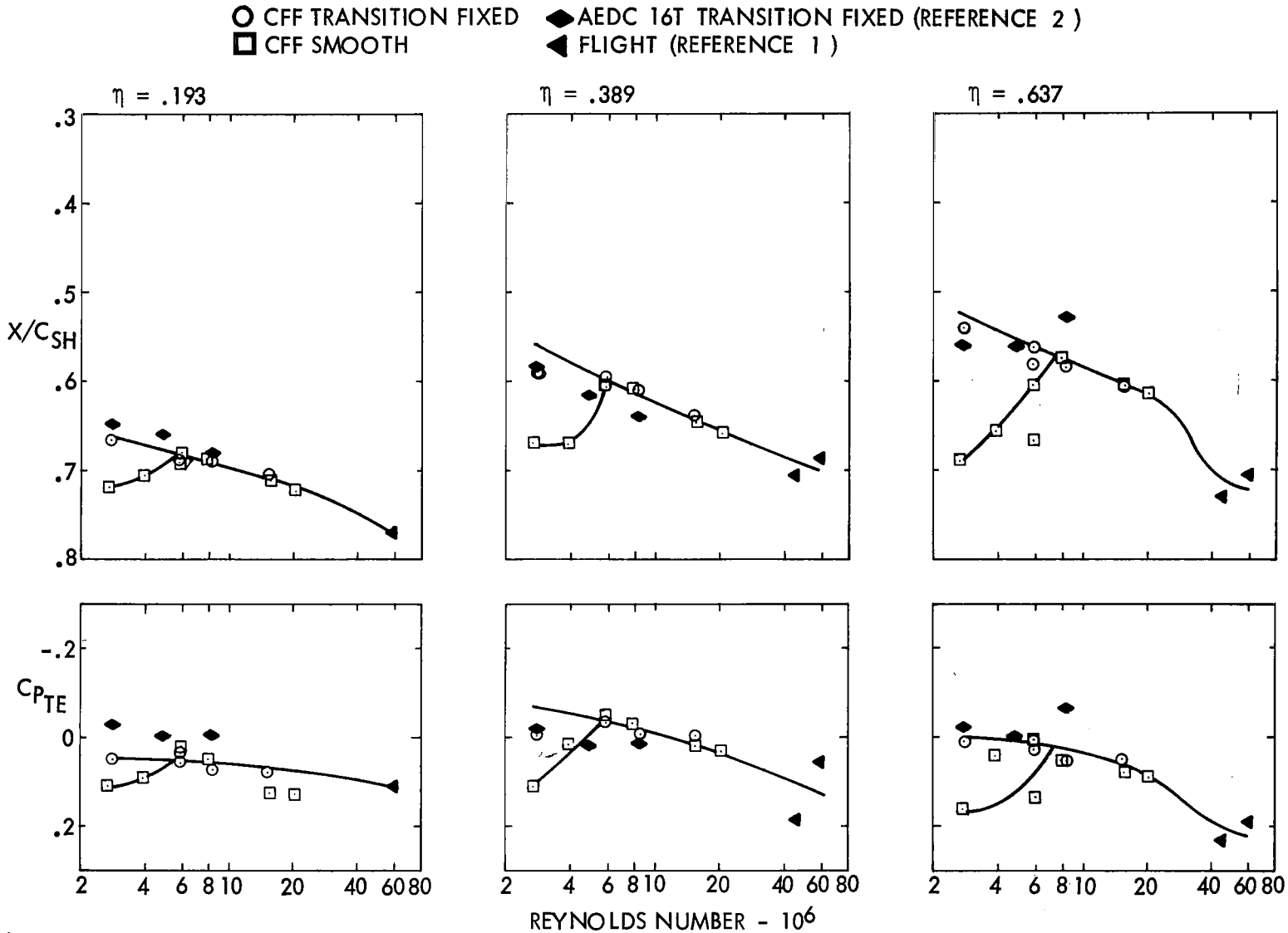

Figure 14 . Scale Effect on Shock Location and Trailing Edge Pressure Recovery
$M = .85$ (a) $\alpha_{CFF} = 1^{o}$

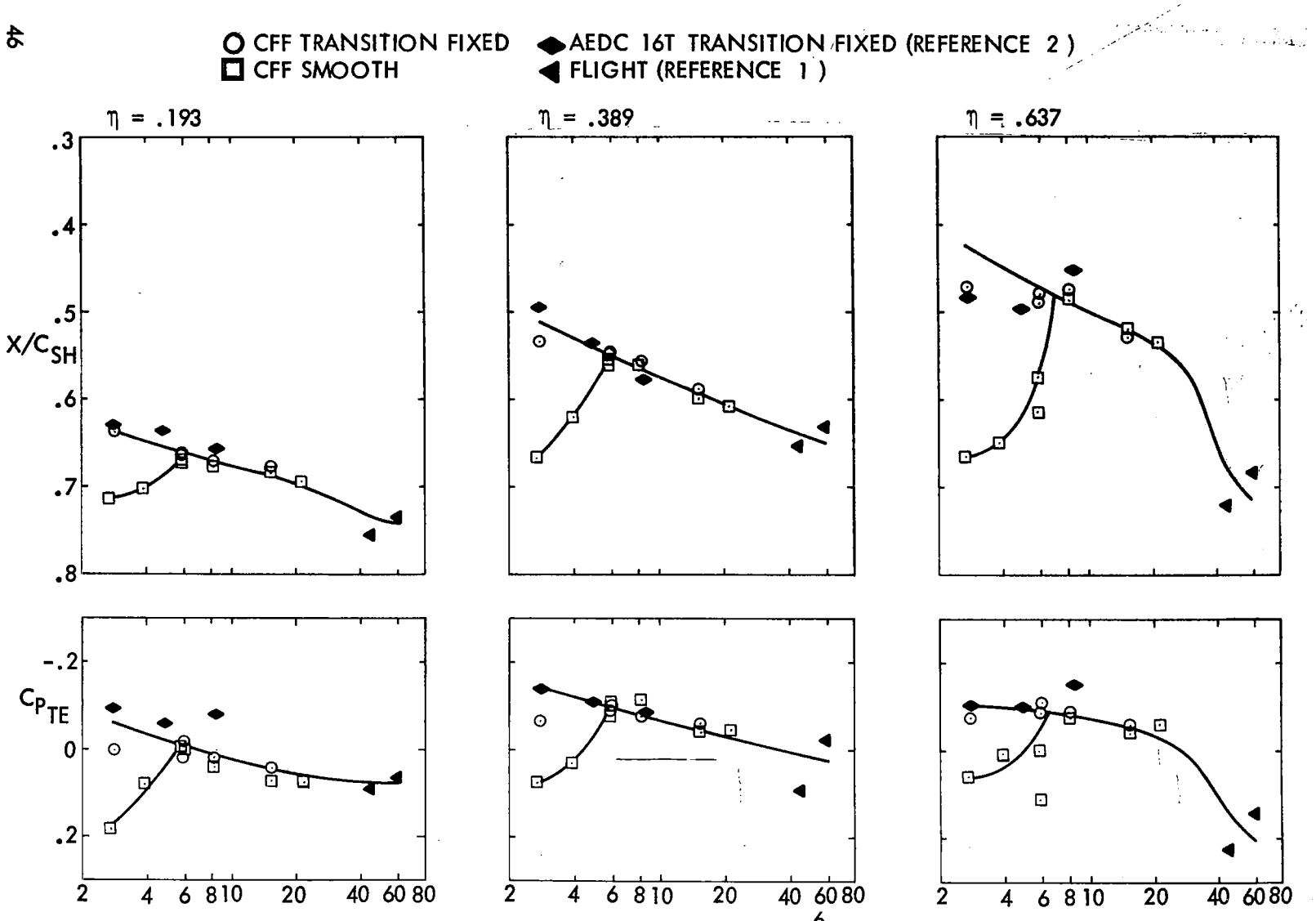

Figure 14. Continued

(b) $\alpha_{CFF} = 2^{o}$

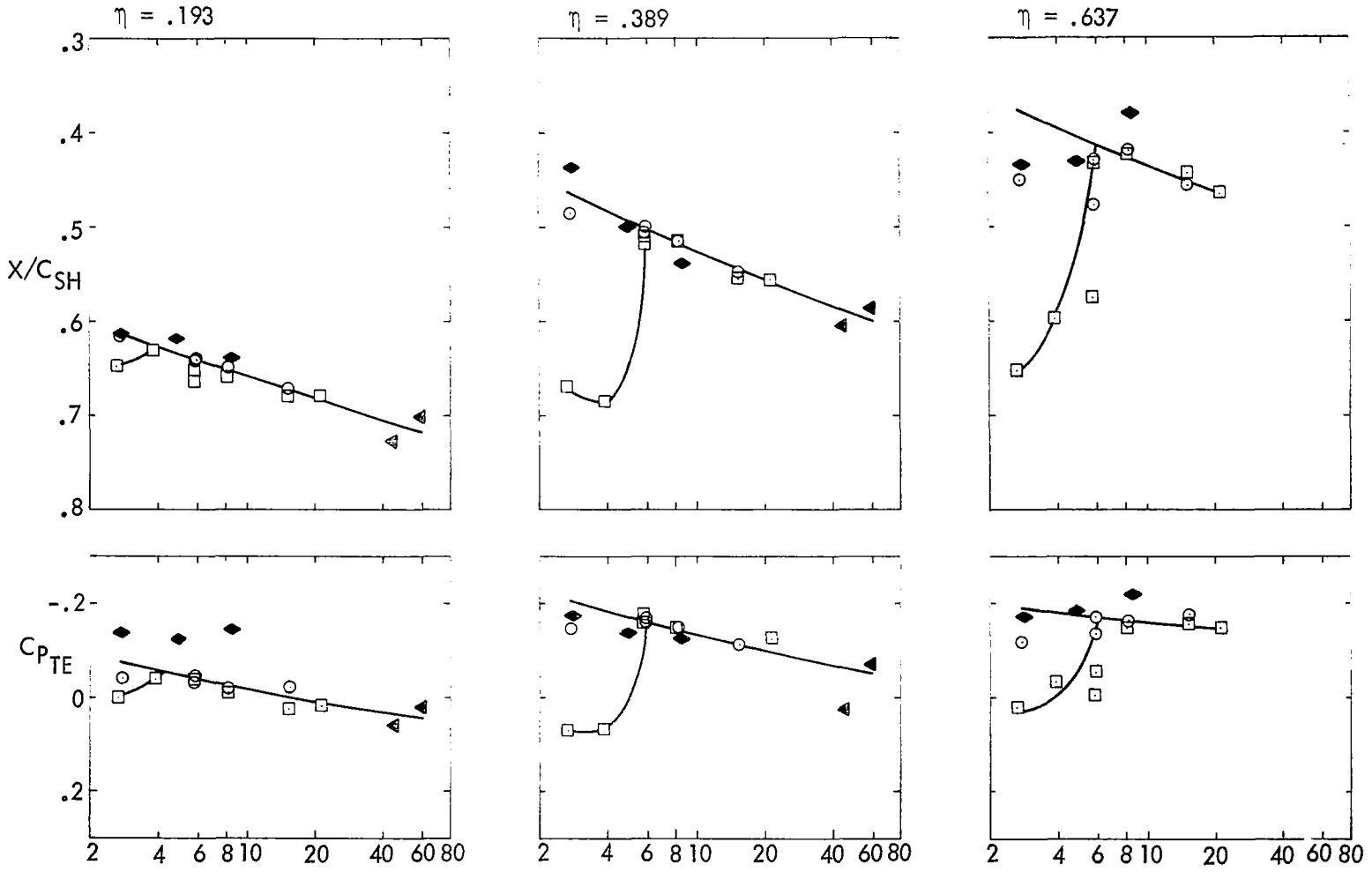

Figure 14. Continued

(c) $\alpha_{CFF} = 3^{o}$

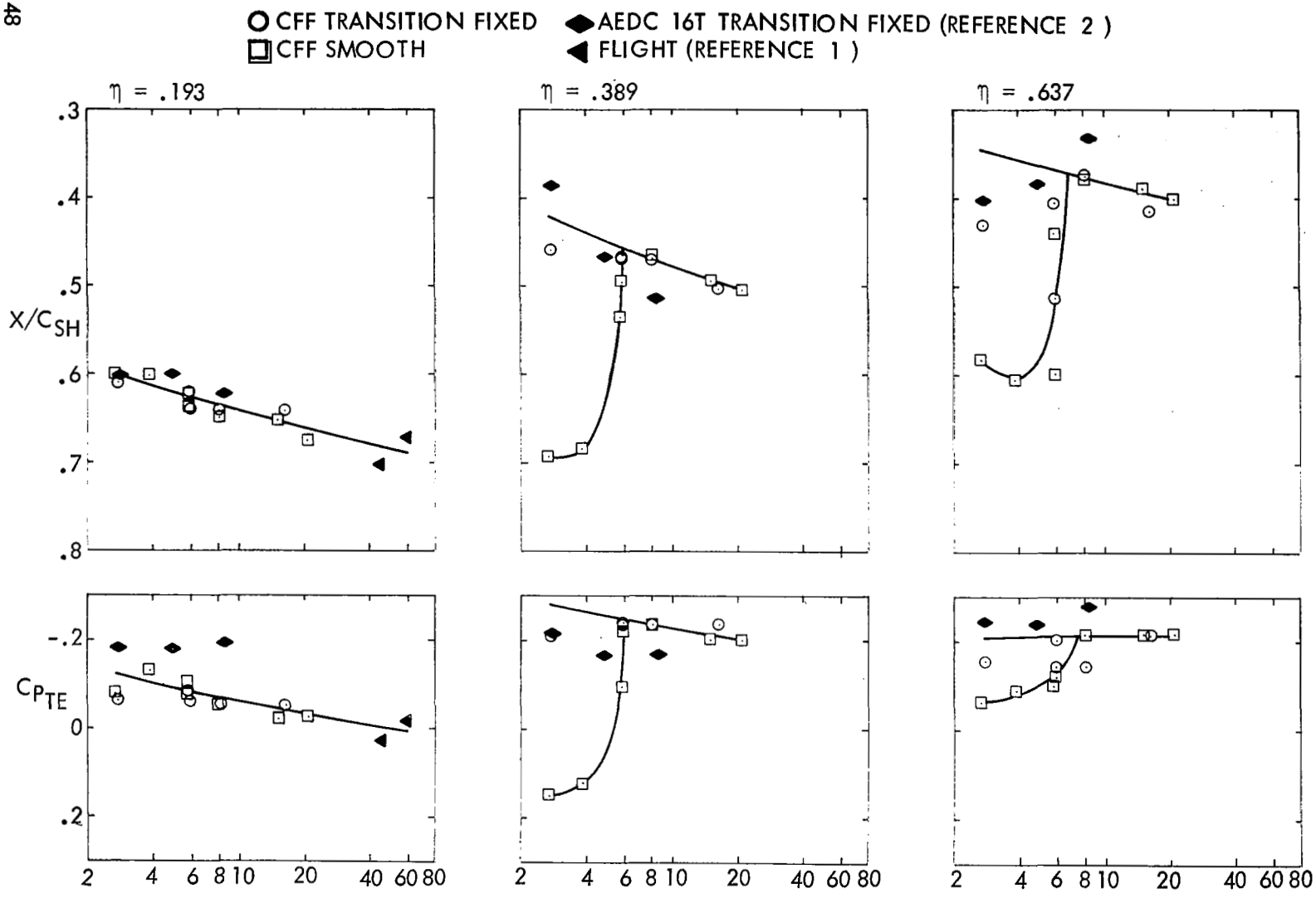

REYNOLDS NUMBER - 10^6

Figure 14 . Concluded

(d) $\alpha_{CFF} = 4^o$

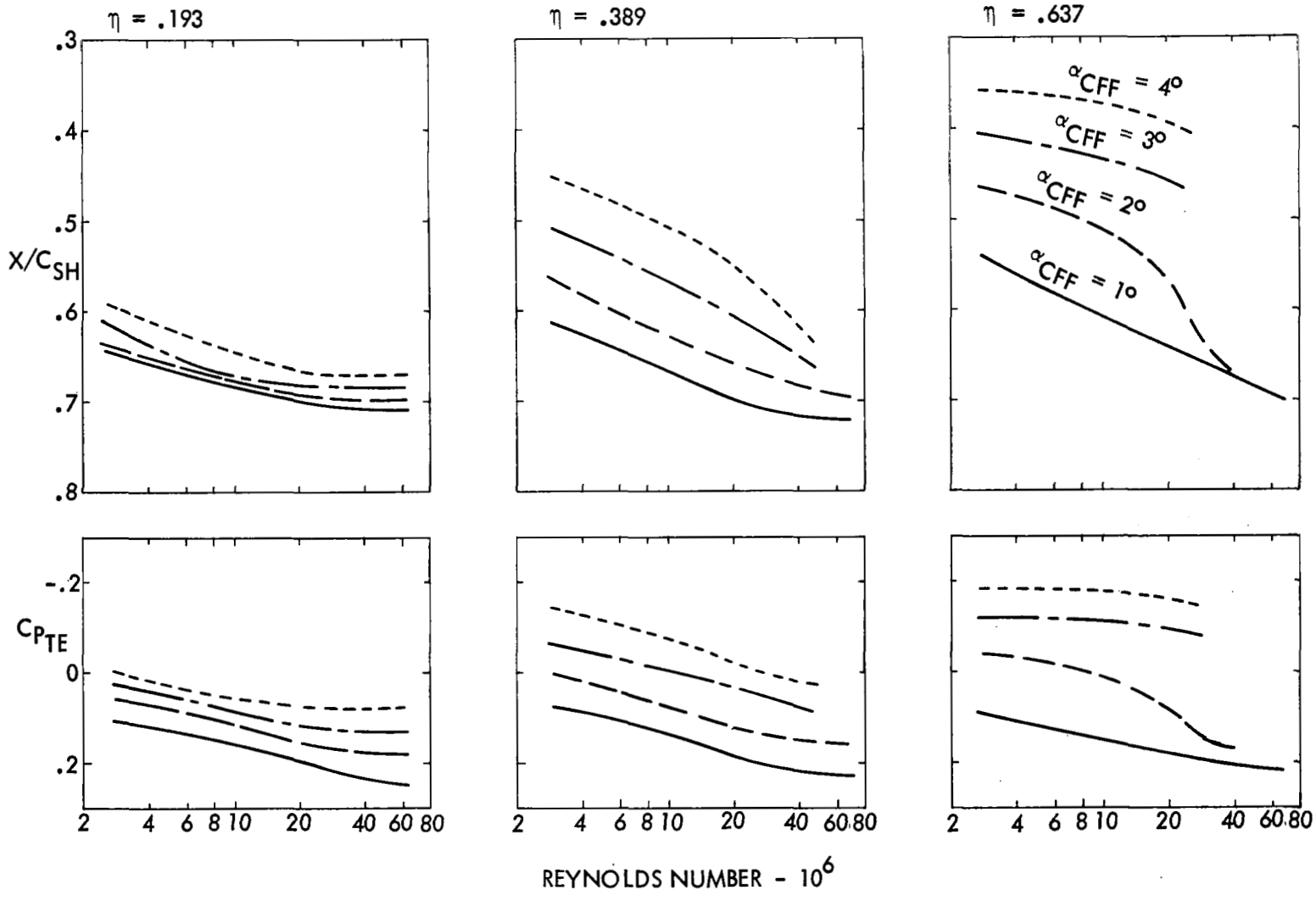

Figure 15. Composite Summary of Flight and Wind Tunnel Scale Effects at M = 0.825

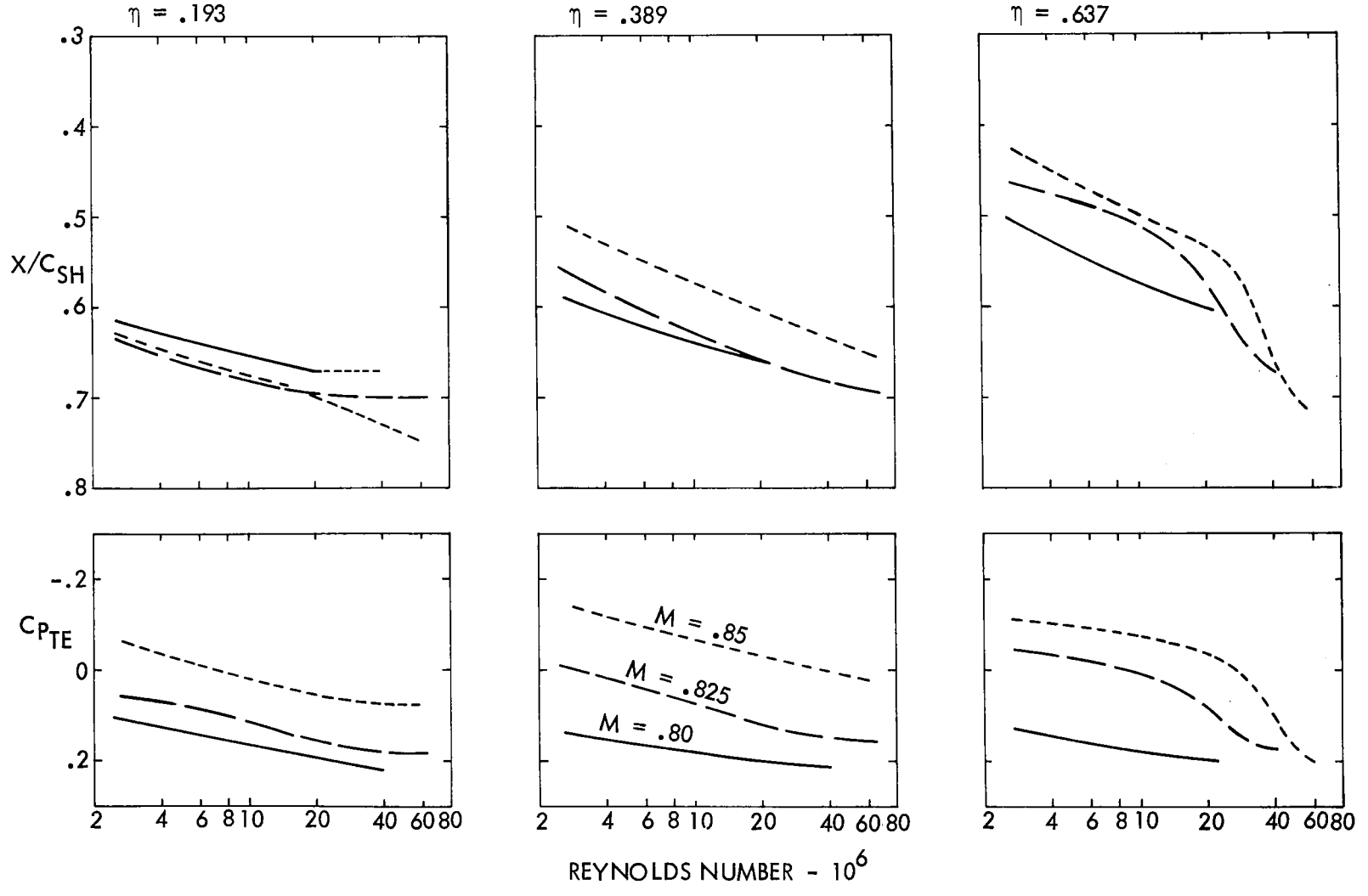

Figure 16. Composite Summary of Flight and Wind Tunnel Scale Effects at 2° Angle of Attack

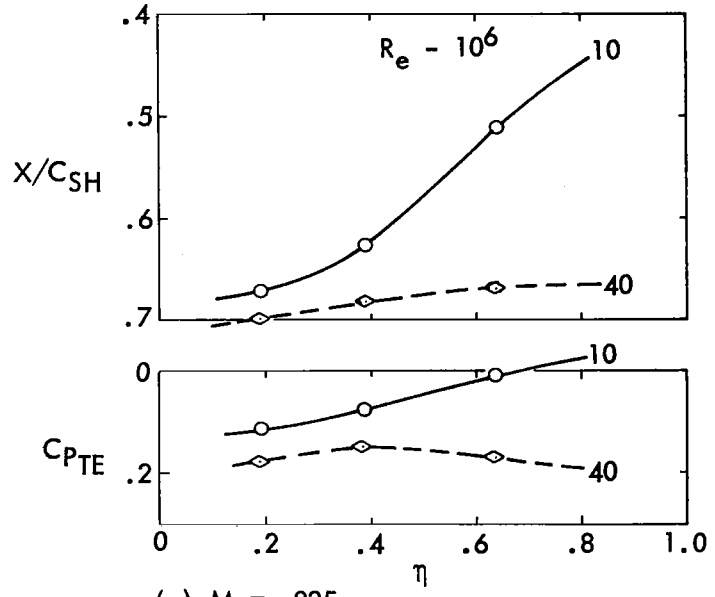

(a) M = .825

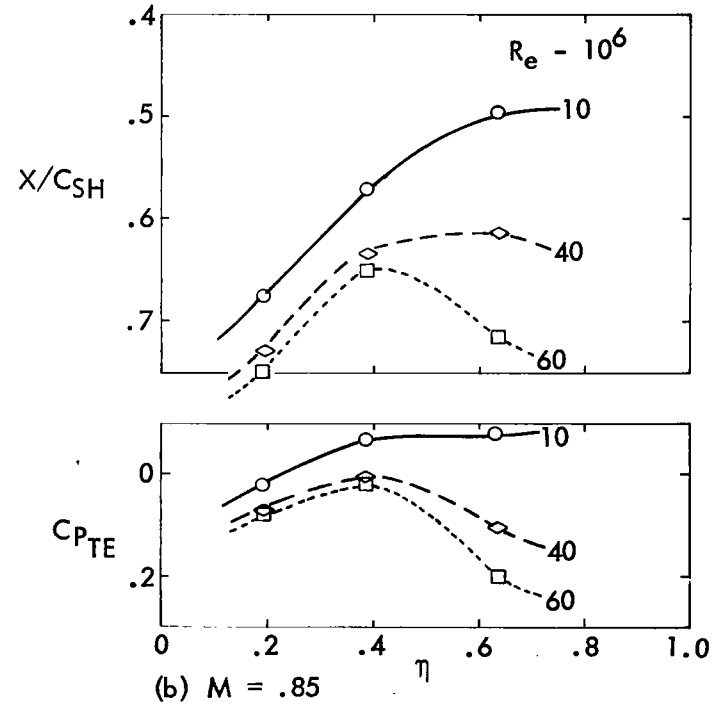

(b) M = .85

Figure 17. Spanwise Variation in Trailing-Edge Pressure Recovery and Shock Location for Low and High Reynolds Numbers, $\alpha_{CFF} = 2^{o}$ at Each η

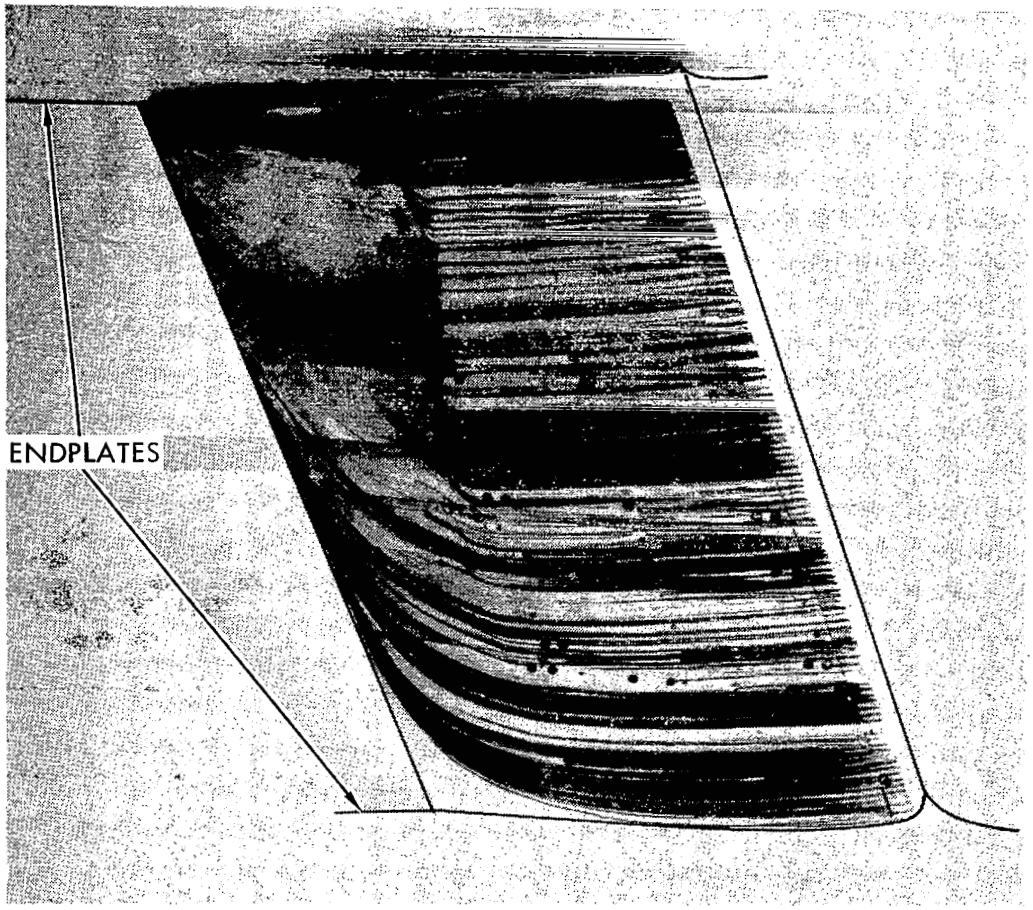

Figure 18. Flow Pattern on C-141 Panel Model

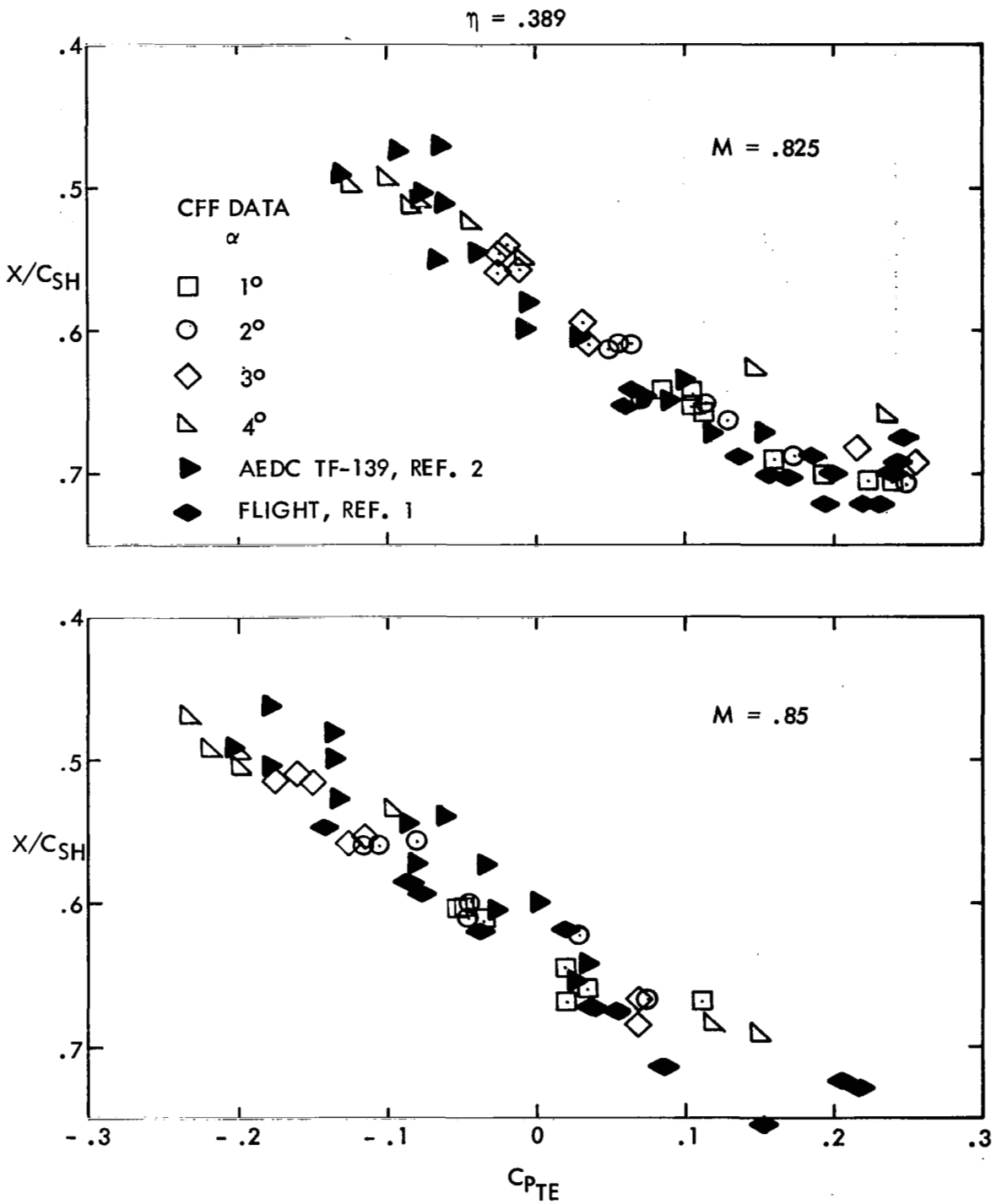

Figure 19. Correlation of T. E. Separation and Shock Location

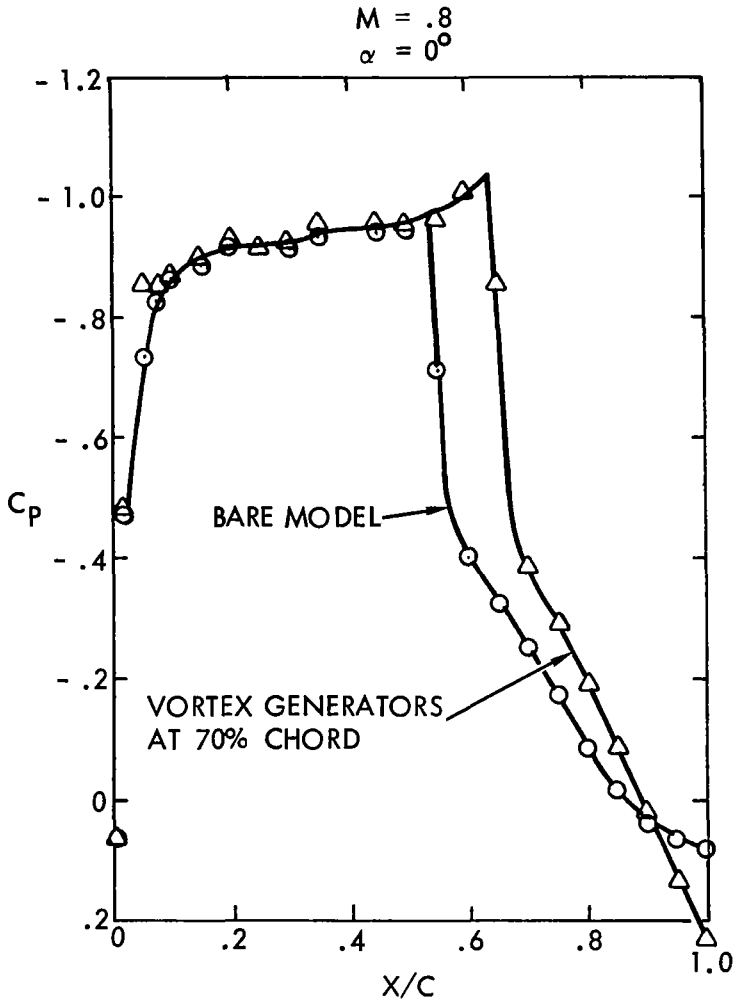

(a) EFFECT OF VORTEX GENERATORS BEHIND SHOCK, REFERENCE 2

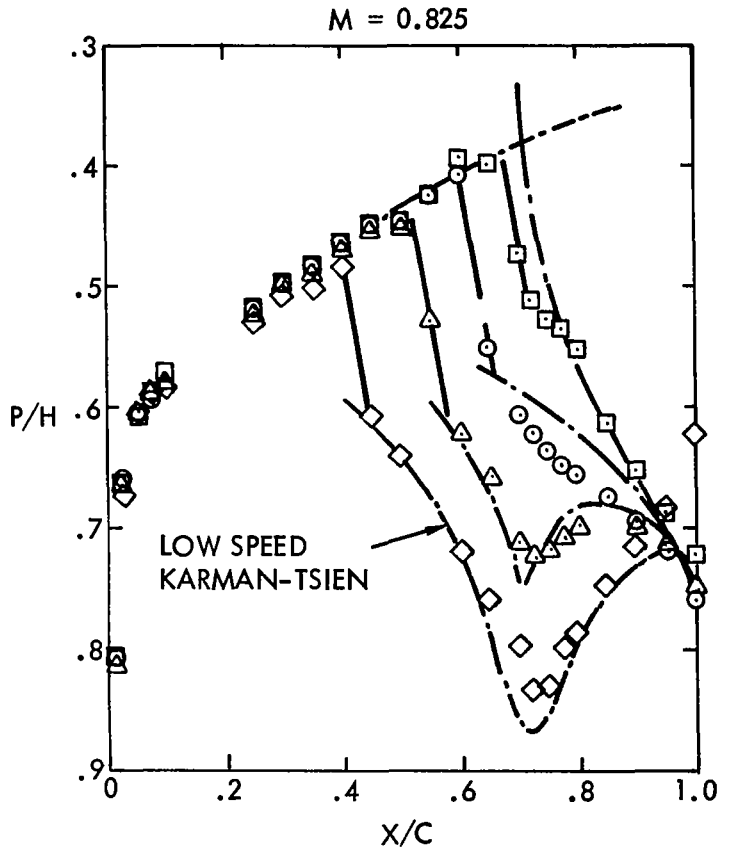

(b) EFFECT OF AILERON DEFLECTION ON SHOCK LOCATION, REFERENCE 11

Figure 20. Downstream Pressure Controls Shock Location

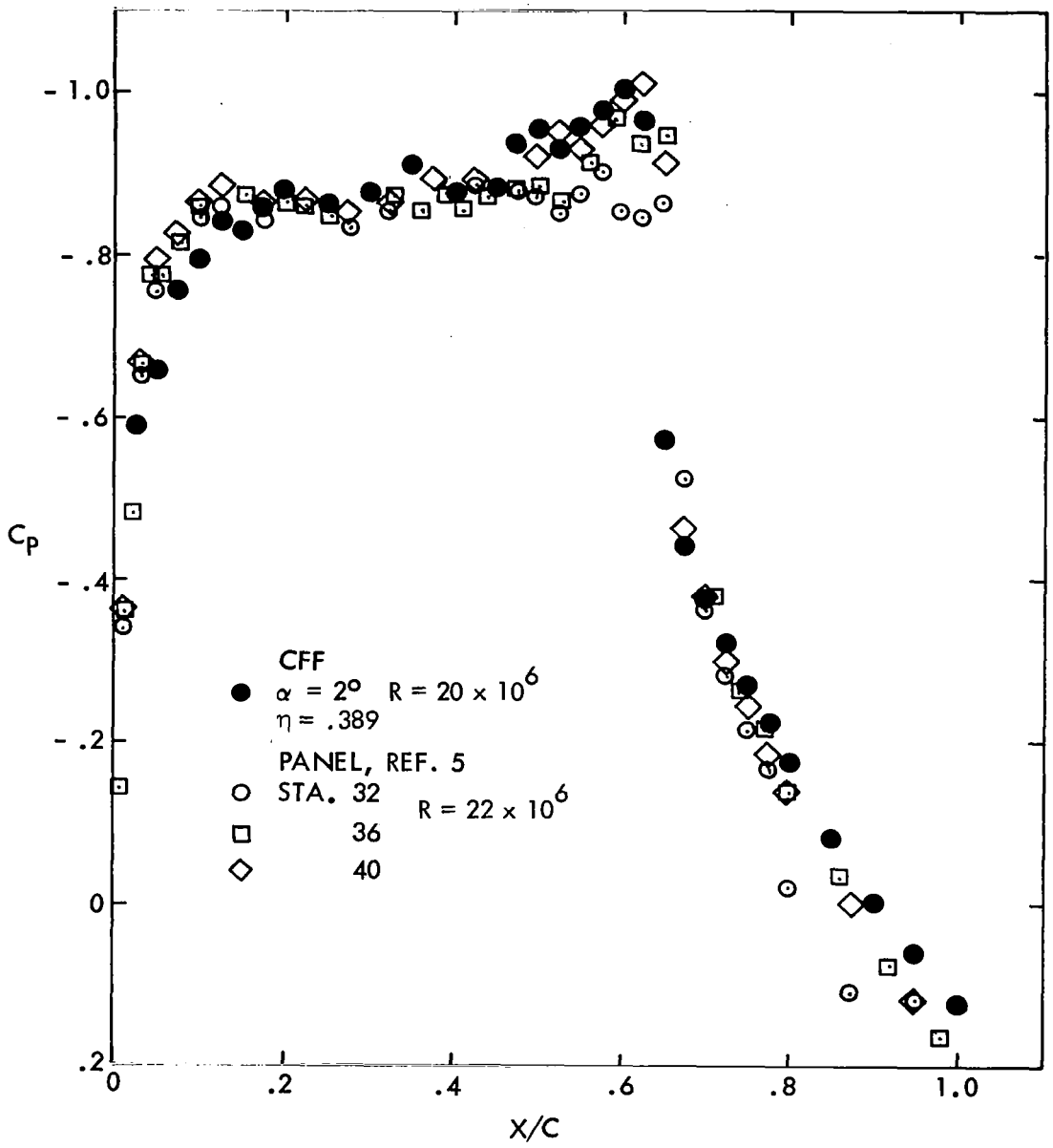

Figure 21. Comparison with Panel Model, M = .825

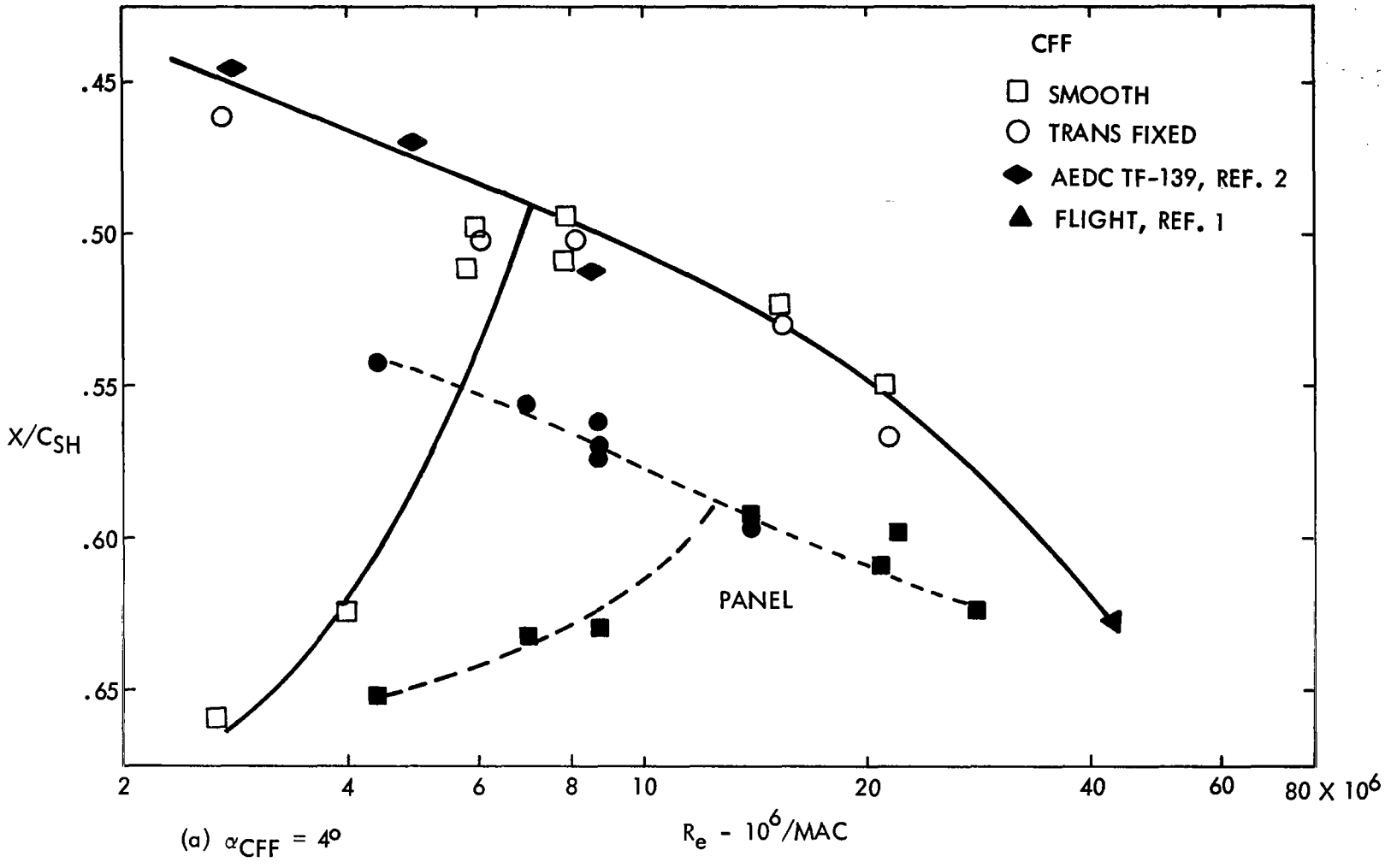

Figure 22. Scale Effect Comparison, M = .825

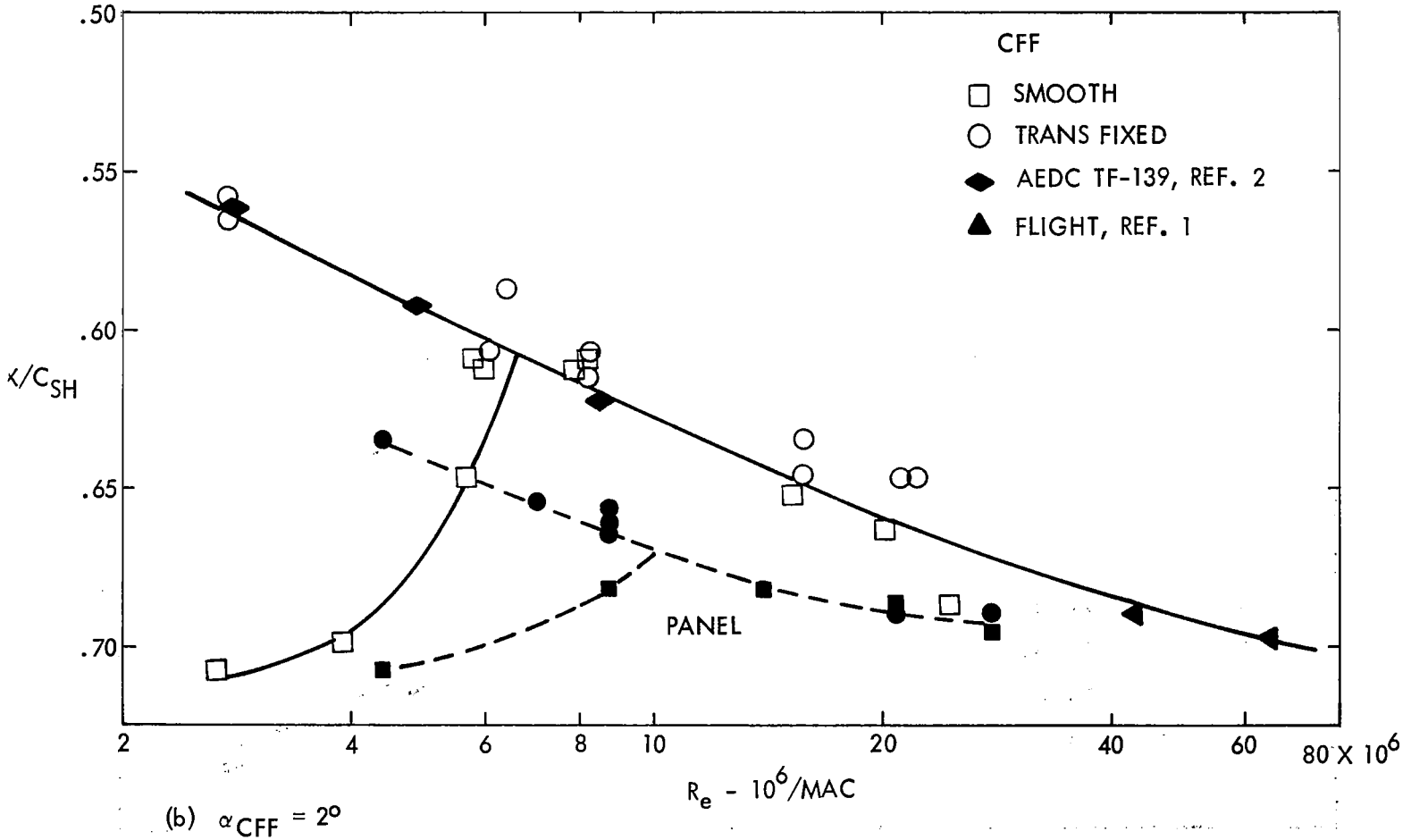

Figure 22. Concluded

APPENDIX A

MACHINE-PLOTTED PRESSURE DISTRIBUTION DATA

The plotting sequence follows the program summary of table 2 in the body of this report. In general, each figure contains plots for the angle-of-attack variation at a spanwise station for each measured condition. Data for all three spanwise stations are plotted in sequence, and the figures are numbered consecutively. A summary of figure numbers is given in table 1A.

TABLE 1A. FIGURE INDEX FOR PLOTTED DATA

FREE TRANSITION

MACH NO.	α	R_e X 10^{-6} ON MAC	SPAN STATION .193	.389	.637
			Fig.	Fig.	Fig.
.75	1°-4°	2.7	1A	2A	3A
.75	0°-4°	6.0	4A	5A	6A
.75	1°-4°	8.2	7A	8A	9A
.75	1°-4°	15.0	10A	11A	12A
.75	1°-4°	20.0	13A	14A	15A
.80	1°-4°	2.7	16A	17A	18A
.80	0°-4°	6.0	19A	20A	21A
.80	1°-4°	8.2	22A	23A	24A
.80	1°-4°	15.0	25A	26A	27A
.80	1°-4°	20.0	28A	29A	30A
.825	1°-4°	2.7	31A	32A	33A
.825	1°-4°	4.4	34A	35A	36A
.825	1°-4°	6.0	37A	38A	39A
.825	1°-4°	6.0	40A	41A	42A
.825	2°	6.0	43A	44A	45A
.825	1°-4°	8.2	46A	47A	48A
.825	1°-4°	8.2	49A	50A	51A
.825	1°-4°	15.0	52A	53A	54A
.825	1°-4°	20.0	55A	56A	57A
.825	2°	VAR	58A	59A	60A
.85	1°-4°	2.7	61A	62A	63A
.85	1°-4°	4.4	64A	65A	66A
.85	1°-4°	6.0	67A	68A	69A
.85	1°-4°	6.0	70A	71A	72A
.85	1°-4°	8.2	73A	74A	75A
.85	1°-4°	15.0	76A	77A	78A
.85	1°-4°	20	79A	80A	81A

FIXED TRANSITION

MACH NO.	α	R_e X 10^{-6} ON MAC	SPAN STATION .193	.389	.637
			Fig.	Fig.	Fig.
.75	1°-4°	6.0	82A	83A	84A
.75	1°-4°	8.2	85A	86A	87A
.8	1°-4°	2.7	88A	89A	90A
.8	1°-4°	6.0	91A	92A	93A
.8	1°-4°	6.0	94A	95A	96A
.8	1°-4°	8.2	97A	98A	99A
.825	1°-4°	2.7	100A	101A	102A
.825	1°-4°	6.0	103A	104A	105A
.825	1°-4°	8.2	106A	107A	108A
.825	1°-4°	15.0	109A	110A	111A
.825	$2^\circ, 4^\circ$	20.0	112A	113A	114A
.825	2°	VAR	115A	116A	117A
.85	1°-4°	2.7	118A	119A	120A
.85	1°-4°	6.0	121A	122A	123A
.85	1°-4°	6.0	124A	125A	126A
.85	1°-4°	8.2	127A	128A	129A
.85	1°-4°	15.0	130A	131A	132A

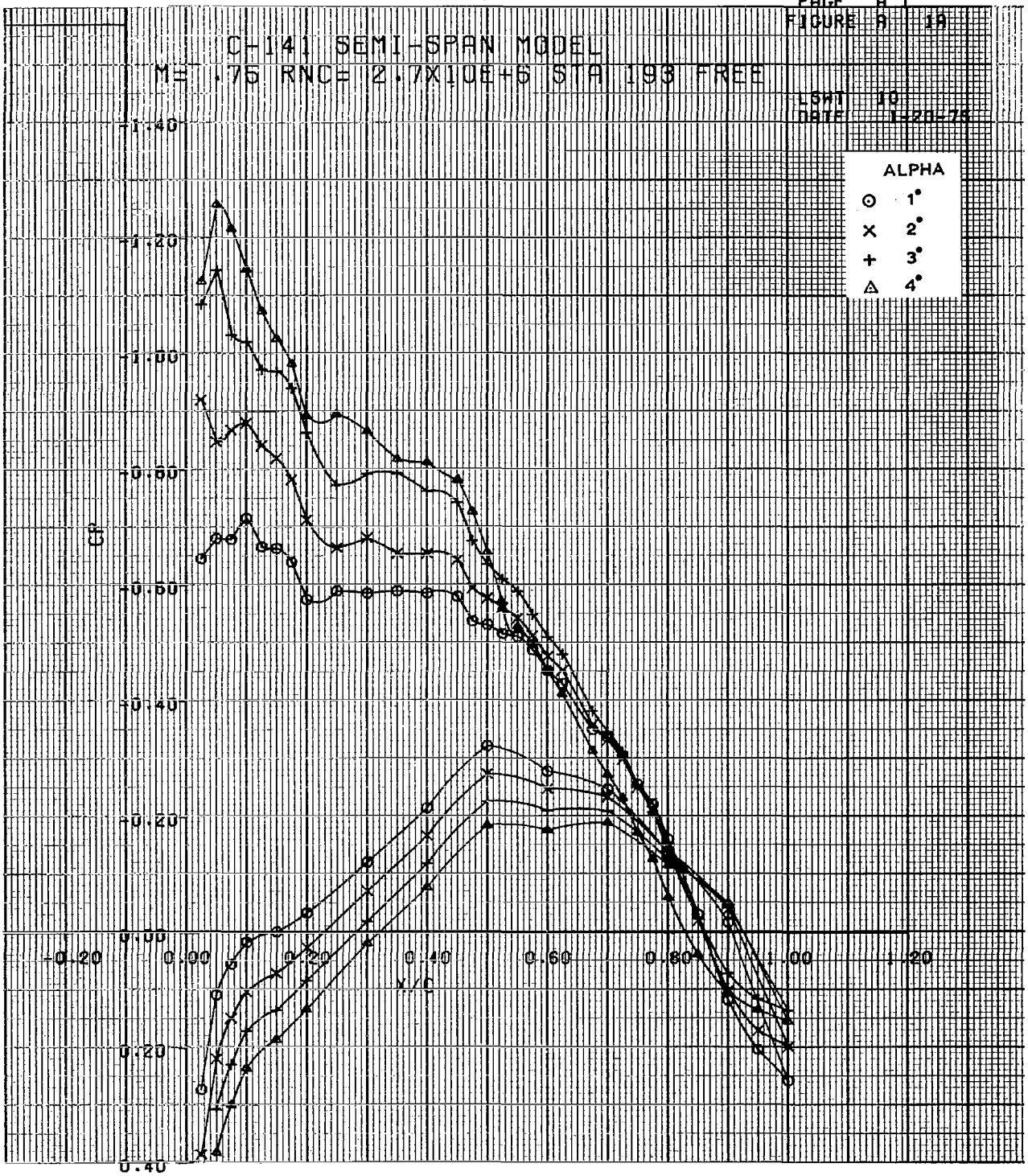
C-141 SEMI-SPAN MODEL
M= .75 RNC= 2.7X10E+6 STA 193 FREE
LSHT 19
DATE 1-20-78
ALPHA
1°
2°
3°
4°
-1.40
-1.20
-1.00
-0.80
-0.60
-0.40
-0.20
0.00
0.20
0.40
CP
-0.20
0.00
0.20
0.40
0.60
0.80
1.00
1.20
X/C

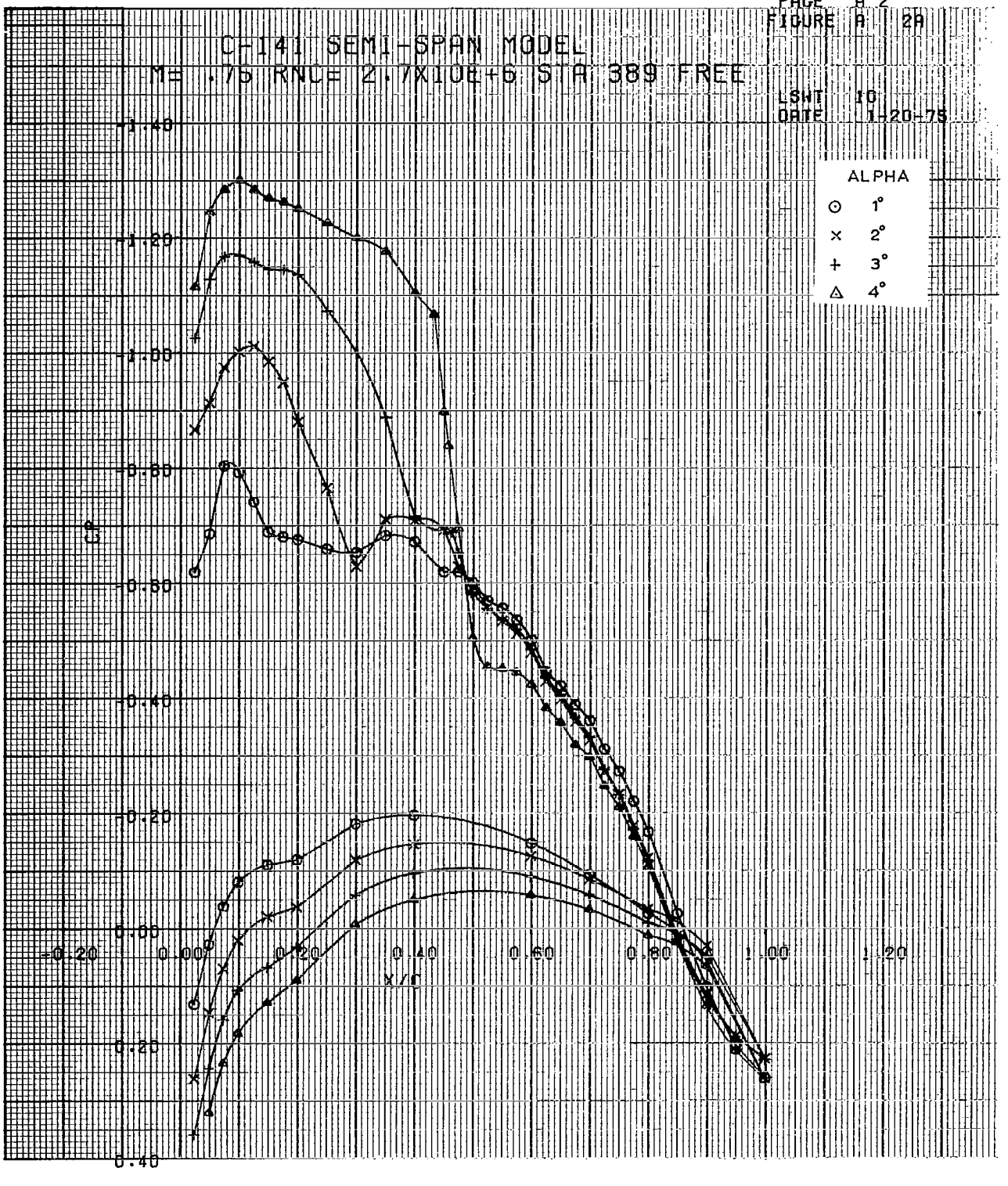
C-141 SEMI-SPAN MODEL
M= .75 RNLC= 2.7X10E+6 STA 389 FREE
LSWT 10
DATE 1-20-75
ALPHA
1°
2°
3°
4°
-1.40
-1.20
-1.00
-0.80
-0.60
-0.40
-0.20
0.00
0.20
0.40
-0.20
0.00
0.20
0.40
0.60
0.80
1.00
1.20
X/C

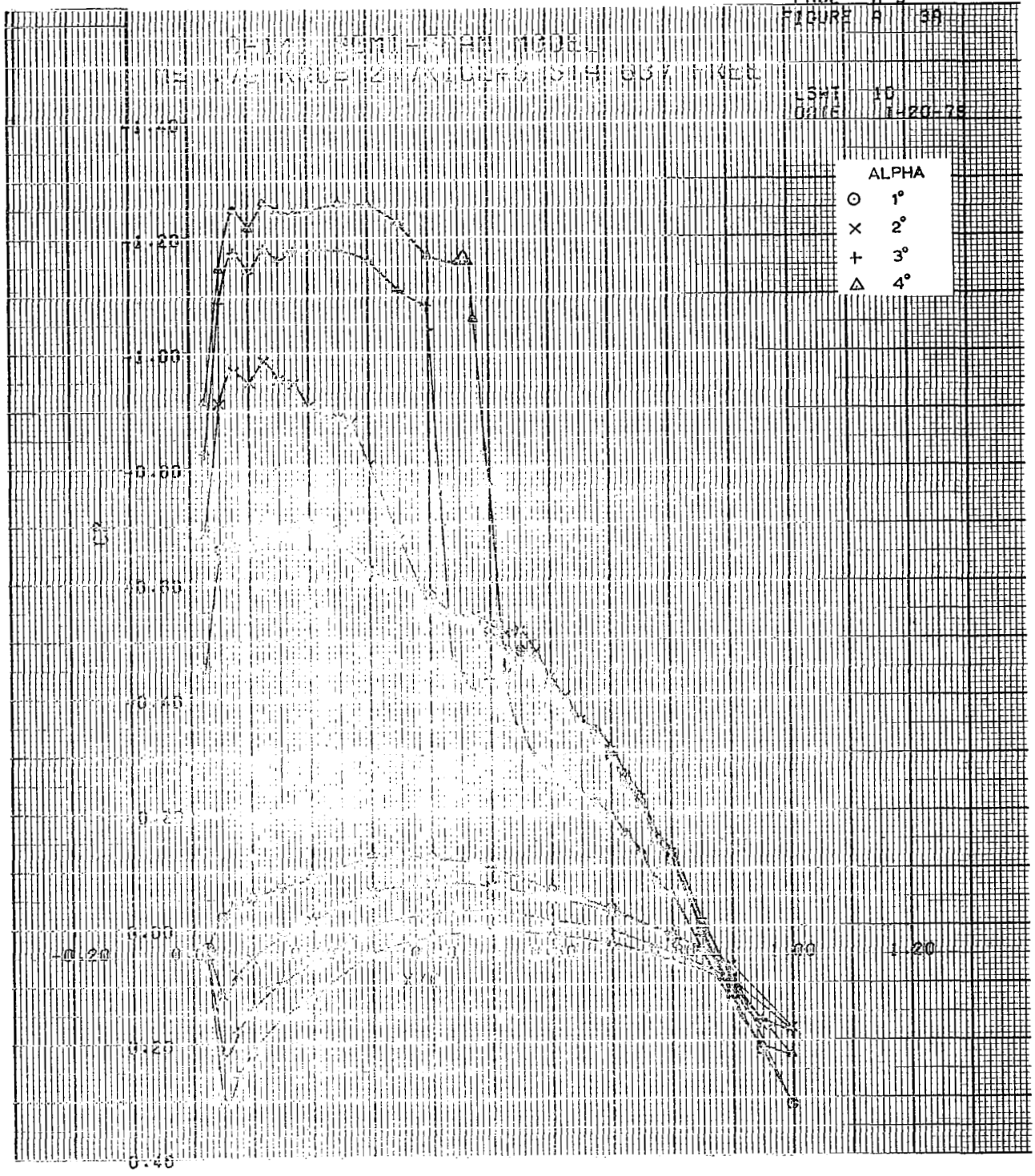
ALPHA
⊙ 1°
× 2°
+ 3°
△ 4°
CL
-1.20
1.20
0.45

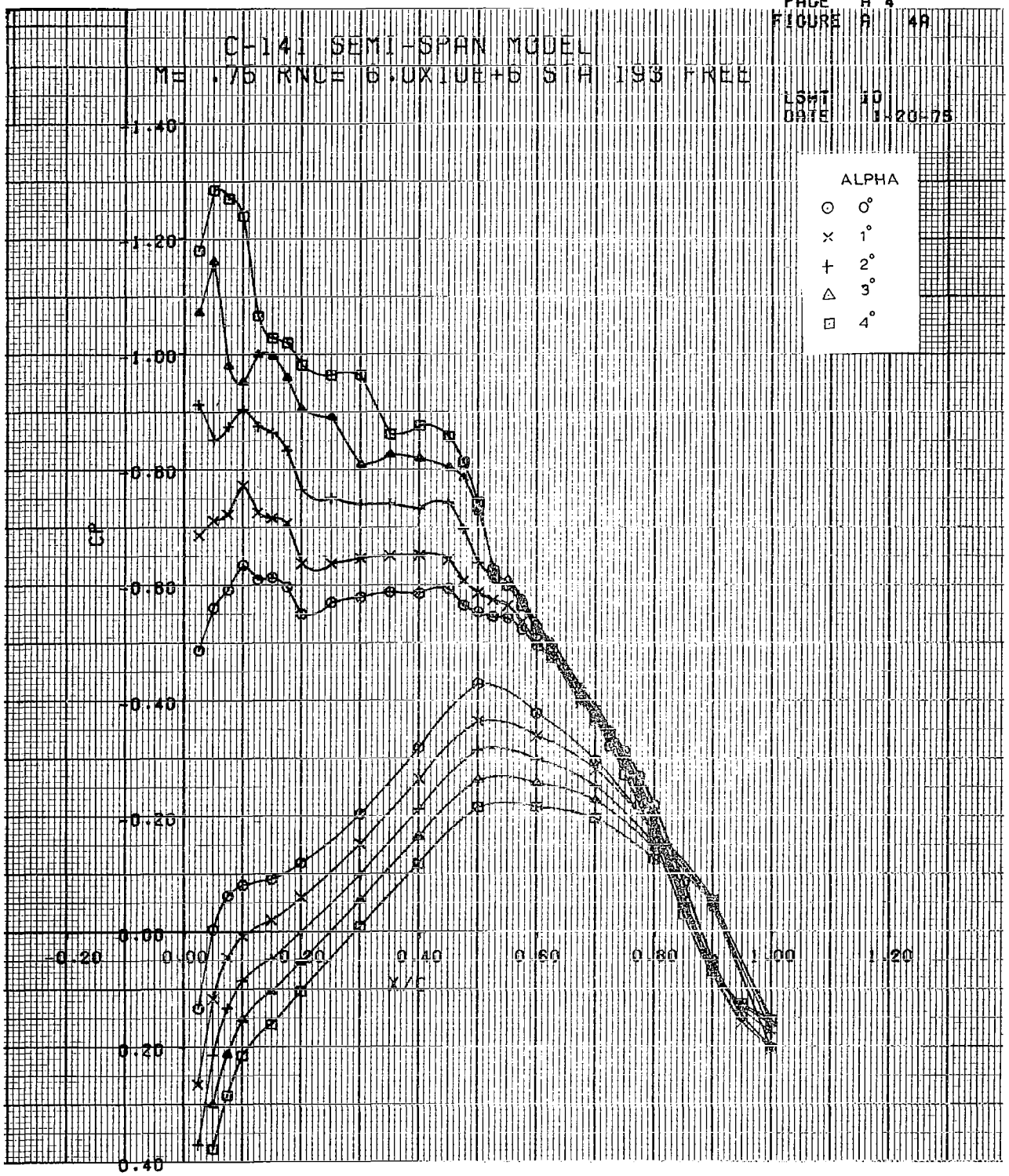
CF-141 SEMI-SPAN MODEL
ME .75 RNCE 6.0X10E+6 S A 193 TREE
LSHT 10
DATE 8-20-75
ALPHA
0°
1°
2°
3°
4°
-1.40
-1.20
-1.00
-0.80
-0.60
-0.40
-0.20
0.00
0.20
0.40
-0.20
0.00
0.20
0.40
0.60
0.80
1.00
1.20
X/C

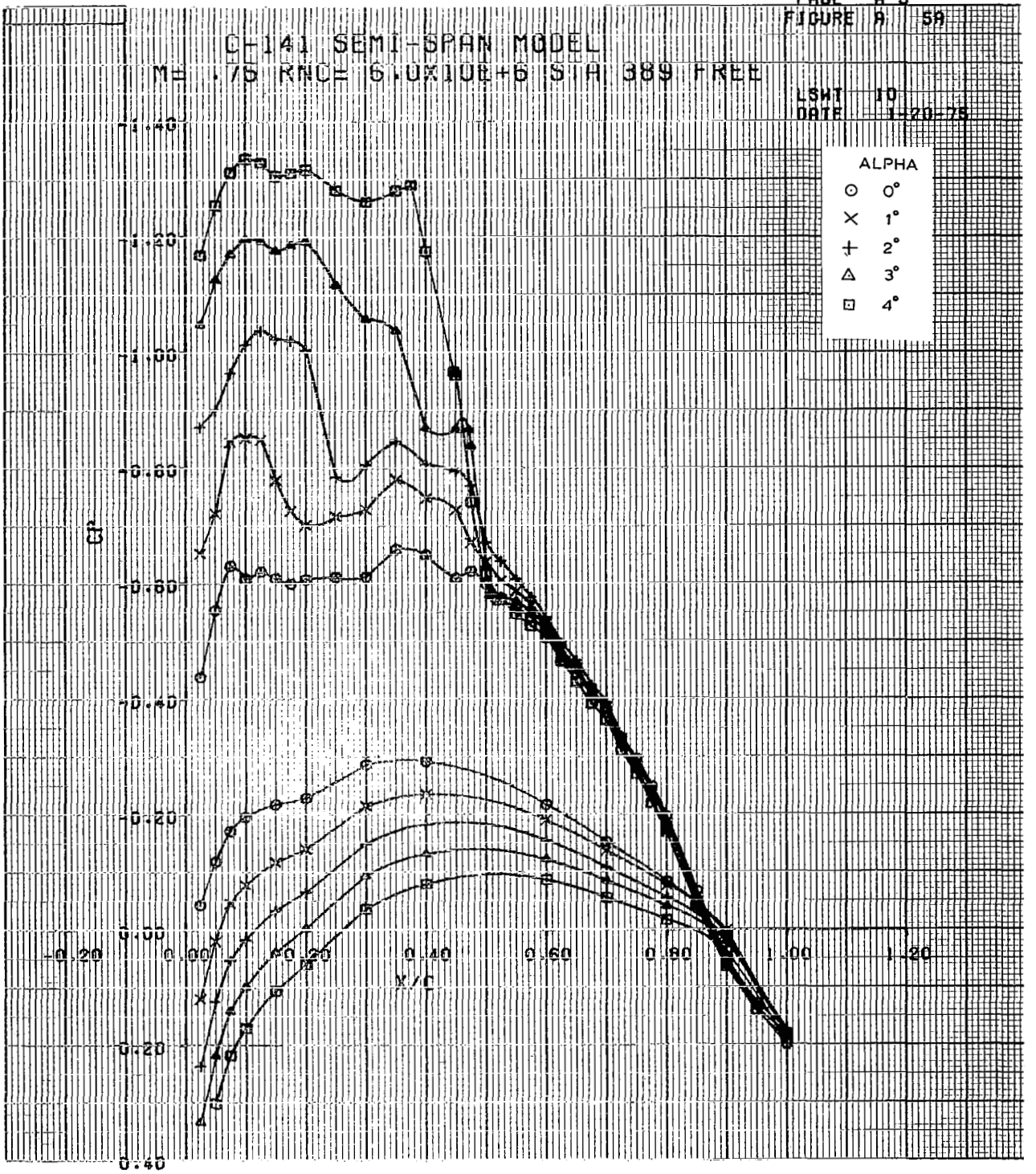
CH141 SEMI-SPAN MODEL
ME .75 RNCE 6.0X10E+6 S A 389 FREE
LSHT 10
DATE 1-20-75
ALPHA
0°
1°
2°
3°
4°
CP
-1.40
-1.20
-1.00
-0.80
-0.60
-0.40
-0.20
0.00
0.20
-0.20
-0.40
-0.20
0.00
0.20
0.40
0.60
0.80
1.00
1.20
X/C

C-141 SEMI-SPAN MODEL
M= .75 RNC= 6.0X10E+6 S H 637 -REF

LSHT 10
DATE 1-20-75

ALPHA
⊙ 0°
× 1°
+ 2°
△ 3°
□ 4°

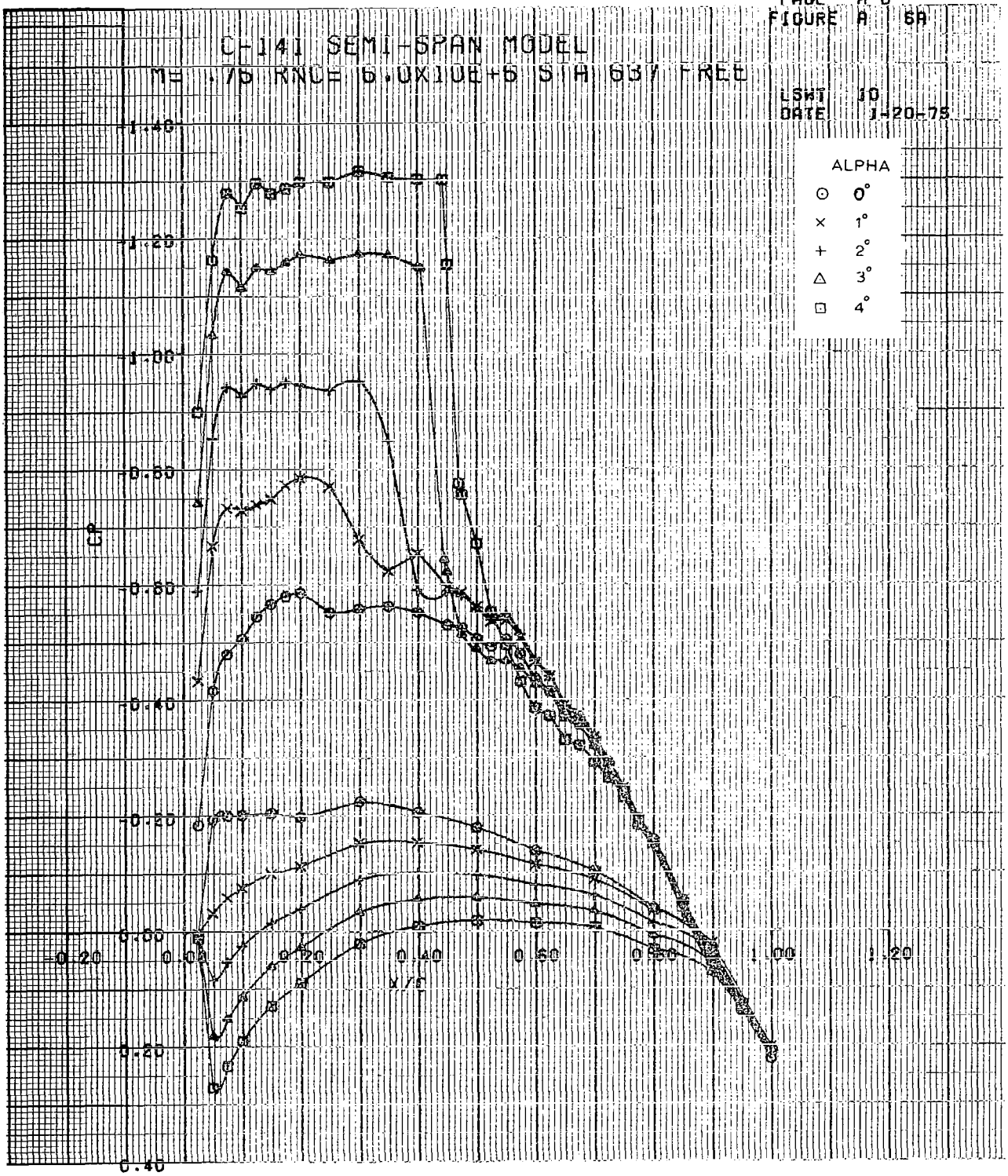

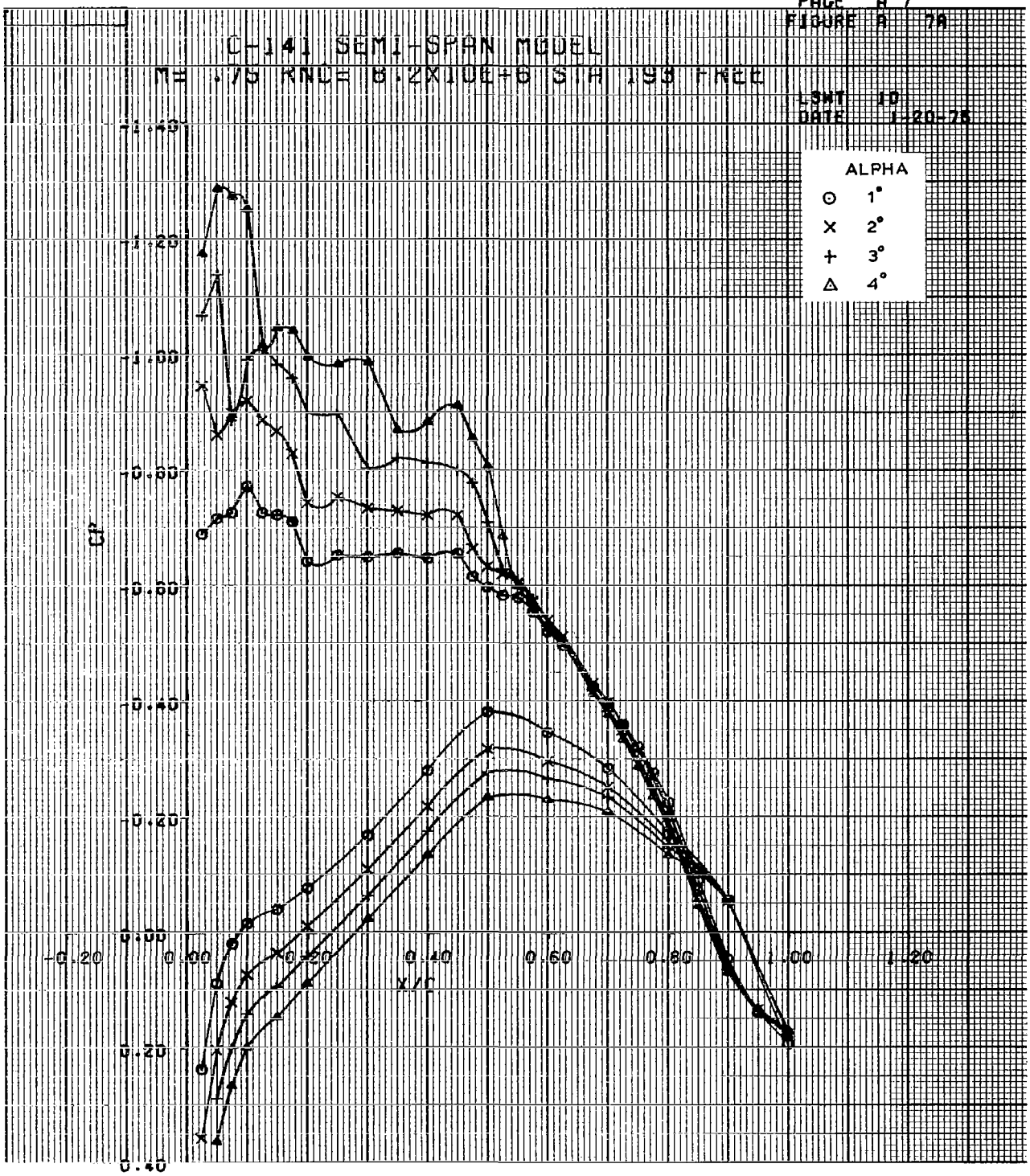
C-141 SEMI-SPAN MODEL
M= .75 RNO= 8.2X10E+6 SIM 195 FREE
LSWT 10
DATE 1-20-75
ALPHA
1°
2°
3°
4°
CP
X/C
-0.20
0.00
0.20
0.40
0.60
0.80
1.00
1.20
0.40

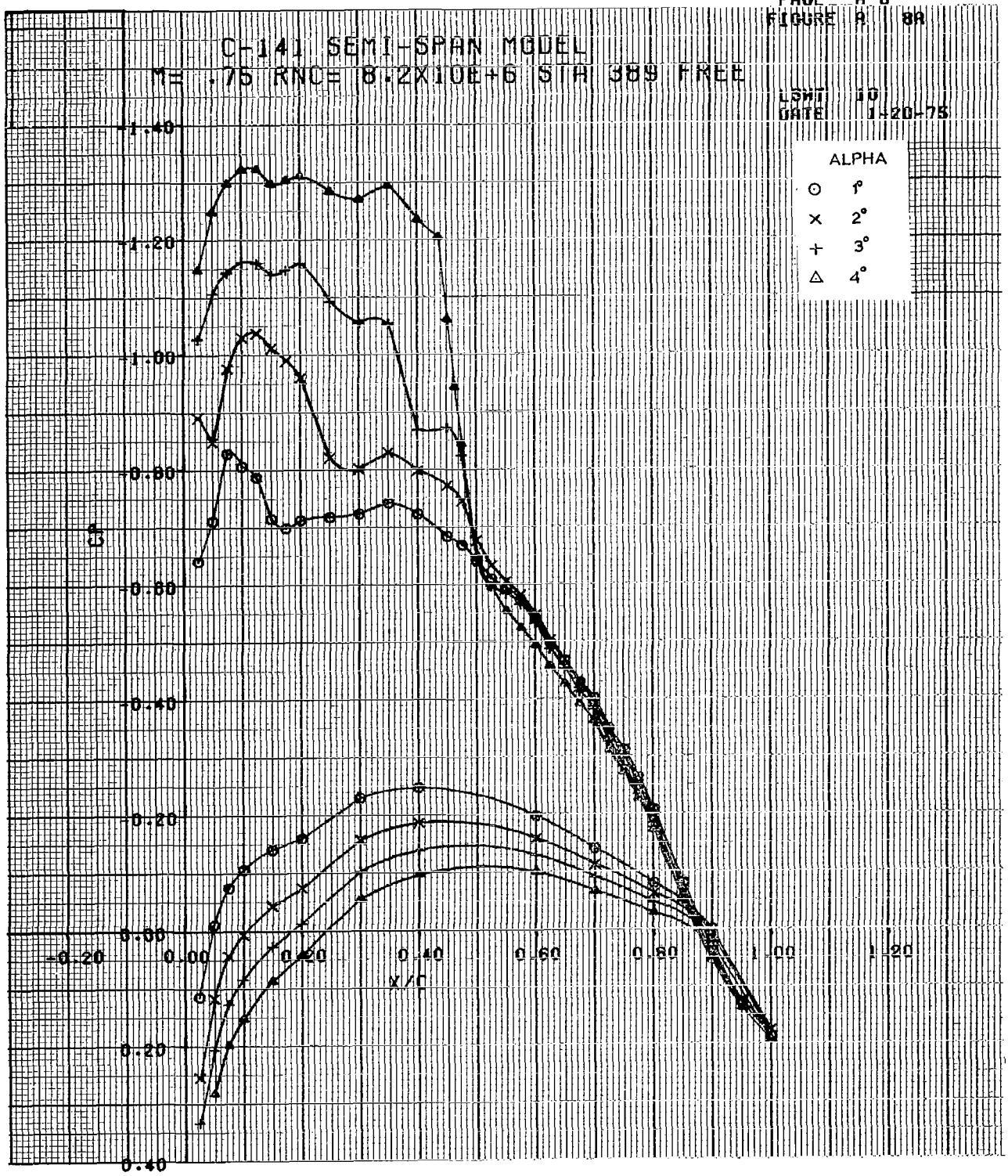
C-141 SEMI-SPAN MODEL
ME .75 RNC= 8.2X10E+6 S H 389 FREE
LSHT 10
DATE 1-20-75
ALPHA
⊙ 1°
× 2°
+ 3°
△ 4°
-1.40
-1.20
-1.00
-0.80
-0.60
-0.40
-0.20
0.00
0.20
0.40
-0.20
0.00
0.20
0.40
0.60
0.80
1.00
1.20
Y/C

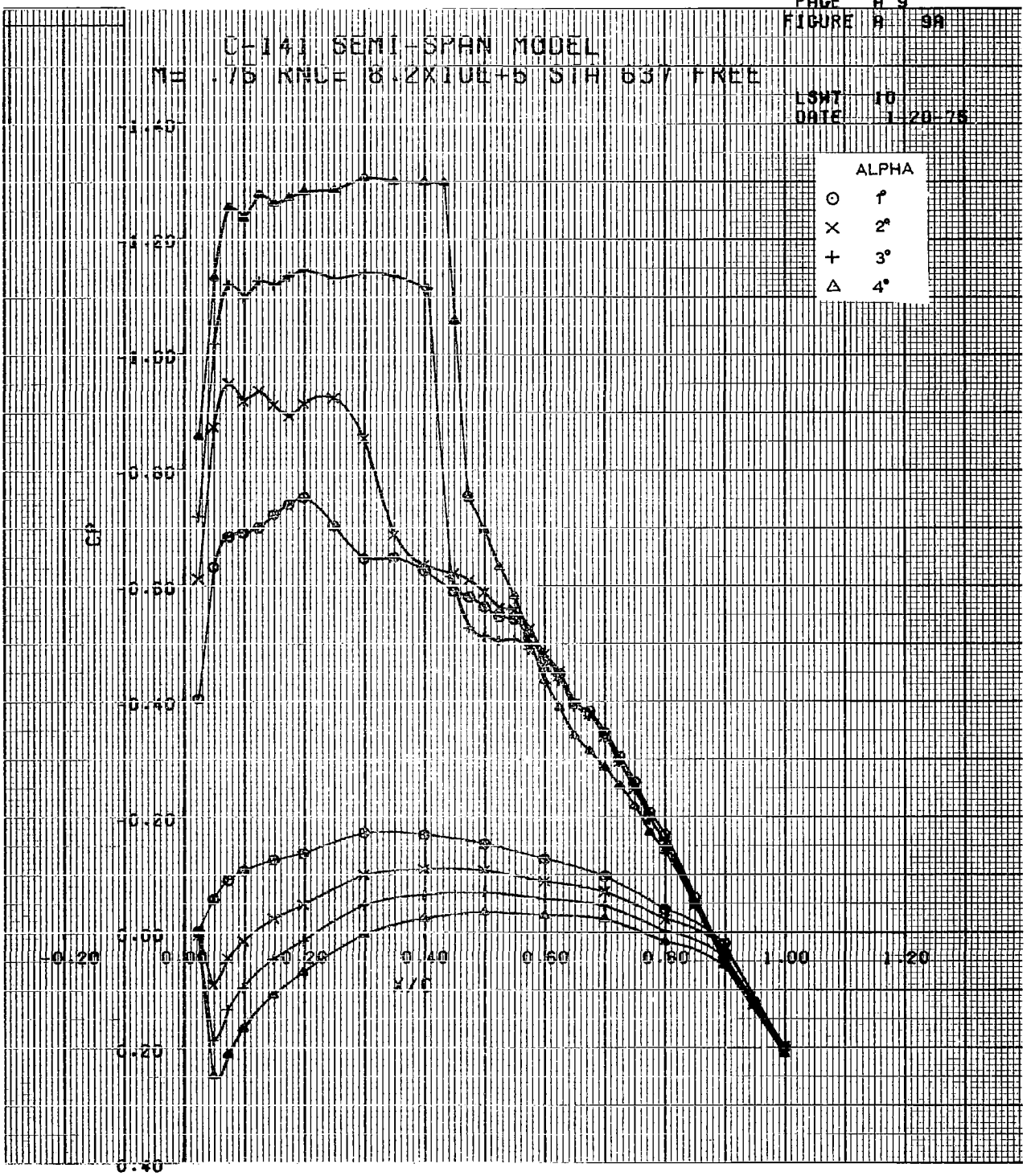
C-141 SEMI-SPAN MODEL
ME .75 RNUE 6.2X10E+6 STH 63Y FREE
LSHT 10
DATE 1-20-76
ALPHA
⊙ 1°
× 2°
+ 3°
△ 4°
CP
-0.20
0.00
0.20
0.40
0.60
0.80
1.00
1.20
X/C
0.40

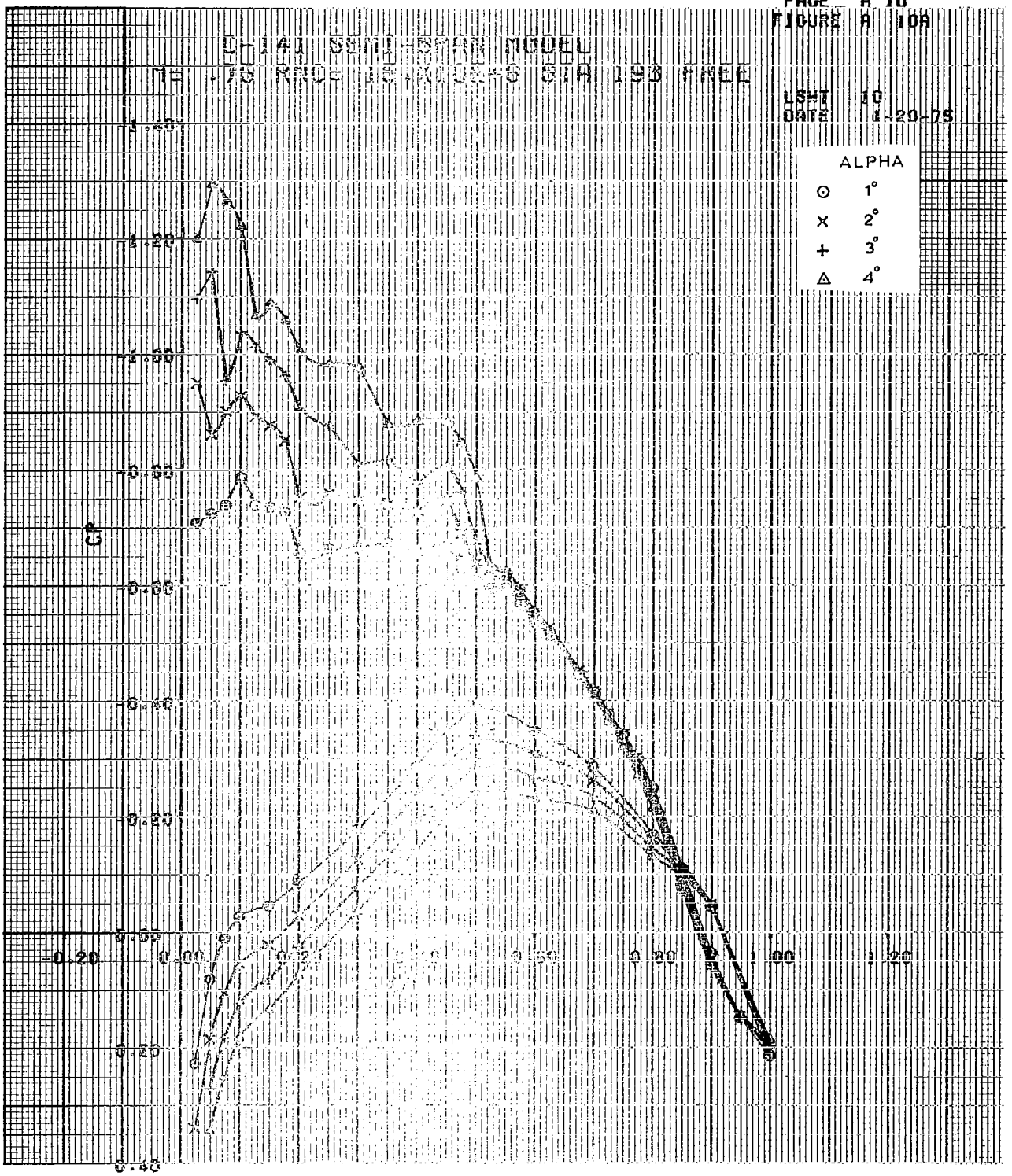
CHAI SEMI-SPAN MODEL
M = .70 R = 2.0 x 10^6 / FT
LSHI 10
DATE 1-20-78
ALPHA
⊙ 1°
× 2°
+ 3°
△ 4°
CP
-1.20
-1.00
-0.80
-0.60
-0.40
-0.20
0.00
0.20
1.00
1.20

FIGURE A 11A

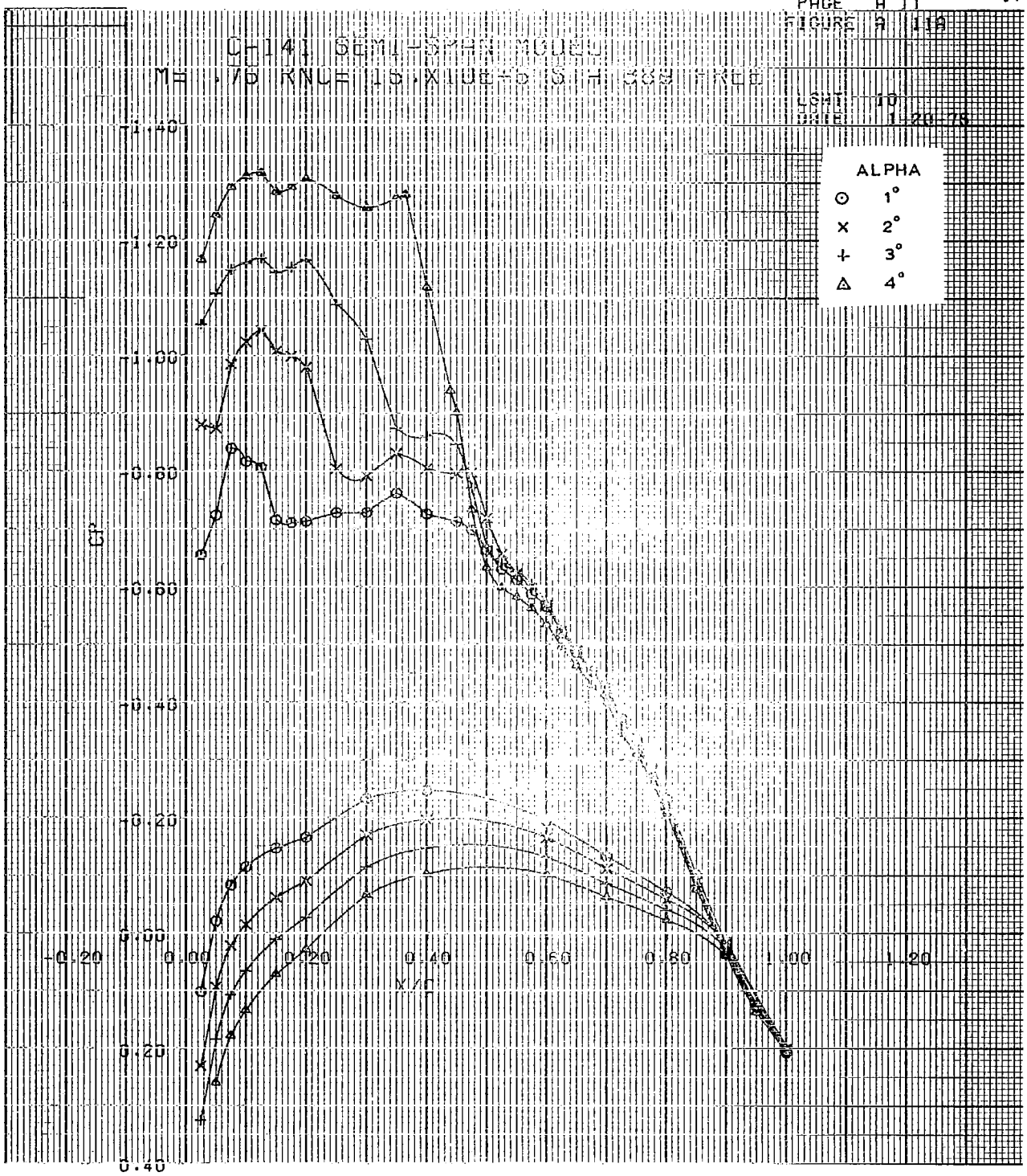
CH141 SEMI-SPAN MODEL
MACH KNUE 1.5 INJECTED SIDE FLOW
LSHT 10
DATE 1-20-78
ALPHA
1°
2°
3°
4°
CP
1.40
1.20
1.00
0.60
0.40
0.20
0.00
0.20
0.40
-0.20
0.00
0.20
0.40
0.60
0.80
1.00
1.20
X/C

FIGURE A 12A

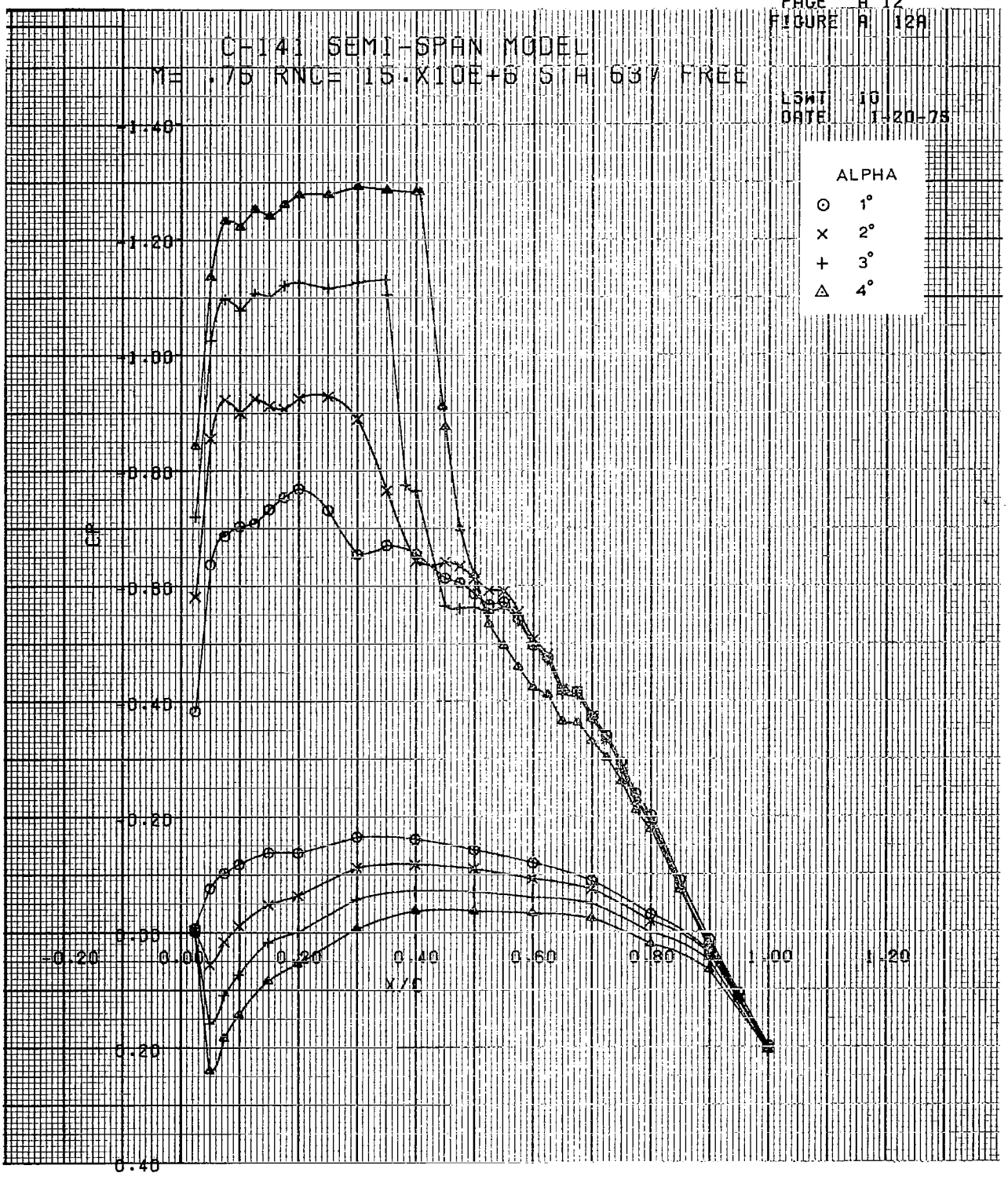
C-141 SEMI-SPAN MODEL
M= .76 RNC= 15.X10E+6 S H 63% FREE
LSHT 10
DATE 1-20-75
ALPHA
1°
2°
3°
4°
-1.40
-1.20
-1.00
-0.80
-0.60
-0.40
-0.20
0.00
0.20
0.40
-0.20
0.00
0.20
0.40
0.60
0.80
1.00
1.20
X/C

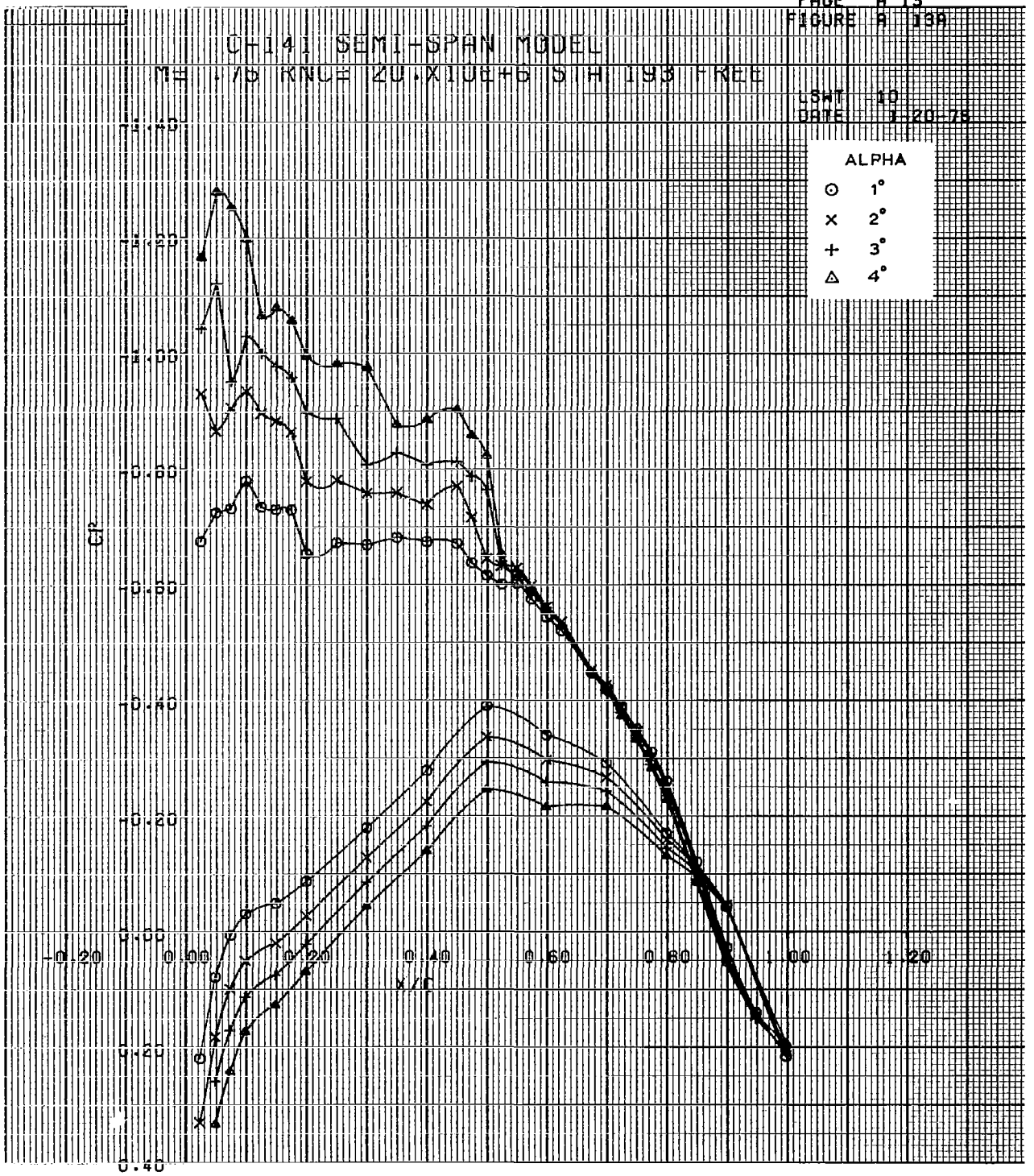
C-141 SEMI-SPAN MODEL
ALPHA
1°
2°
3°
4°
LSHT 10
DATE 1-20-78
Cl
x/c
-0.20
0.00
0.20
0.40
0.60
0.80
1.00
1.20
0.40

FIGURE A 14A

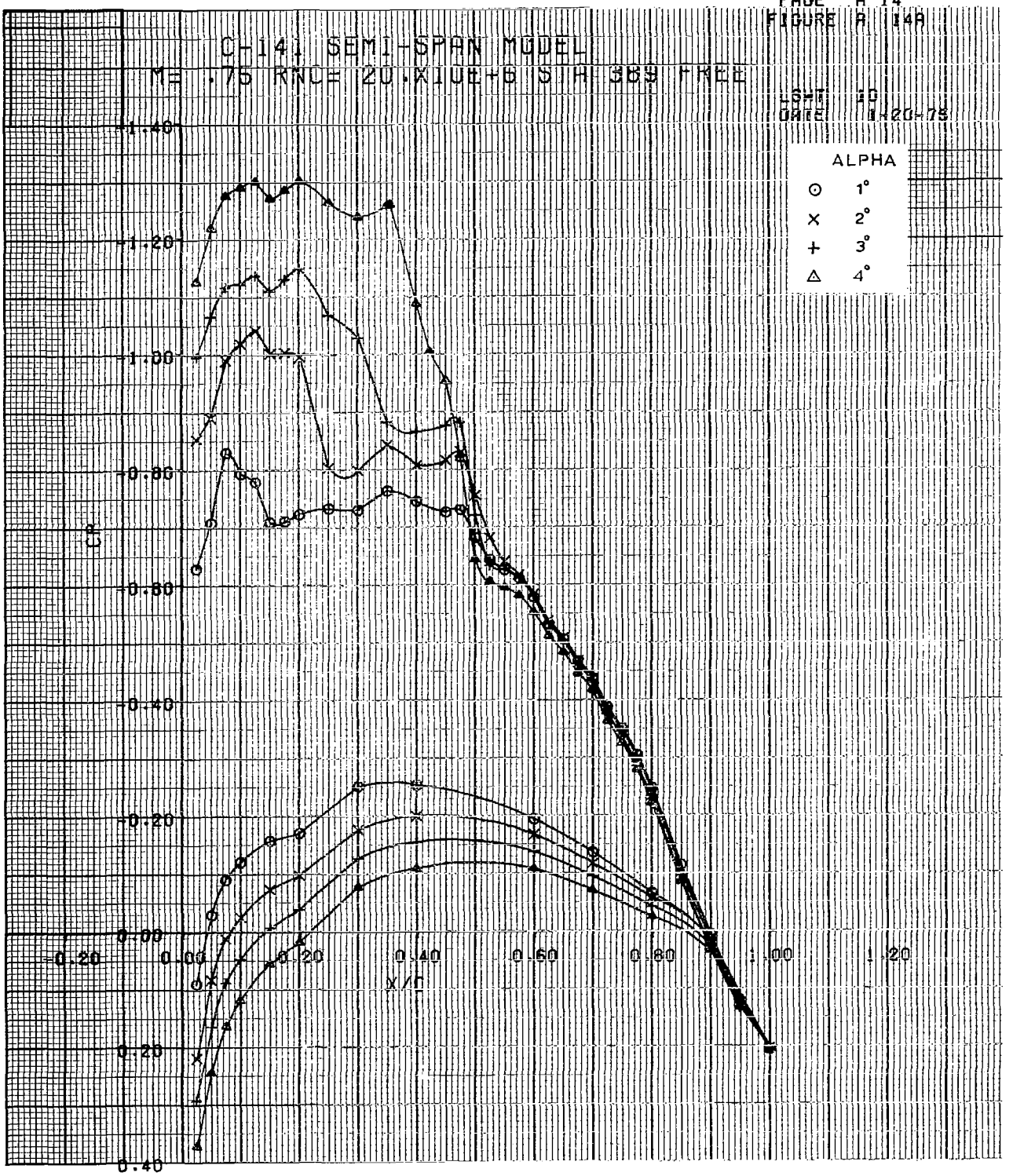
C-14, SEMI-SPAN MODEL
M= .75 RNC= 20.X10E+6 S/A 369 FREE
SHT HD
DATE 1-20-78
ALPHA
1°
2°
3°
4°
CL
-1.40
-1.20
-1.00
-0.80
-0.60
-0.40
-0.20
0.00
0.20
0.40
-0.20
0.00
0.20
0.40
0.60
0.80
1.00
1.20
X/H

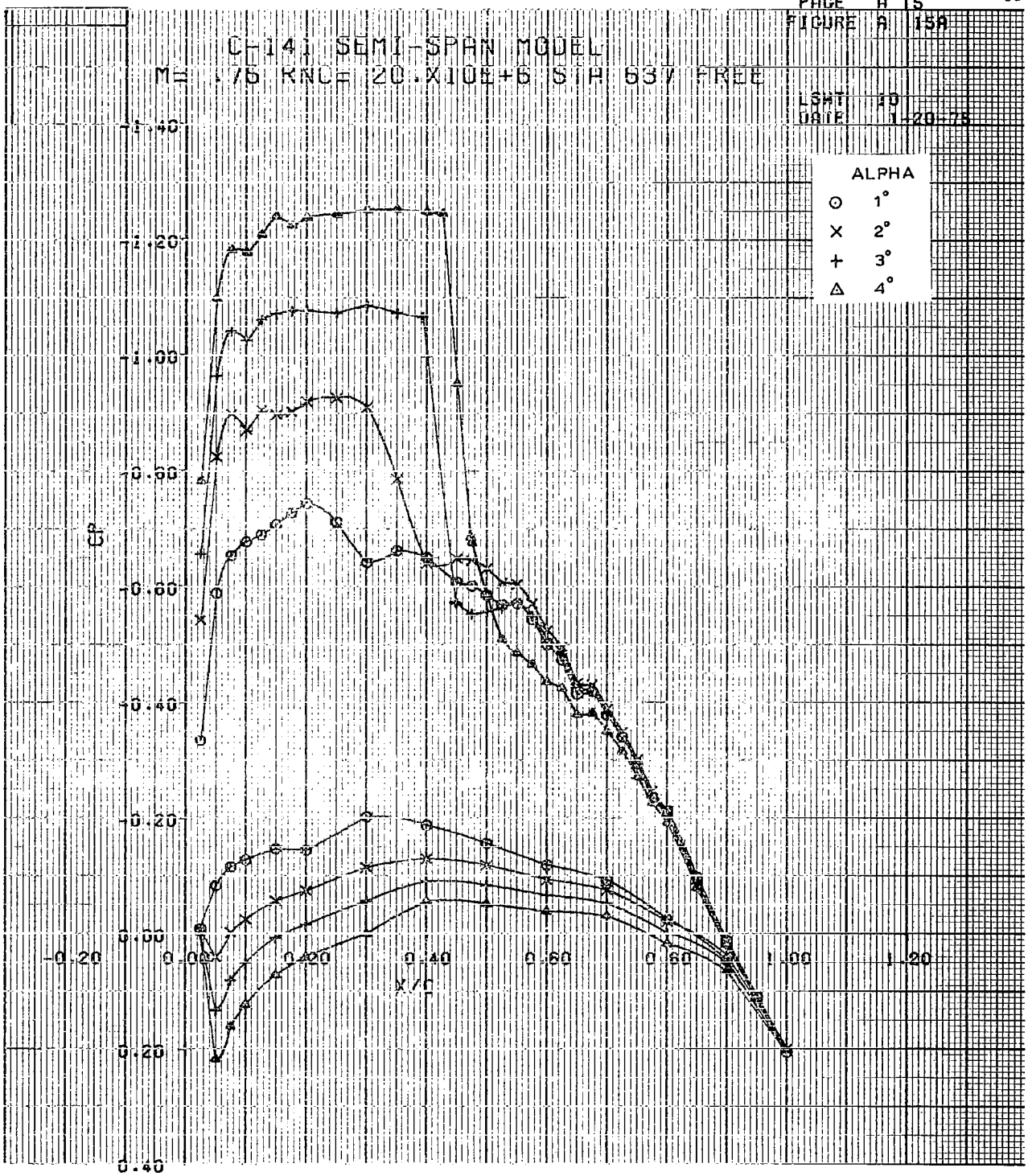
(F-14) SEMI-SPAN MODEL
ME .76 RNCE 20.X10E+6 SIR 537 FREE
LSHT 40
DATE 1-20-75
ALPHA
1°
2°
3°
4°
CP
X/C
-0.20
0.00
0.20
0.40
0.60
0.80
1.00
1.20
-0.40
-0.20
0.00
0.20
0.40
0.60
0.80
1.00
1.20
1.40

FIGURE A 16A

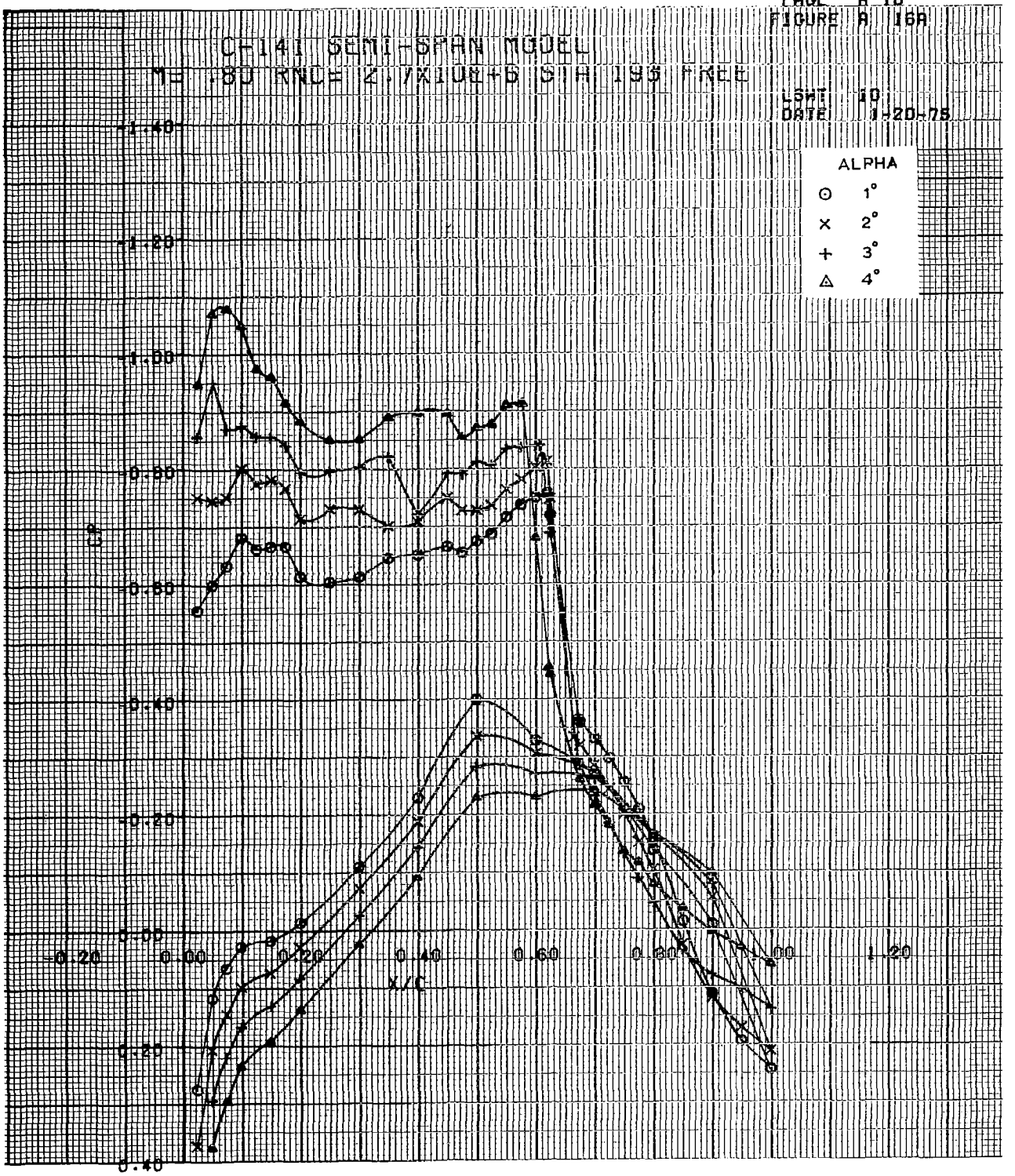
CF-141 SEMI-SPAN MODEL
M= .80 RNUE 2.7X10E+6 SIH 135 TNEE
LSHT 10
DATE 1-20-75
ALPHA
1°
2°
3°
4°
-1.40
-1.20
-1.00
-0.80
-0.60
-0.40
-0.20
0.00
0.20
-0.40
-0.20
0.00
0.20
0.40
0.60
0.80
1.00
1.20
X/C

FIGURE A 17A

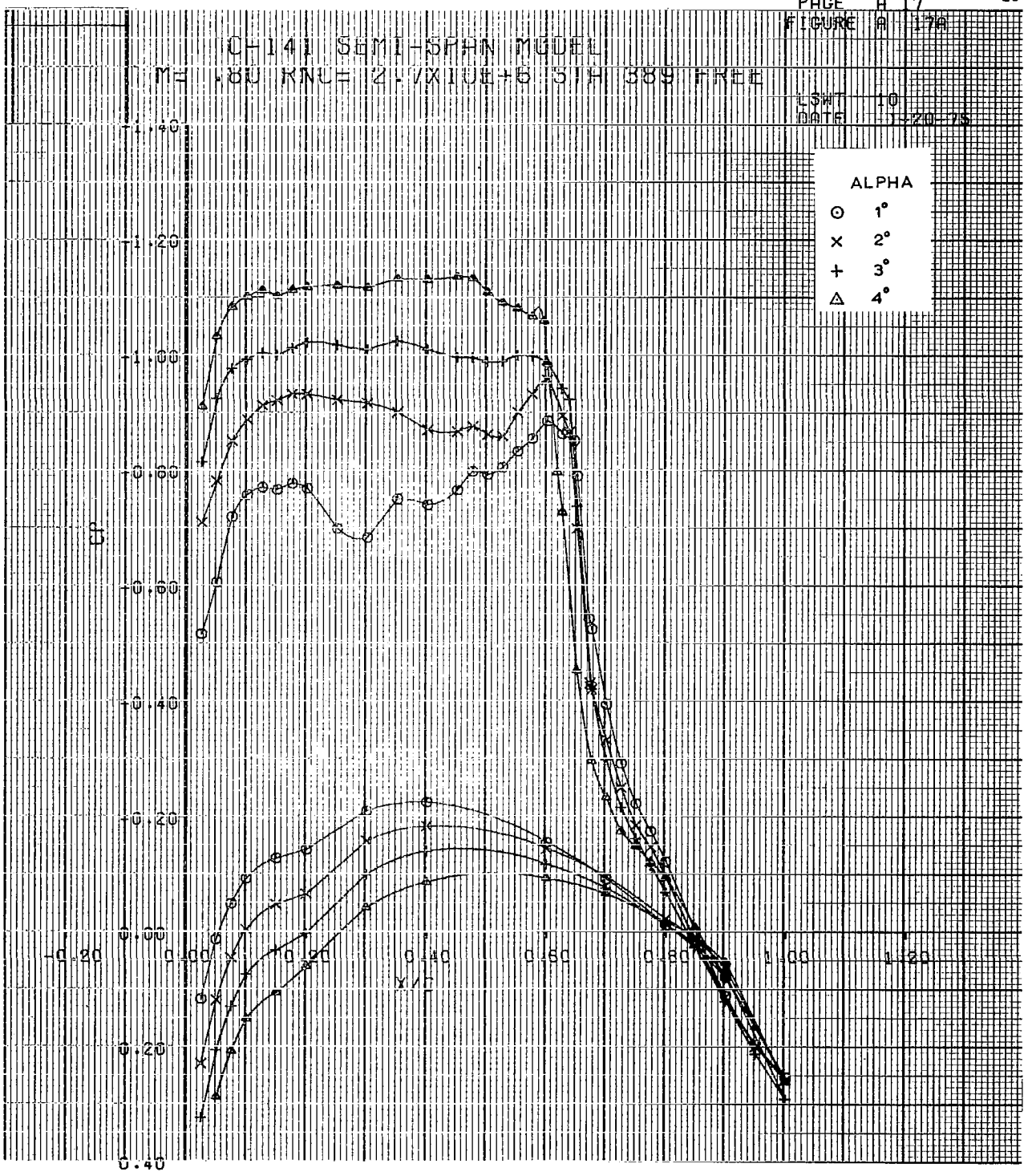
C-141 SEMI-SPAN MODEL
M = .82 KNOTS = 2.VXIDE+6 S/F 389 FREE
LSWT 10
DATE 1-20-75
ALPHA
1°
2°
3°
4°
Cp
X/C

FIGURE A 18A

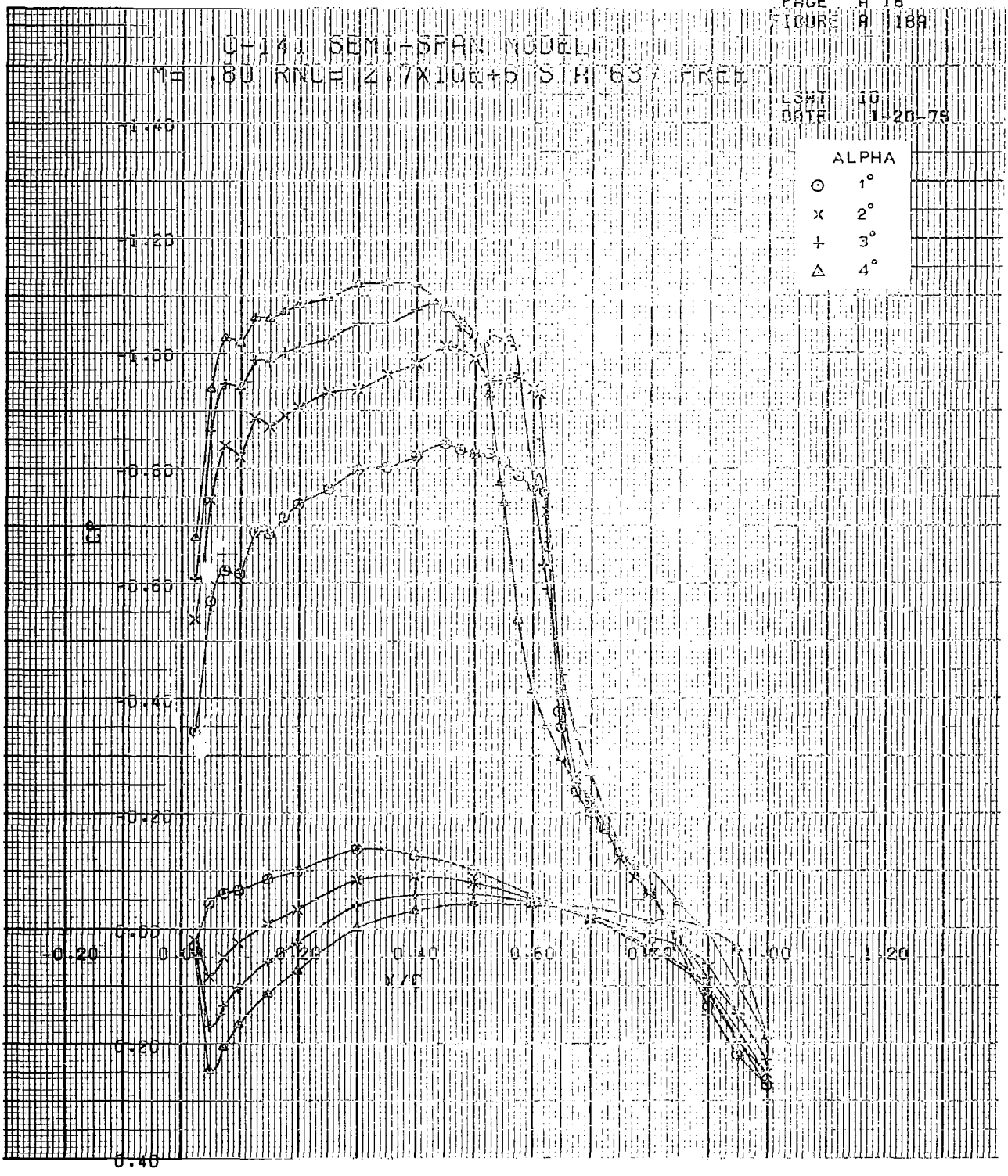
CH141 SEMI-SPAN MODEL
M= .80 RNO= 2.7X10E+6 SIR 63 FREE
LSHL 10
DATE 1-20-78
ALPHA
1°
2°
3°
4°
1.40
1.20
1.00
0.80
0.60
0.40
0.20
0.00
-0.20
0.40
0.20
0.00
0.20
0.40
0.60
0.80
1.00
1.20
X/C

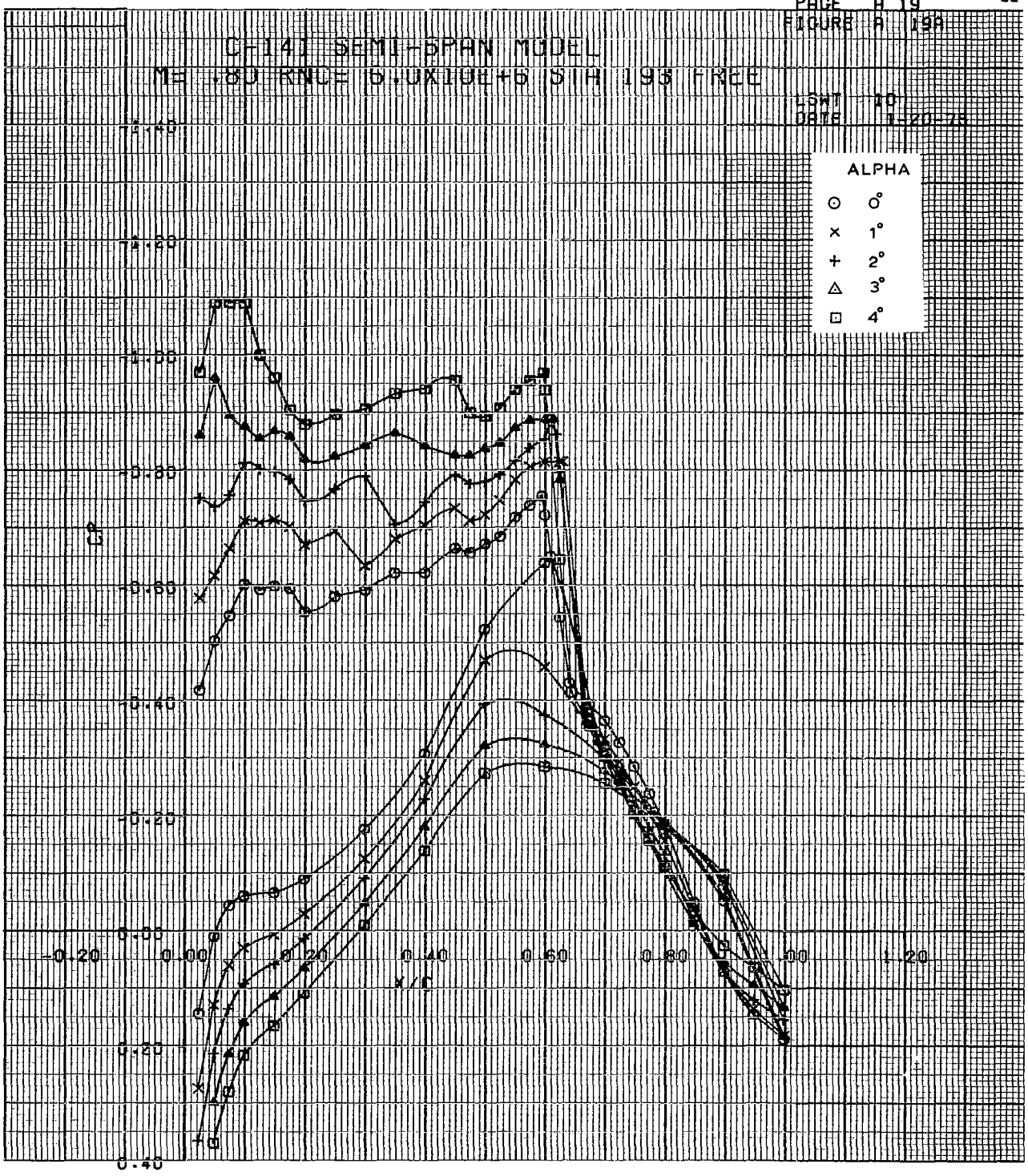
C-141 SEMI-SPAN MODEL
M= .80 RNC= 6.0X10E+6 STH 195 FREE
LSWT 10
DATE 1-NOV-78
ALPHA
0°
1°
2°
3°
4°
CP
-0.80
-0.60
-0.40
-0.20
0.00
0.20
0.40
-0.20
0.00
0.20
0.40
0.60
0.80
1.00
1.20
X/C

FIGURE A 20B

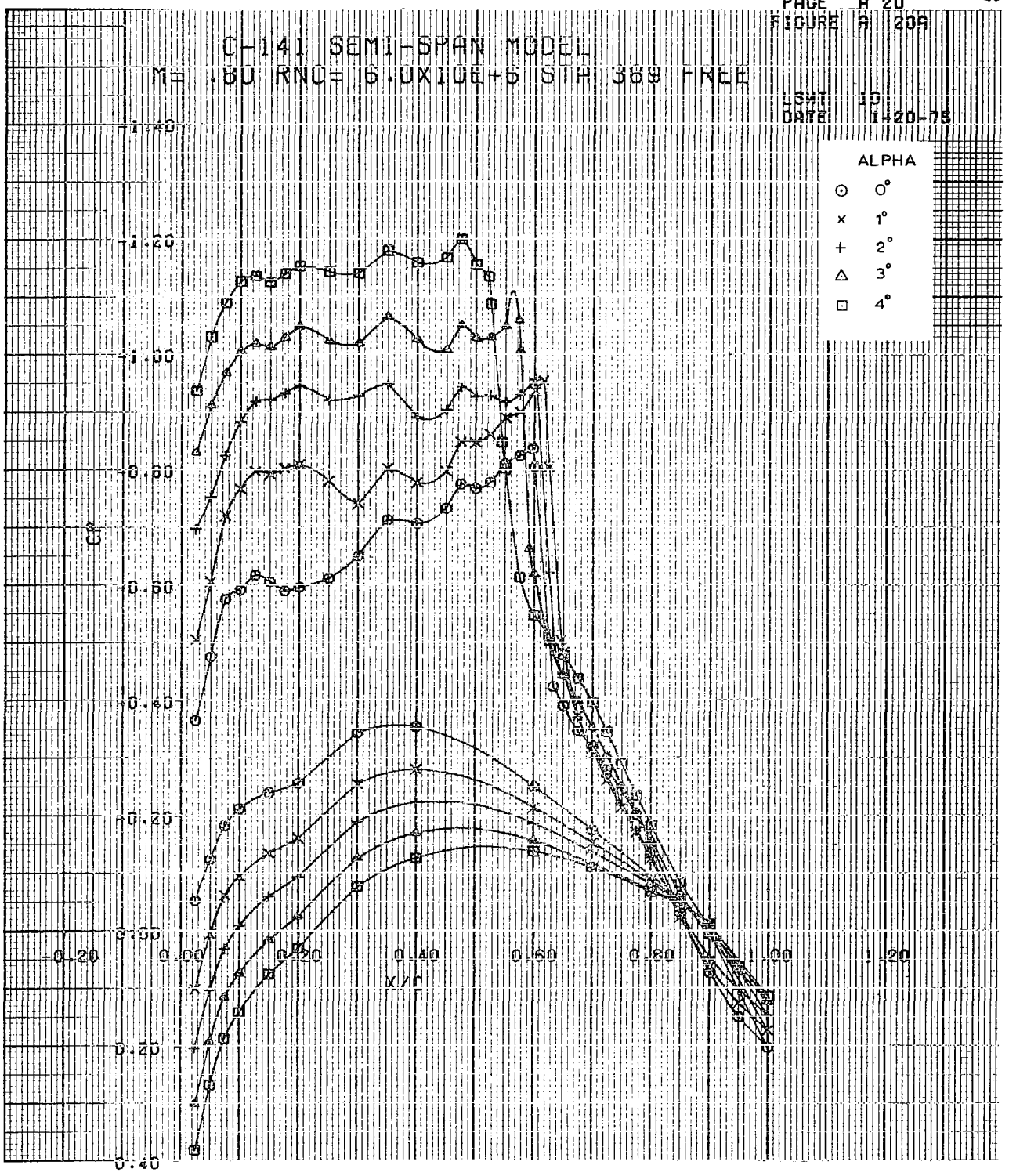
C-141 SEMI-SPAN MODEL
M= .60 RNC= 6.0X10E+6 S-H SEC FREE
CONF 5D
DATE 1-20-78
ALPHA
⊙ 0°
× 1°
+ 2°
△ 3°
⊡ 4°
CP
X/C
1.40
1.20
1.00
0.80
0.60
0.40
0.20
0.00
-0.20
0.00
0.20
0.40
0.60
0.80
1.00
1.20

C-141 SEMI-SPAN MODEL
M= .80 RNC= 6.0X10E+6 SIA 63Y FREE

LSHE 10
DATE 1-20-75

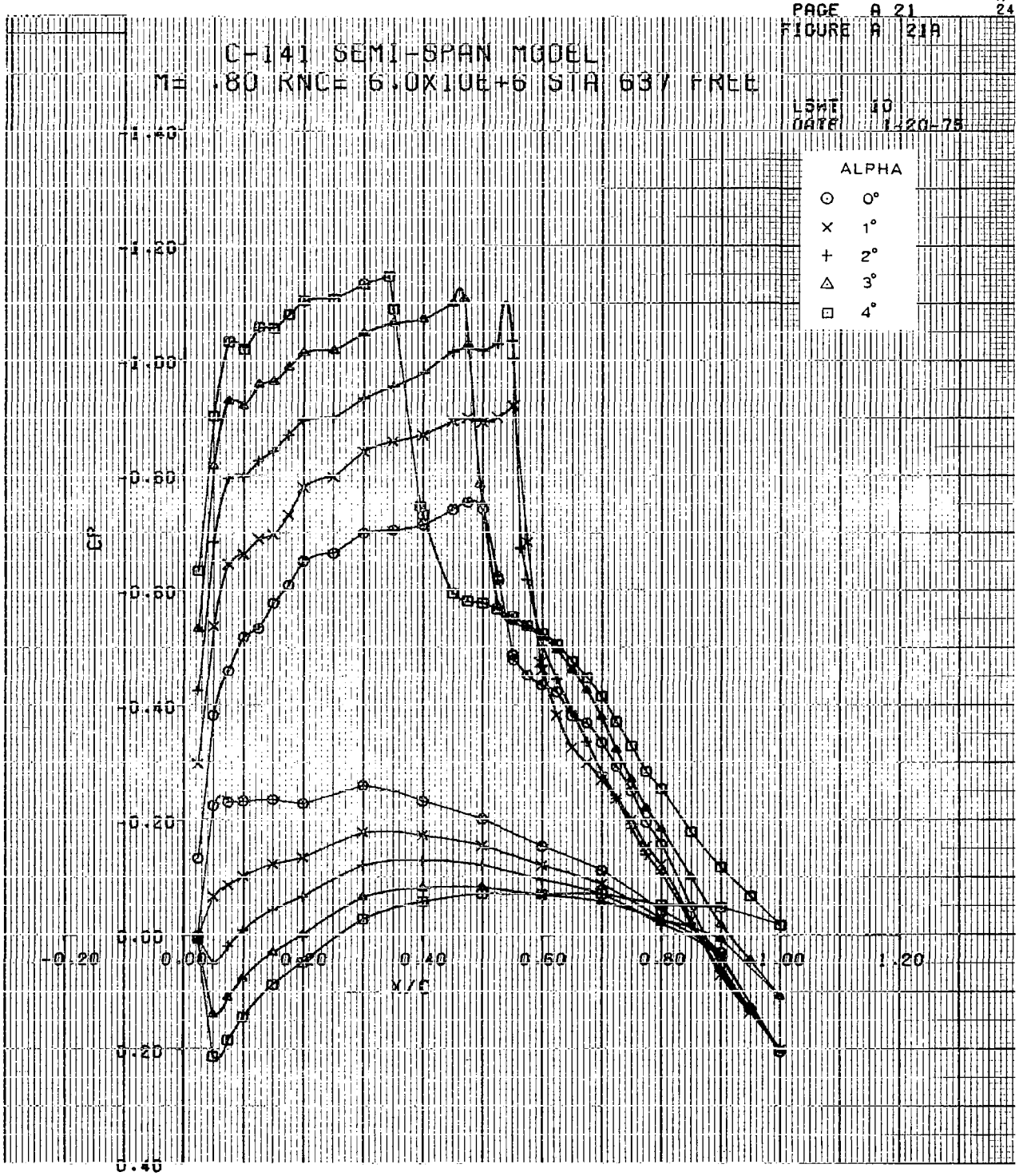

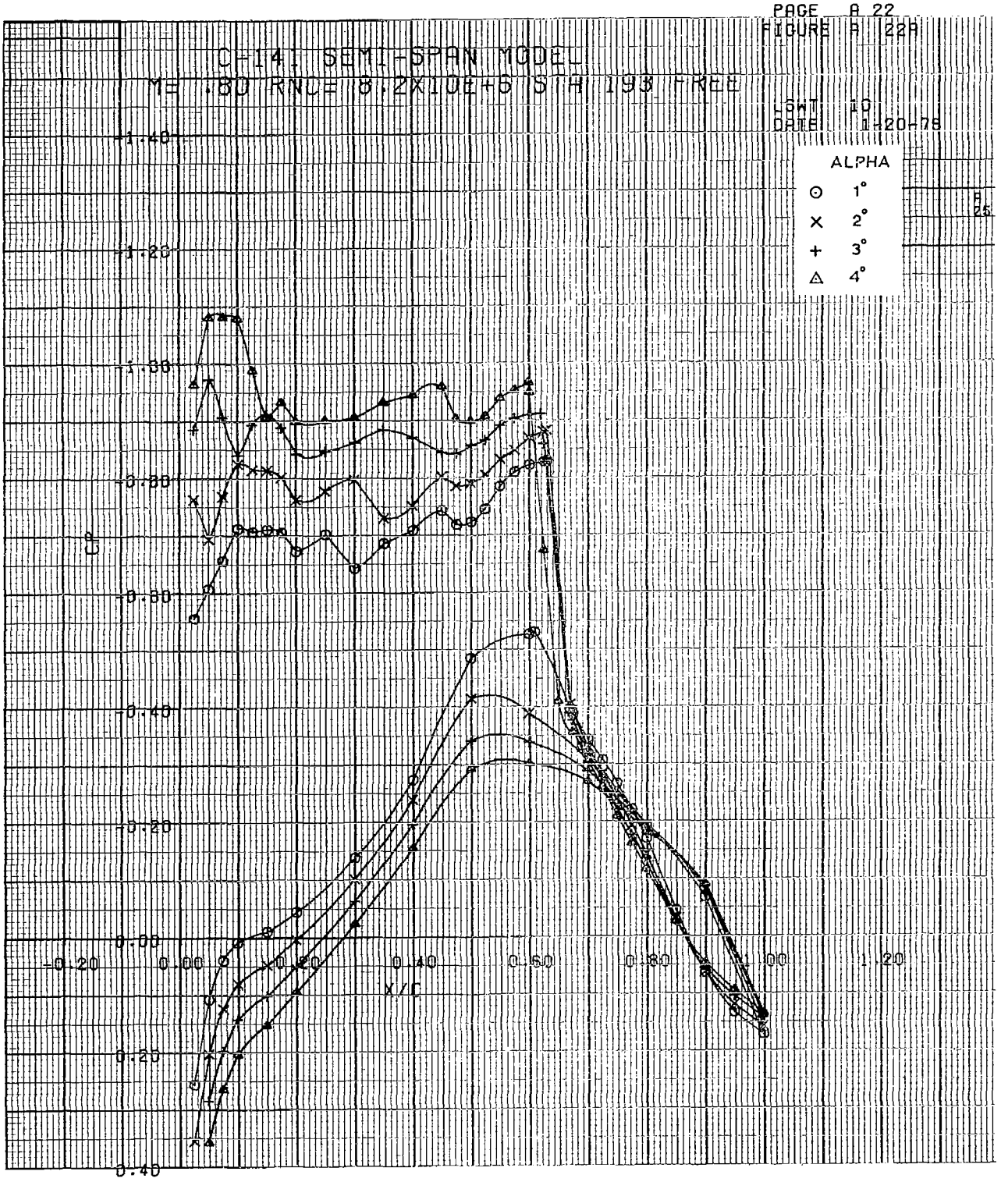
C-14, SEMI-SPAN MODEL
M= .80 RNL= 8.2X10E+6 S/H .193 FREE
LSWT 10
DATE 1-20-78
ALPHA
1°
2°
3°
4°
-1.40
-1.20
-1.00
-0.80
-0.60
-0.40
-0.20
0.00
0.20
-0.20
0.00
0.20
0.40
0.60
0.80
1.00
1.20
X/C
-0.40

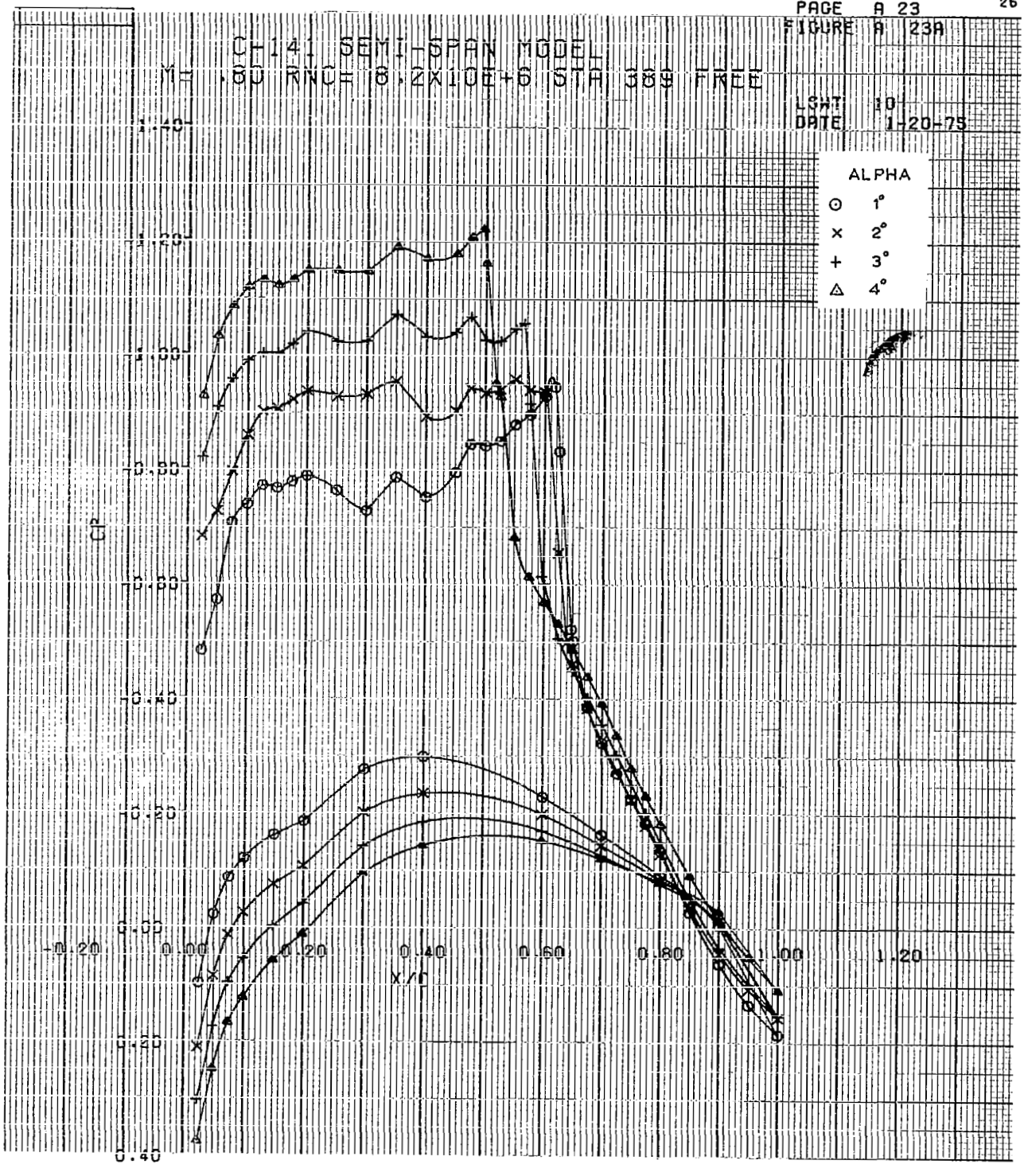
LSHT 10
DATE 1-20-75
ALPHA
⊙ 1°
× 2°
+ 3°
△ 4°
CP
X/C
1.40
0.40
-0.20
0.00
0.20
0.40
0.60
0.80
1.00
1.20

FIGURE A 24A

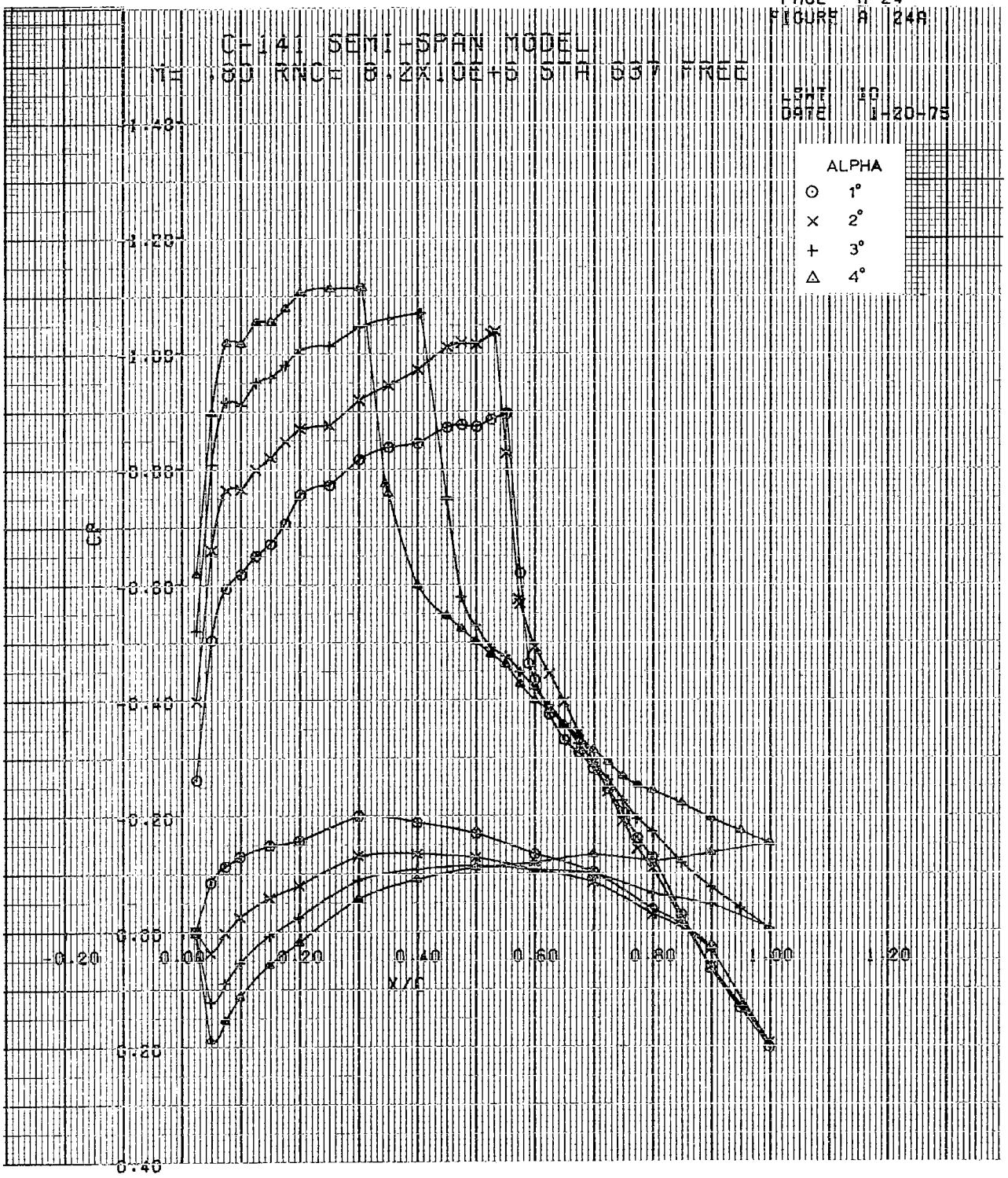

FIGURE A 25A

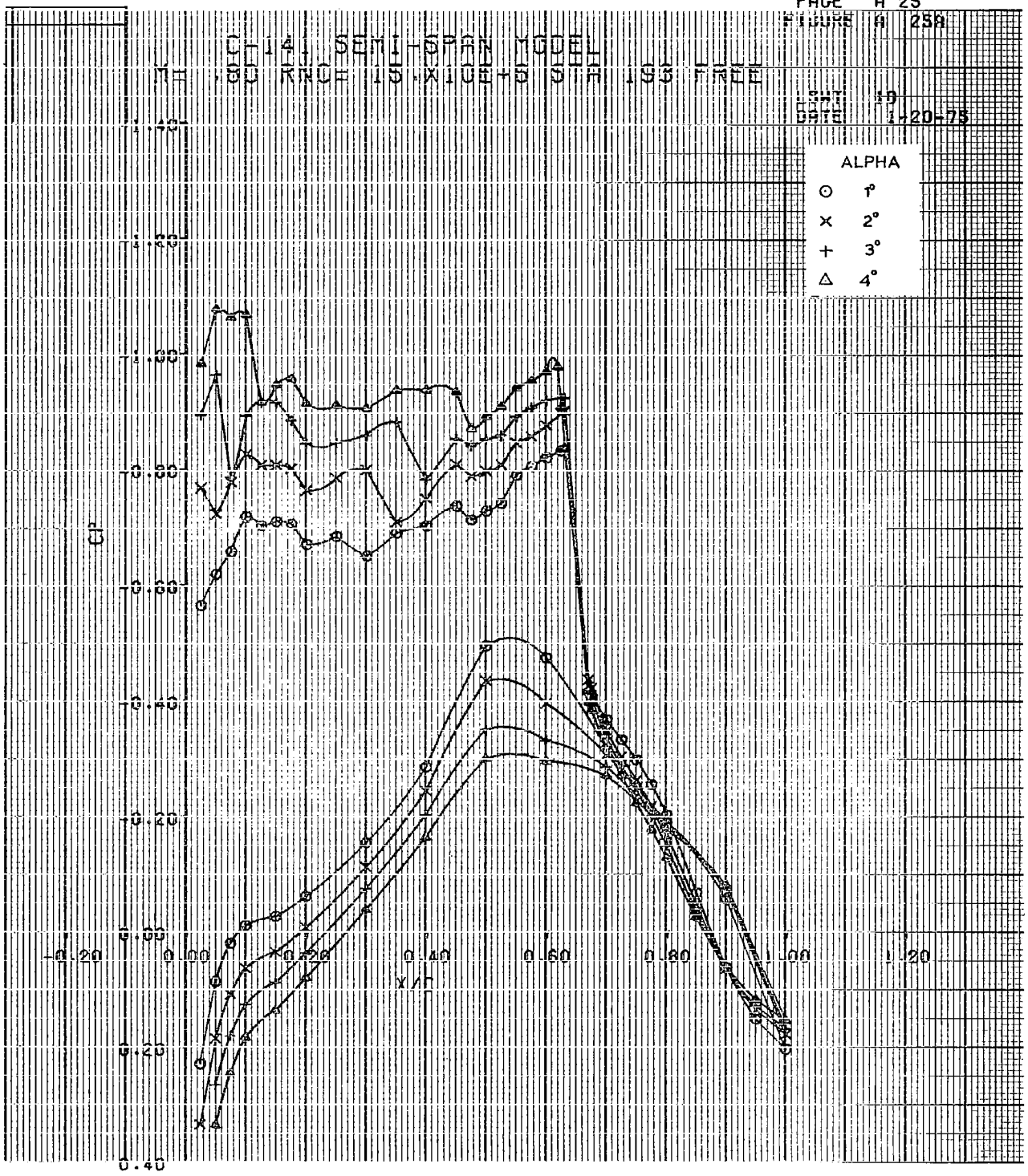

C-141 SEMI-SPAN MODEL
M= .80 RNC= 15.X10E+6 STA 389 FREE

LSHT 10
DATE 1-20-75

ALPHA
⊙ 1°
× 2°
+ 3°
△ 4°

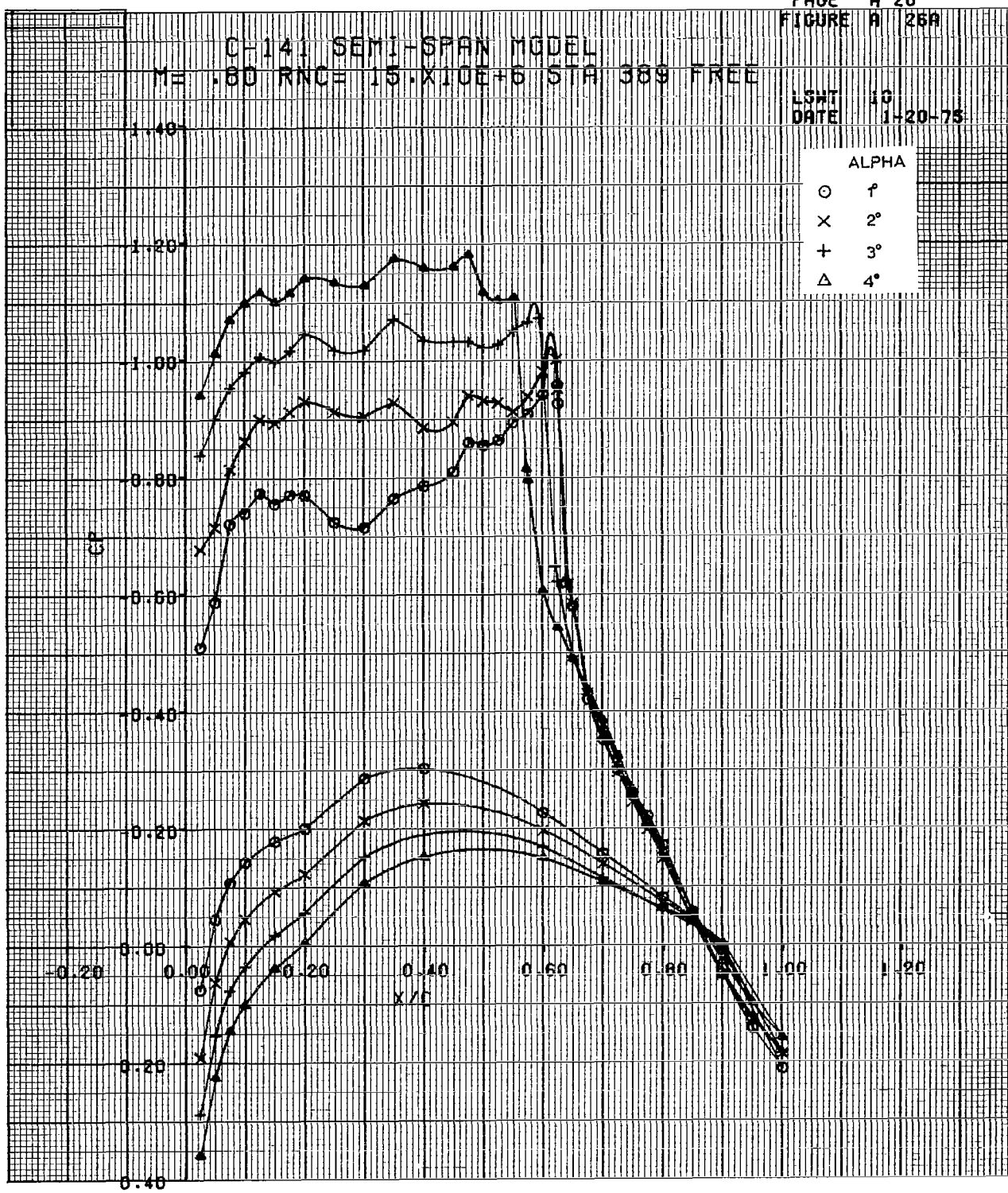

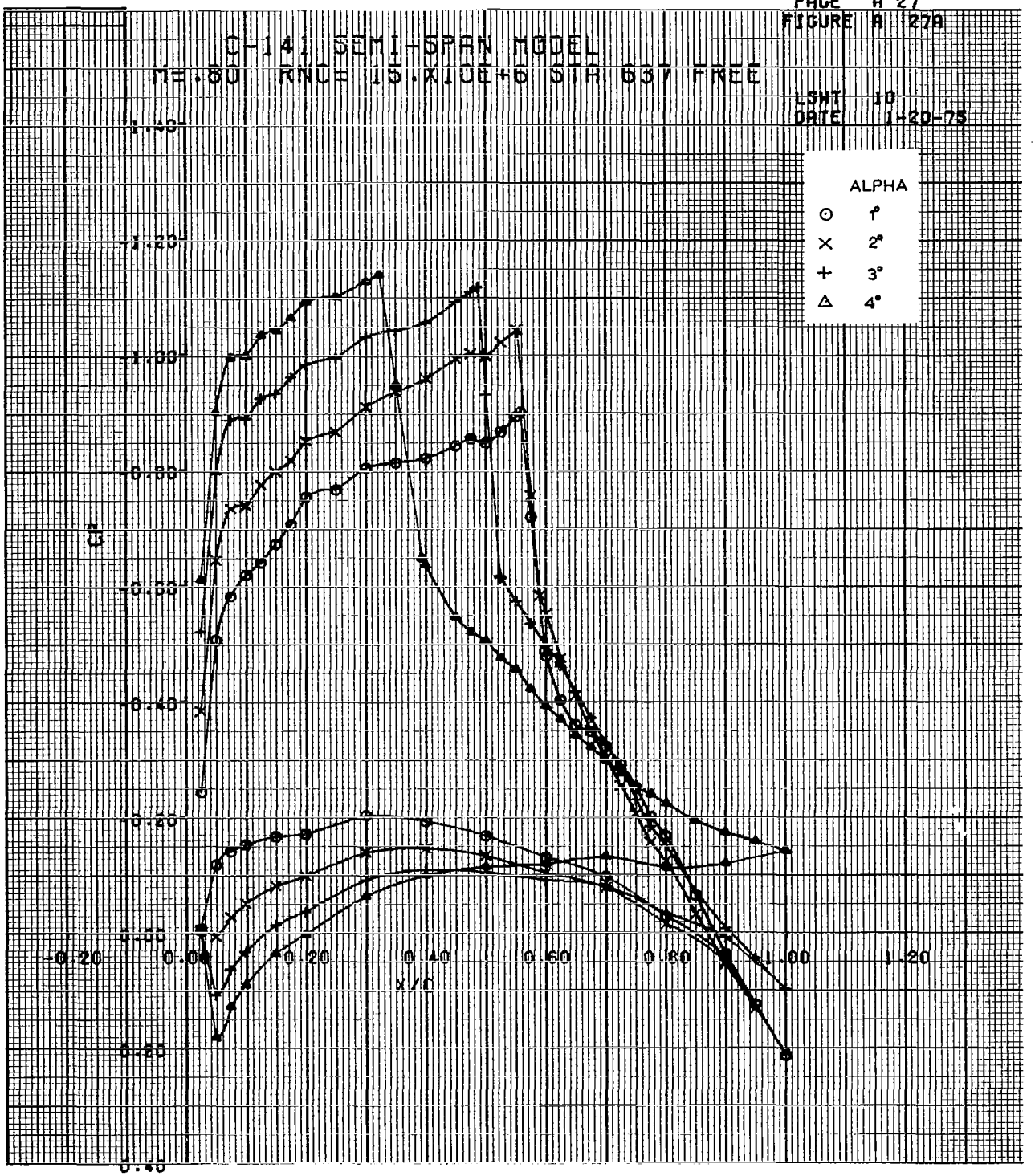
CH-141 SEMI-SPAN MODEL
ALPHA
1°
2°
3°
4°
LSWT 10
DATE 1-20-75
-1.20
-1.00
-0.80
-0.60
-0.40
-0.20
0.00
0.20
0.40
0.60
0.80
1.00
1.20
X/C

FIGURE A 28A

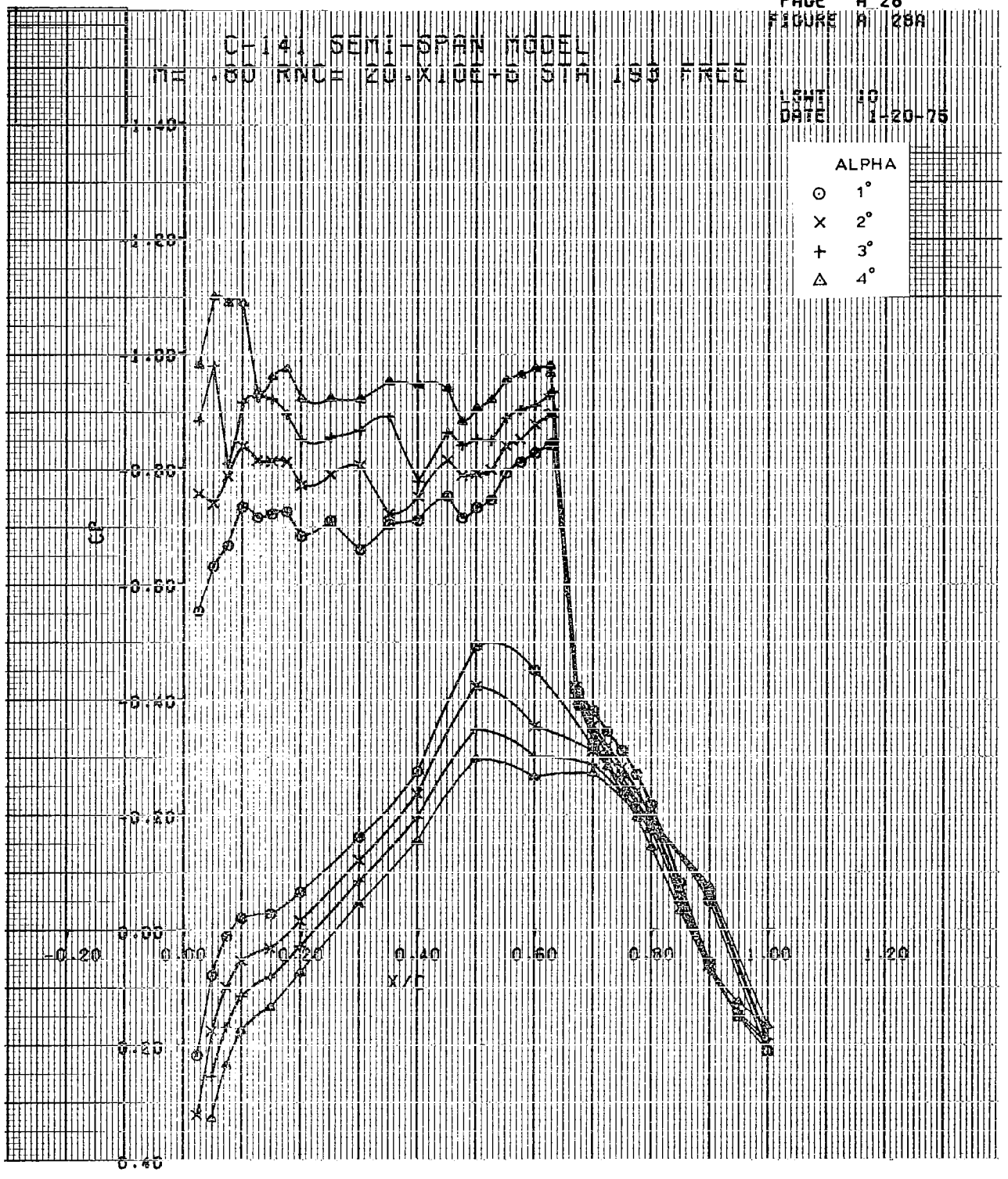
DATE 1-20-75
ALPHA
⊙ 1°
× 2°
+ 3°
△ 4°
CP
X/C
-0.20
0.00
0.20
0.40
0.60
0.80
1.00
1.20
-1.40
-1.20
-1.00
-0.80
-0.60
-0.40
-0.20
0.00
0.20
0.40
0.60

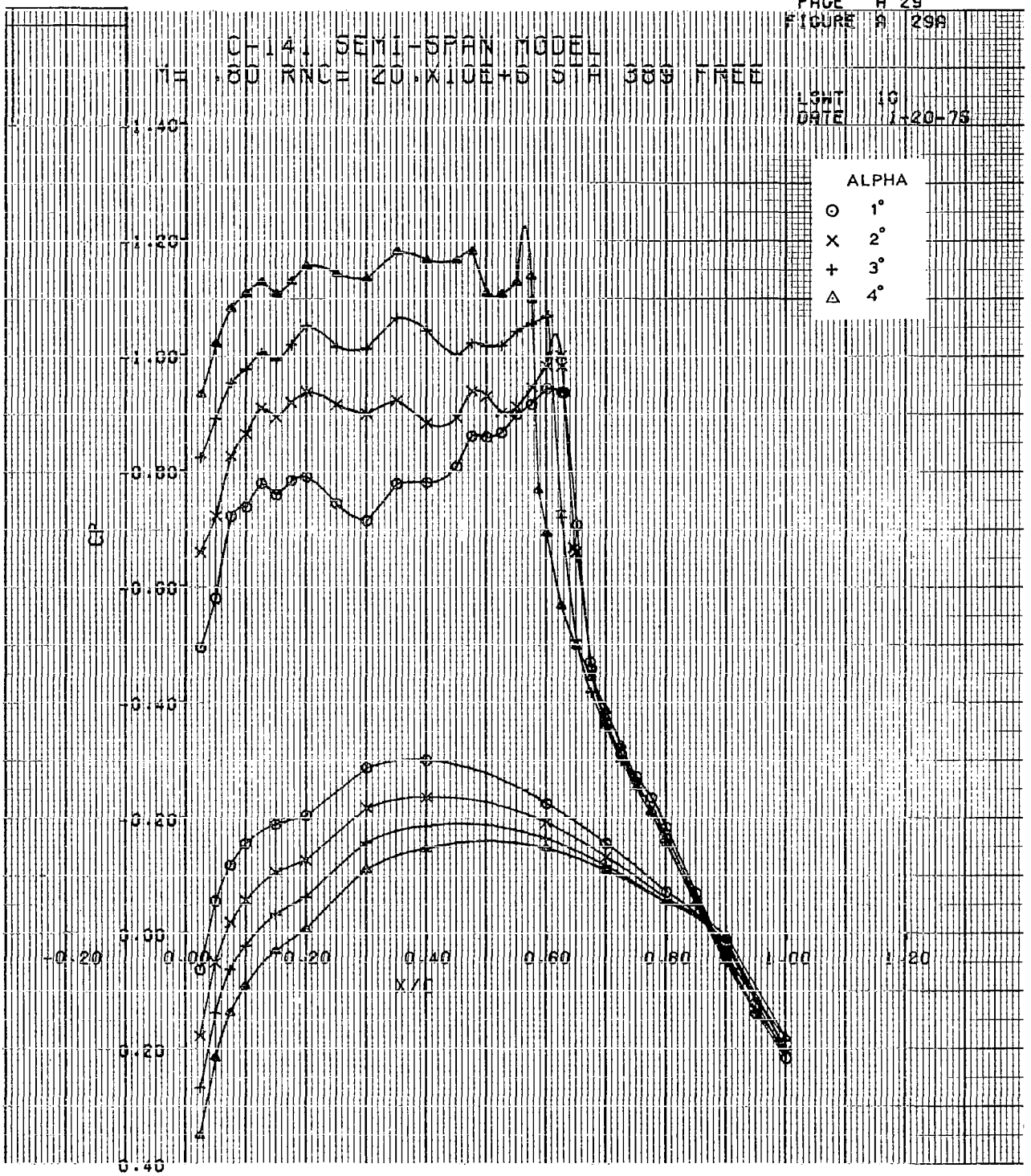
ALPHA
1°
2°
3°
4°
X/C
-0.20
0.00
0.20
0.40
0.60
0.80
1.00
1.20
0.40
0.20

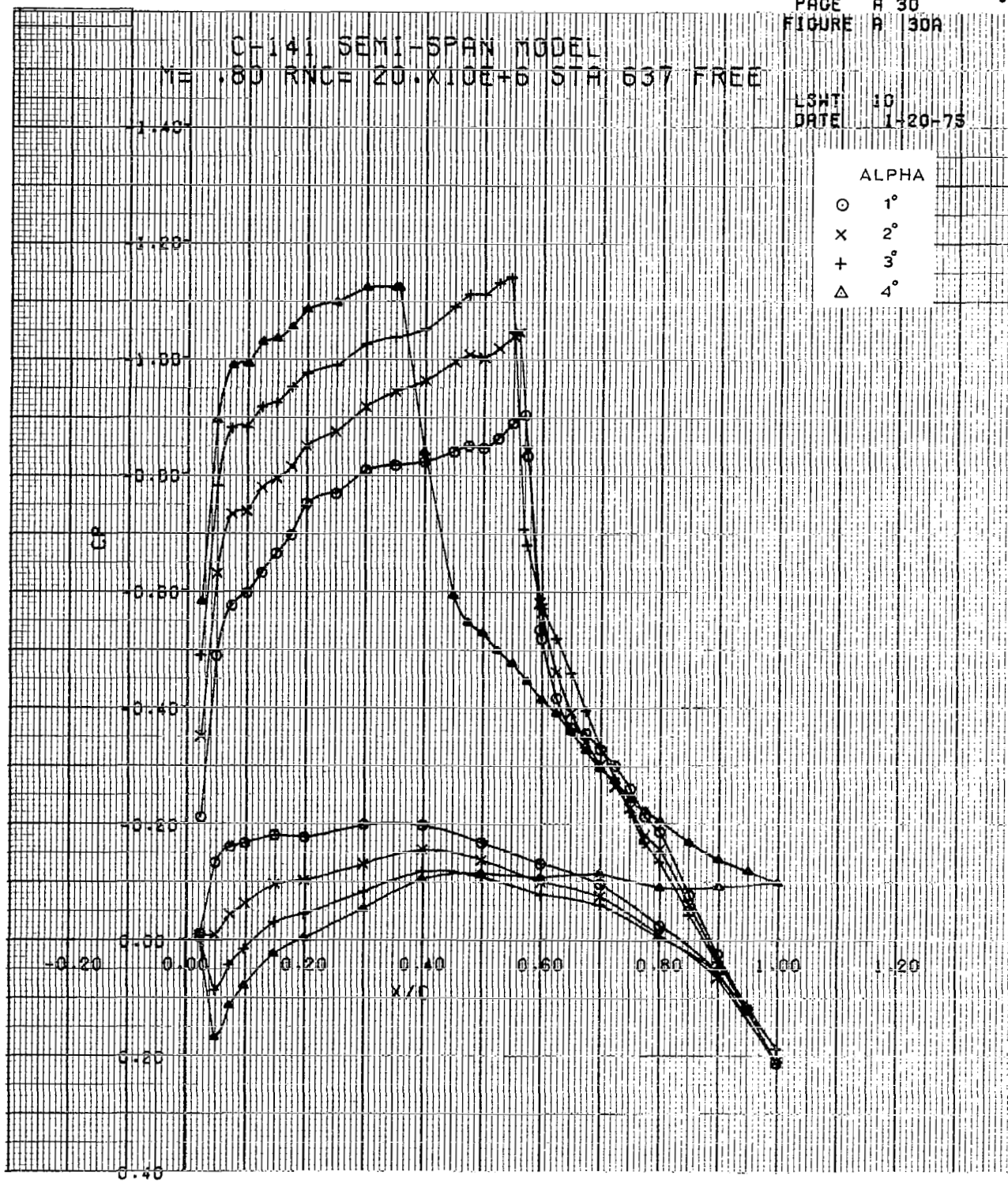
CF-141 SEMI-SPAN MODEL
M= .80 RNC= 20.X10E+6 S-A 637 FREE
LSHT 10
DATE 1-20-75
ALPHA
1°
2°
3°
4°
CP
X/C
-1.40
-1.20
-1.00
-0.80
-0.60
-0.40
-0.20
0.00
0.20
0.40
-0.20
-0.40
-0.20
0.00
0.20
0.40
0.60
0.80
1.00
1.20

FIGURE A 31A

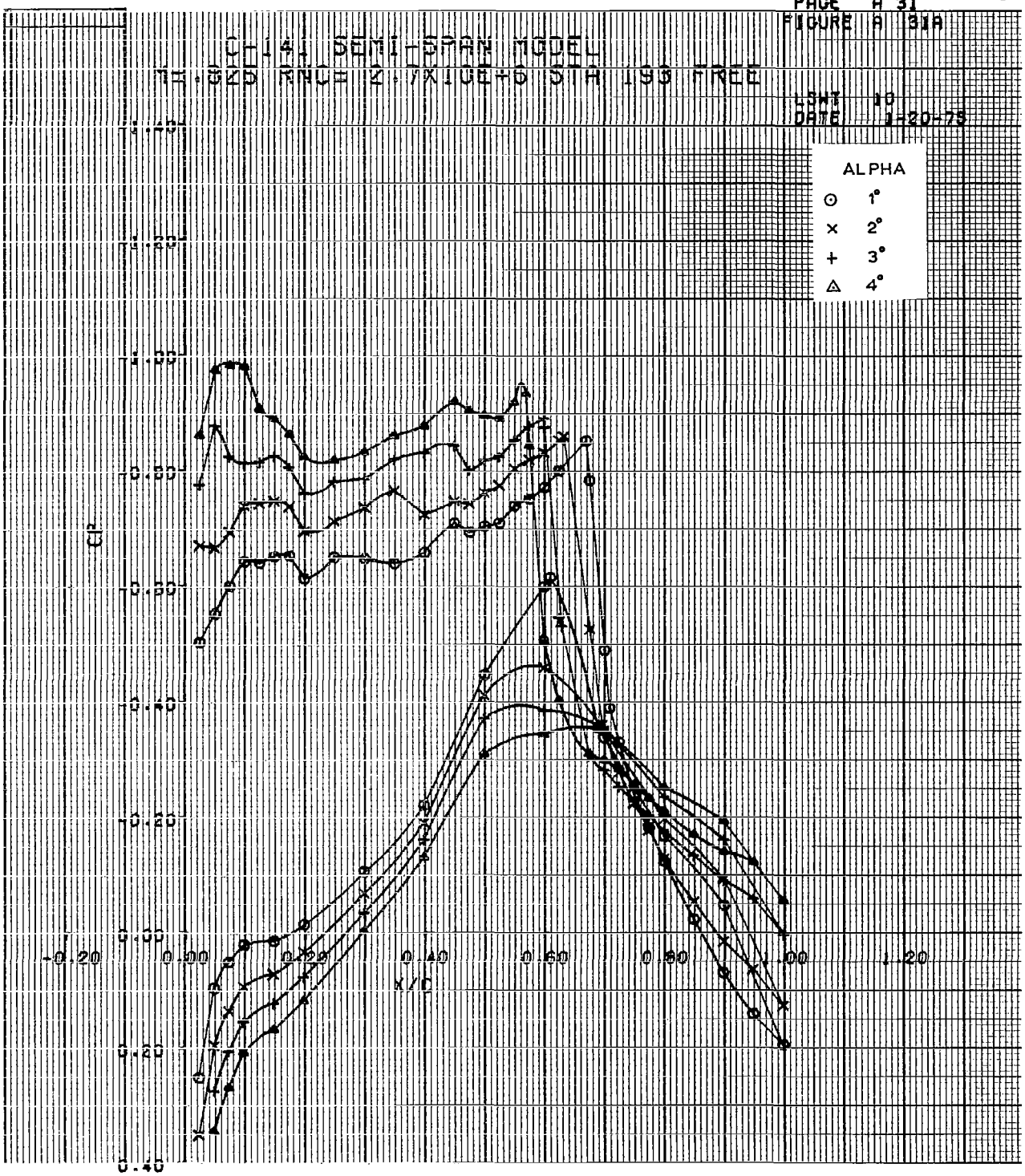
LSWT 10
DATE 1-20-75
ALPHA
⊙ 1°
× 2°
+ 3°
△ 4°
Cl²
X/C
-0.20
0.00
0.20
0.40
0.60
0.80
1.00
1.20
0.40

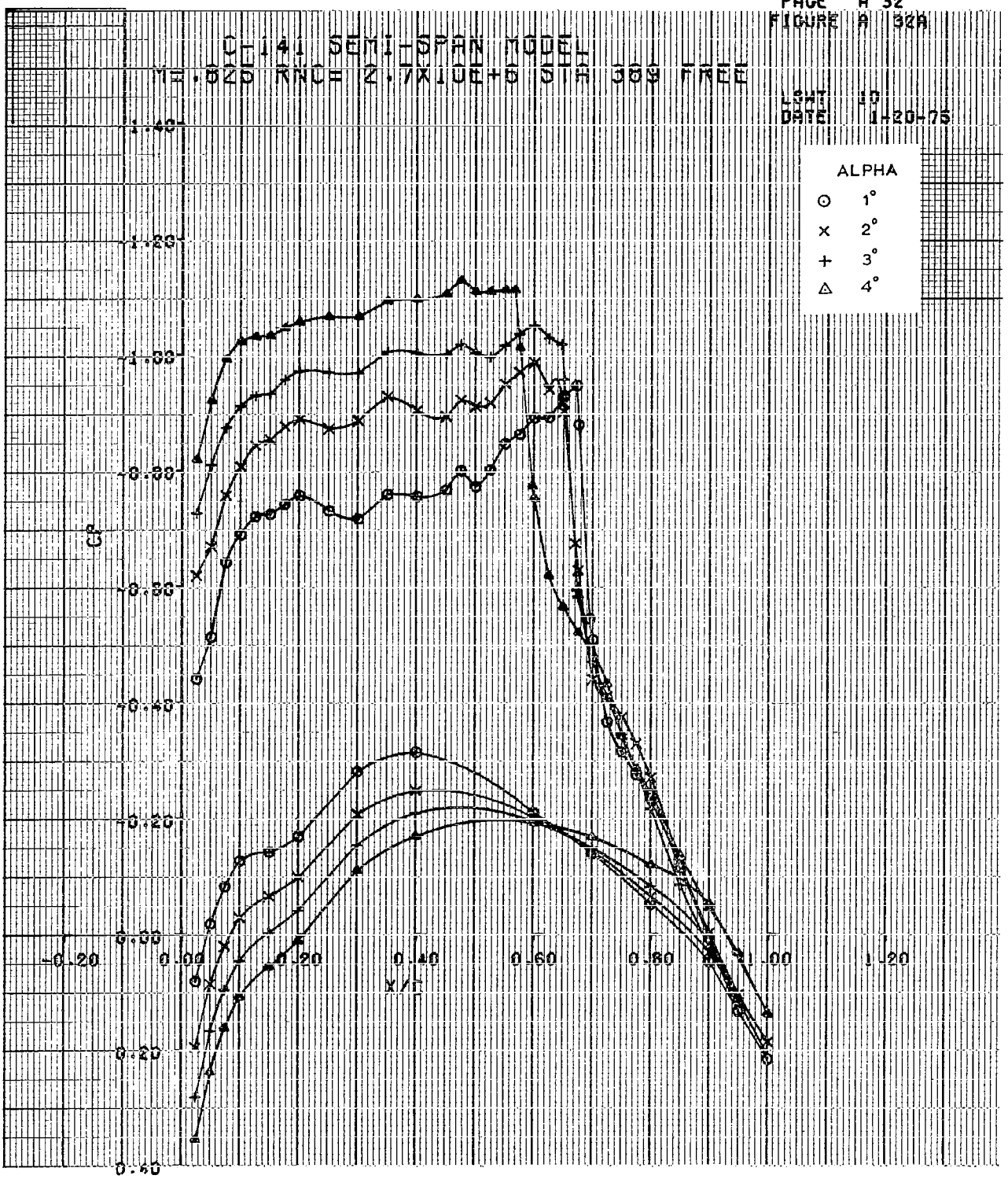
ALPHA
1°
2°
3°
4°
CP
X/L
-0.20
0.00
0.20
0.40
0.60
0.80
1.00
1.20
-0.40
-0.20
0.00
0.20
0.40

C-141 SEMI-SPAN MODEL
M=.820 RNO= 2.7X10E+06 WITH 63% TREE

RUN 10
DATE 1-20-75

ALPHA
⊙ 1°
× 2°
+ 3°
△ 4°

C_P

X/C

-0.20 0.00 0.20 0.40 0.60 0.80 1.00 1.20

0.40
0.20
0.00
-0.20
-0.40
-0.60
-0.80
-1.00
-1.20
-1.40

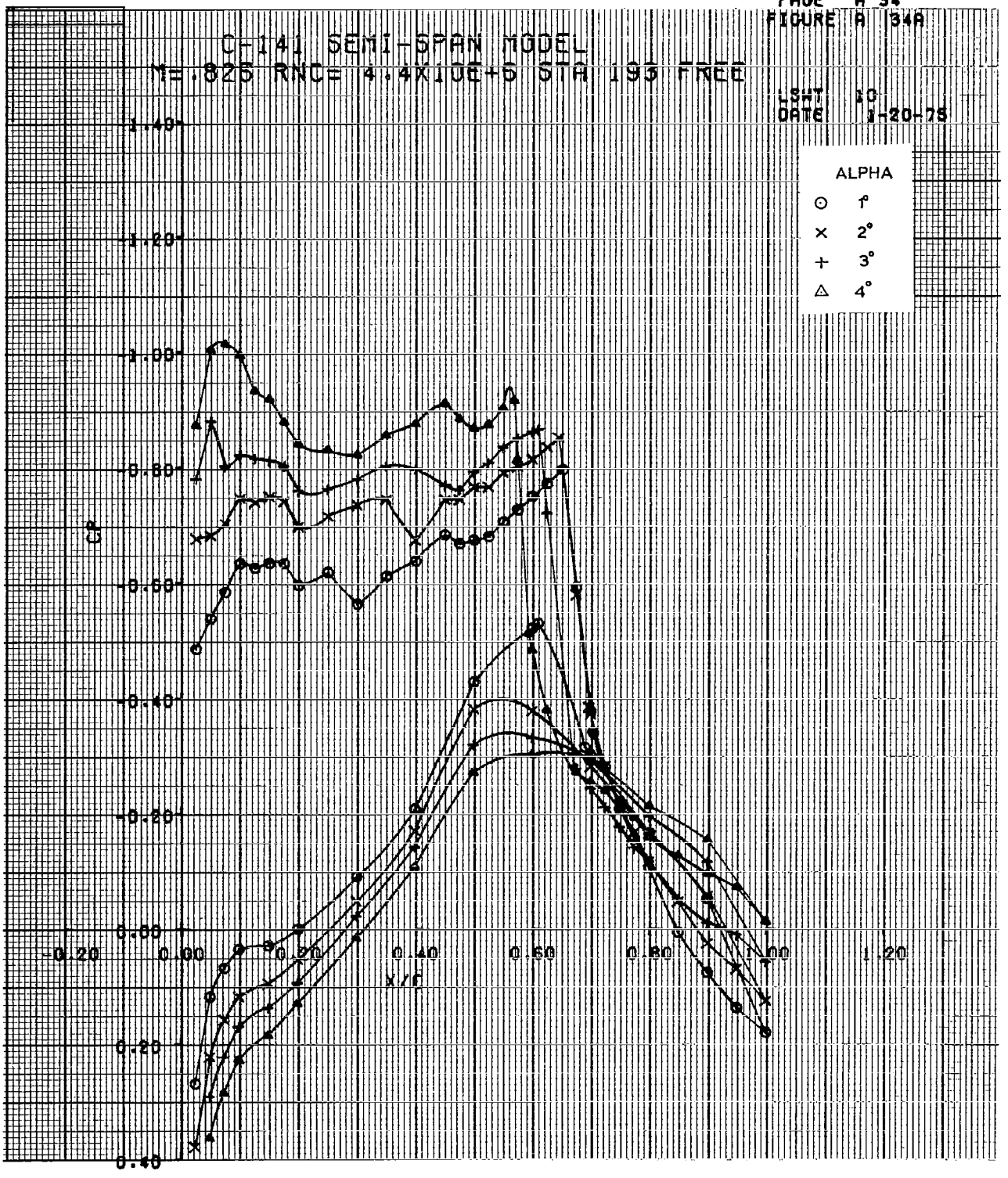
C-141 SEMI-SPAN MODEL
M=.825 RNC= 4.4X10E+6 SIH 193 FREE
LSHT 10
DATE 1-20-78
ALPHA
⊙ 1°
× 2°
+ 3°
△ 4°
CP
-1.40
-1.20
-1.00
-0.80
-0.60
-0.40
-0.20
0.00
0.20
0.40
-0.20
0.00
0.20
0.40
0.60
0.80
1.00
1.20
X/C

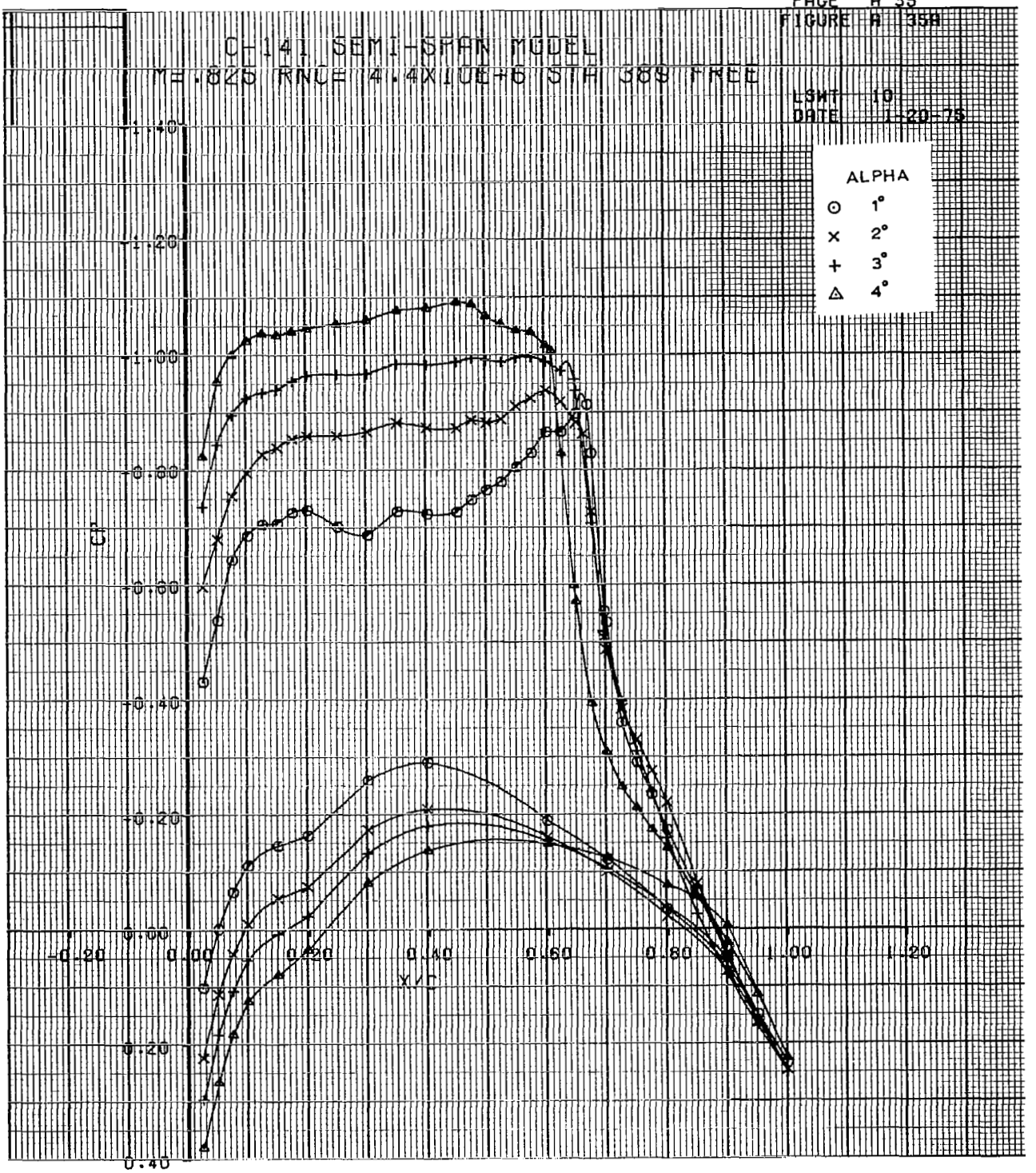
CF-141 SEMI-SPAN MODEL
M=.825 RNUE 4.4X10E+6 STA 388 FREE
LSHT 10
DATE 1-20-75
ALPHA
⊙ 1°
× 2°
+ 3°
△ 4°
CL
1.40
1.20
1.00
+0.80
+0.60
+0.40
+0.20
0.00
0.20
0.40
-0.20
0.00
0.20
0.40
0.60
0.80
1.00
1.20
X/C

C-141 SEMI-SPAN MODEL
M=.825 RNC= 4.4X10E+6 STH 637 FREE

LSWT 10
DATE 1-20-75

ALPHA
⊙ 1°
× 2°
+ 3°
△ 4°

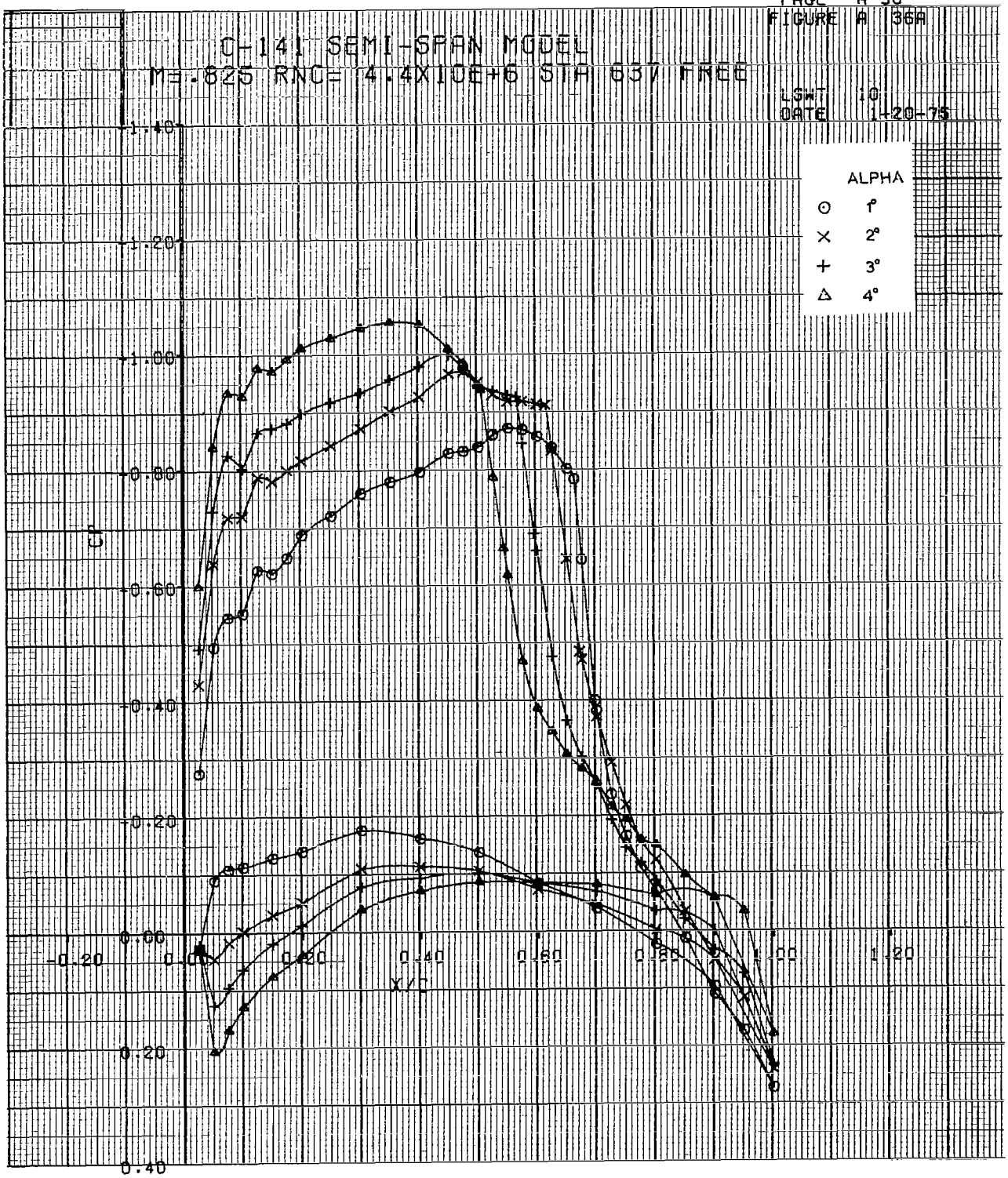

C-141 SEMI-SPAN MODEL
M=.825 RNL=6.0X10E+6 STH 193 FREE

LSWT 10
DATE 1-20-78

ALPHA
⊙ 1°
× 2°
+ 3°
△ 4°

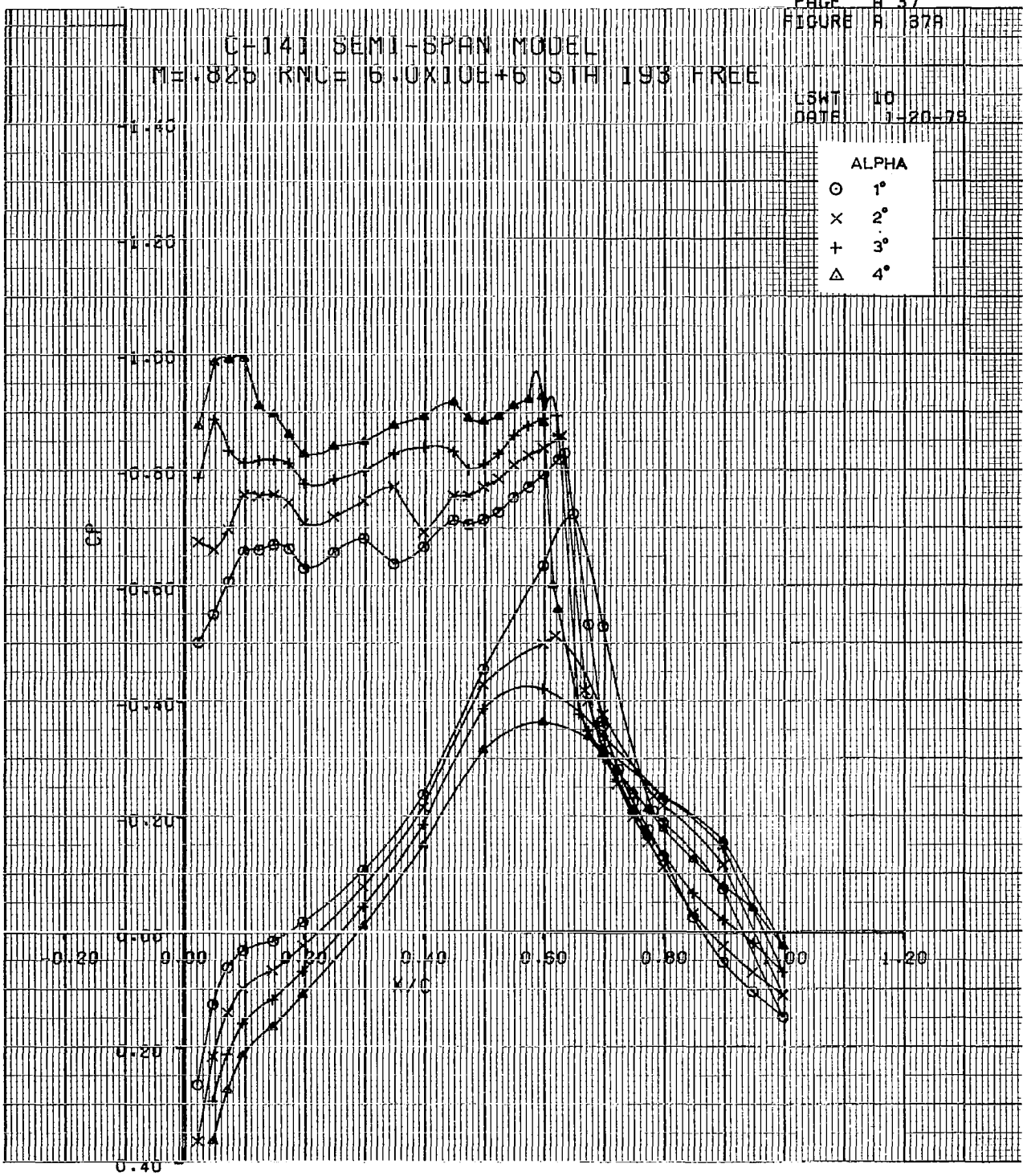

CL14: SEMI-SPAN MODEL
ME.82D KNUE S.UXLUE+6 SA 38S FREE

LIMIT 10
DATE 1420-75

ALPHA
⊙ 1°
× 2°
+ 3°
△ 4°

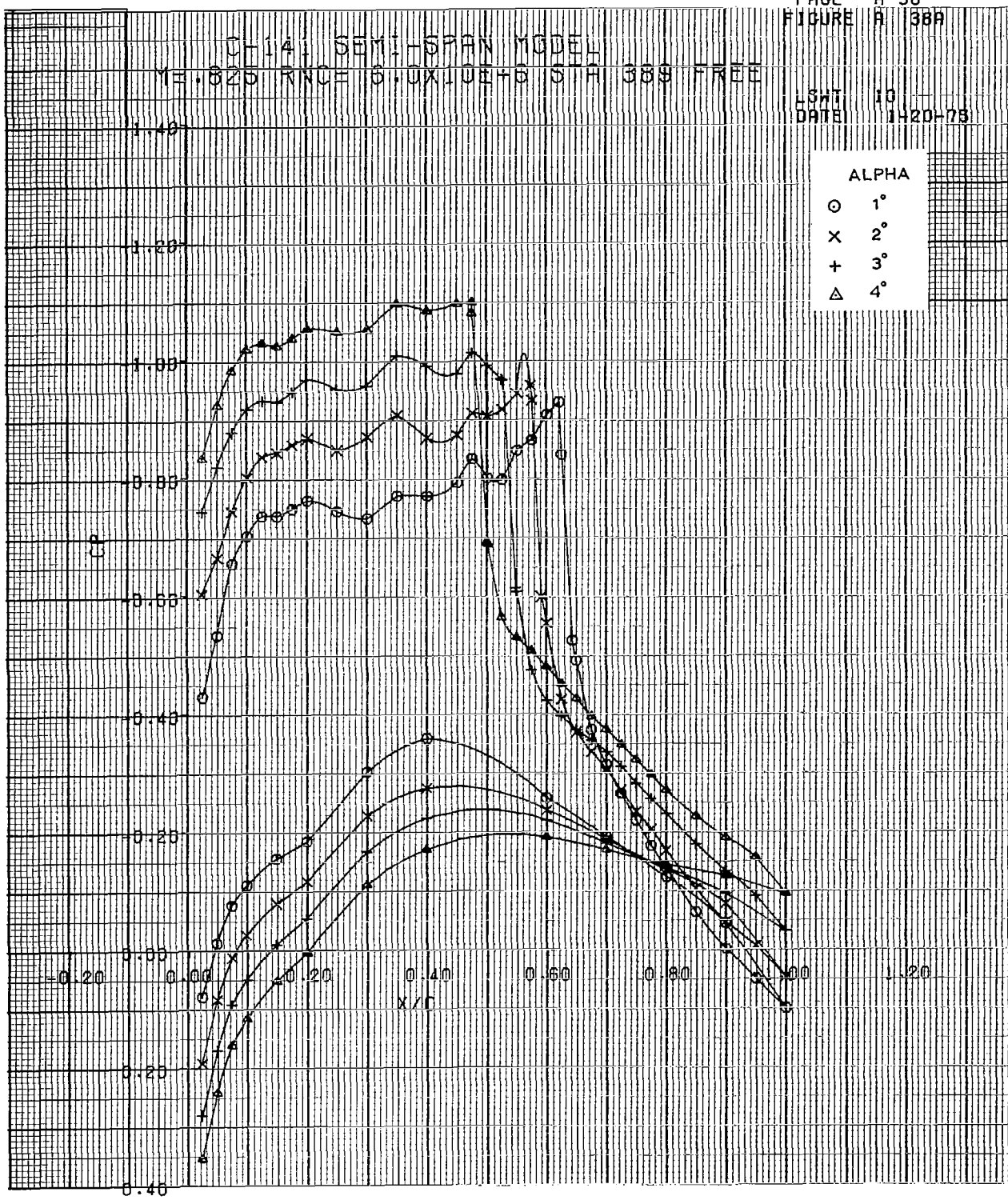

FIGURE A 39A

CT 14, SEMI-SPAN MODEL
M∞ .825 RN/ft 6.0x10E+6 S.F. 63% FREE

LSWT 10
DATE 1-20-75

ALPHA
⊙ 1°
× 2°
+ 3°
△ 4°

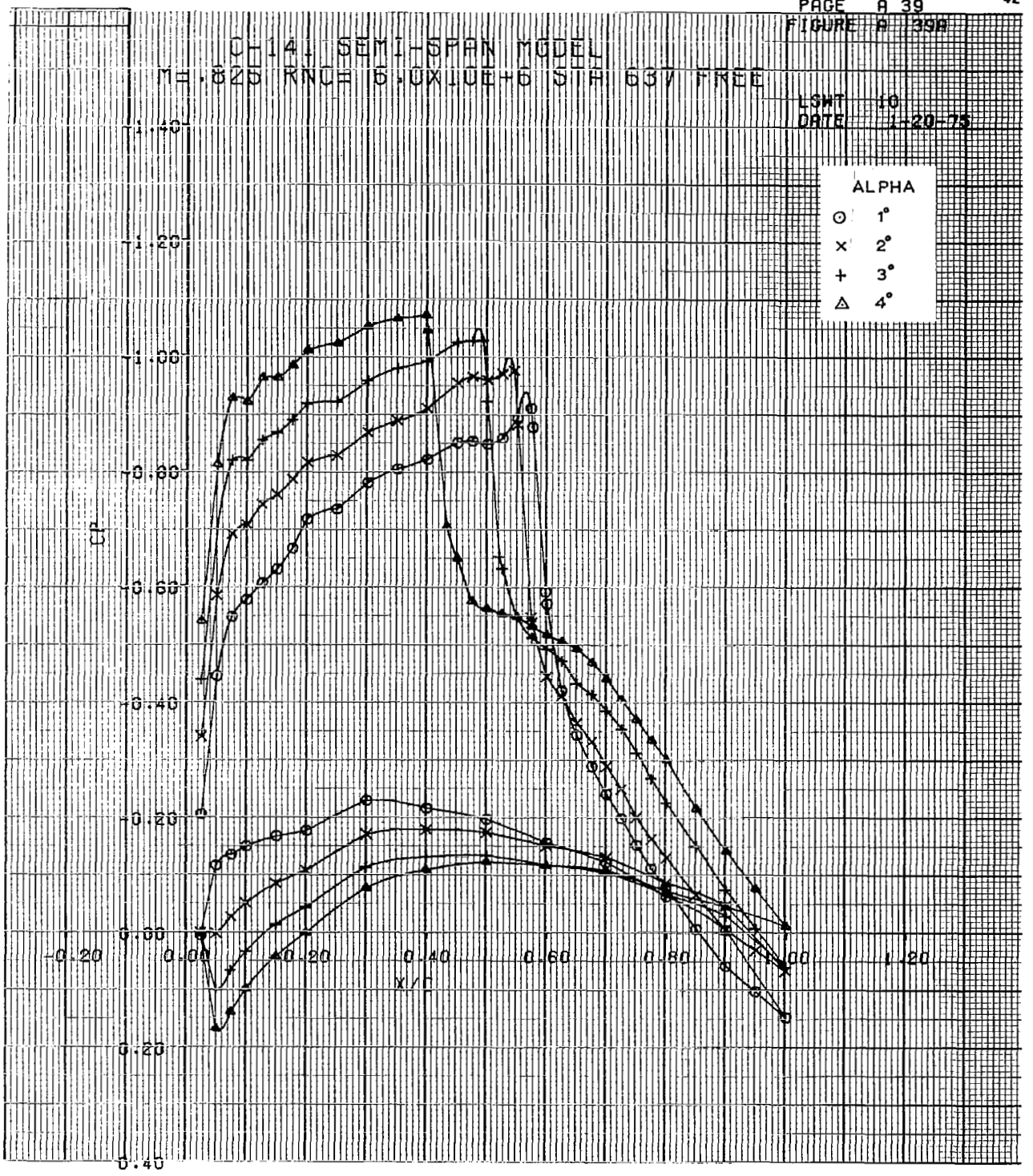

C-141 SEMI-SPAN MODEL
M=.825 RNC= 6.0X10E+6 STA 193 FREE

LSHT 10
DATE 1-20-78

ALPHA
⊙ 1°
× 2°
+ 3°
△ 4°

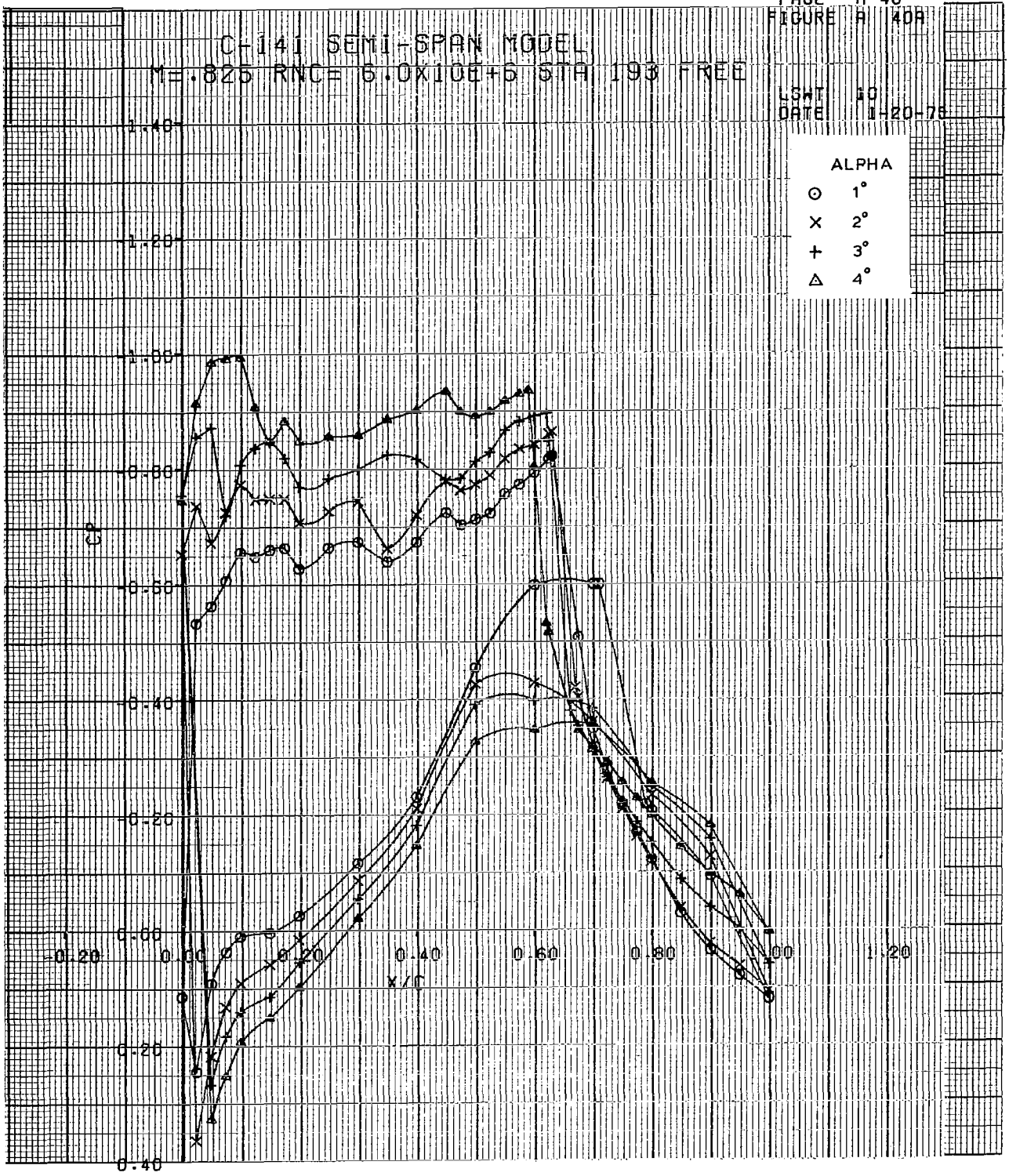

FIGURE A 41A

C-141 SEMI-SPAN MODEL
M=.825 RNC= 6.0X10E+6 STA 389 FREE

LSHT 10
DATE 1-20-75

ALPHA
⊙ 1°
× 2°
+ 3°
△ 4°

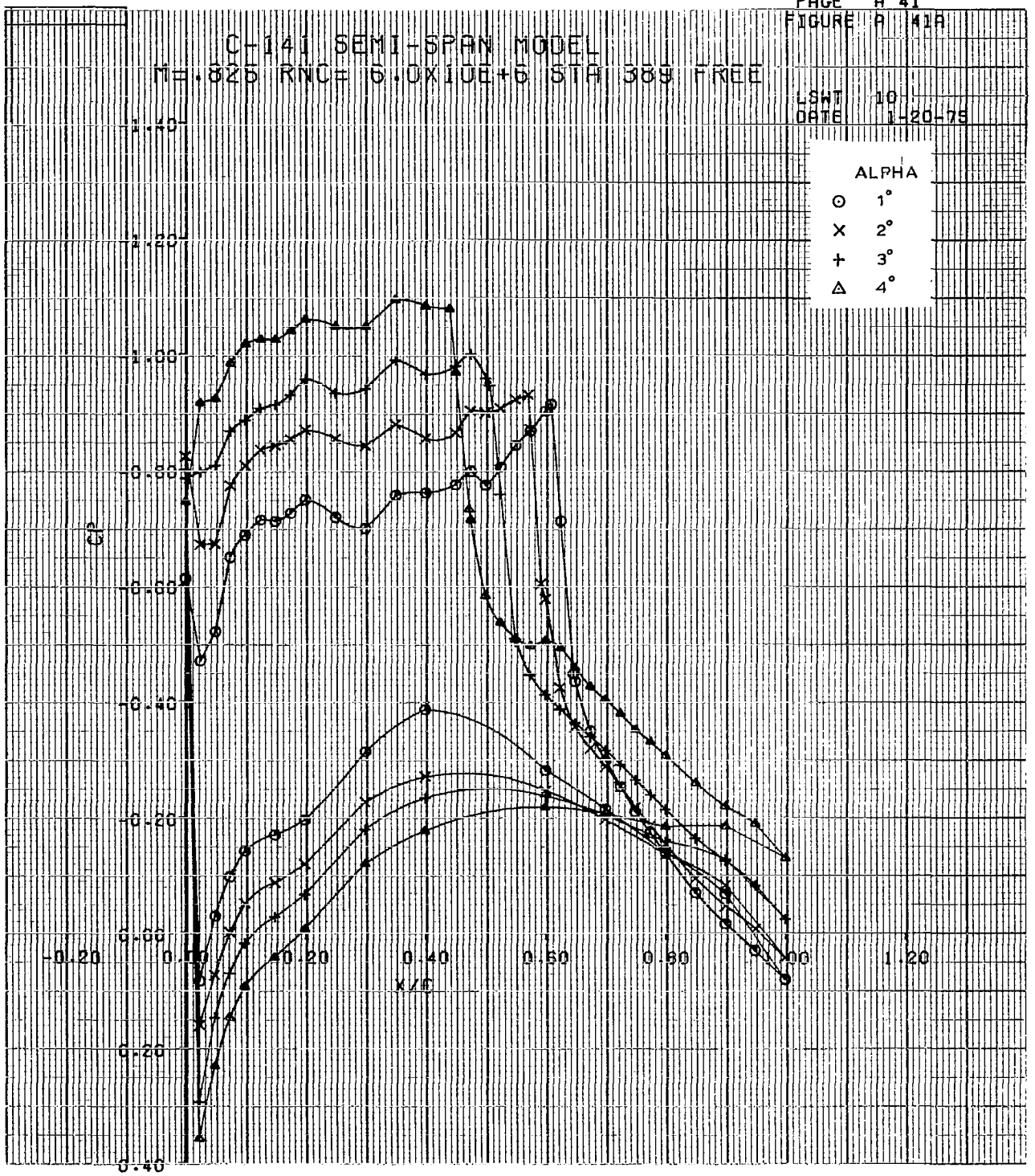

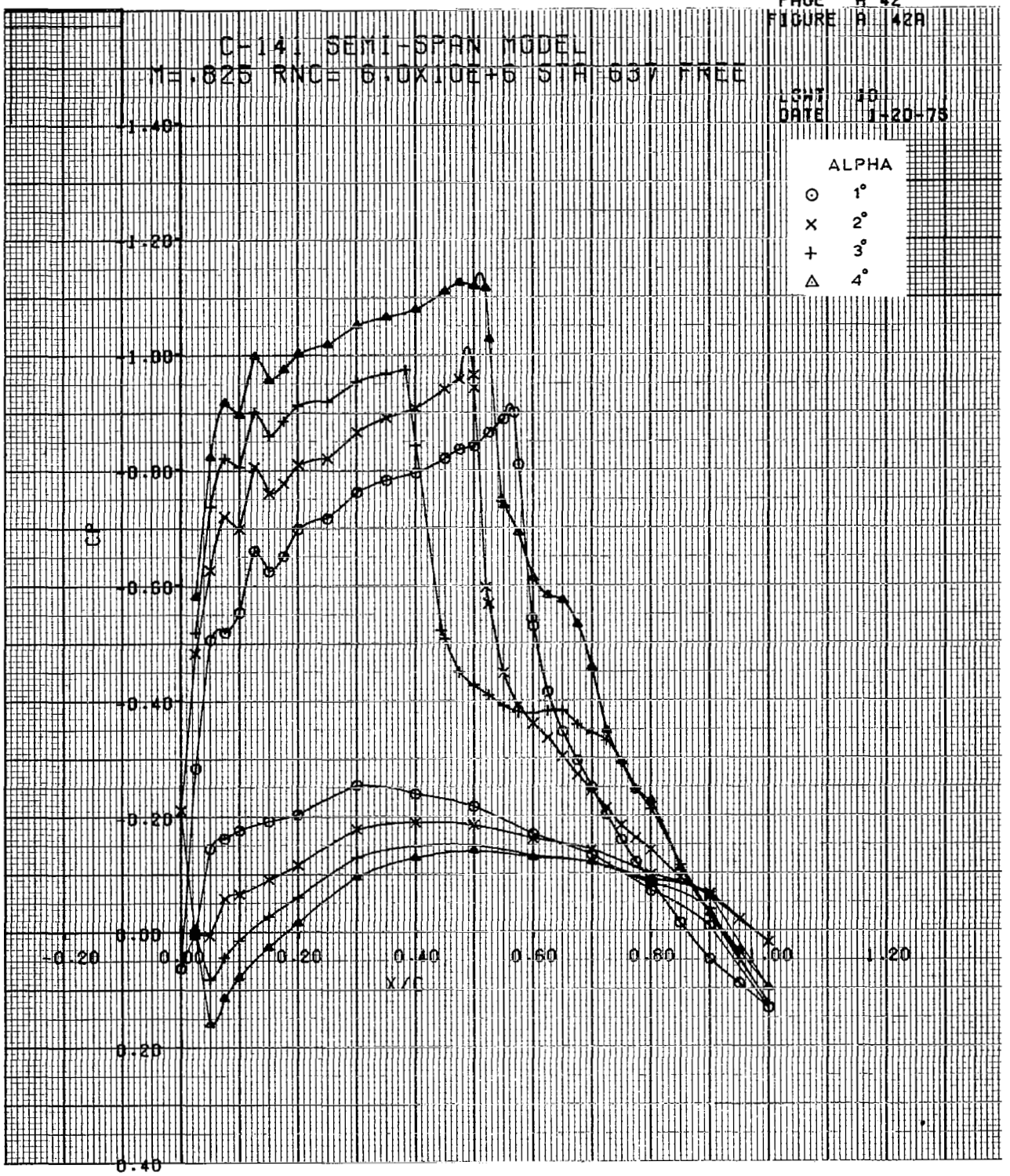
C-14, SEMI-SPAN MODEL
M=.825 RNC= 6.0X10E+6 S A 63J FREE
LSHT 10
DATE 1-20-75
ALPHA
1°
2°
3°
4°
-1.40
-1.20
-1.00
-0.80
-0.60
-0.40
-0.20
0.00
0.20
0.40
-0.20
0.00
0.20
0.40
0.60
0.80
1.00
1.20
X/C

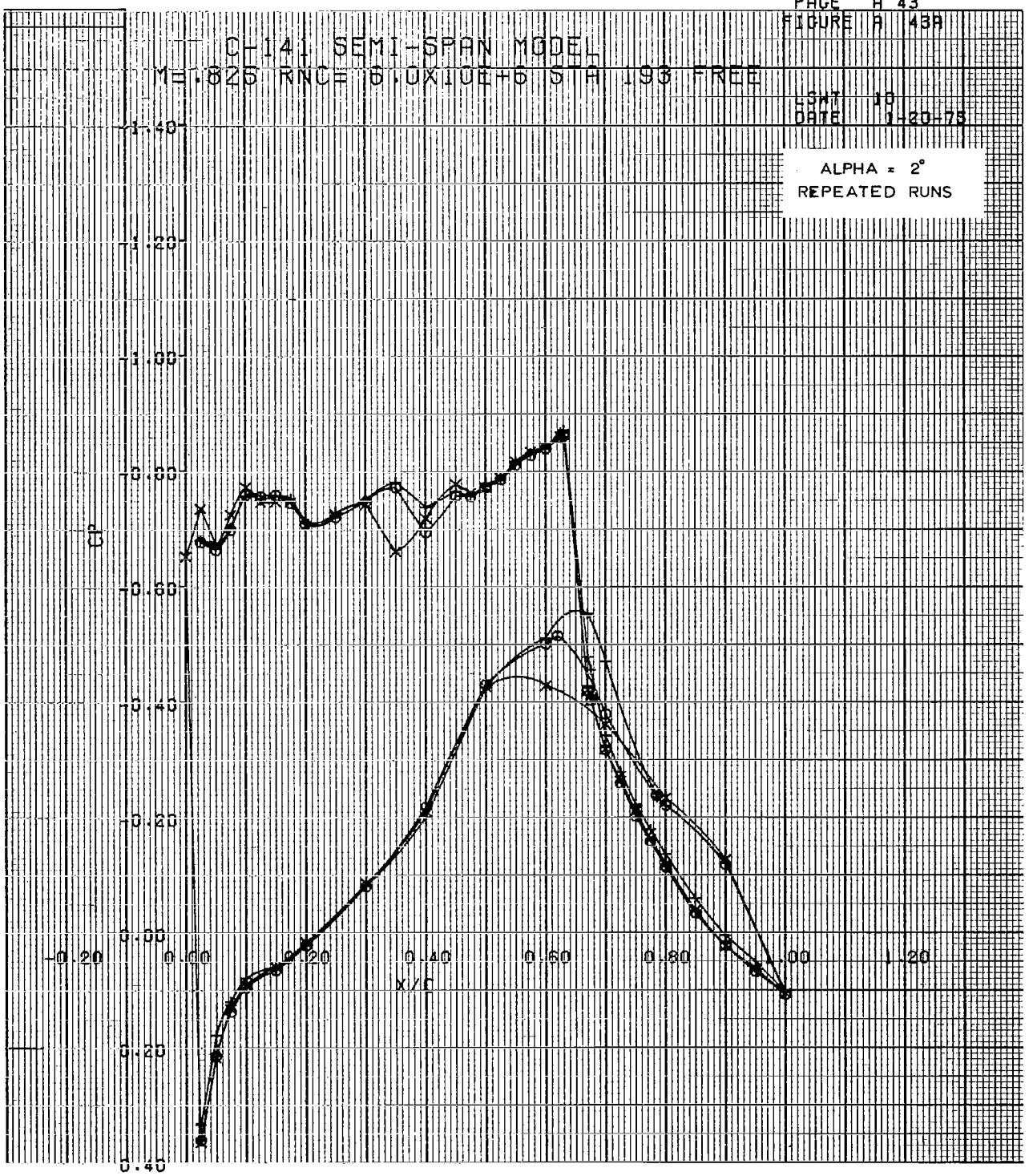
CL14, SEMI-SPAN MODEL
M=.825 RNC= 6.0X10E+6 S/F .193 FREE
CNT 10
DATE 1-20-75
ALPHA = 2°
REPEATED RUNS
CP
X/C
1.40
1.20
1.00
0.80
0.60
0.40
0.20
0.00
-0.20
-0.40
-0.20
0.00
0.20
0.40
0.60
0.80
1.00
1.20

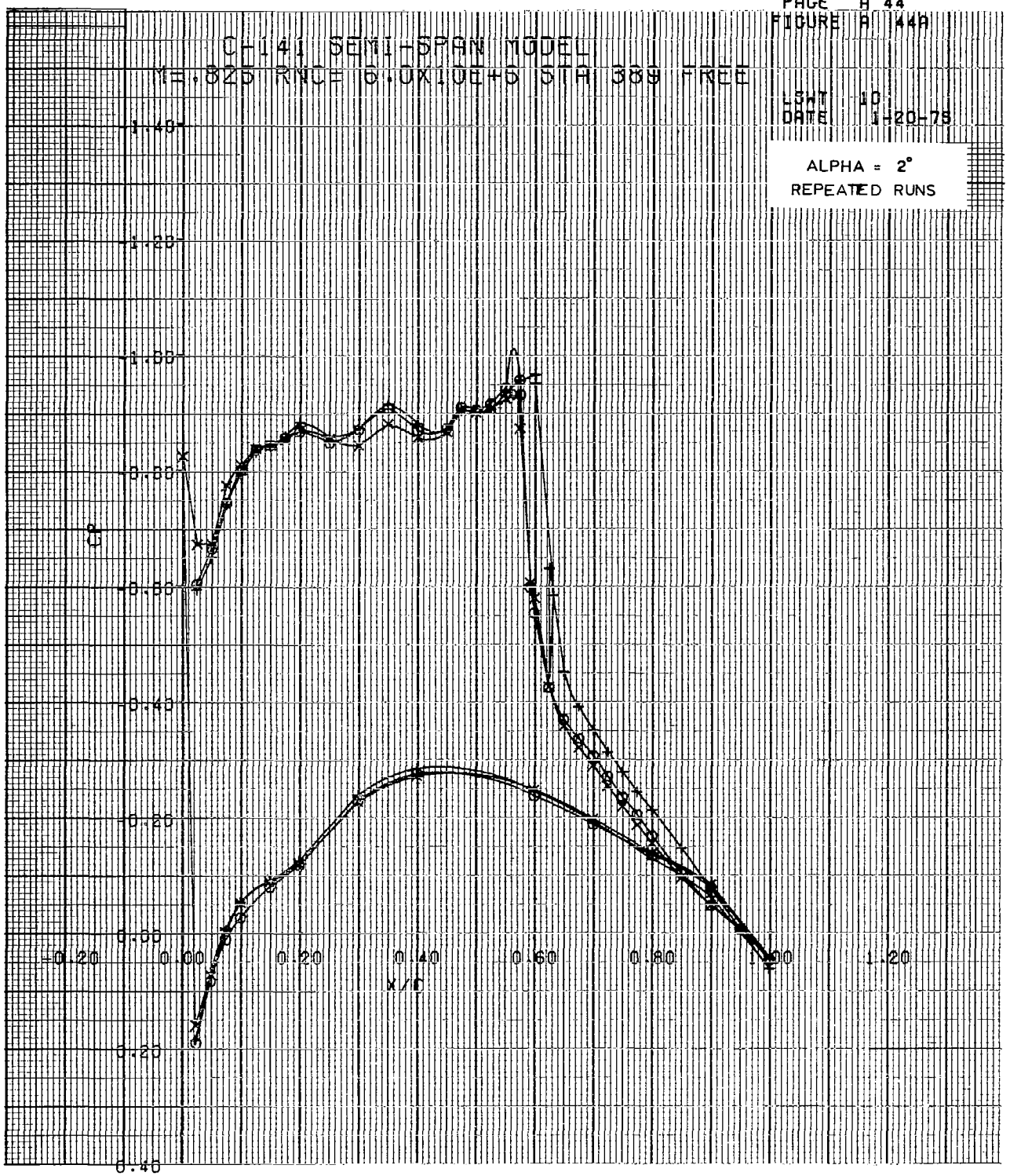
C-141 SEMI-SPAN MODEL
M=.825 RNC= 6.0X10E+6 STR 385 FREE
RUN 10
DATE 1-20-78
ALPHA = 2°
REPEATED RUNS
Cp
1.40
1.20
1.00
0.80
0.60
0.40
0.20
0.00
0.20
0.40
0.60
0.80
1.00
1.20
X/C

FIGURE A 46A

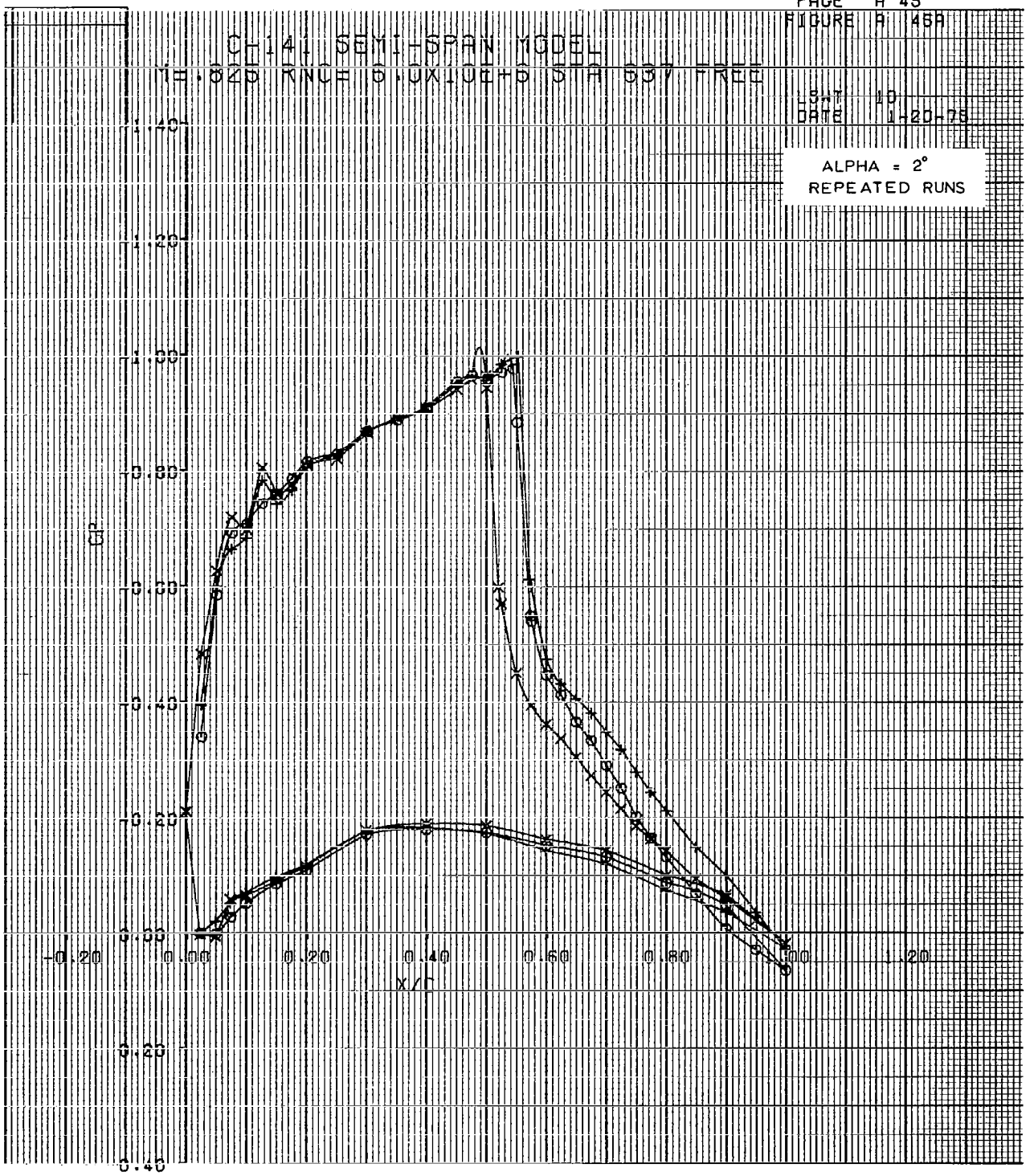
C-14 SEMI-SPAN MODEL
M = 0.820 RNUB = 6.0X10**6 STRIP GRIT FREE
RUN 10
DATE 1-20-76
ALPHA = 2°
REPEATED RUNS
CP
X/C
-0.20
0.00
0.20
0.40
0.60
0.80
1.00
1.20
-1.40
-1.20
-1.00
-0.80
-0.60
-0.40
-0.20
0.00
0.20
0.40

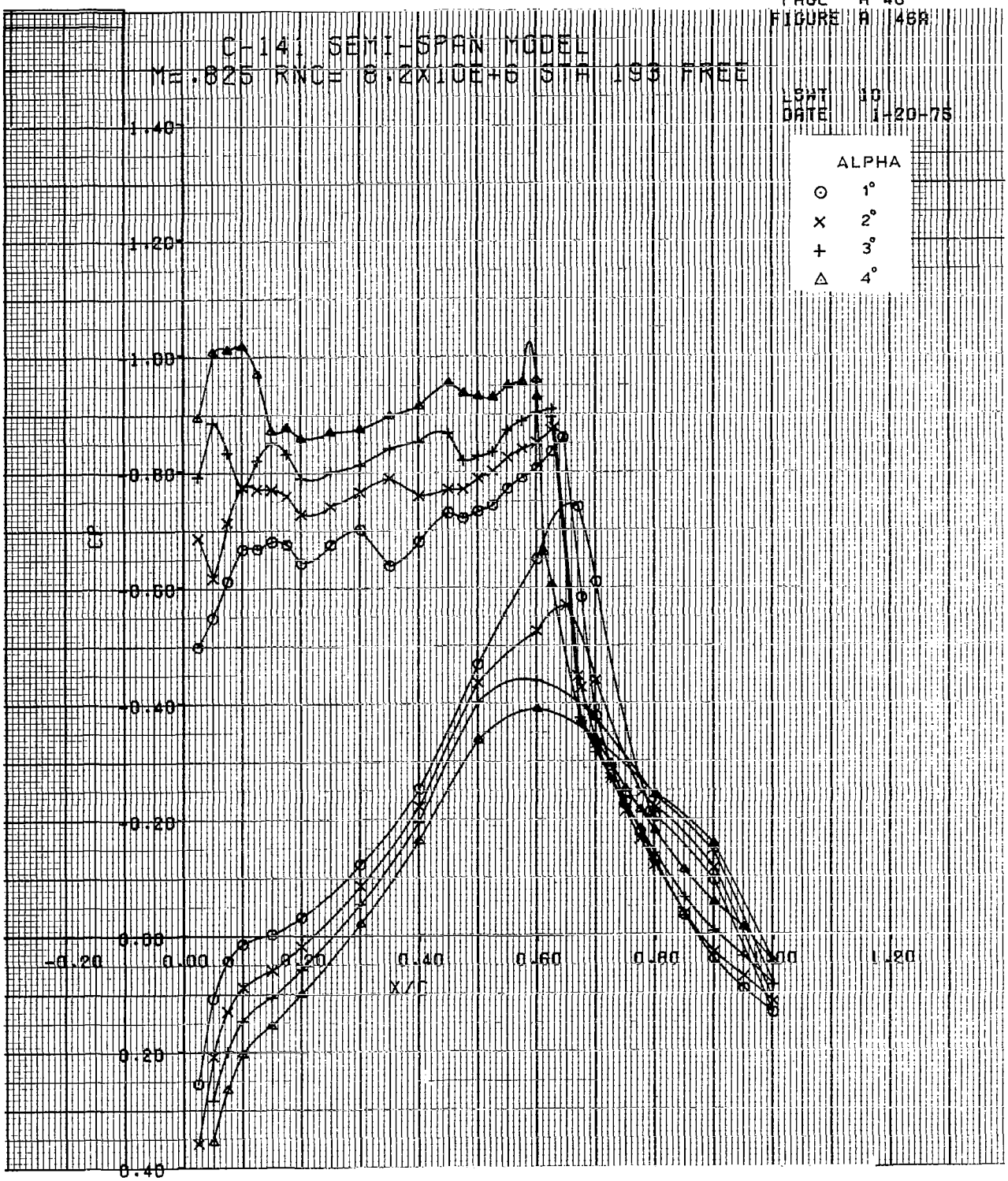
CL-14, SEMI-SPAN MODEL
M=.825 RNCE 8.2X10E+6 SLH 1SS FREE
LSWT 10
DATE 1-20-75
ALPHA
1°
2°
3°
4°
CL
X/C
1.40
1.20
1.00
0.80
0.60
0.40
0.20
0.00
-0.20
-0.40
-0.20
0.00
0.20
0.40
0.60
0.80
1.00
1.20

C-141 SEMI-SPAN MODEL
M=.825 RNC= 8.2X10E+6 STA 389 FREE

LSHT 10
DATE 1-20-75

ALPHA
⊙ 1°
× 2°
+ 3°
△ 4°

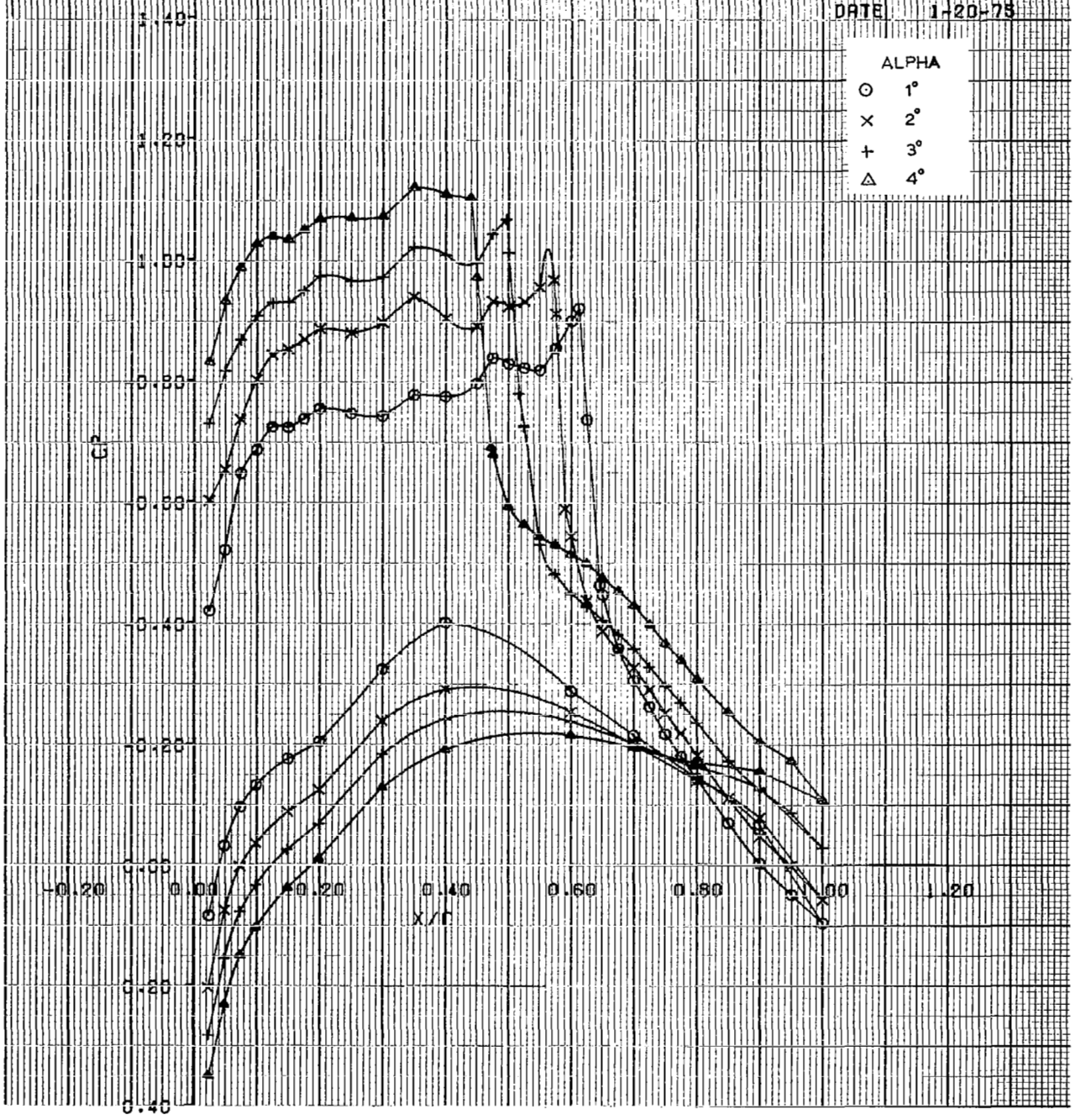

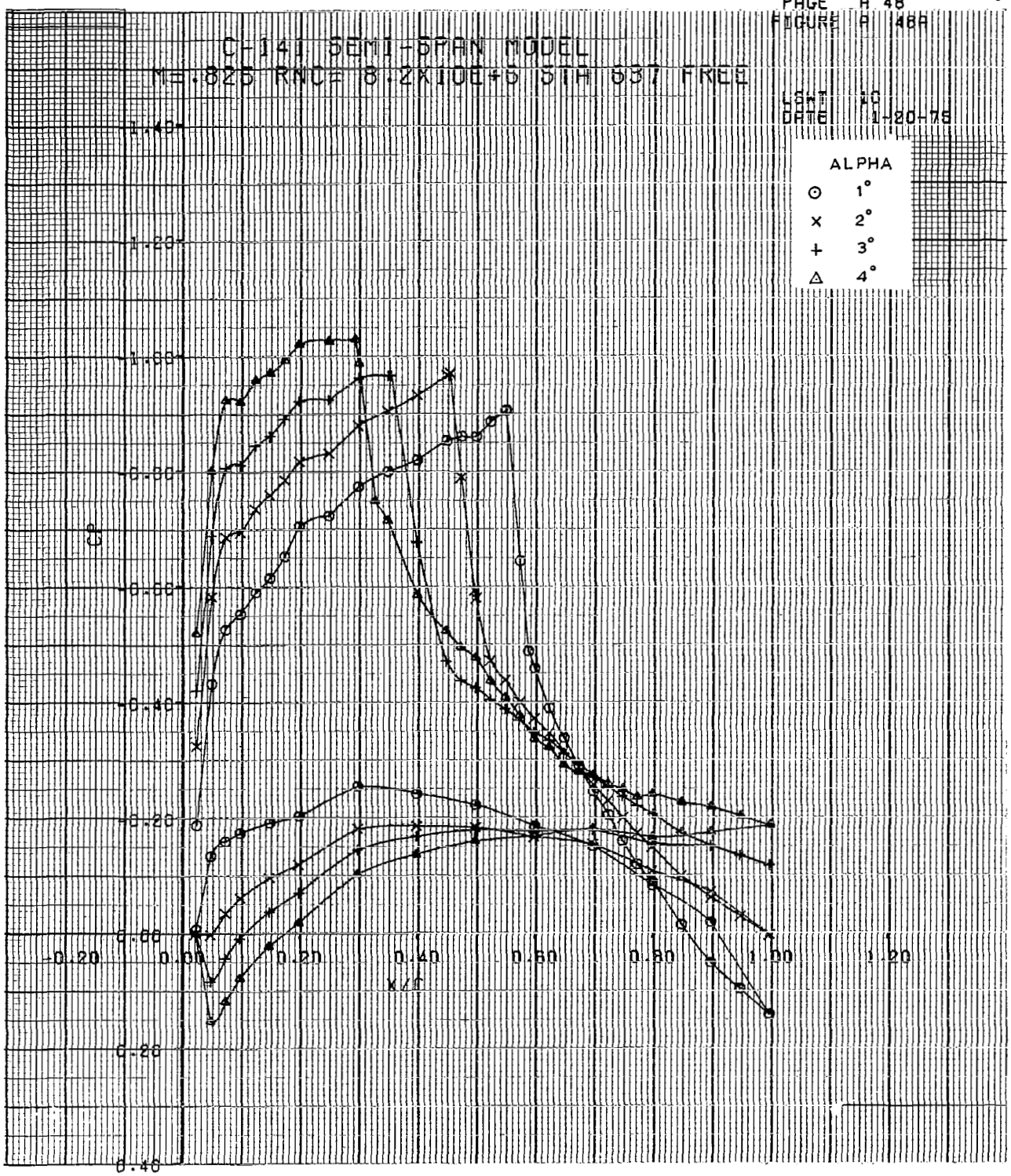
C-141 SEMI-SPAN MODEL
M=.825 RNC= 8.2X10E+6 5TH 65% FREE
LOAT
DATE 1-20-75
ALPHA
⊙ 1°
× 2°
+ 3°
△ 4°
1.40
1.20
1.00
0.80
0.60
0.40
0.20
0.00
-0.20
-0.40
-0.60
-0.80
-1.00
-1.20
-1.40
CL
CD
-0.20
0.00
0.20
0.40
0.60
0.80
1.00
1.20
X/C

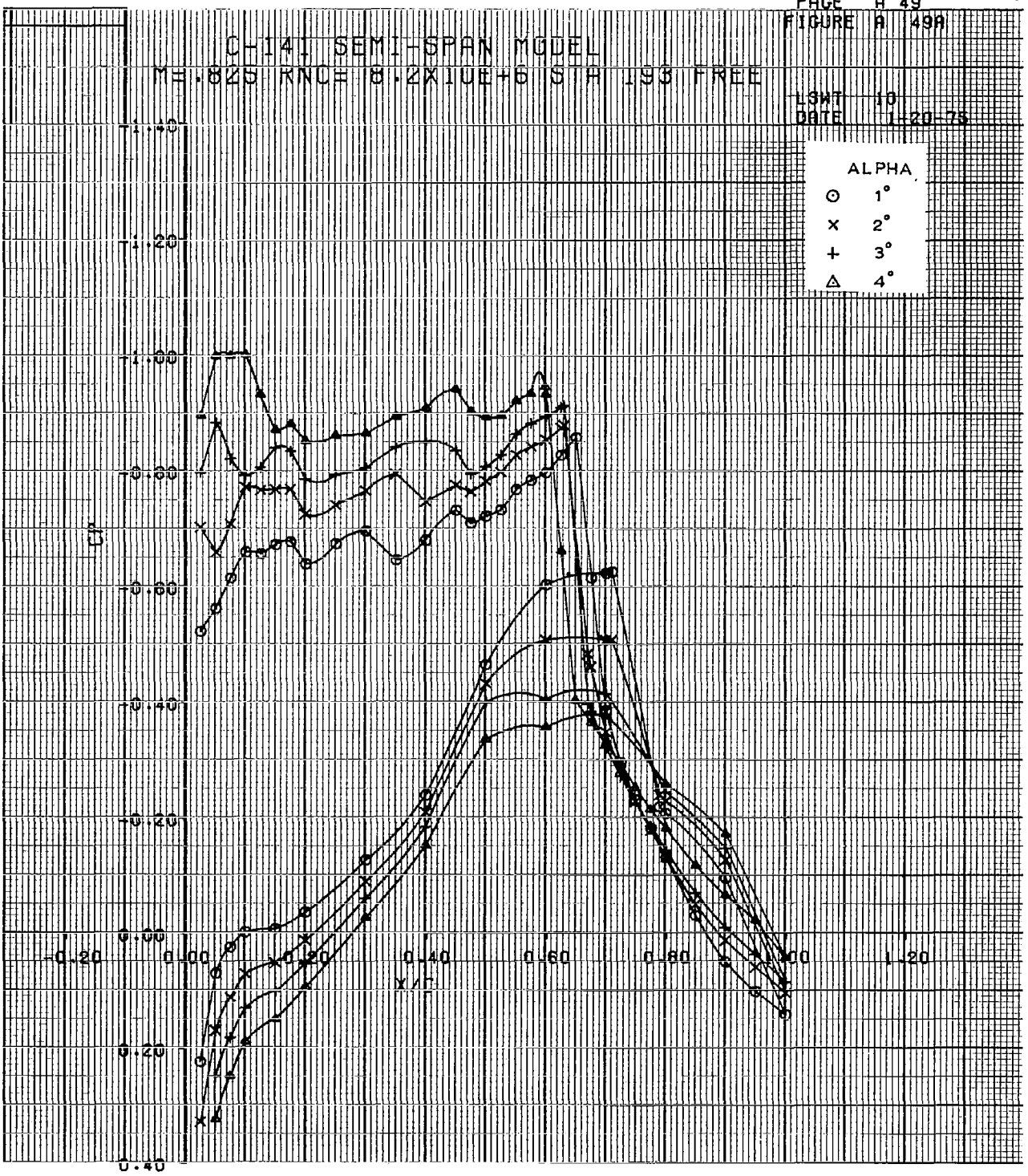
C-141 SEMI-SPAN MODEL
M=.825 RNC= 8.2X10E+6 S A 193 FREE
LSWT 10
DATE 1-20-75
ALPHA
⊙ 1°
× 2°
+ 3°
△ 4°
CL
Y/B
-0.20
0.00
0.20
0.40
0.60
0.80
1.00
1.20

FIGURE A 50A

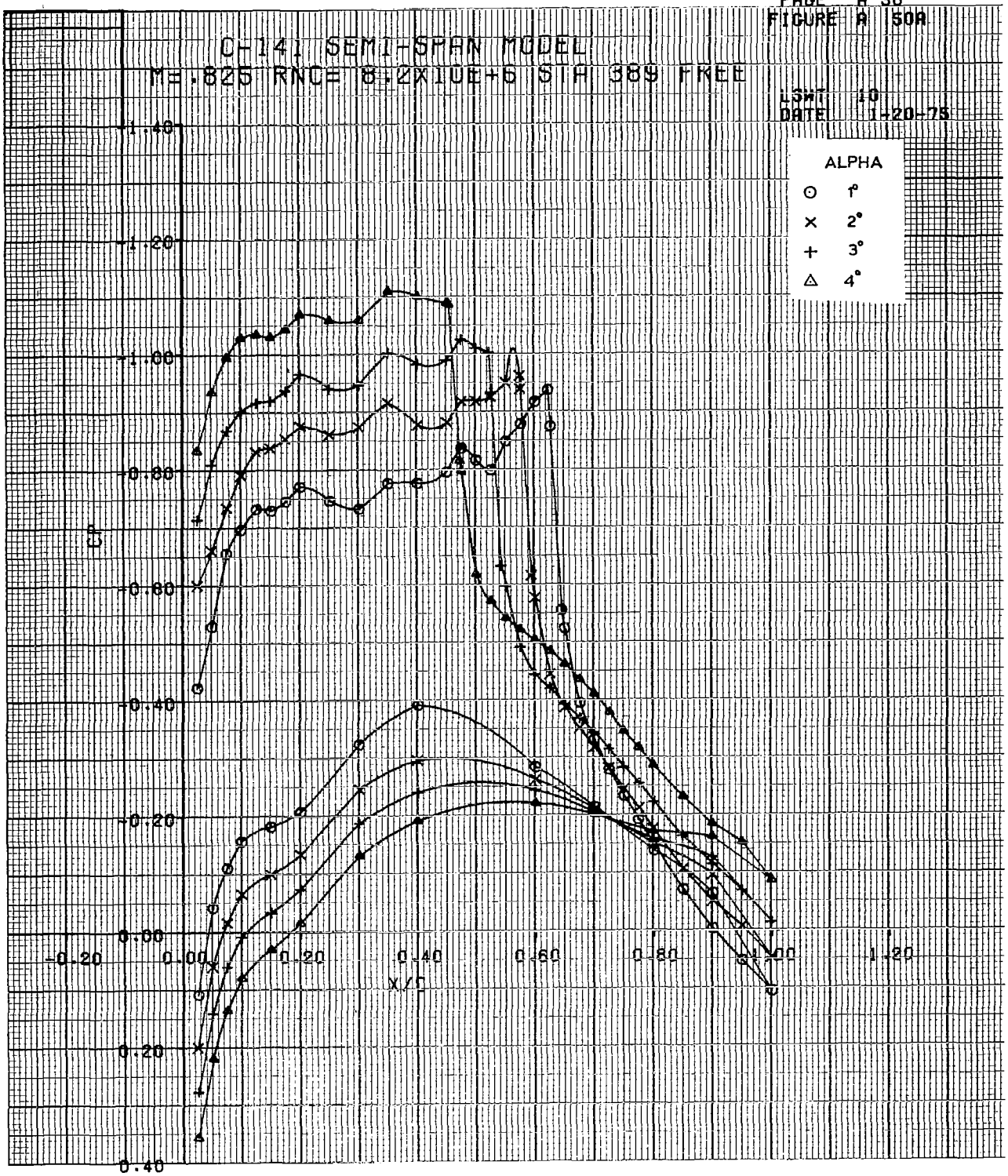
CH-141 SEMI-SPAN MODEL
M= .825 RNC= 8.2X10E+6 SIM 389 FREE
LIMIT 10
DATE 1-20-75
ALPHA
⊙ 1°
× 2°
+ 3°
△ 4°
CP
1.40
1.20
1.00
0.80
0.60
0.40
0.20
0.00
0.20
-0.20
0.00
0.20
0.40
0.60
0.80
1.00
1.20
X/C

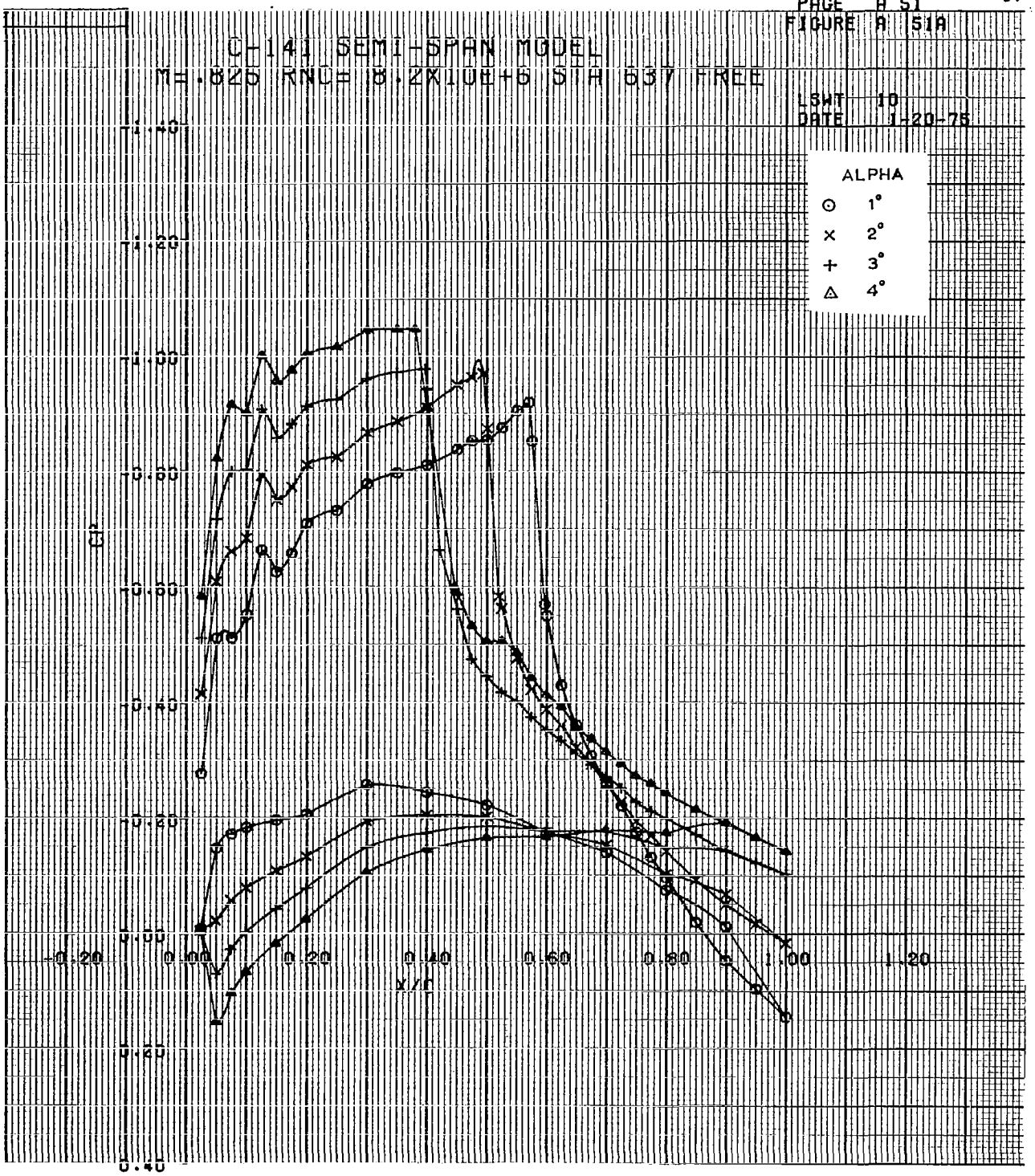
CL-141 SEMI-SPAN MODEL
M=.825 RNUM= 8.2X10E+6 SIM 65% FREE
LSHT 10
DATE 1-20-75
ALPHA
1°
2°
3°
4°
CP
X/C
-0.20
0.00
0.20
0.40
0.60
0.80
1.00
1.20
0.40

FIGURE A 52A

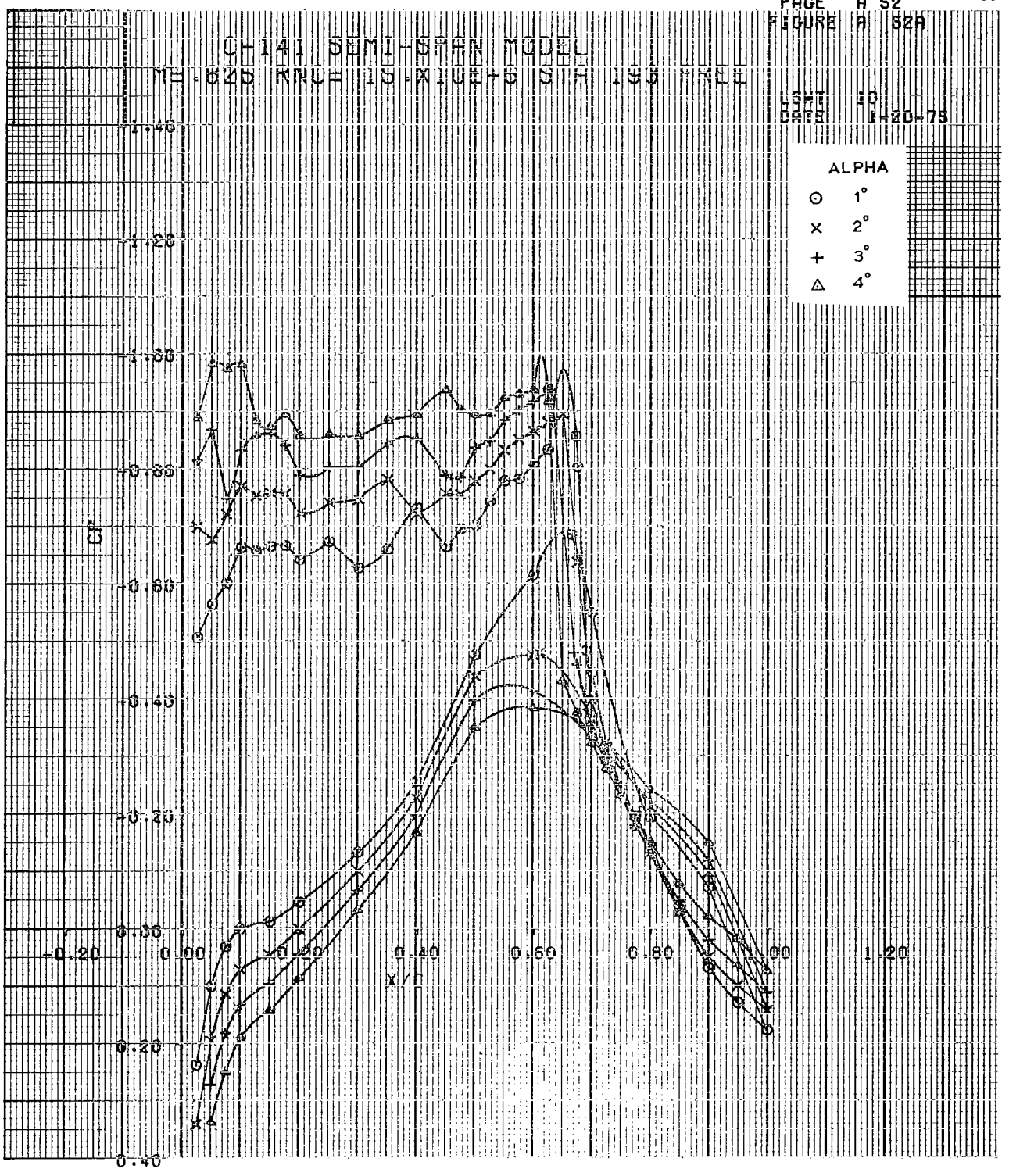
ALPHA
1°
2°
3°
4°
CASE 5C
DATE 1-20-75
-1.40
-1.20
-1.00
-0.80
-0.60
-0.40
-0.20
0.00
0.20
0.40
-0.20
0.00
0.20
0.40
0.60
0.80
1.00
1.20
X/C

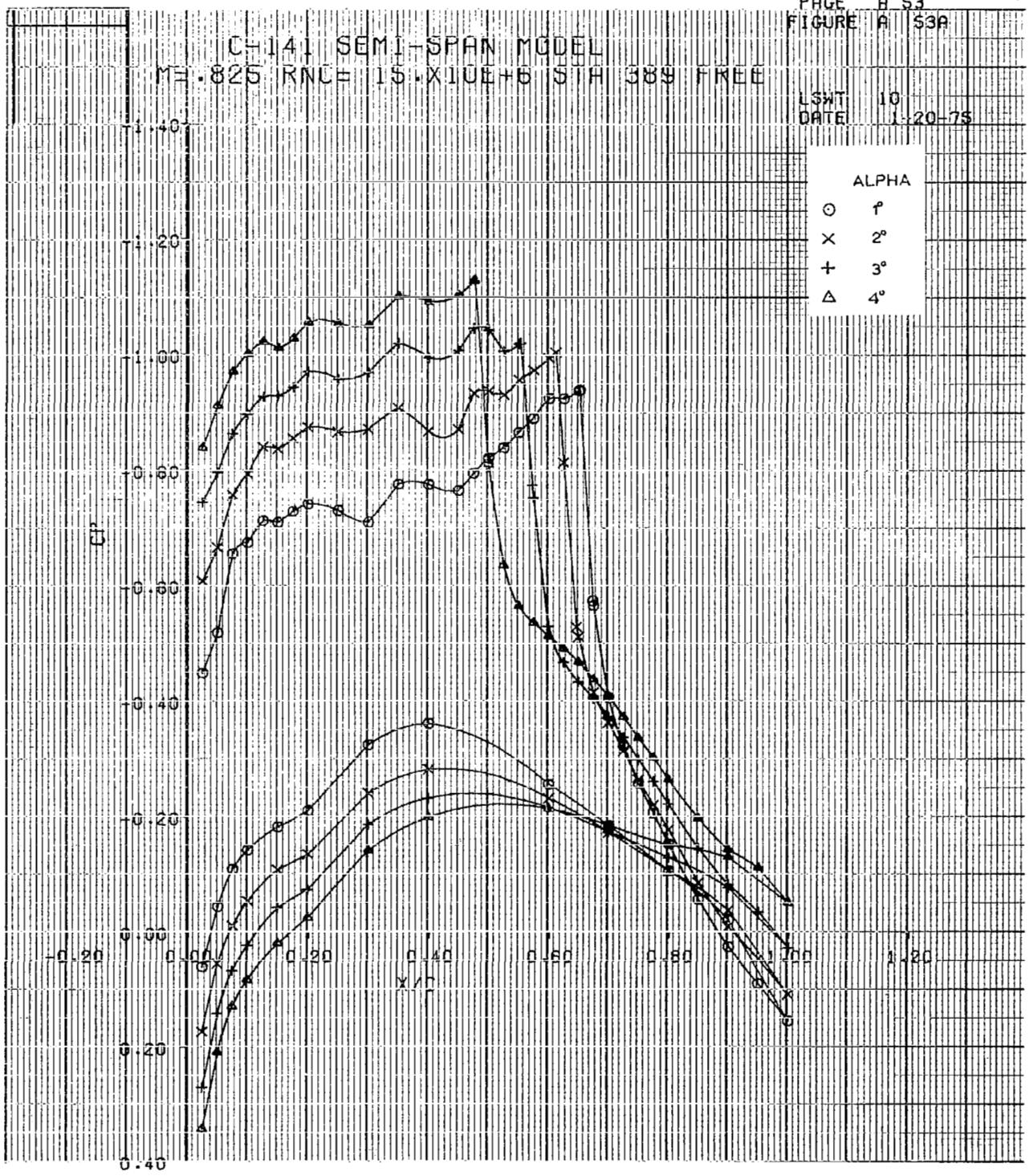
C-141 SEMI-SPAN MODEL
M=.825 RNC= 15.X10E+6 S H 389 FREE
LSWT 10
DATE 1-20-75
ALPHA
1°
2°
3°
4°
CL
Y/R
1.40
1.20
1.00
0.80
0.60
0.40
0.20
0.00
-0.20
0.00
0.20
0.40
0.60
0.80
1.00
1.20

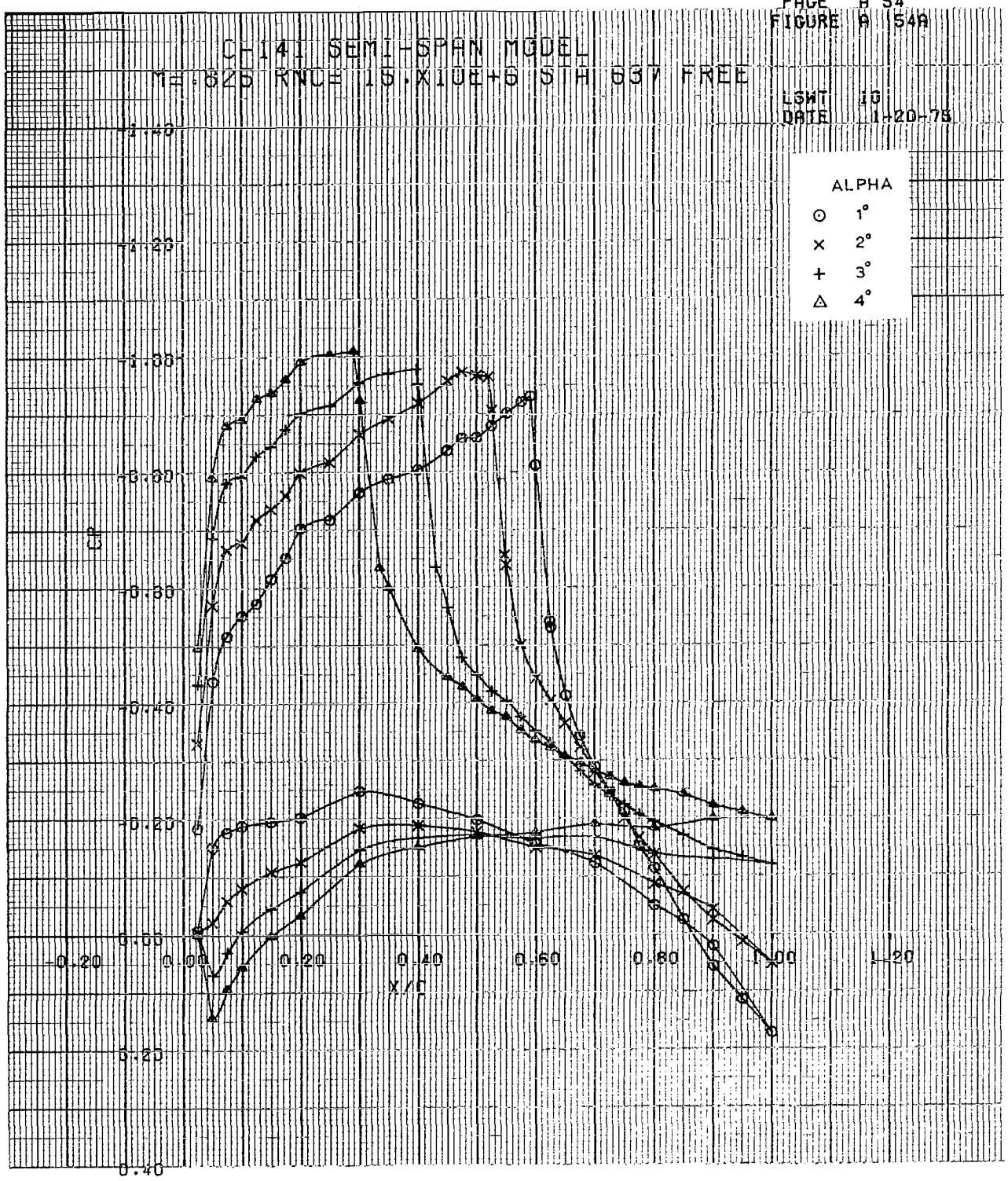
C-141 SEMI-SPAN MODEL
M=.625 RNC= 15.X10E+6 S H 63Y FREE
LSHT 10
DATE 1-20-75
ALPHA
⊙ 1°
× 2°
+ 3°
△ 4°
CP
X/C
-0.20
0.00
0.20
0.40
0.60
0.80
1.00
1.20
-1.40
-1.20
-1.00
-0.80
-0.60
-0.40
-0.20
0.00
0.20
0.40

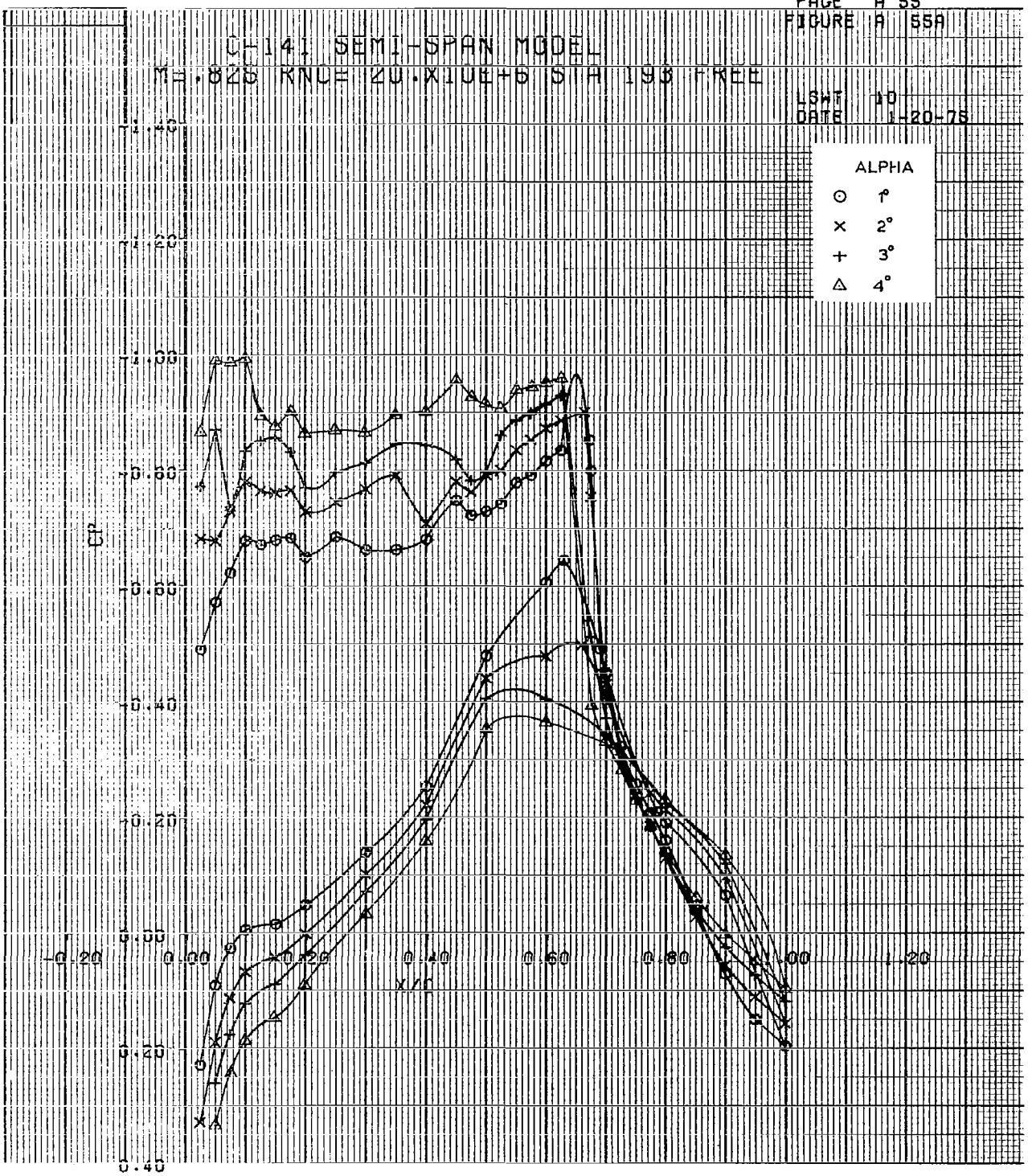
C-141 SEMI-SPAN MODEL
M=.825 RNUE 2U.X1UE+6 S A 193 FREE
LSHT 10
DATE 1-20-75
ALPHA
1°
2°
3°
4°
CP
X/C
-0.20
0.00
0.20
0.40
0.60
0.80
1.00
1.20
0.40
0.20
0.00
-0.20
-0.40
-0.60
-0.80
-1.00

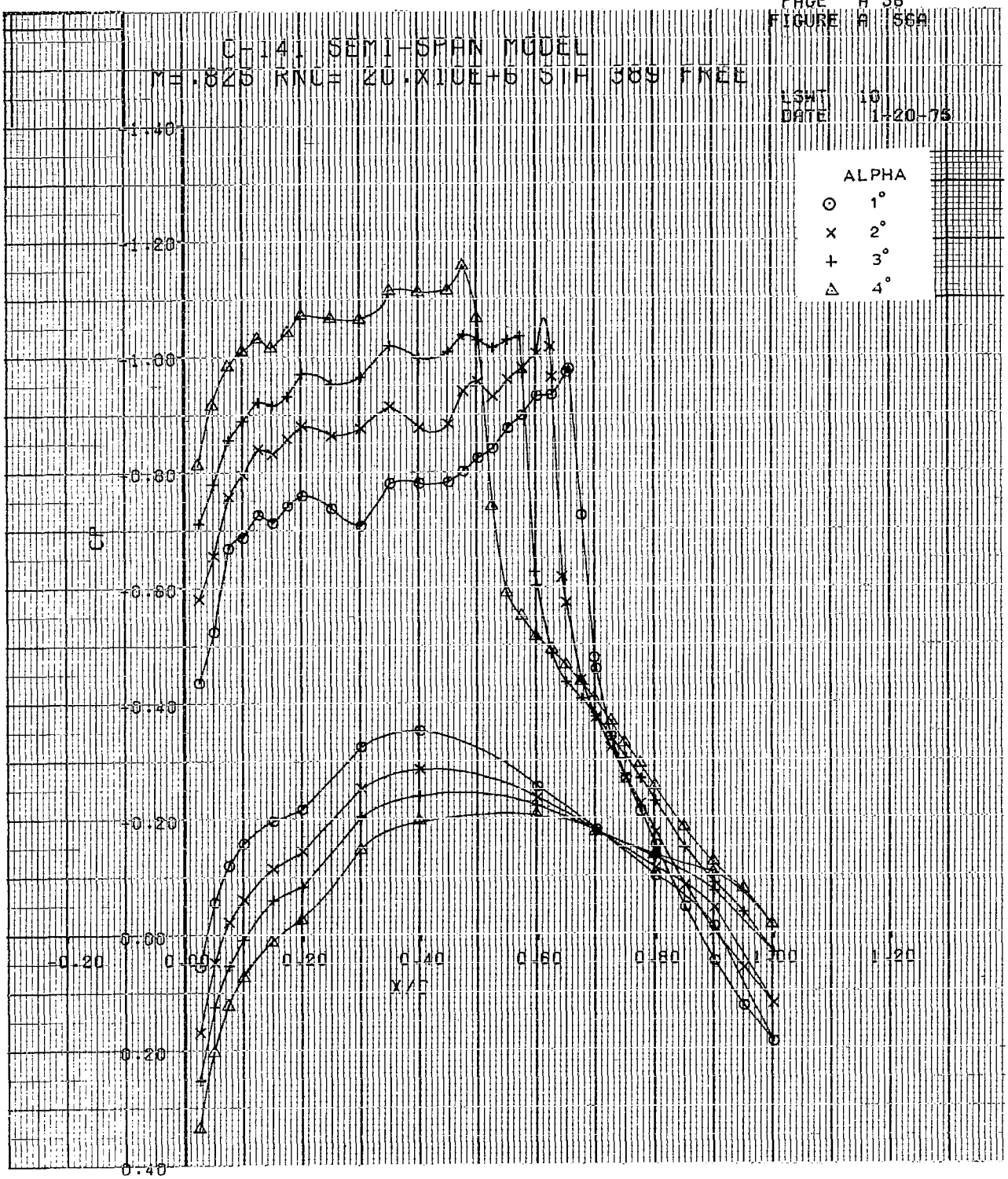
CF-14 SEMI-SPAN MODEL
M=.825 RNC= 20.X10E+6 SIM 505 TNEL
LGHT 10
DATE 1-20-75
ALPHA
1°
2°
3°
4°
CP
X/C
-1.40
-1.20
-1.00
-0.80
-0.60
-0.40
-0.20
0.00
0.20
0.40
-0.20
0.00
0.20
0.40
0.60
0.80
1.00
1.20

FIGURE A 57A

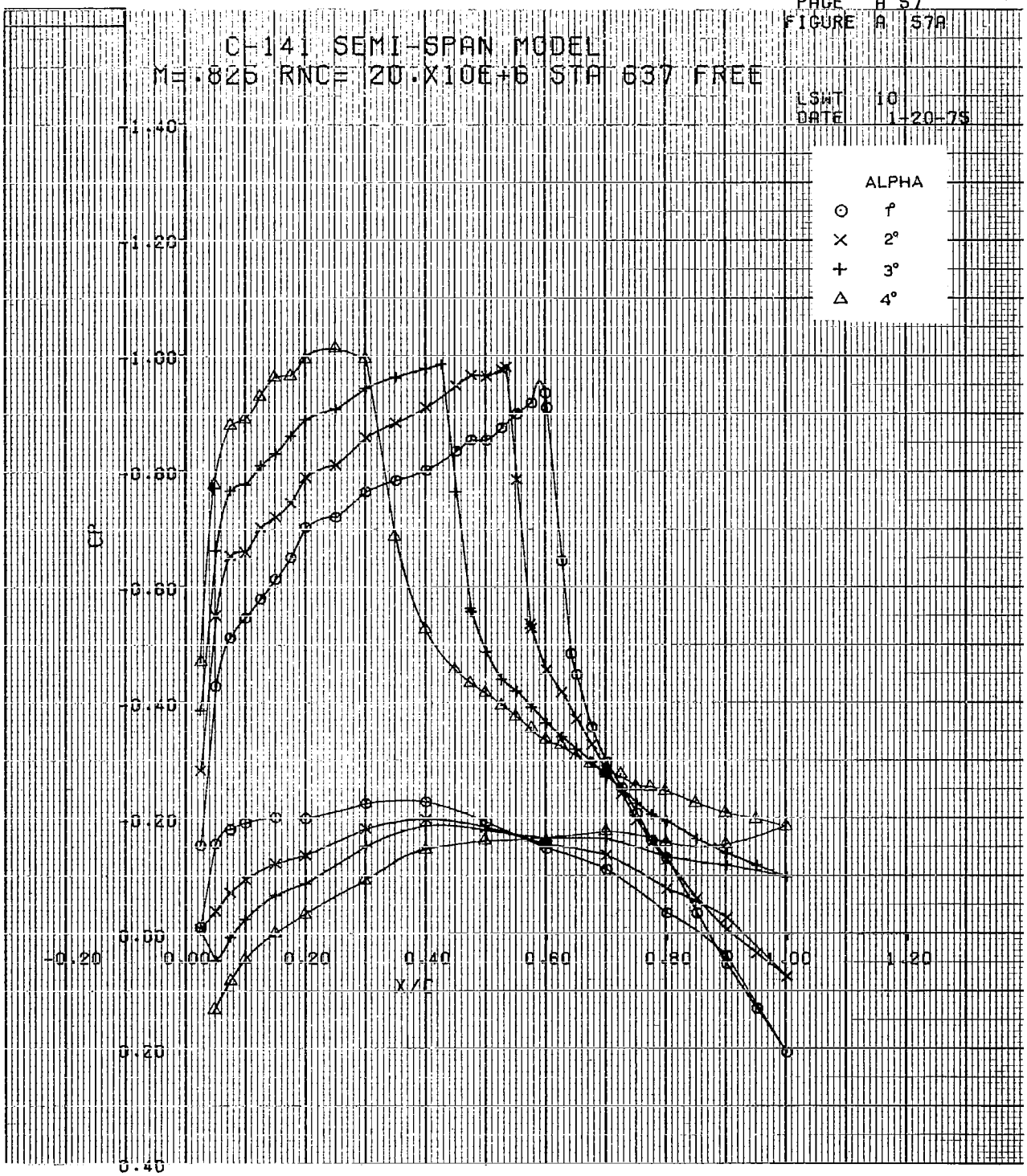
C-141 SEMI-SPAN MODEL
M=.825 RNC= 20.X10E+6 STA 637 FREE
LSWT 10
DATE 1-20-75
ALPHA
1°
2°
3°
4°
CL
X/C
1.20
1.00
0.80
0.60
0.40
0.20
0.00
-0.20
-0.40

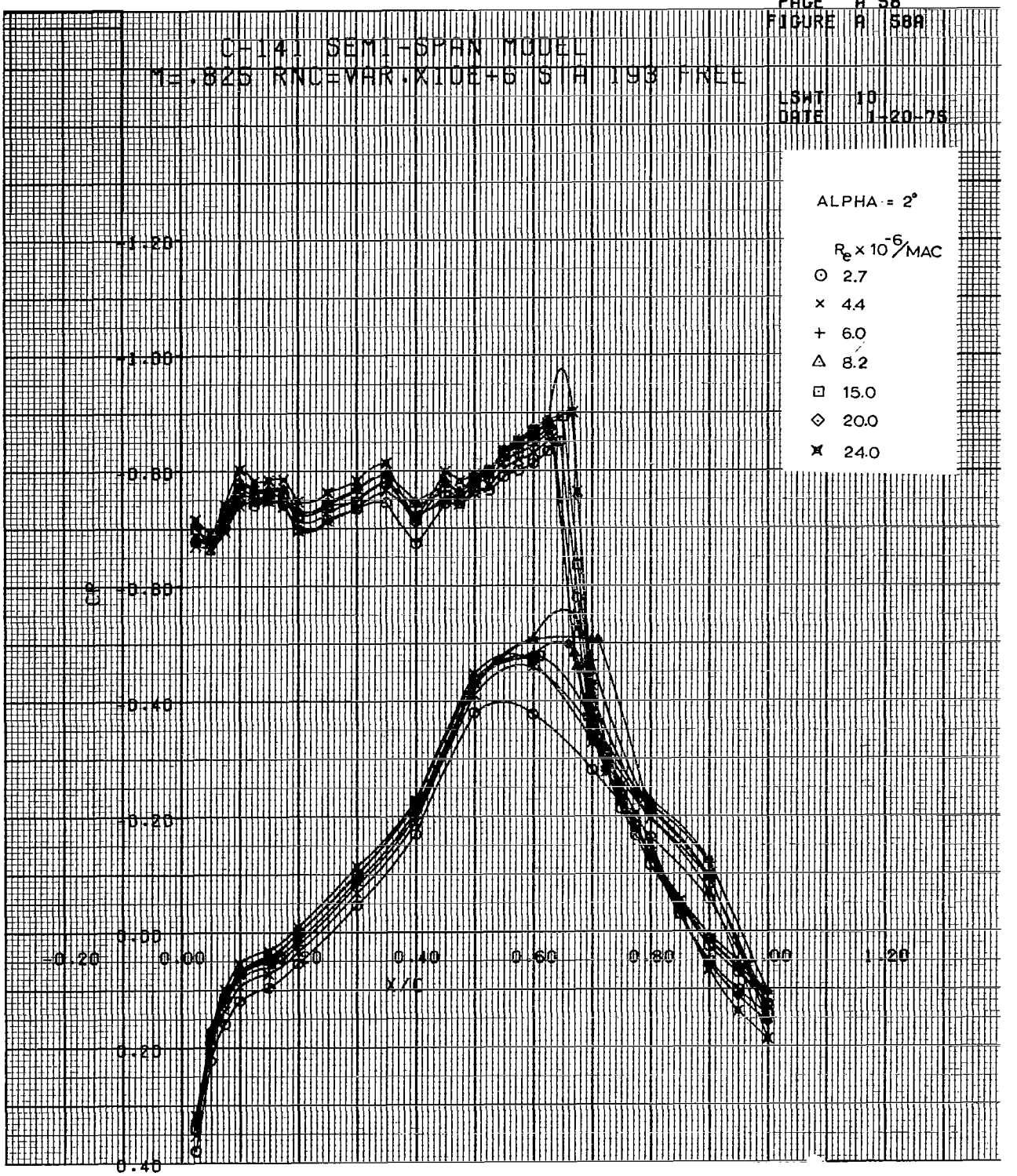
C-141 SEMI-SPAN MODEL
M=.825 RNC=VAR.X10E+6 S A 193 FREE
LSHT 10
DATE 1-20-75
ALPHA = 2°
$R_e \times 10^{-6}$/MAC
⊙ 2.7
× 4.4
+ 6.0
△ 8.2
⊡ 15.0
◇ 20.0
⋈ 24.0
C_p
X/C
-1.20
-1.00
-0.80
-0.60
-0.40
-0.20
0.00
0.20
0.40
0.60
0.80
1.00
1.20
0.40

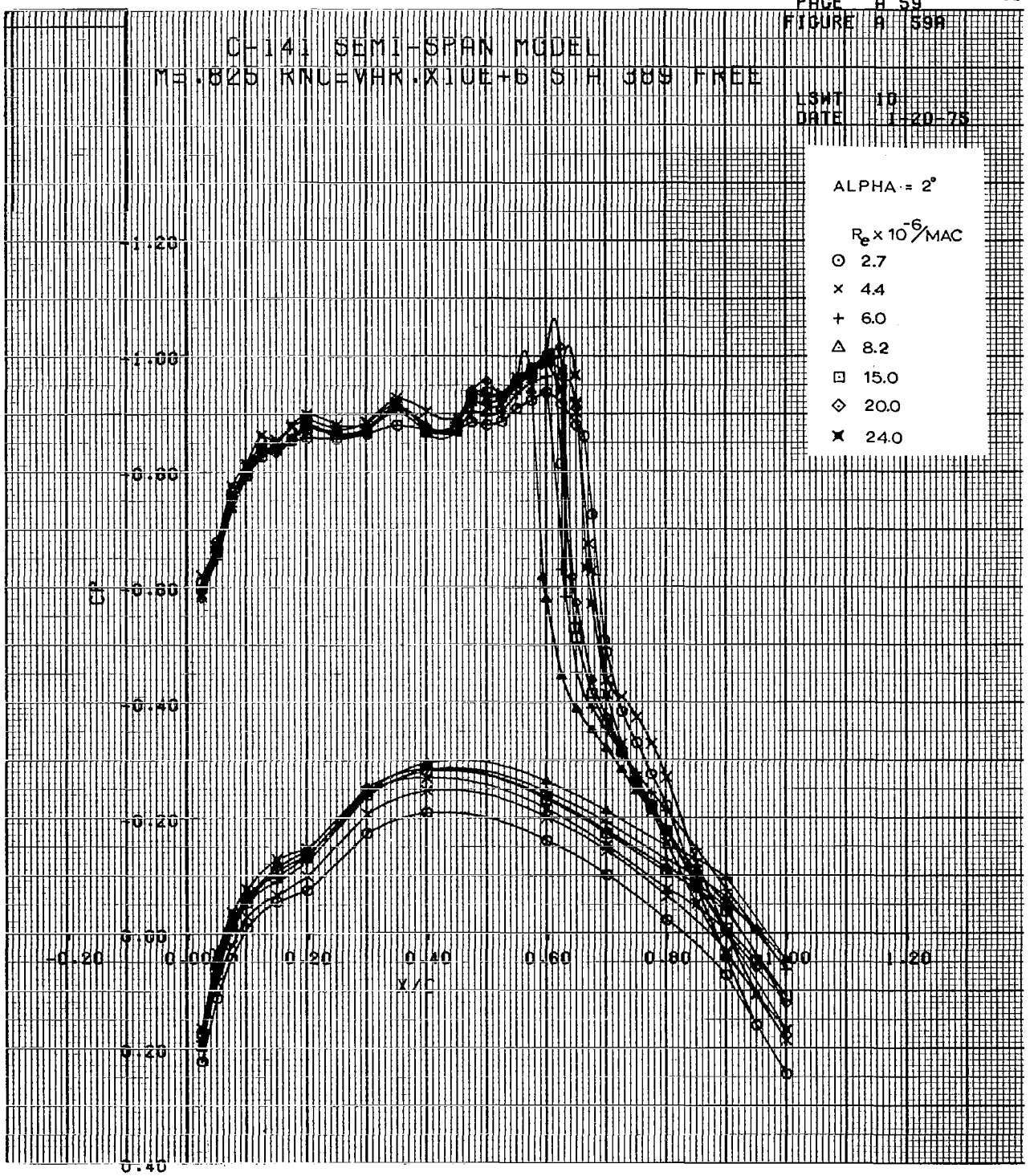
C-141 SEMI-SPAN MODEL
M=.825 RNC=VHK.X10E+6 S H 389 FREE
LSWT 10
DATE 1-20-75
ALPHA = 2°
$R_e \times 10^{-6}$/MAC
2.7
4.4
6.0
8.2
15.0
20.0
24.0
CP
X/C
1.20
1.00
0.80
0.60
0.40
0.20
0.00
-0.20
-0.40
-0.60
-0.80
-1.00
-1.20
-0.20
0.00
0.20
0.40
0.60
0.80
1.00
1.20

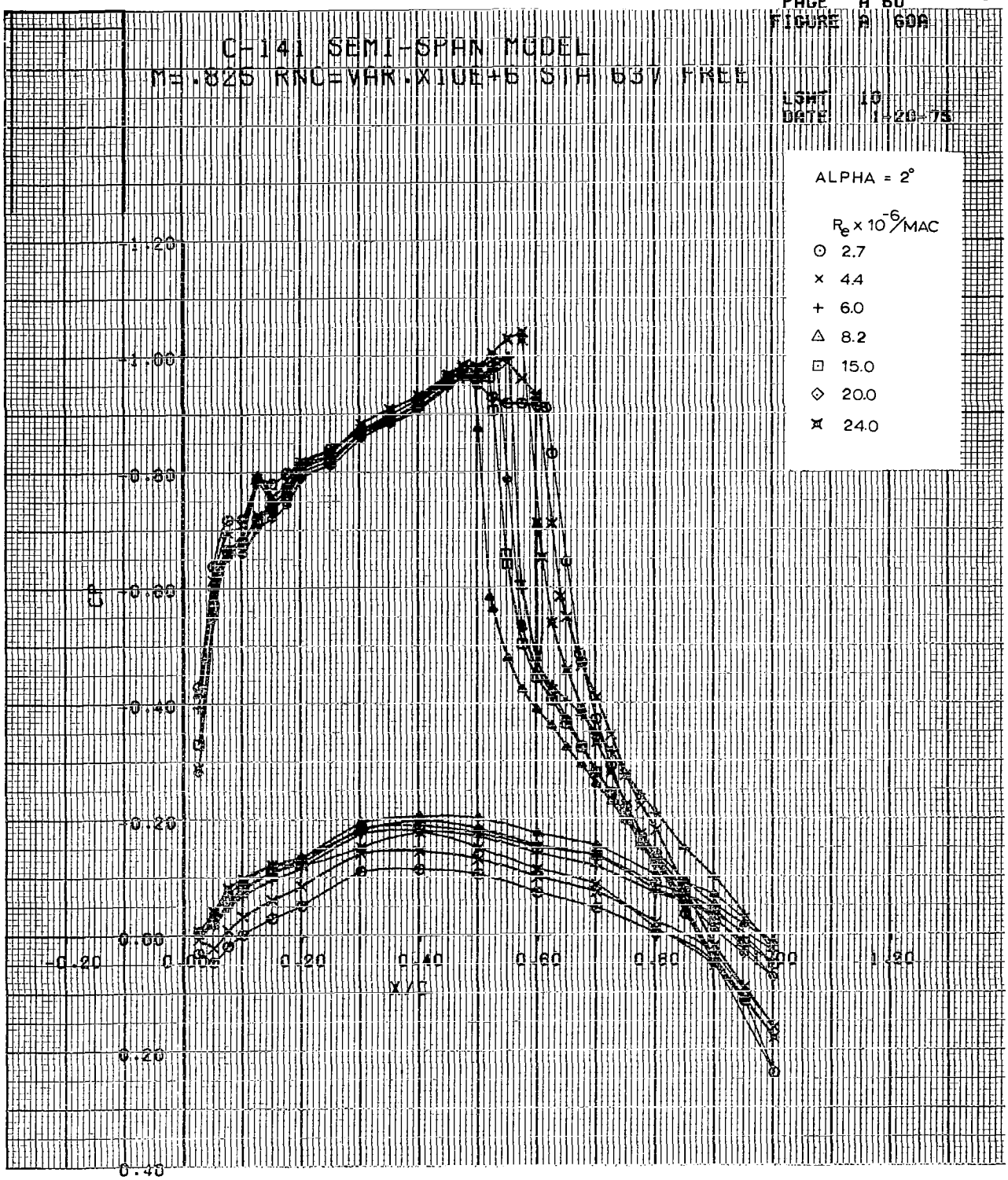
C-141 SEMI-SPAN MODEL
M=.825 RNC=MAK.X1UE+6 SIM 63V FREE
LSHT 10
DATE 1-20-75
ALPHA = 2°
Re x 10^-6/MAC
2.7
4.4
6.0
8.2
15.0
20.0
24.0
CL
CD
1.20
1.00
0.80
0.40
0.20
0.00
-0.20
-0.40
-0.20
0.00
0.20
0.40
0.60
0.80
1.00
1.20

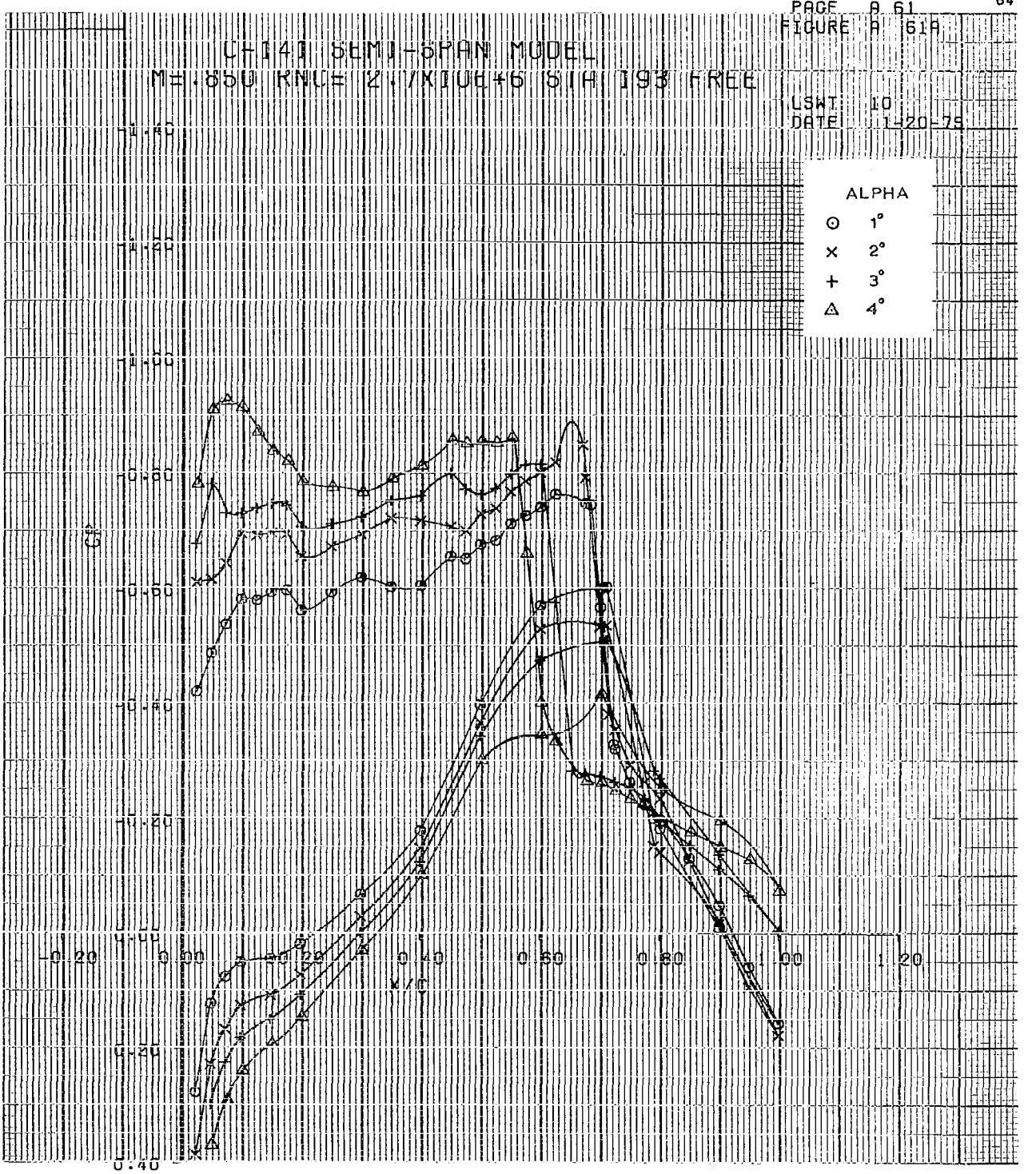
LSWT 10
DATE 1-20-75
ALPHA
1°
2°
3°
4°
CL
K/C
0.40

FIGURE A 62A

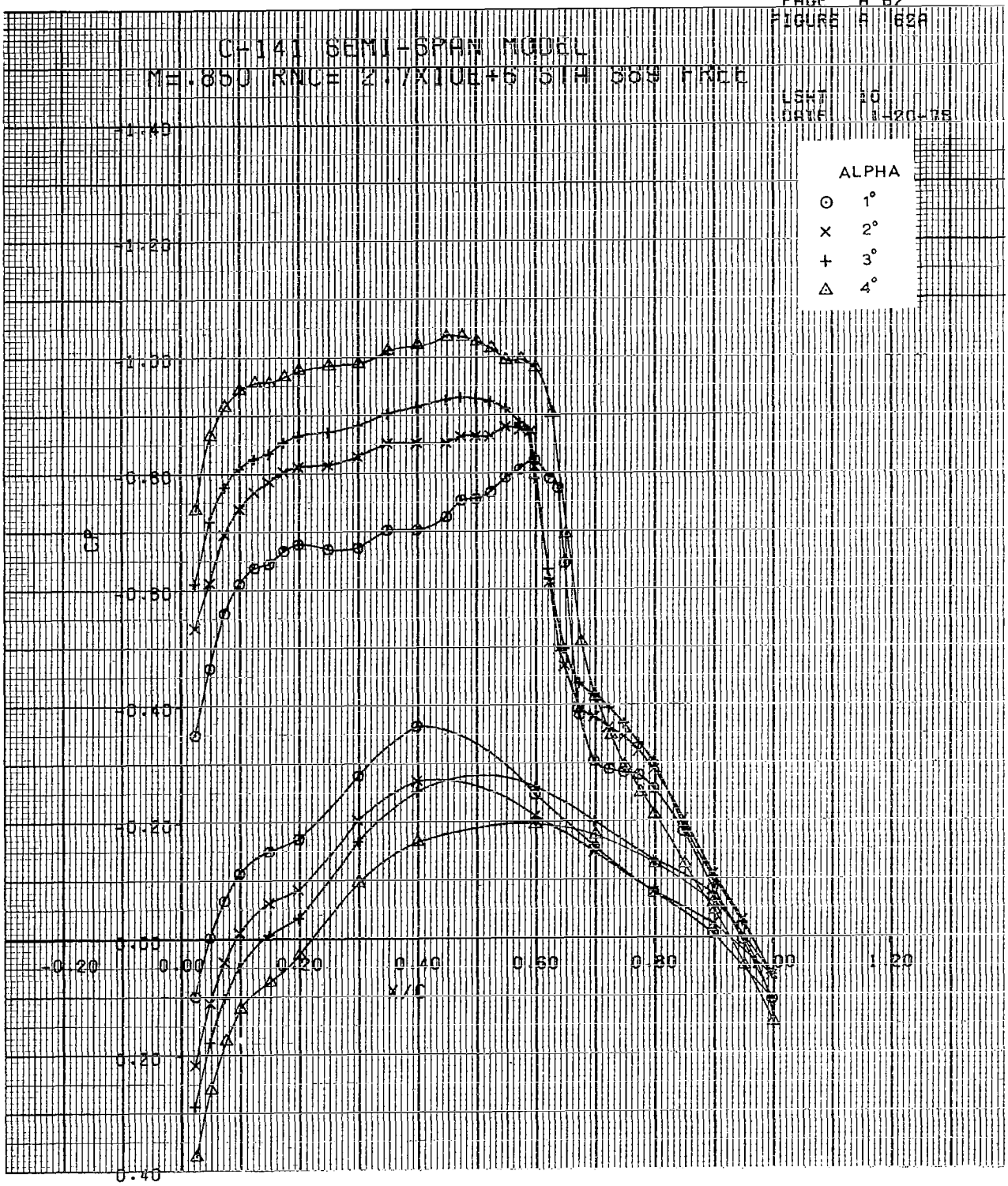
C-141 SEMI-SPAN MODEL
M=.850 RNC= 2./X10E+6 SLR 000 FREE
ALPHA
1°
2°
3°
4°
-1.40
-1.20
-1.00
-0.80
-0.60
-0.40
-0.20
0.00
0.20
0.40
-0.20
0.00
0.20
0.40
0.60
0.80
1.00
1.20
X/C

FIGURE A 63A

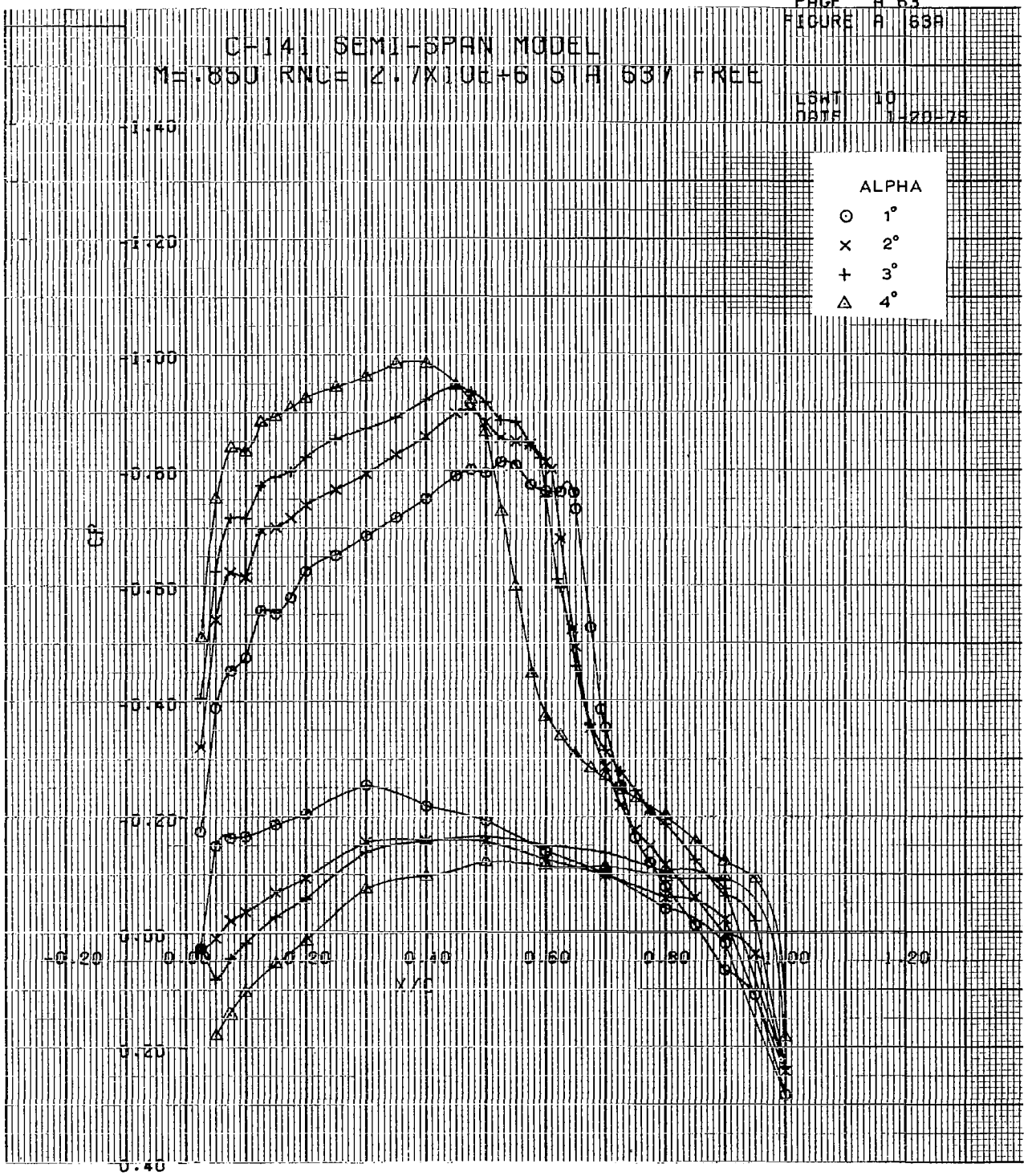
C-141 SEMI-SPAN MODEL
M=.850 RNC= 2.7X10E+6 S/A 63/ FREE
LSHT 10
DATA 1-20-78
ALPHA
1°
2°
3°
4°
CL
Y/S
1.40
1.20
1.00
0.80
0.60
0.40
0.20
0.00
-0.20
0.20
0.40
0.60
0.80
1.00
1.20

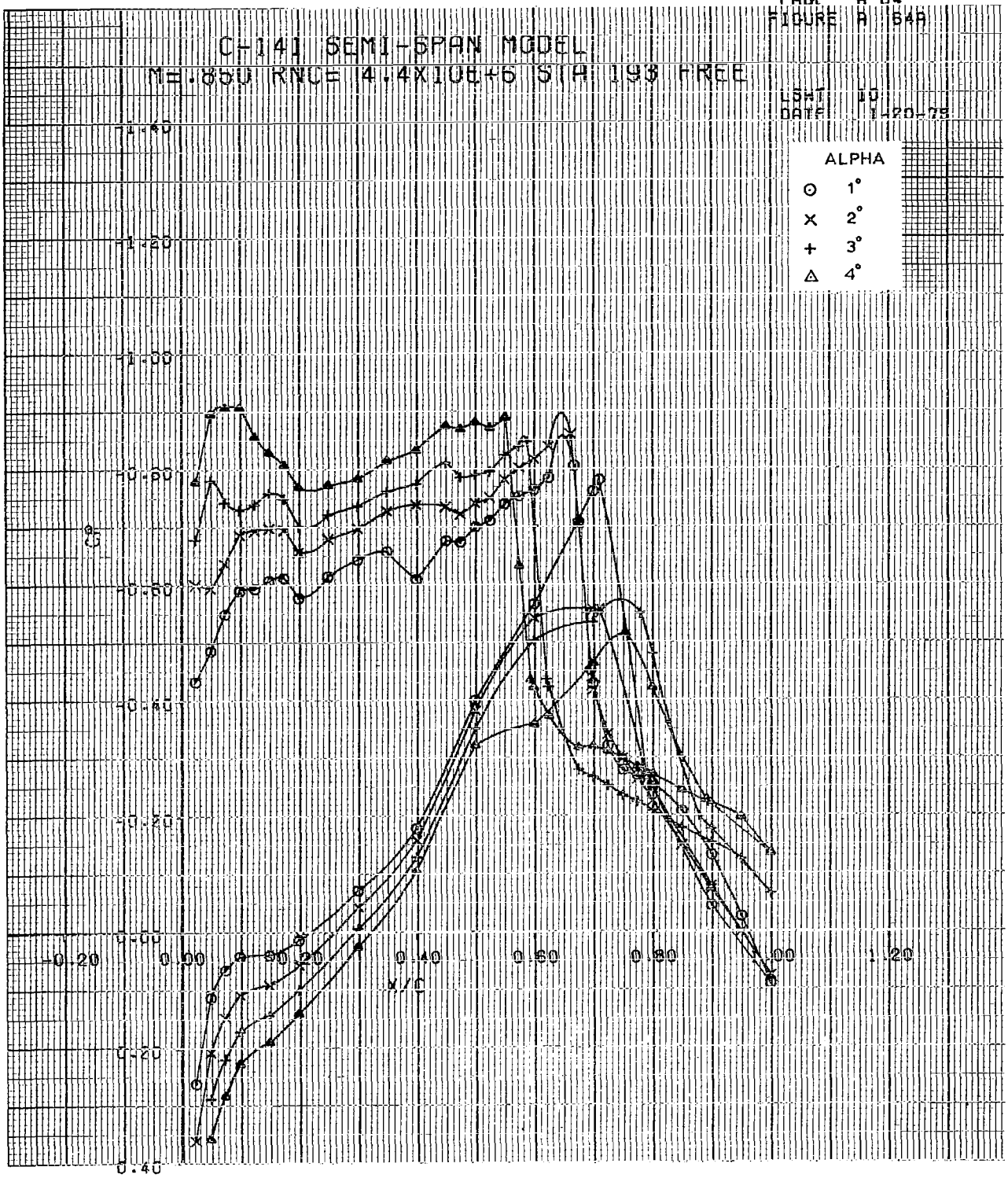
C-141 SEMI-SPAN MODEL
M=.850 RNUE=4.4X10E+6 STA 193 FREE
LOAD LO
DATE 1-20-75
ALPHA
1°
2°
3°
4°
-1.60
-1.20
-1.00
-0.80
-0.60
-0.40
-0.20
0.00
0.40
-0.20
0.00
0.20
0.40
0.60
0.80
1.00
1.20
X/C

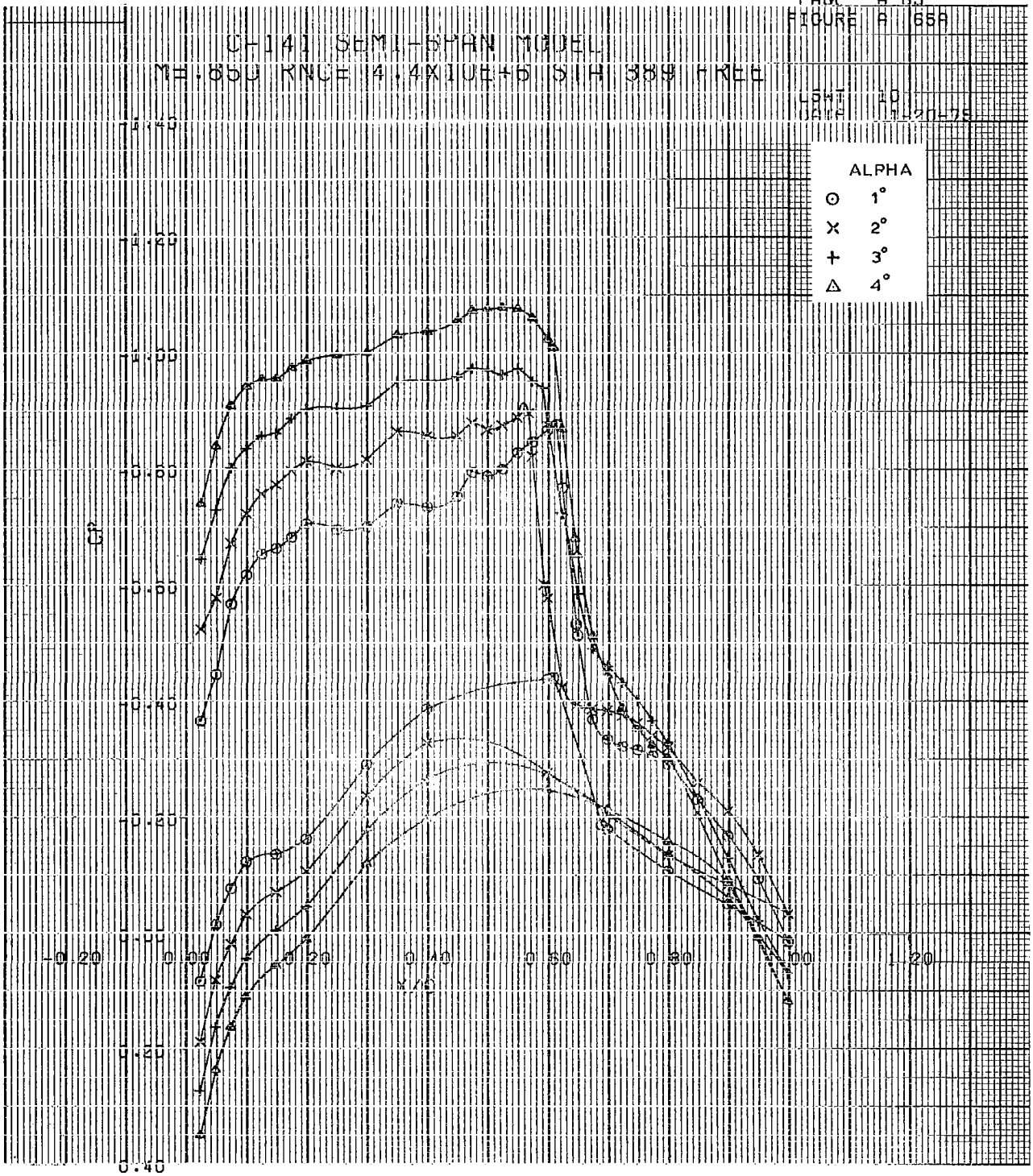
CL141 SEMI-SPAN MODEL
MACH KNUM 4.4XICE+6 SH 38S FKEP
ALPHA
⊙ 1°
X 2°
+ 3°
△ 4°
CL
0.40

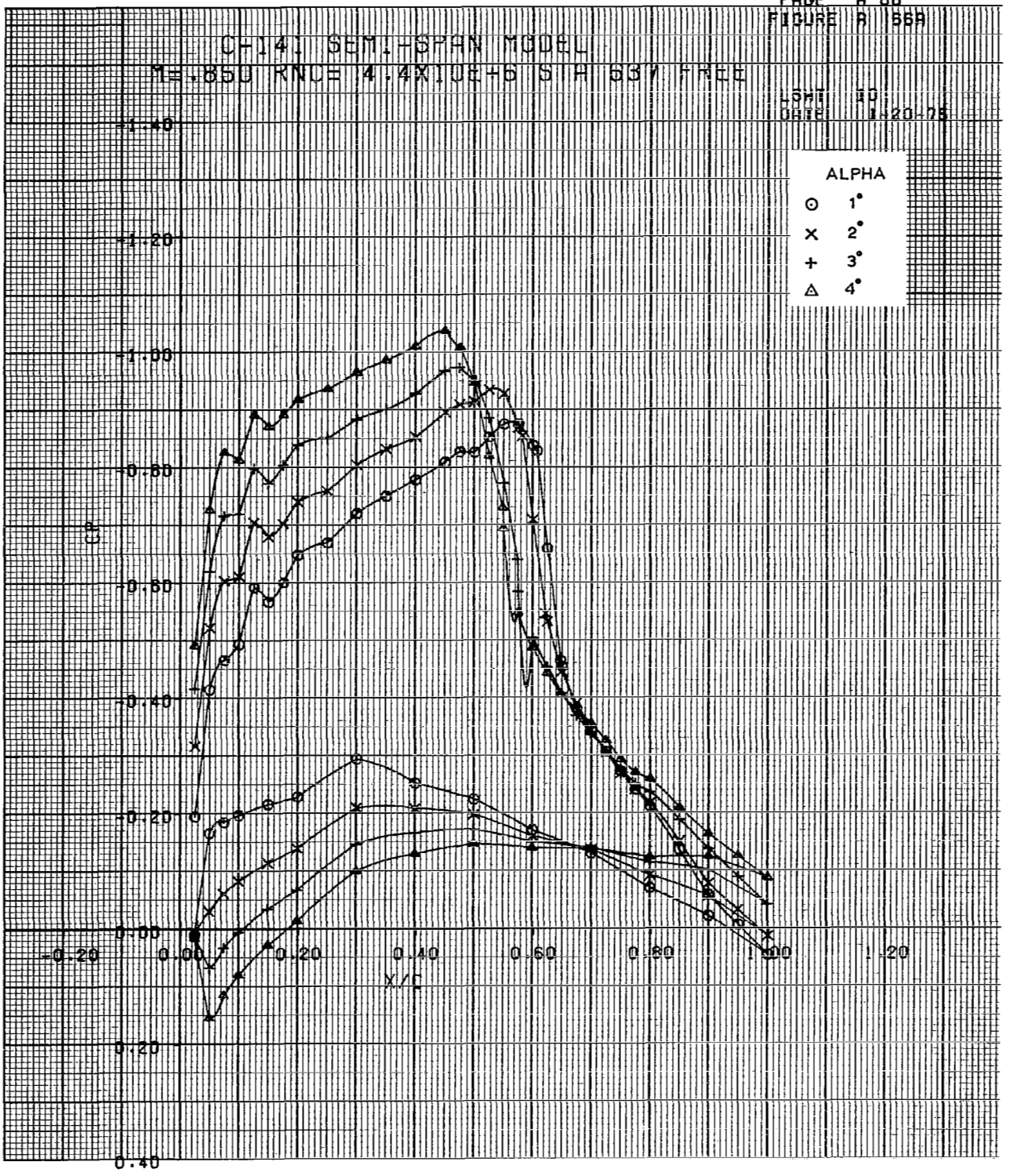
CH14, SEMI-SPAN MODEL
M=.850 RNCB 4.4X10E+6 S/A 63Y FREE
SHOT 50
DATE 1-20-75
ALPHA
1°
2°
3°
4°
-1.40
-1.20
-1.00
-0.80
-0.60
-0.40
-0.20
0.00
0.20
0.40
-0.20
0.00
0.20
0.40
0.60
0.80
1.00
1.20
X/C

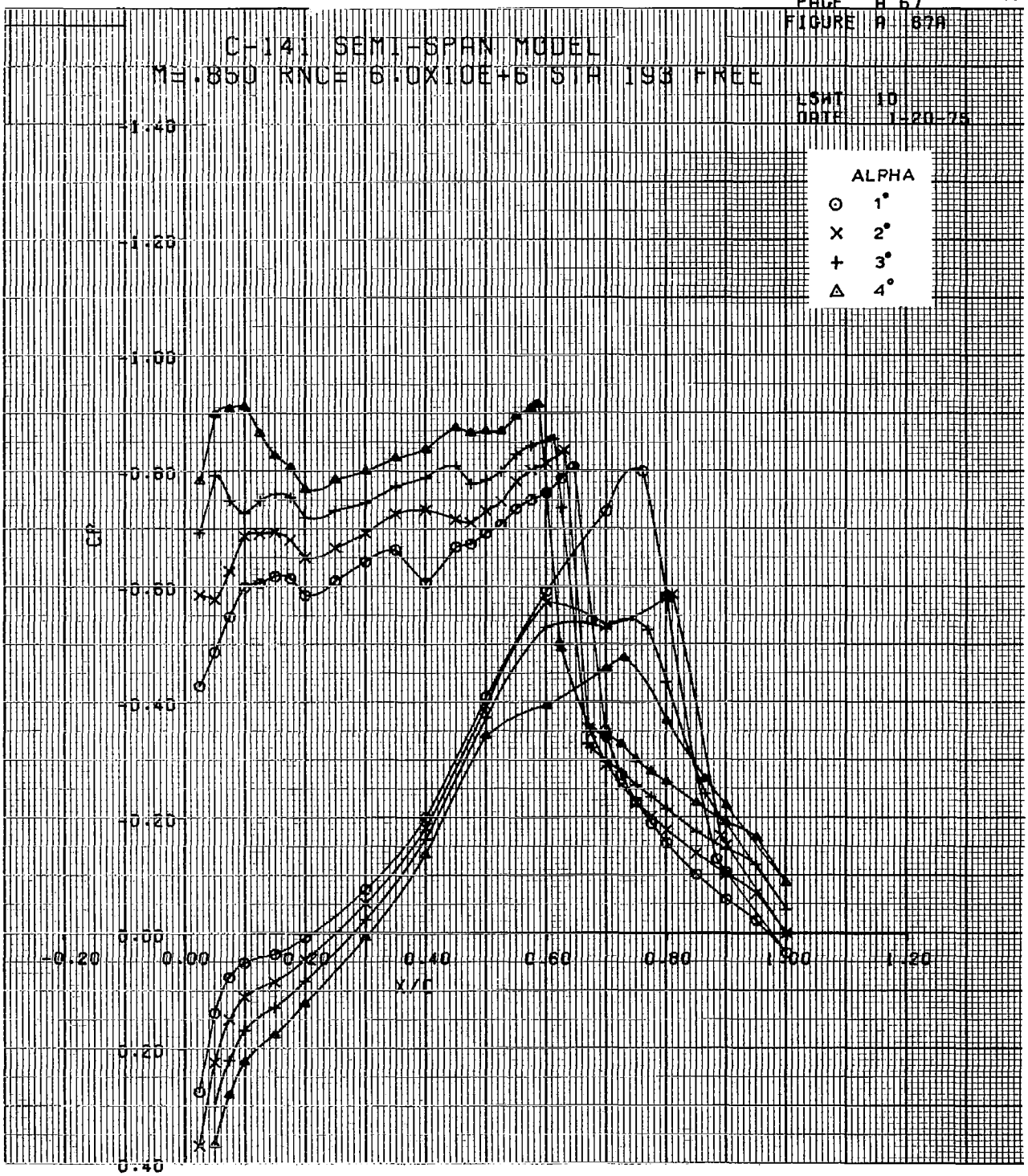
C-141 SEMI-SPAN MODEL
M=.850 RNCE= 6.0X10E+6 S/A 193 FREE
SHT 10
DATE 1-20-75
ALPHA
1°
2°
3°
4°
-1.40
-1.20
-1.00
-0.80
-0.60
-0.40
-0.20
0.00
0.20
-0.20
0.00
0.40
0.60
0.80
1.00
1.20
X/C

FIGURE A 68A

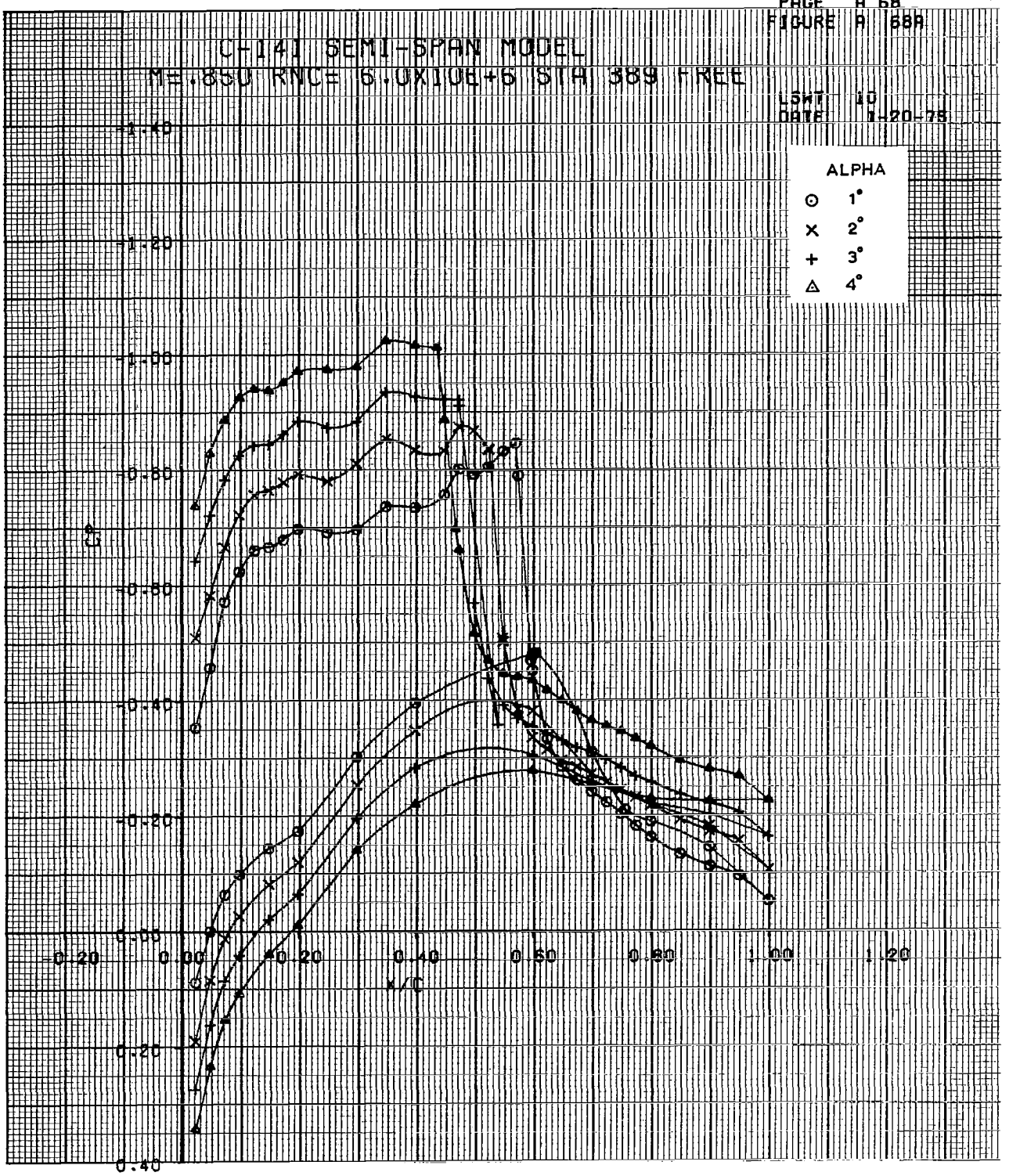
C-141 SEMI-SPAN MODEL
M=.850 RNC= 6.0X10E+6 STA 389 FREE
LSWT 10
DATE 1-20-75
ALPHA
1°
2°
3°
4°
CL
X/C
-1.40
-1.20
-1.00
-0.80
-0.60
-0.40
-0.20
0.00
0.20
0.40
0.60
0.80
1.00
1.20
-0.40

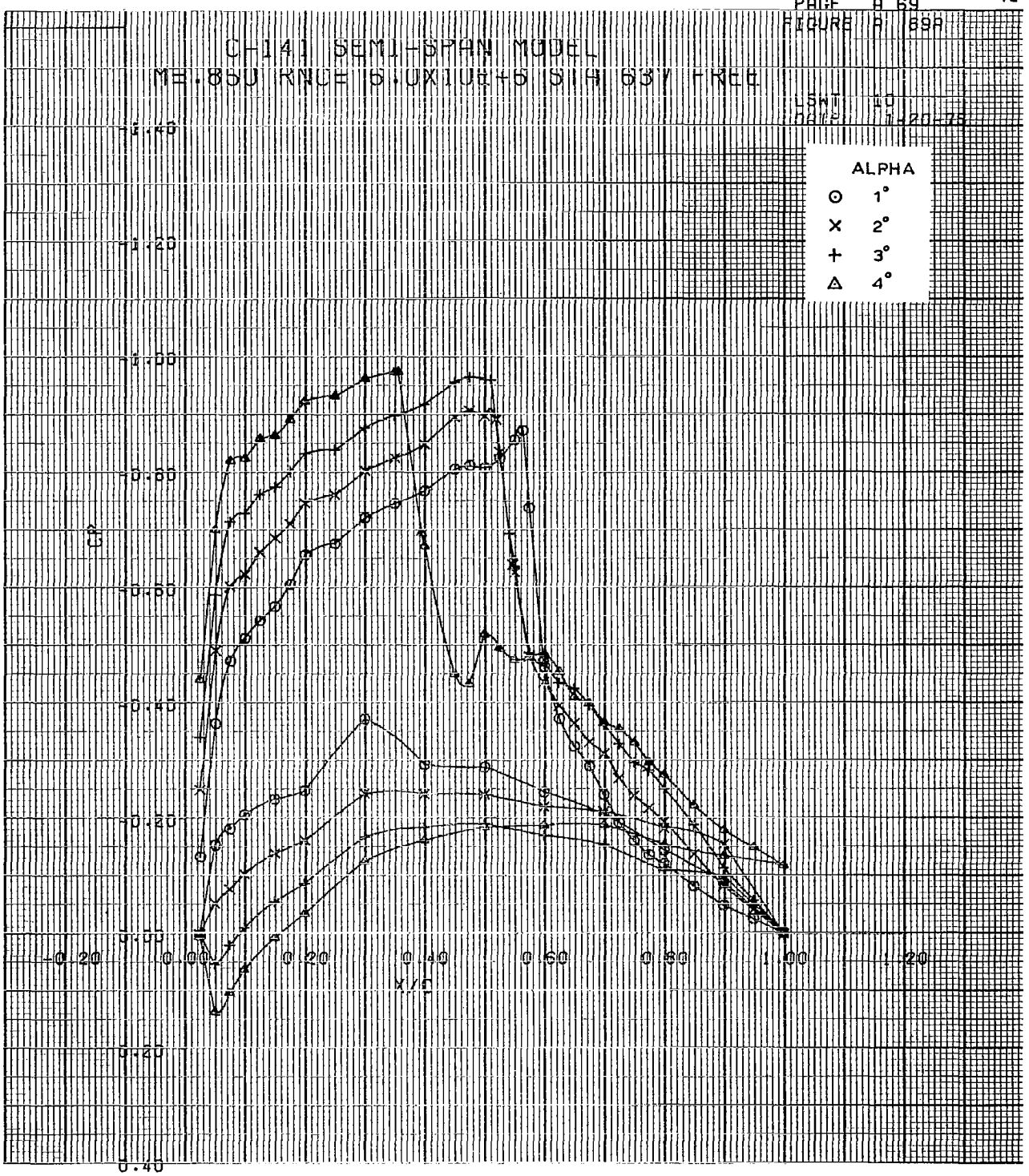
CH-141 SEMI-SPAN MODEL
ALPHA
1°
2°
3°
4°
CP
X/C
-0.20
0.00
0.20
0.40
0.60
0.80
1.00
1.20
-0.40
-0.20
0.00
0.20
0.40

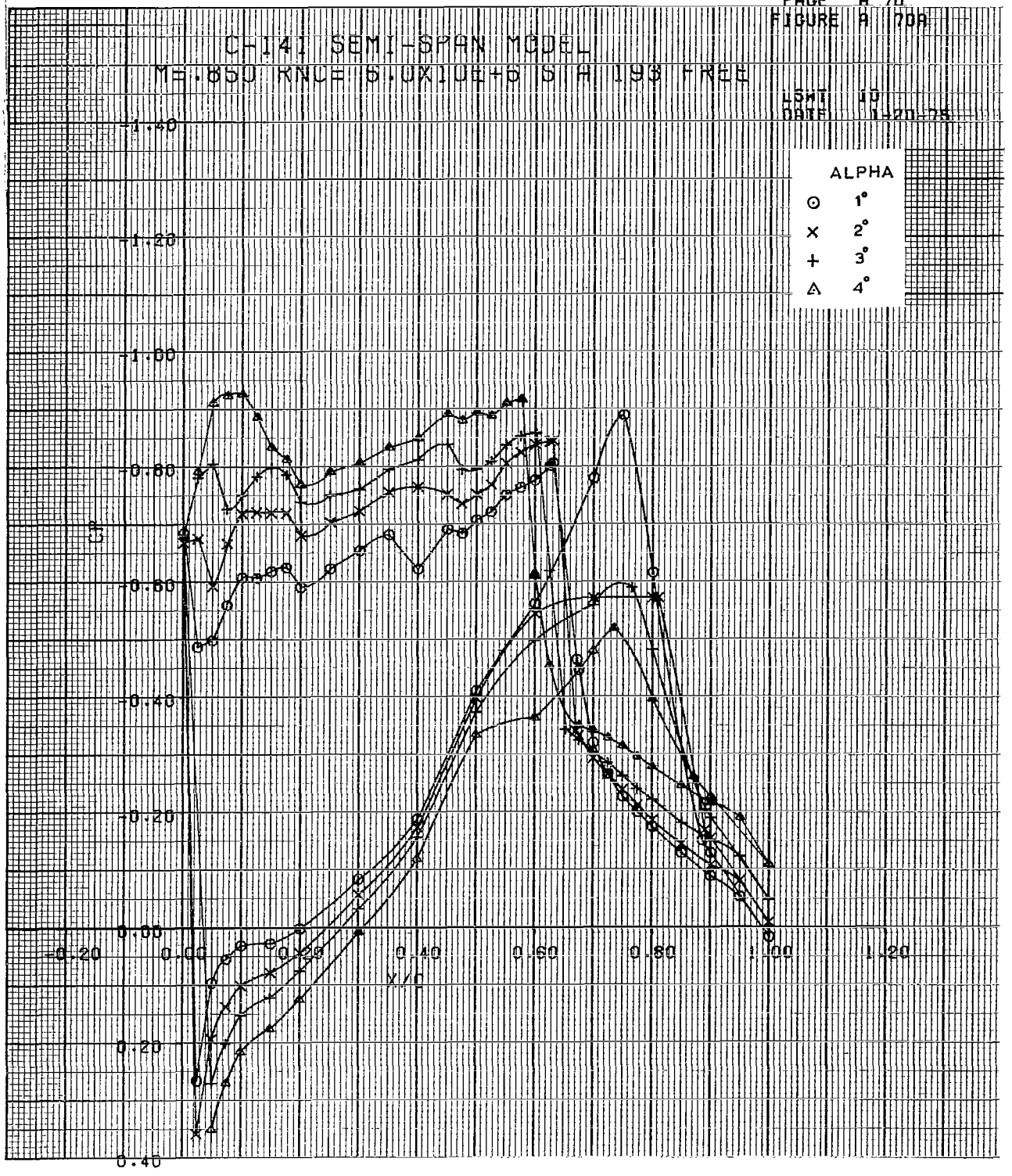
CH141 SEMI-SPAN MODEL
M=.850 RNCE 6.0X10E+6 S/A 193 FREE
LSHT 10
DATE 1-20-75
ALPHA
1°
2°
3°
4°
-1.40
-1.20
-1.00
-0.80
-0.60
-0.40
-0.20
0.00
0.20
0.40
-0.20
0.00
0.20
0.40
0.60
0.80
1.00
1.20
Y/C

C-141 SEMI-SPAN MODEL
M=.850 RNC= 6.0X10E+6 STA 389 FREE

LSWT 10
DATE 1-20-75

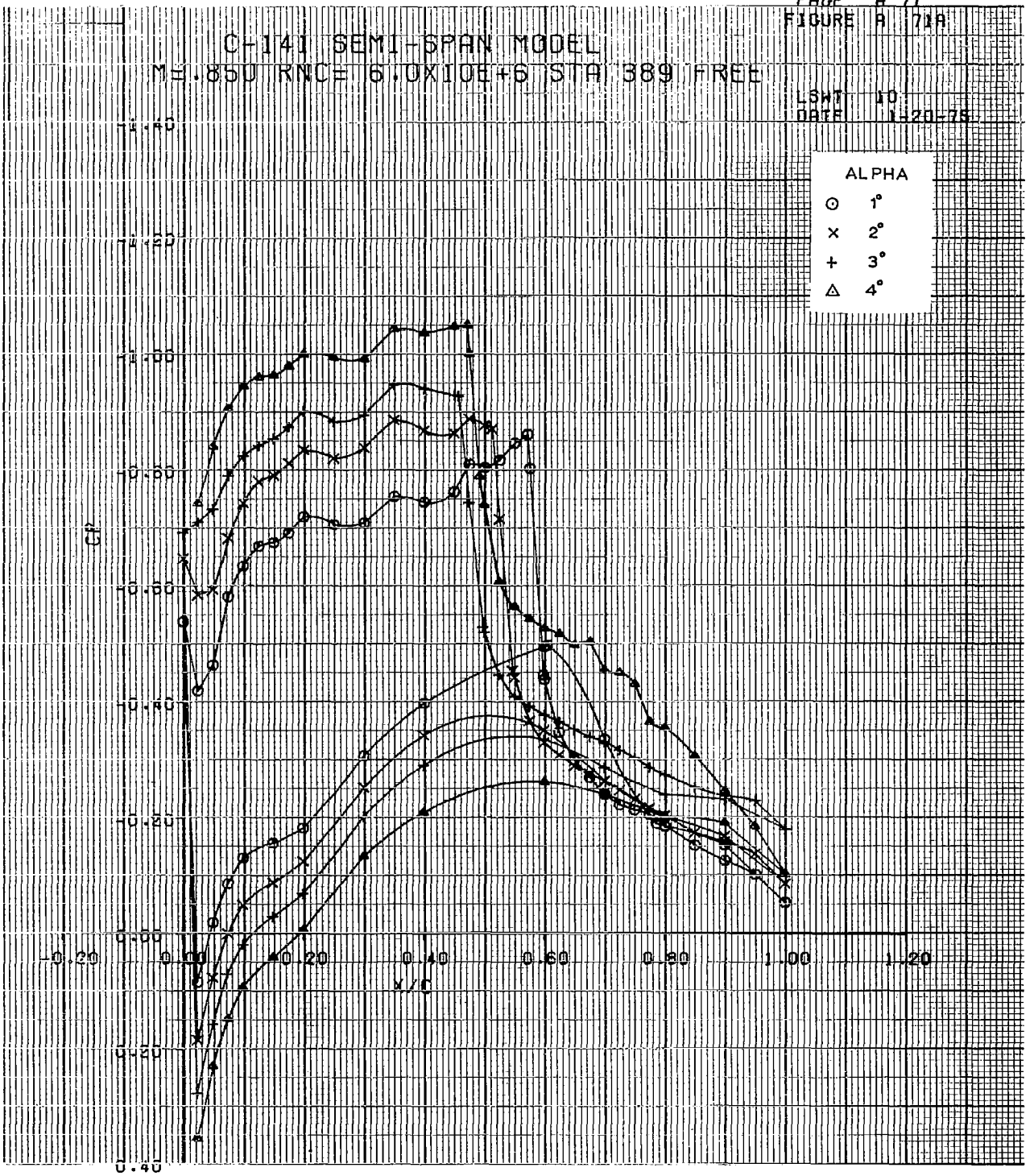

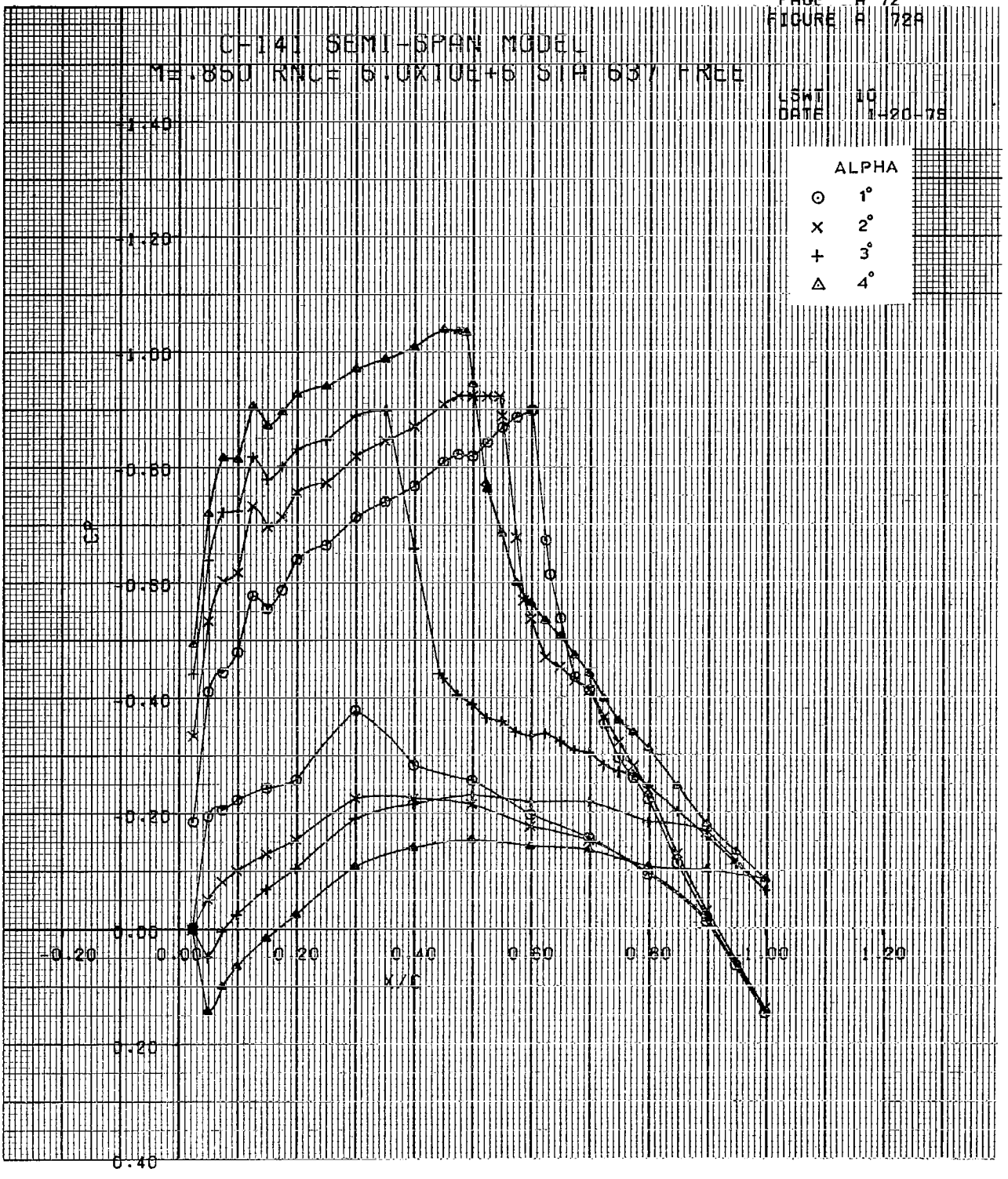
CF-141 SEMI-SPAN MODEL
M=.850 RNC= 6.0X10E+6 SIA 637 FREE
LSWT 10
DATE 1-20-78
ALPHA
1°
2°
3°
4°
CP
-1.40
-1.20
-1.00
-0.80
-0.60
-0.40
-0.20
0.00
0.20
0.40
-0.20
0.00
0.20
0.40
0.60
0.80
1.00
1.20
X/C

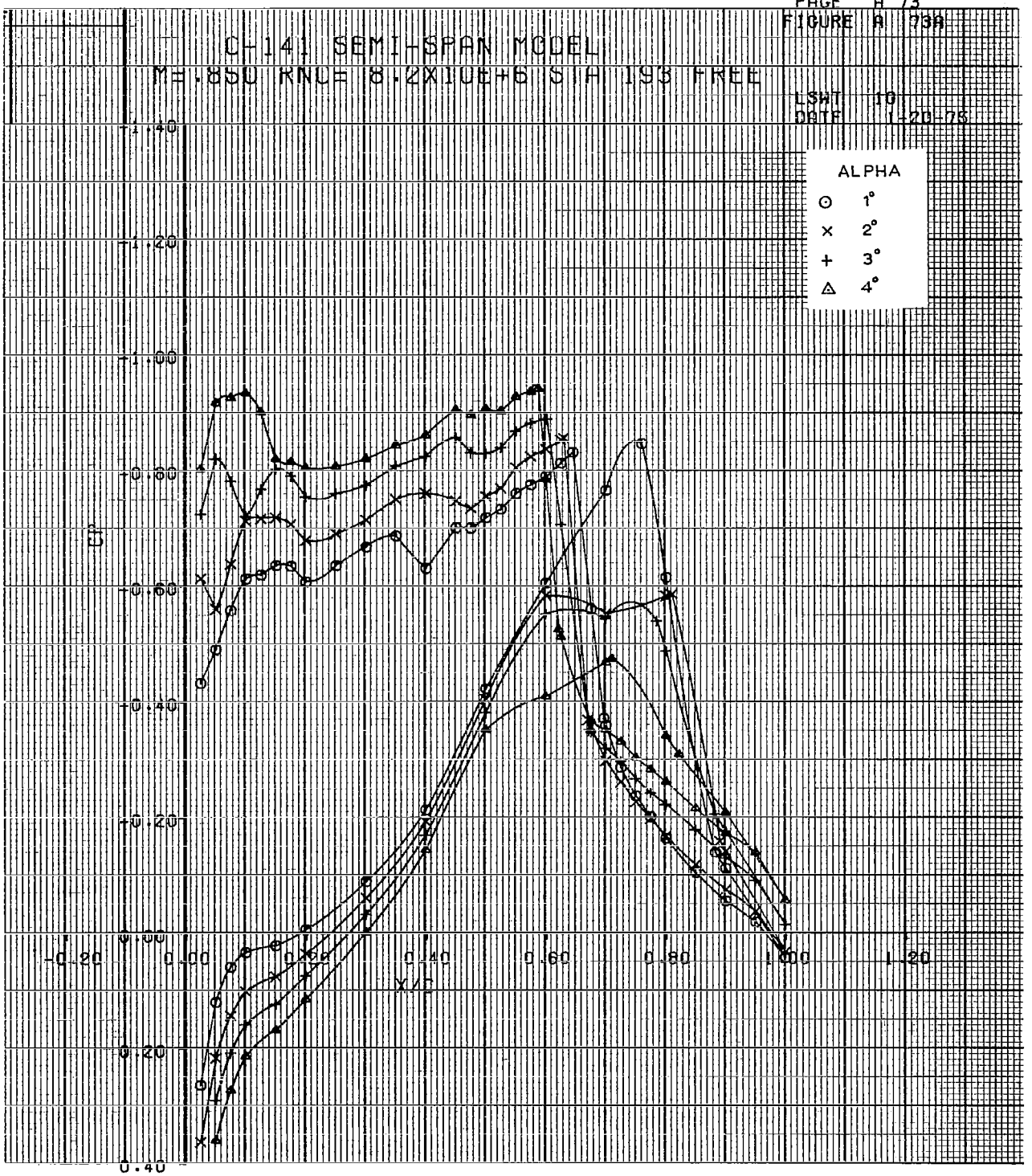
CH-141 SEMI-SPAN MODEL
M=.850 RNC= 8.2X10E+6 S/A 193 FREE
LSWT 10
DATE 1-20-75
ALPHA
⊙ 1°
× 2°
+ 3°
△ 4°
CL
1.40
1.20
1.00
0.80
0.60
0.40
0.20
0.00
-0.20
-0.40
-0.20
0.00
0.20
0.40
0.60
0.80
1.00
1.20
X/C

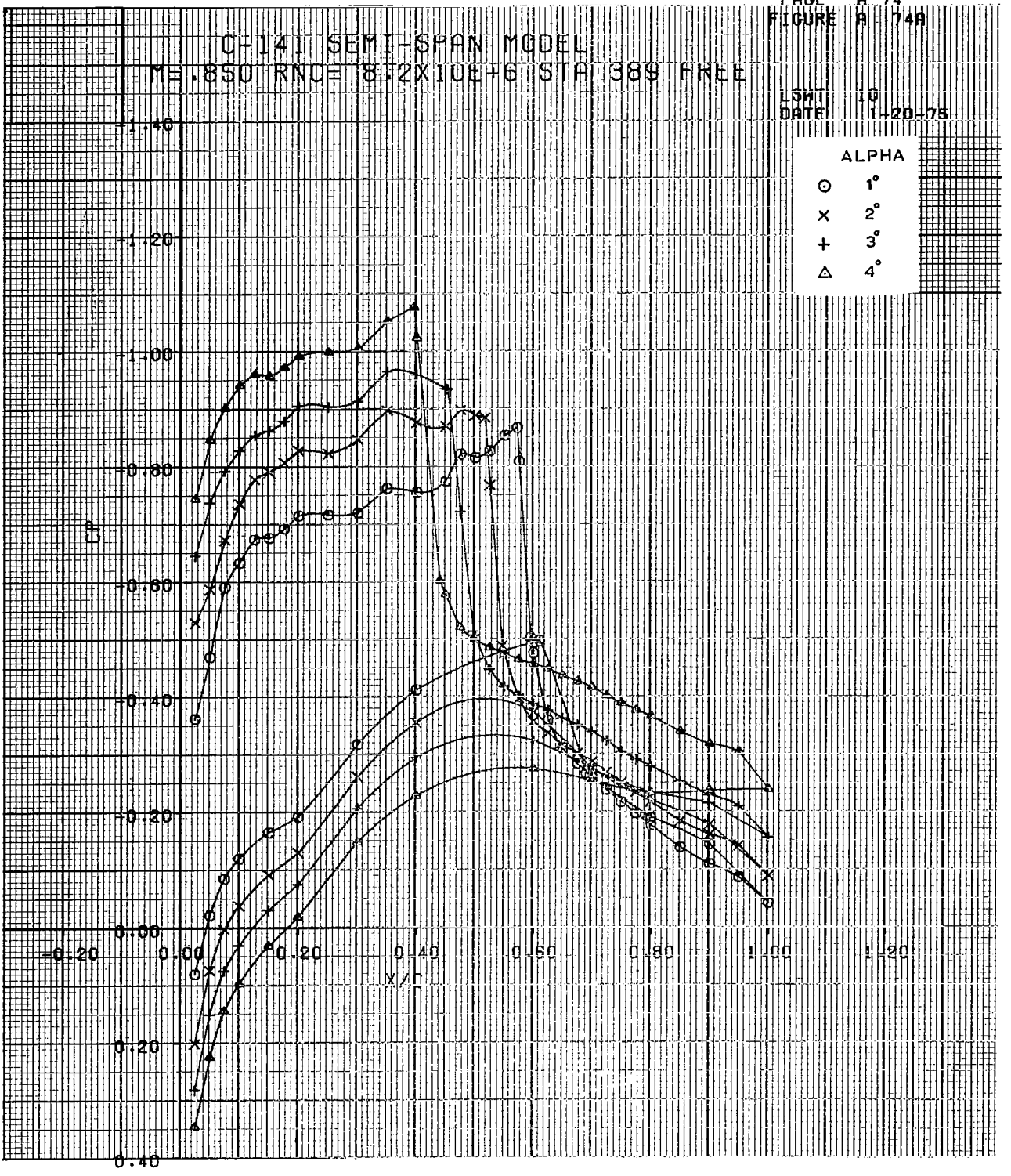
C-141 SEMI-SPAN MODEL
M=.850 RNC= 8.2X10E+6 STA 389 FREE
LSHT 10
DATE 1-20-75
ALPHA
1°
2°
3°
4°
-1.40
-1.20
-1.00
-0.80
-0.60
-0.40
-0.20
0.00
0.20
0.40
-0.20
0.00
0.20
0.40
0.60
0.80
1.00
1.20
X/C

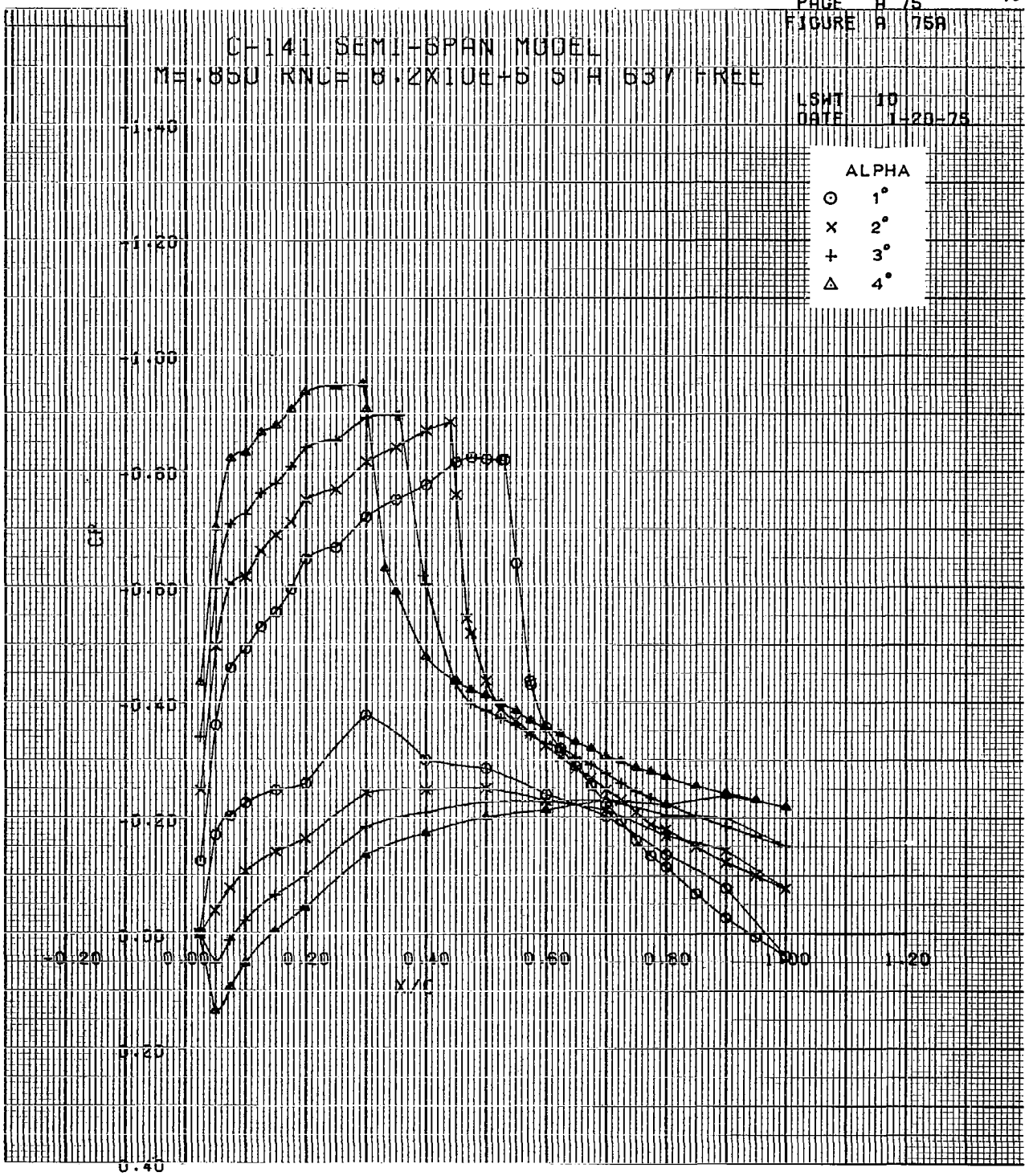
CH-141 SEMI-SPAN MODEL
ME.850 RNUE 8.2X10E+6 S/H 63% FREE
LSHT 10
DATE 1-20-75
ALPHA
1°
2°
3°
4°
CL
1.40
1.20
1.00
0.80
0.60
0.40
0.20
0.00
-0.20
0.00
0.20
0.40
0.60
0.80
1.00
1.20
X/C

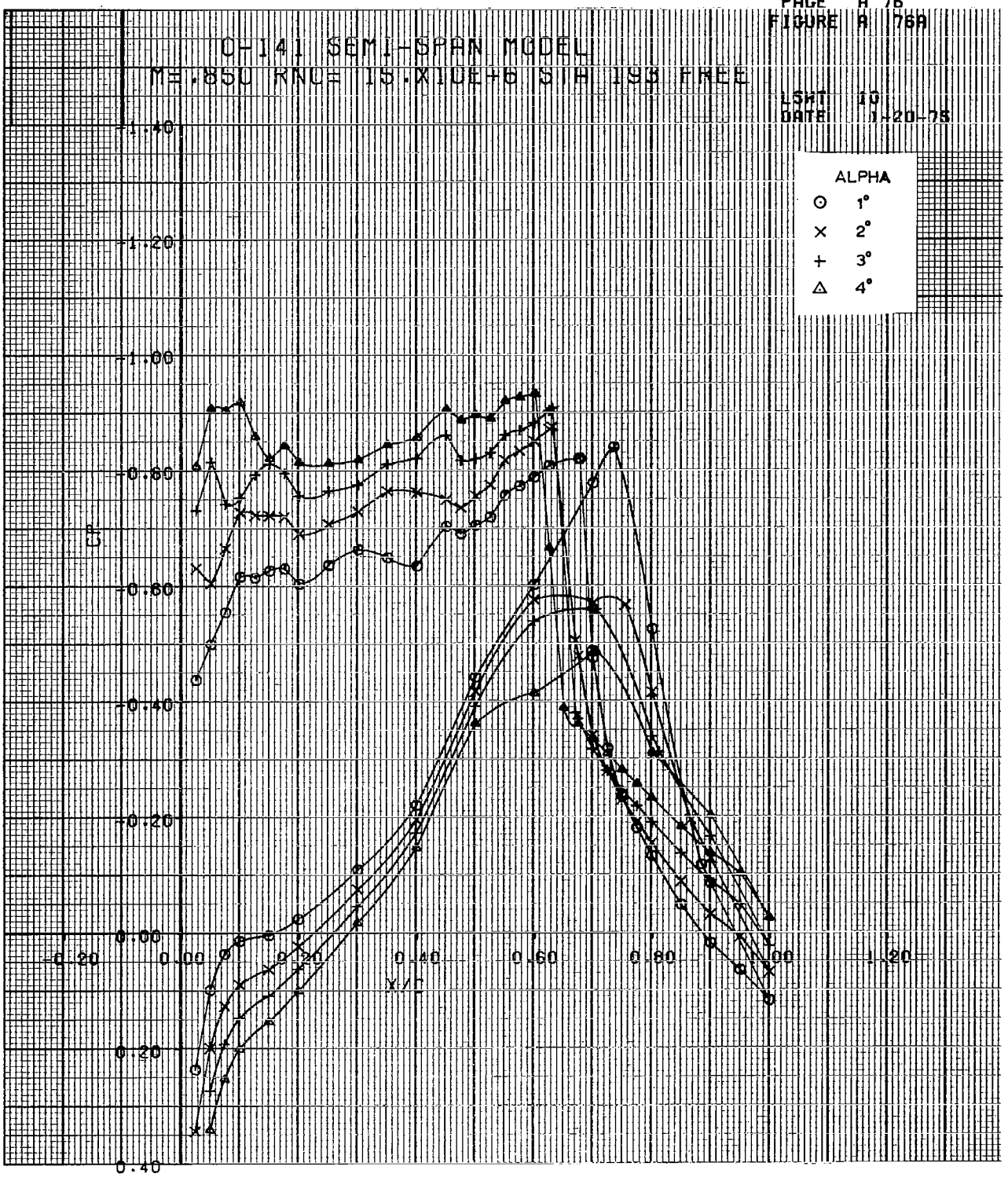
C-141 SEMI-SPAN MODEL
M=.850 RNC= 15.X10E+6 SIM ISS FREE
LSHT 10
DATE 1-20-78
ALPHA
1°
2°
3°
4°
-1.40
-1.20
-1.00
-0.80
-0.60
-0.40
-0.20
0.00
0.20
0.40
-0.20
0.00
0.20
0.40
0.60
0.80
1.00
1.20
X/C

FIGURE A 77A

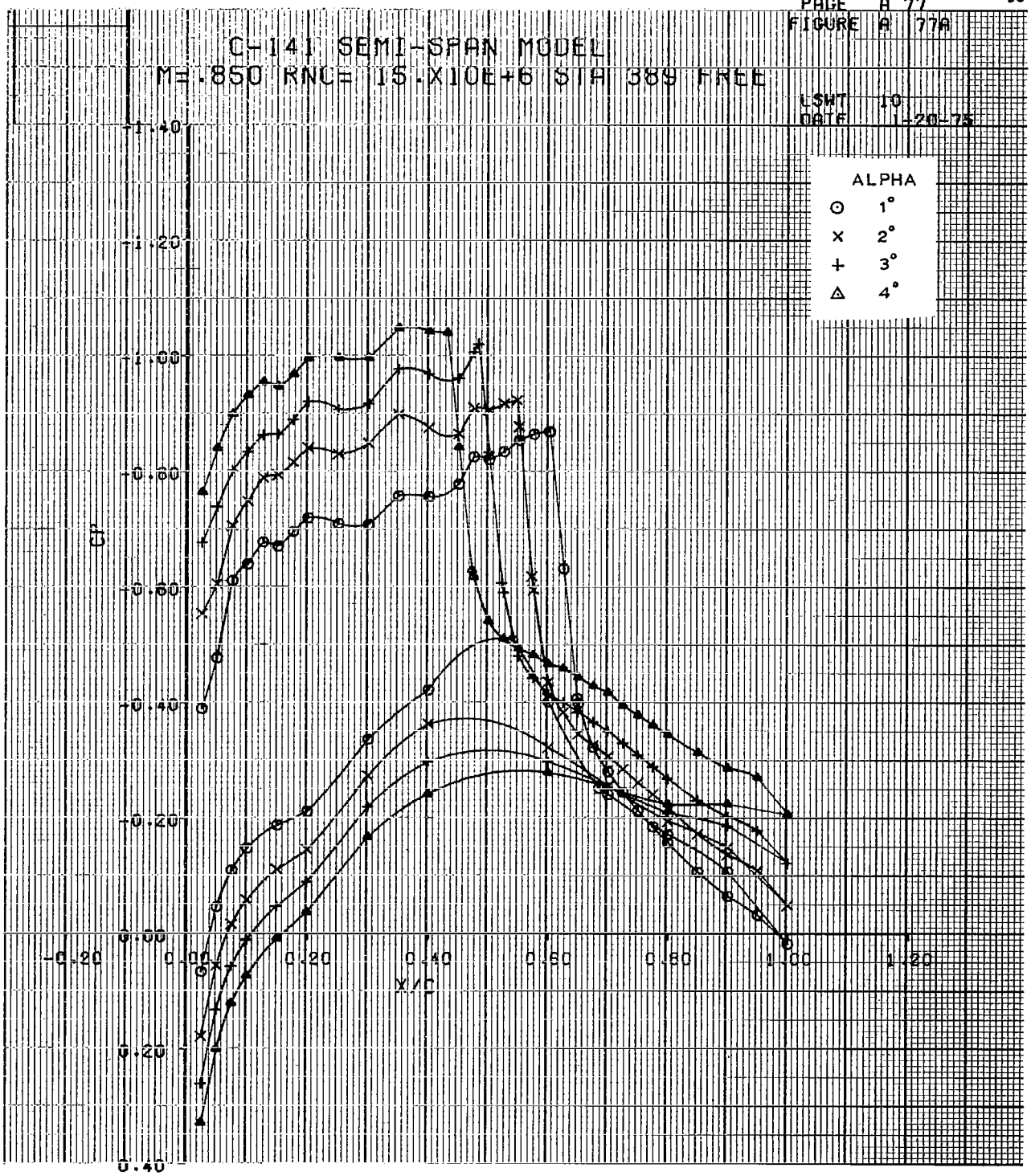
C-141 SEMI-SPAN MODEL
M=.850 RNC= 15.X10E+6 STA 389 FREE
LSWT 10
DATE 1-20-75
ALPHA
1°
2°
3°
4°
CP
X/C
1.40
1.20
1.00
0.80
0.60
0.40
0.20
0.00
-0.20
0.00
0.20
0.40
0.60
0.80
1.00
1.20
0.40

FIGURE A 78A

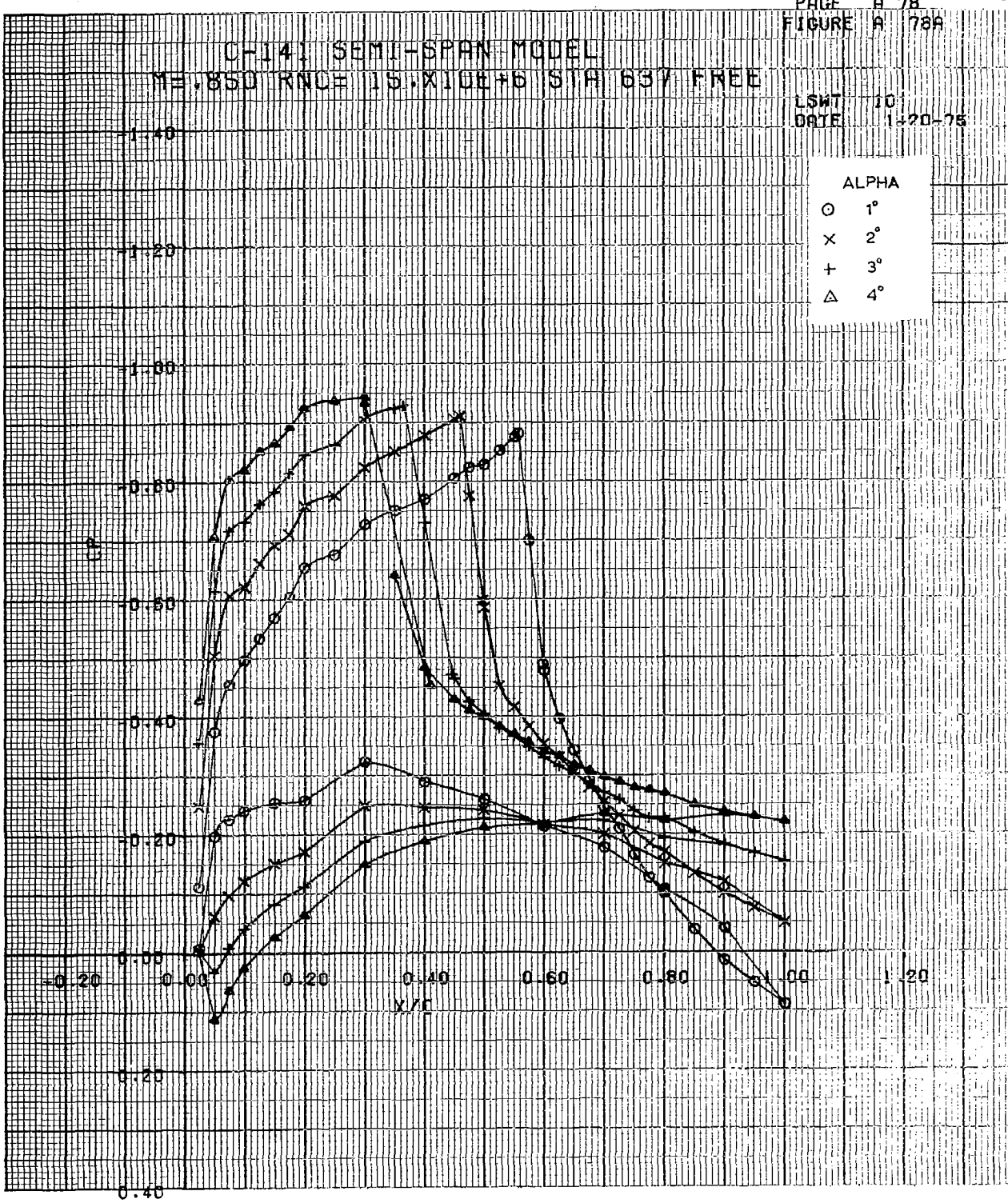
C-141 SEMI-SPAN MODEL
M=.850 RNC= 15.X10E+6 STA 637 FREE
LSWT 10
DATE 1-20-75
ALPHA
1°
2°
3°
4°
-1.40
-1.20
-1.00
-0.80
-0.60
-0.40
-0.20
0.00
0.20
-0.20
0.00
0.20
0.40
0.60
0.80
1.00
1.20
Y/C
0.40

CH-141 SEMI-SPAN MODEL
M=.850 KNUM 20.X10E+6 SHA 193 FREE

LSHT 10
DATE 1-20-75

ALPHA
⊙ 1°
× 2°
+ 3°
△ 4°

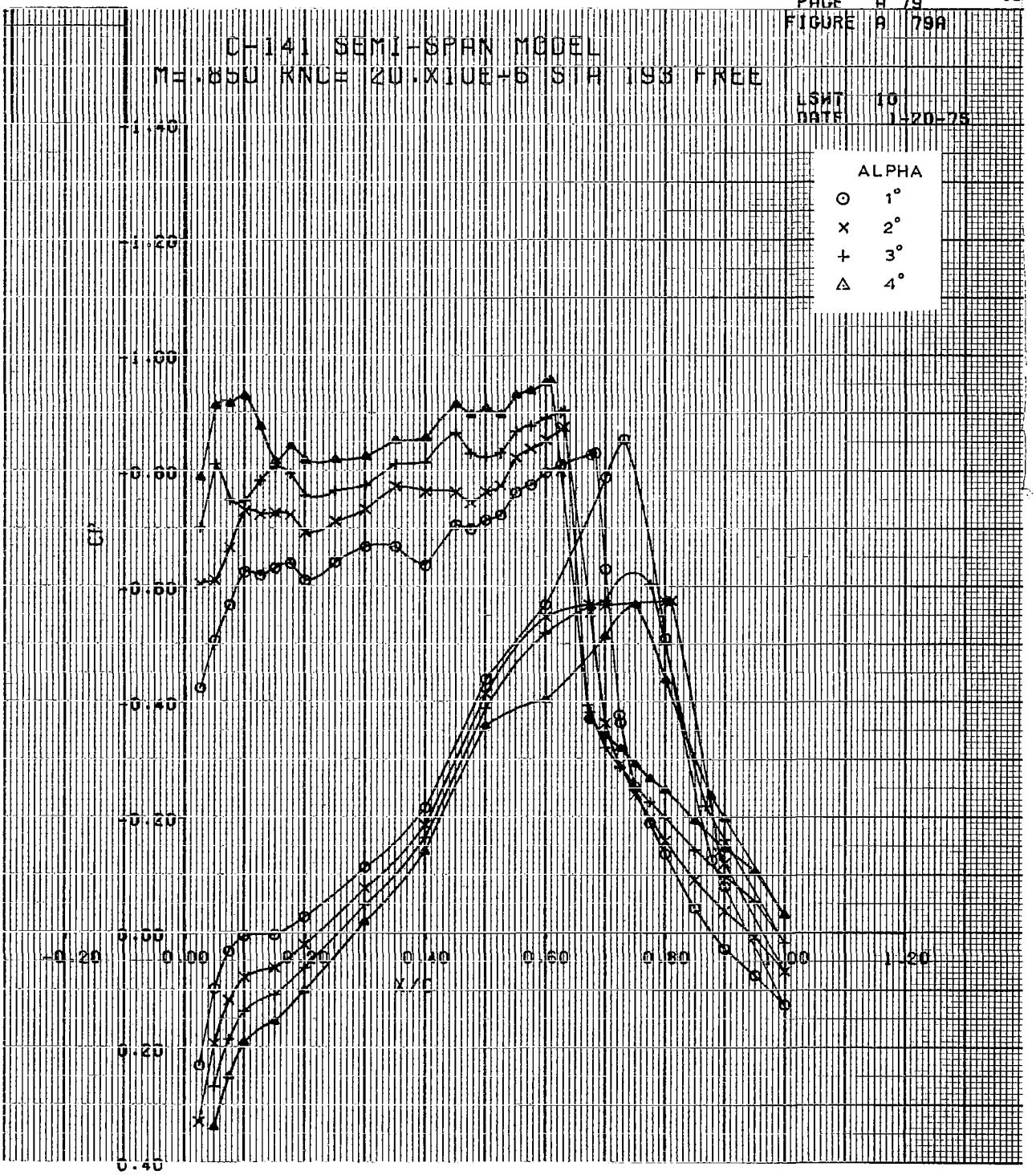

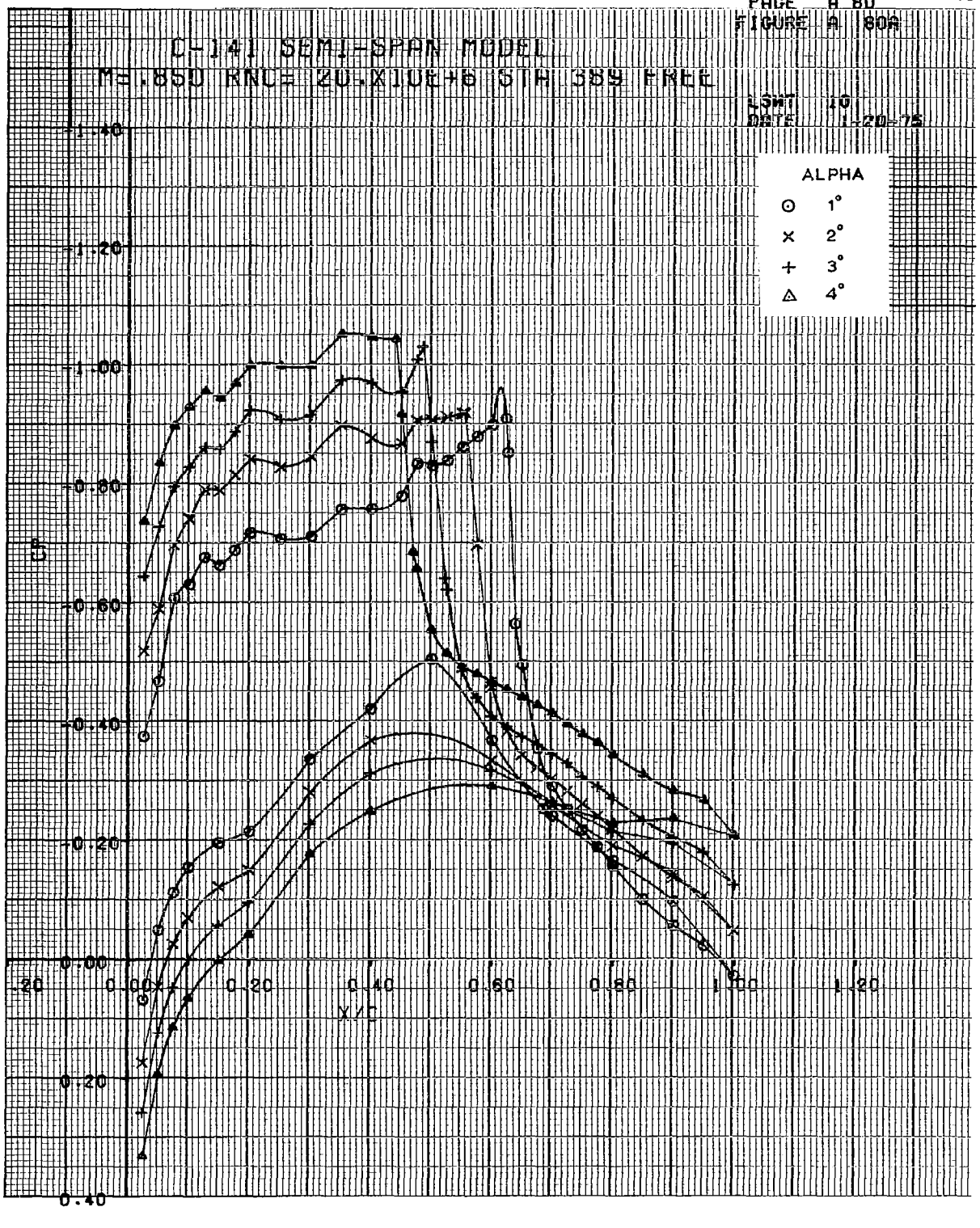
C-141 SEMI-SPAN MODEL
M=1.850 RNC= 20.X10E+6 STH 389 FREE
LSHT 10
DATE 1-20-75
ALPHA
⊙ 1°
× 2°
+ 3°
△ 4°
CP
-1.40
-1.20
-1.00
-0.80
-0.60
-0.40
-0.20
0.00
0.20
-.20
0.00
0.20
0.40
0.60
0.80
1.00
1.20
X/C

C-141 SEMI-SPAN MODEL
M=.850 RNC= 20.XJUE=6 STA 637 FREE

LSM1 40
DATE I=20-75

ALPHA
⊙ 1°
× 2°
+ 3°
△ 4°

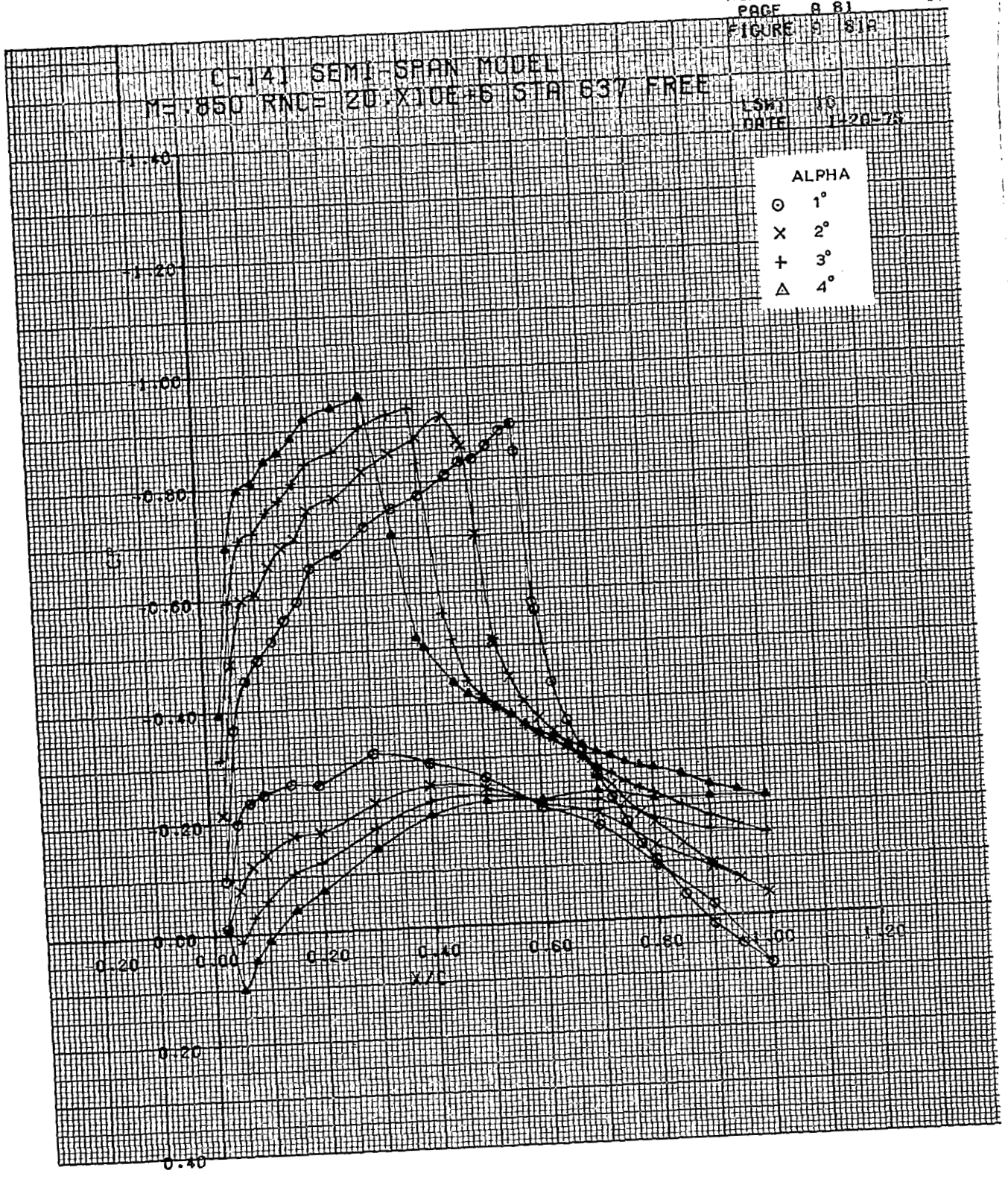

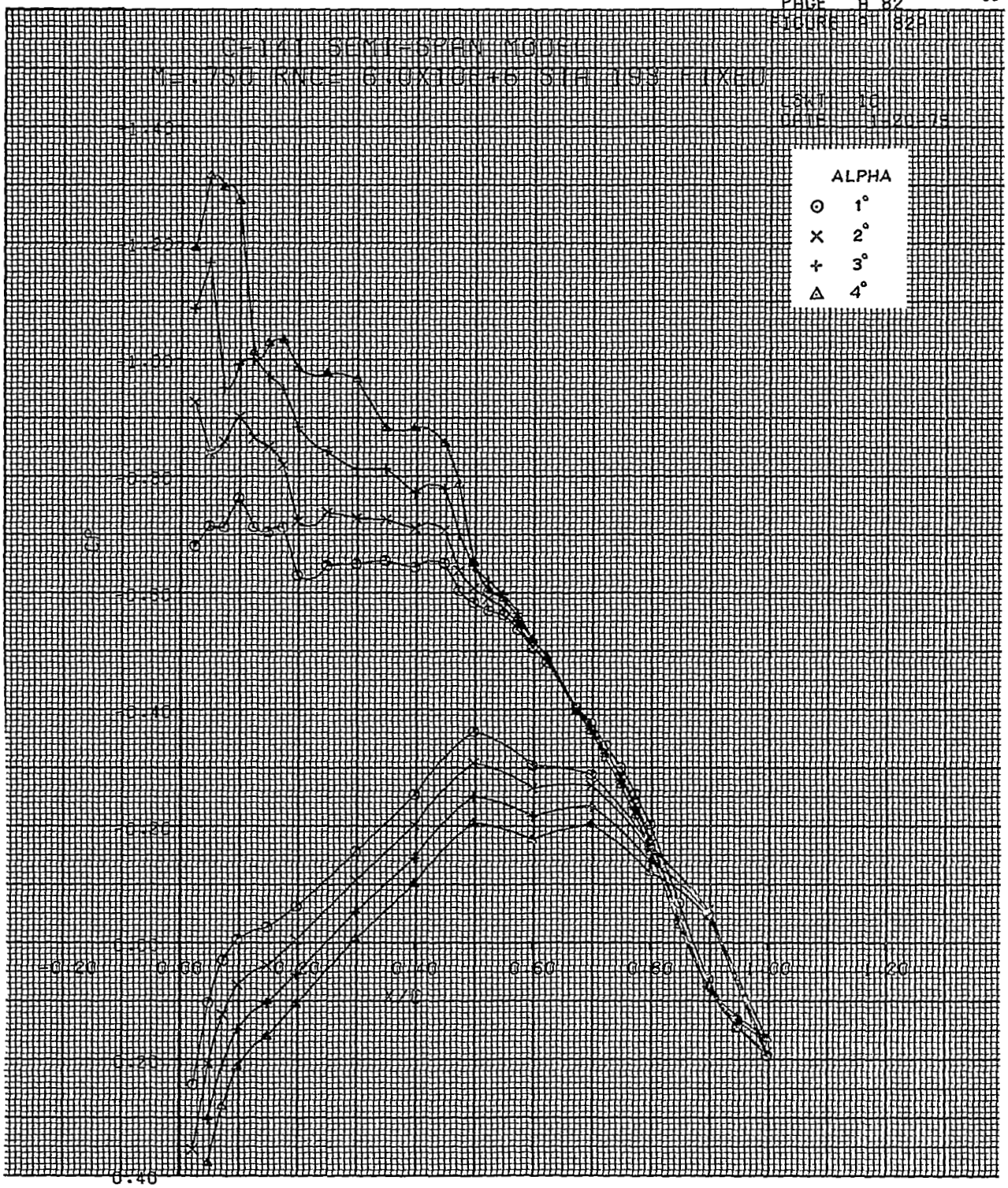
C-141 SEMI-SPAN MODEL
M= .750 RNC= 6.0X10+6 STR 155 FIXED
LSWT 10
DATE 11-20-75
ALPHA
1°
2°
3°
4°
-0.40
-0.20
0.00
0.20
0.40
0.60
0.80
1.00
1.20
XCP
0.40

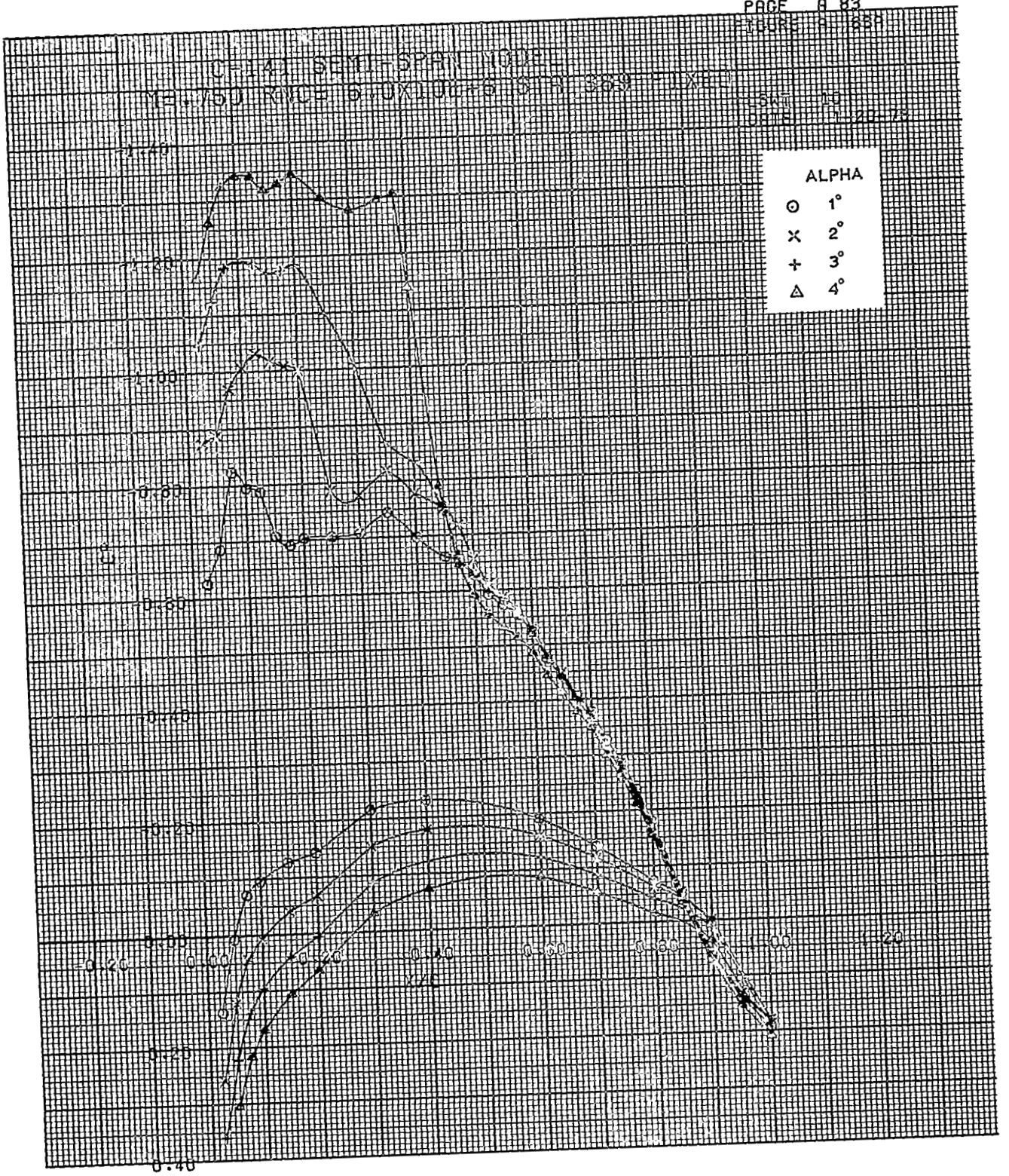
C-141 SEMI-SPAN MODEL
ALPHA
1°
2°
3°
4°
1.20
1.00
0.80
0.60
0.40
0.20
0.00
-0.20
-0.40
-0.60
-0.80
-1.00
-1.20
-0.20
0.00
0.20
0.40
0.60
0.80
1.00
1.20

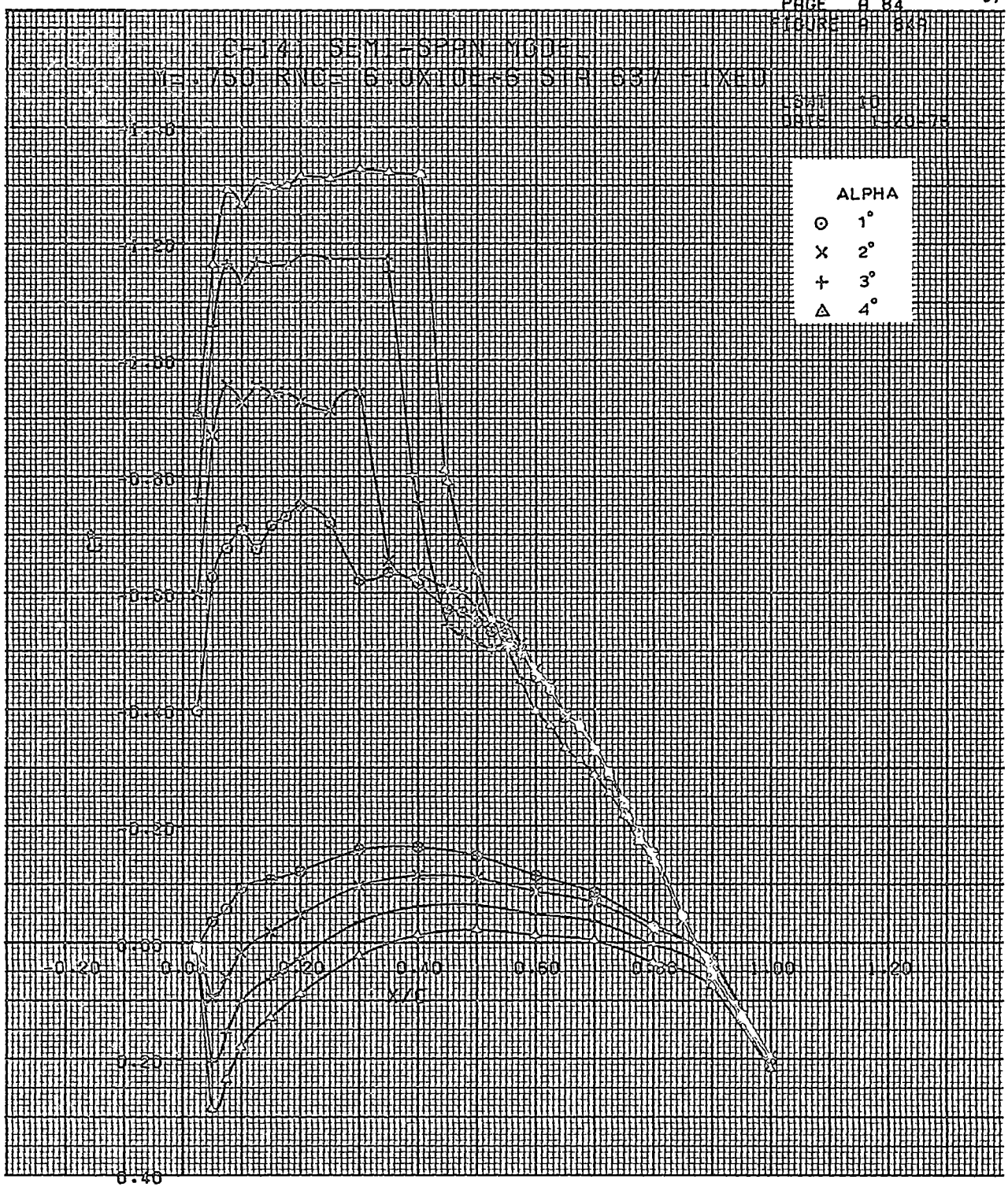
CF-14 SEMI-SPAN MODEL
M=.750 RNC= 6.0X10**6 S R 637 = IXED
ALPHA
1°
2°
3°
4°
-0.20
0.0
0.20
0.40
0.60
0.80
1.00
1.20
0.40

C-141 SEMI-SPAN MODEL
M=.750 RNC= 8.2X10E+6 STA 193 FIXED

LSWT 10
DATE 1-20-78

ALPHA
⊙ 1°
× 2°
+ 2°
△ 4°

C_p

1.40
1.20
1.00
0.80
0.60
0.40
0.20
0.00
-0.20
-0.40

-0.20 0.00 0.20 0.40 0.60 0.80 1.00 1.20

X/C

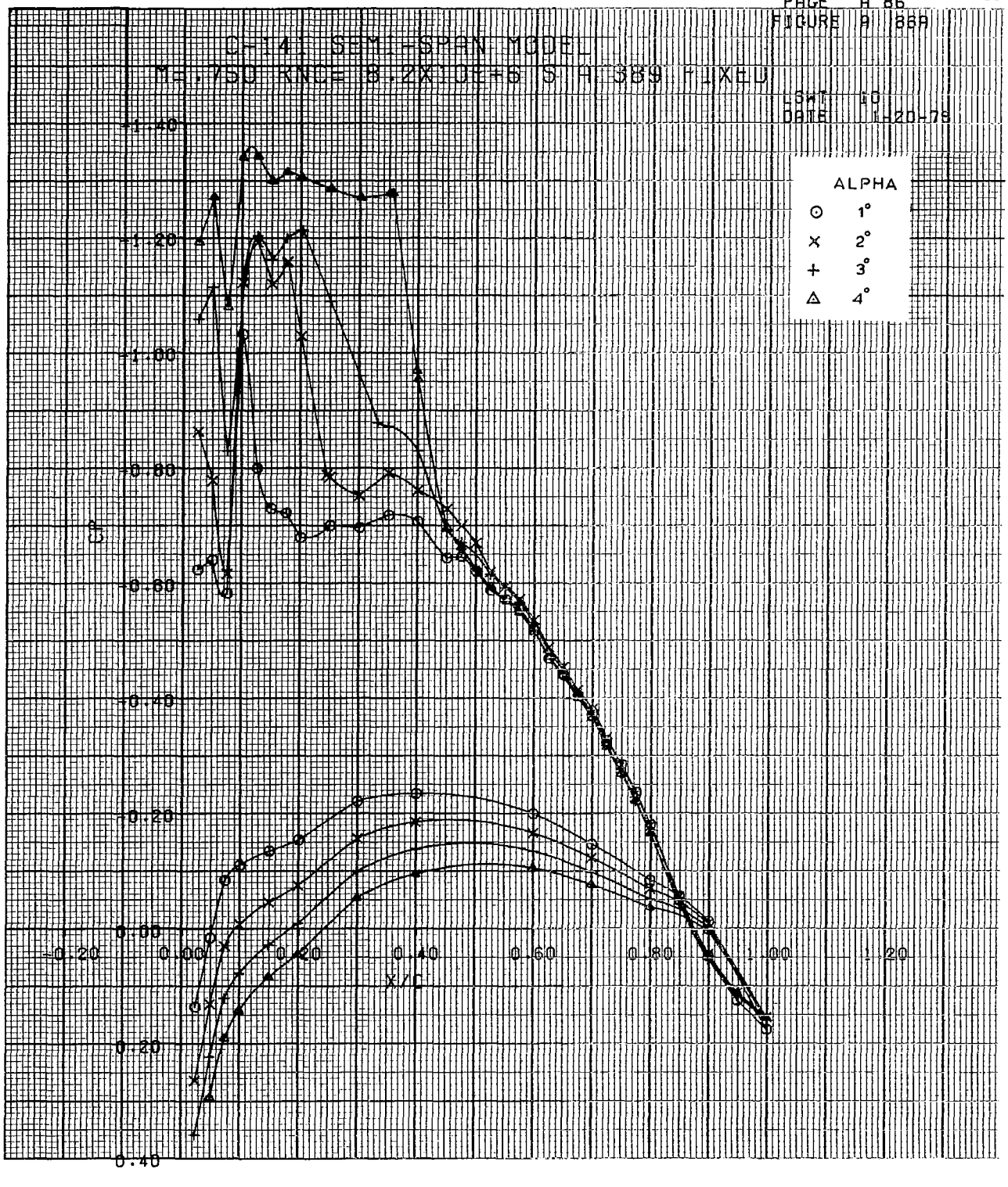
C-14 SEMI-SPAN MODEL
M=.750 RNC= 8.2X10E+6 S A 3&9 FIXED
LSWT 10
DATE 11-20-78
ALPHA
1°
2°
3°
4°
-1.40
-1.20
-1.00
-0.80
-0.60
-0.40
-0.20
0.00
0.20
0.40
-0.20
0.00
0.20
0.40
0.60
0.80
1.00
1.20
X/C

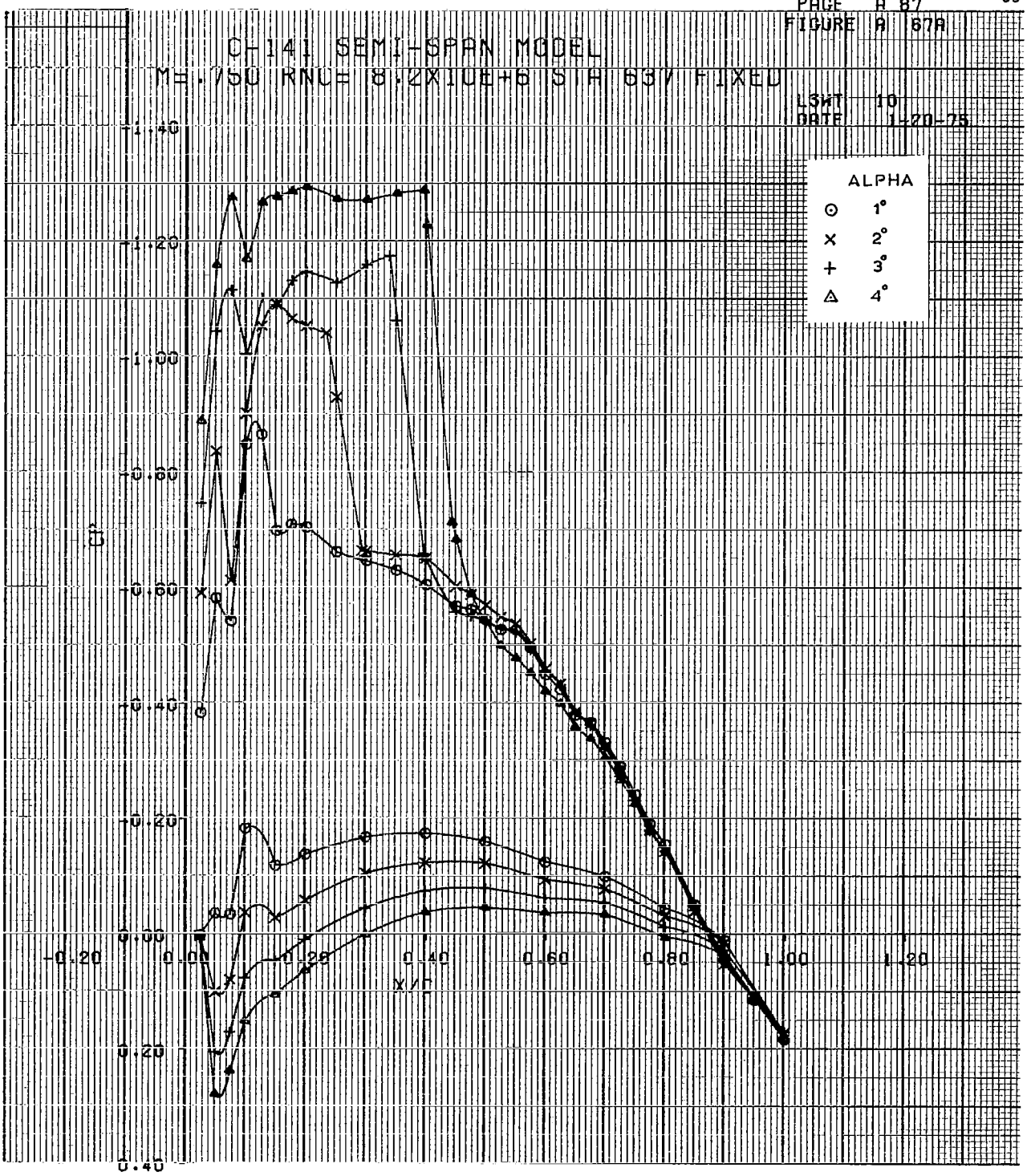
CF-141 SEMI-SPAN MODEL
M=.750 RNU= 8.2X10E+6 S/A 63/ FIXED
LSHT 10
DATE 1-20-75
ALPHA
1°
2°
3°
4°
CP
X/C
1.40
1.20
1.00
0.80
0.60
0.40
0.20
0.00
-0.20
0.20
0.40
-0.20
0.00
0.20
0.40
0.60
0.80
1.00
1.20

FIGURE A 86A

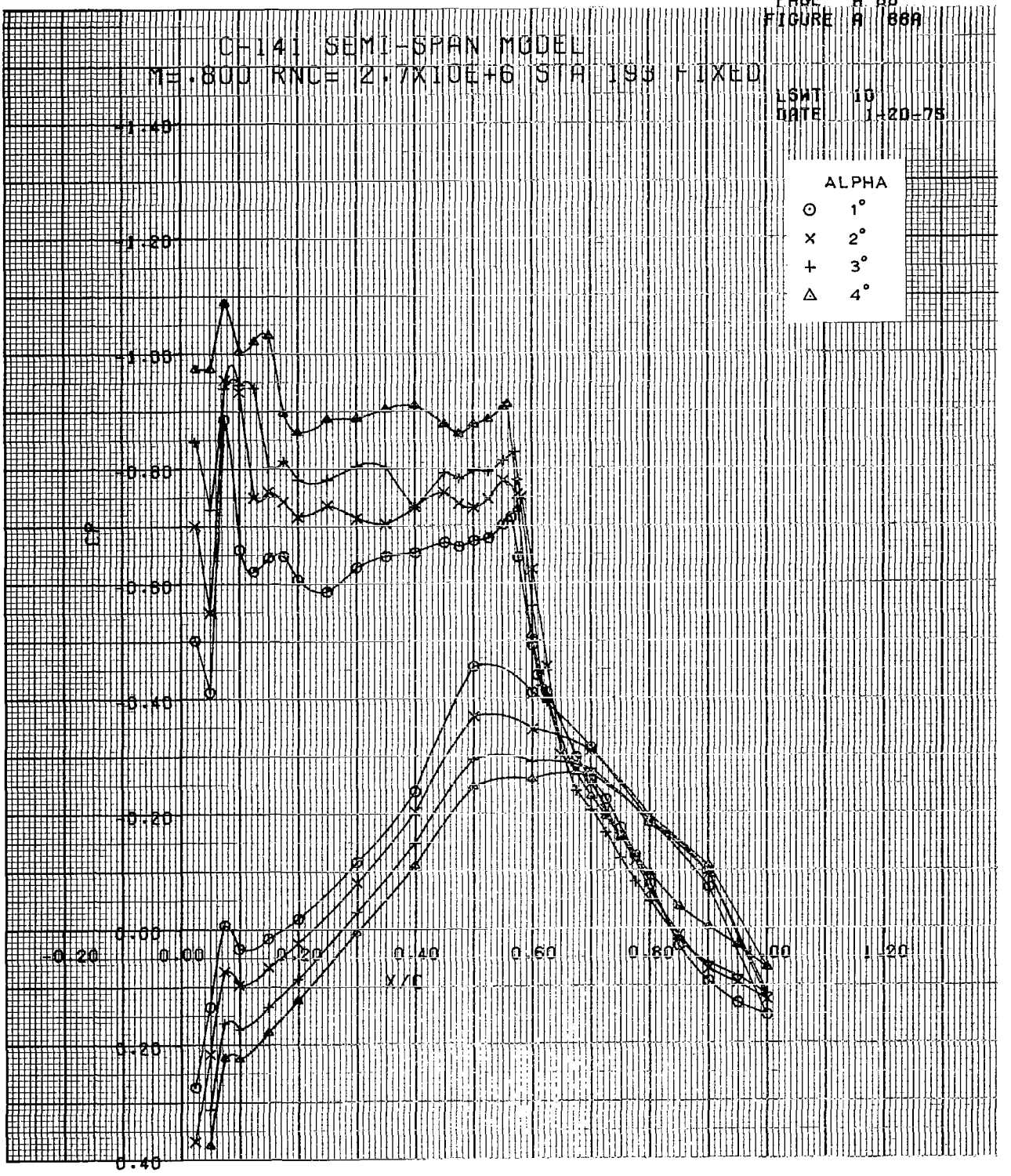
CH141 SEMI-SPAN MODEL
M=.800 RNC= 2.7X10E+6 STA 195 FIXED
LSHT 10
DATE 1-20-75
ALPHA
⊙ 1°
× 2°
+ 3°
△ 4°
-1.40
-1.20
-1.00
-0.80
-0.60
-0.40
-0.20
0.00
0.20
0.40
-0.20
0.00
0.20
0.40
0.60
0.80
1.00
1.20
X/C

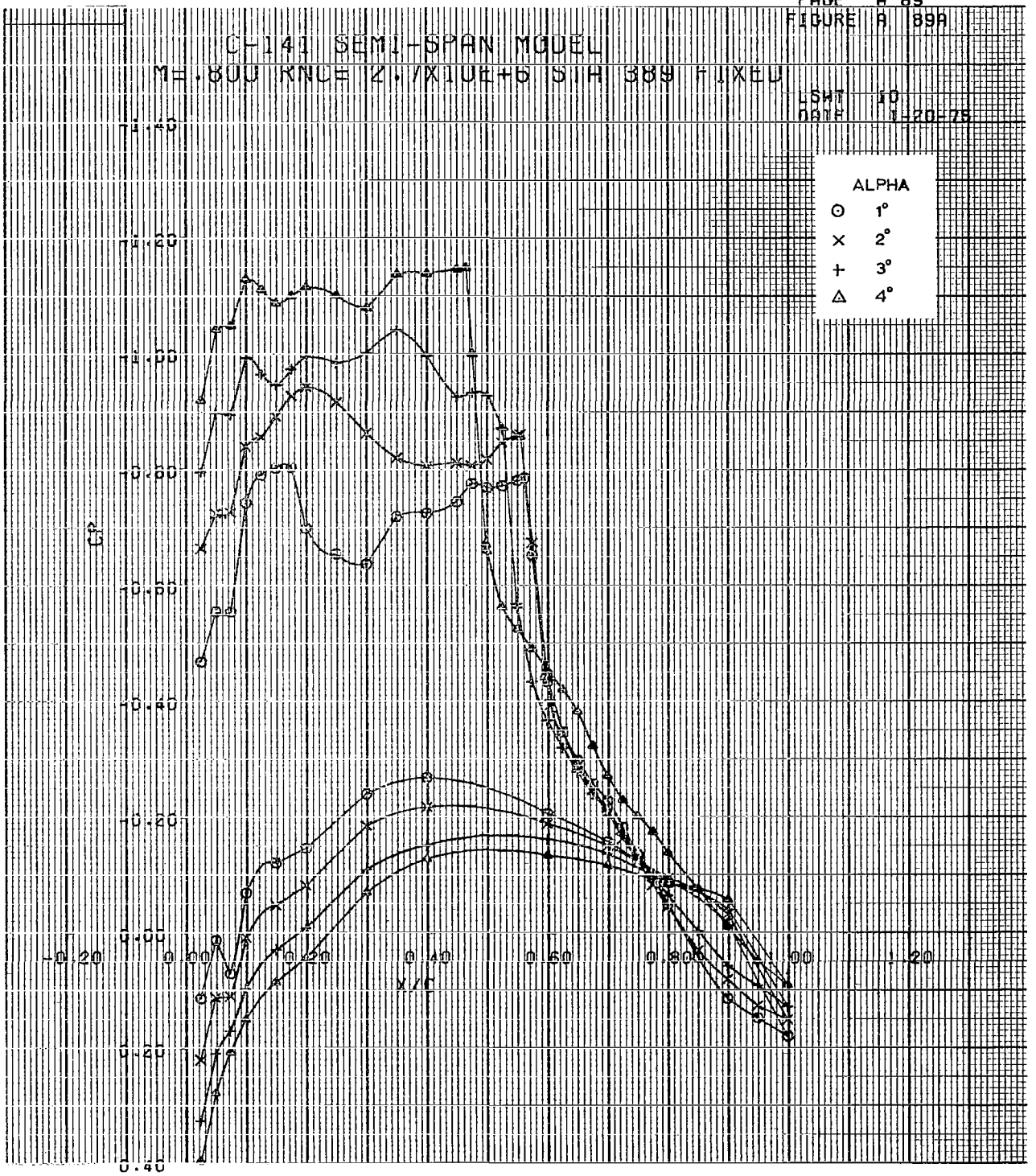
C-141 SEMI-SPAN MODEL
M=.800 KNCE Z=.7X10E+6 SHA 389 FIXED
LSHT 10
DATE 1-20-75
ALPHA
⊙ 1°
× 2°
+ 3°
△ 4°
CP
X/C

FIGURE A 90A

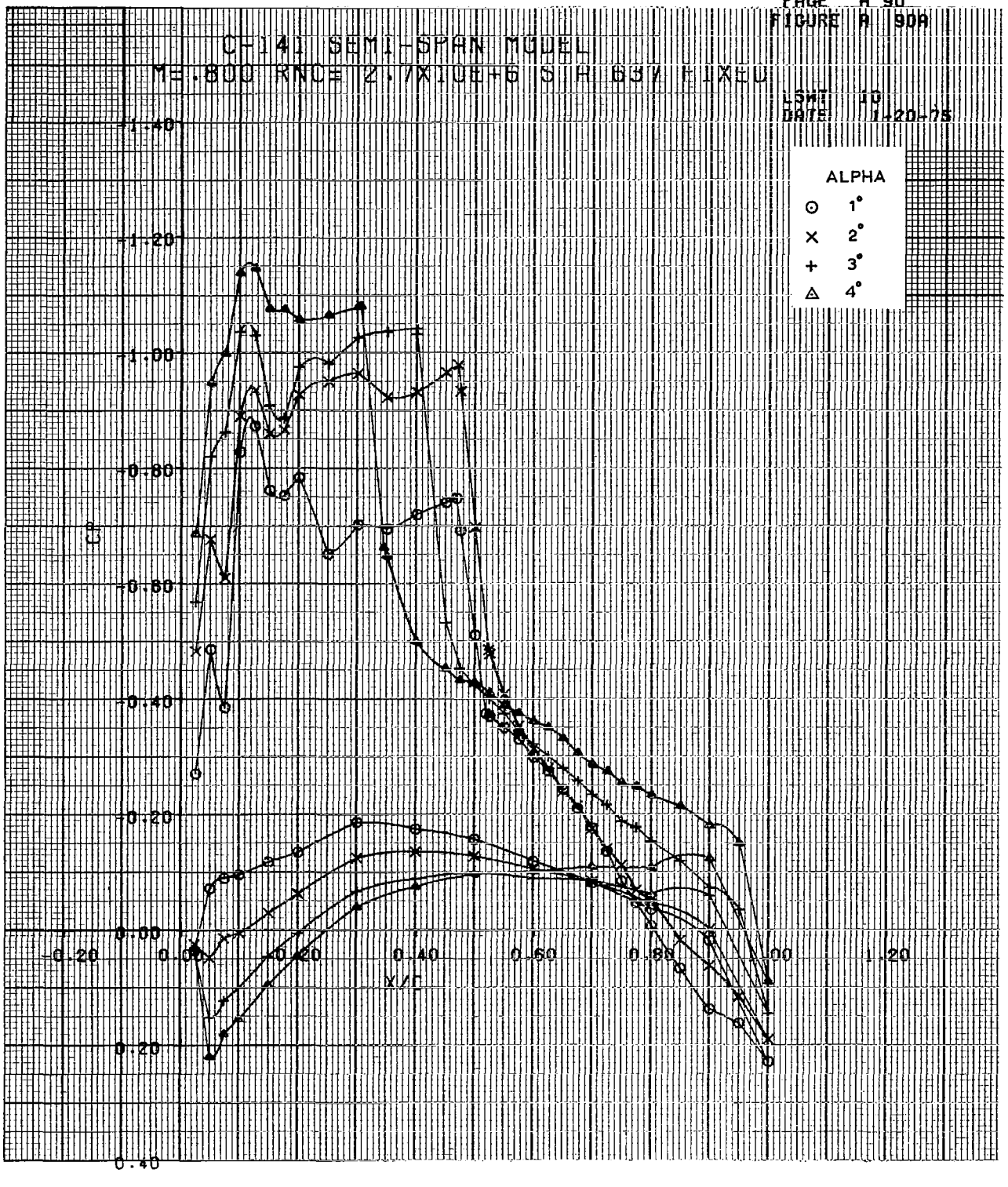
CF-141 SEMI-SPAN MODEL
M=.800 RNC= 2.7X10E+6 S.H. 63% FIXED
LSMT 10
DATE 1-20-75
ALPHA
1°
2°
3°
4°
-1.40
-1.20
-1.00
-0.80
-0.60
-0.40
-0.20
0.00
0.20
0.40
-0.20
0.00
0.20
0.40
0.60
0.80
1.00
1.20
Y/S

C-141 SEMI-SPAN MODEL
M=.800 RNC= 6.0X10E+6 STN 193 FIXED

LSHT 10
DATE 1-20-75

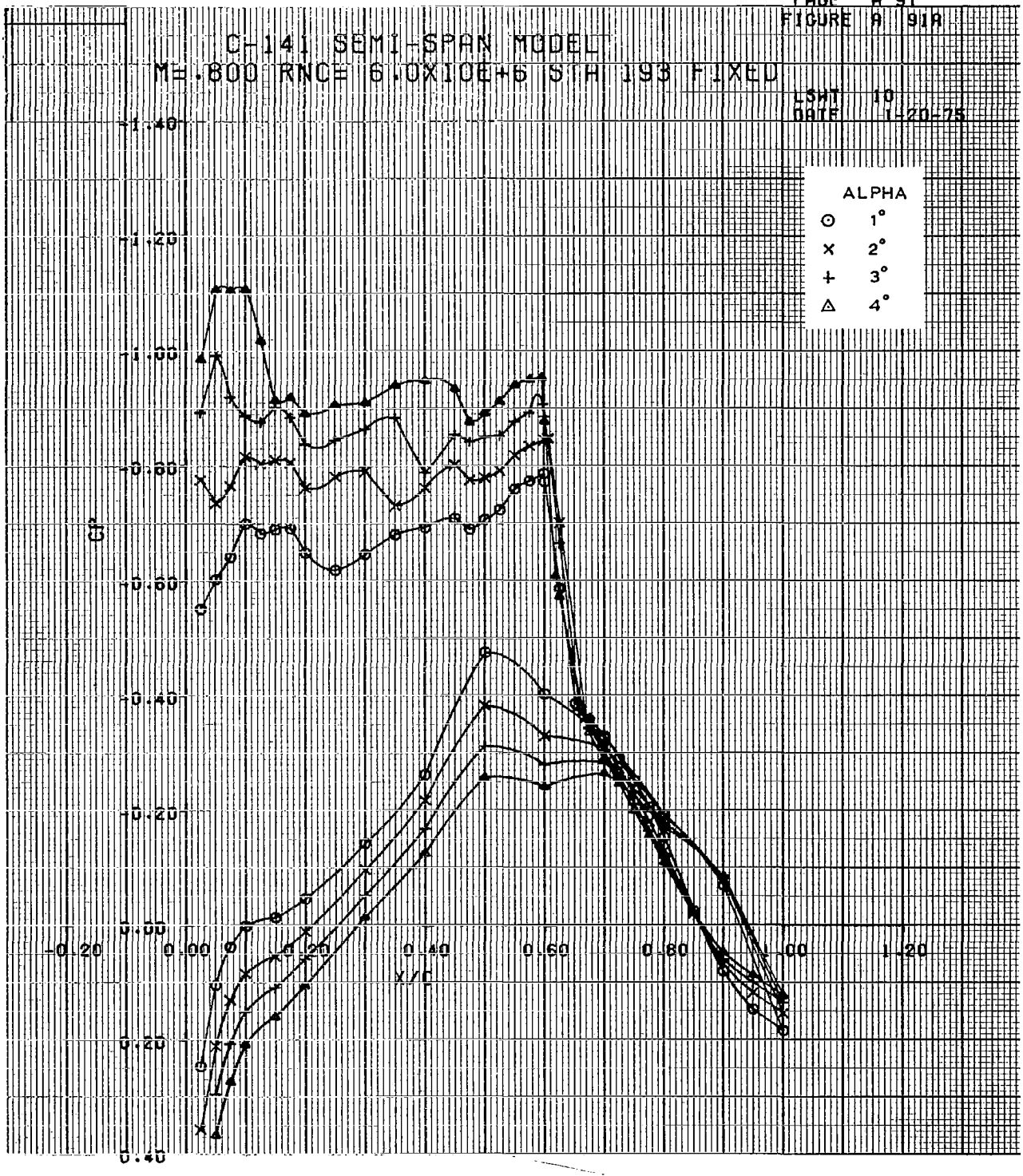

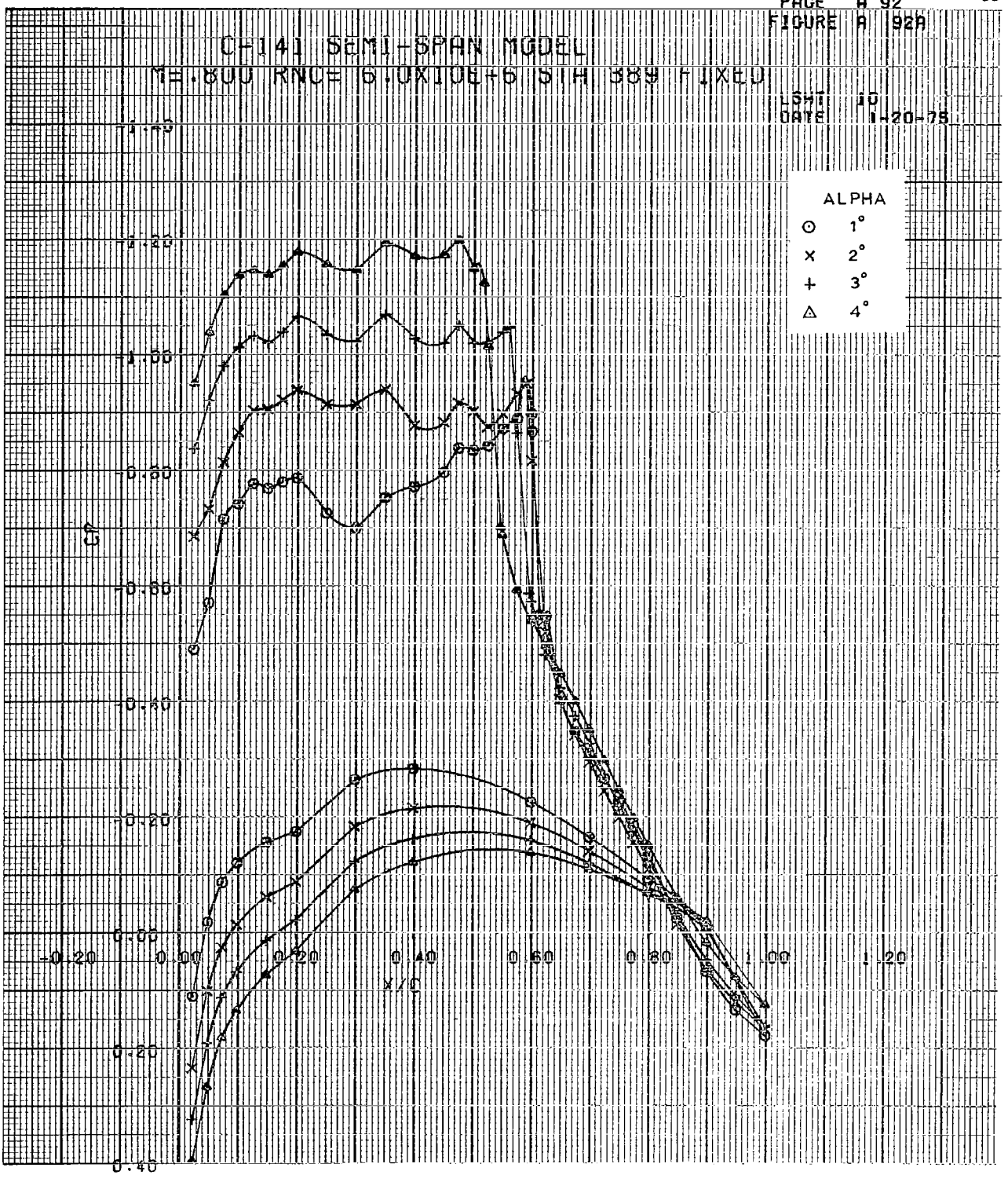
C-141 SEMI-SPAN MODEL
M=.800 RNC= 6.0X10E+6 SIM 38% FIXED
LSHT 10
DATE 1-20-75
ALPHA
⊙ 1°
× 2°
+ 3°
△ 4°
CP
-1.00
-0.80
-0.60
-0.40
-0.20
0.00
0.20
0.40
-0.20
0.00
0.20
0.40
0.60
0.80
1.00
1.20
X/C

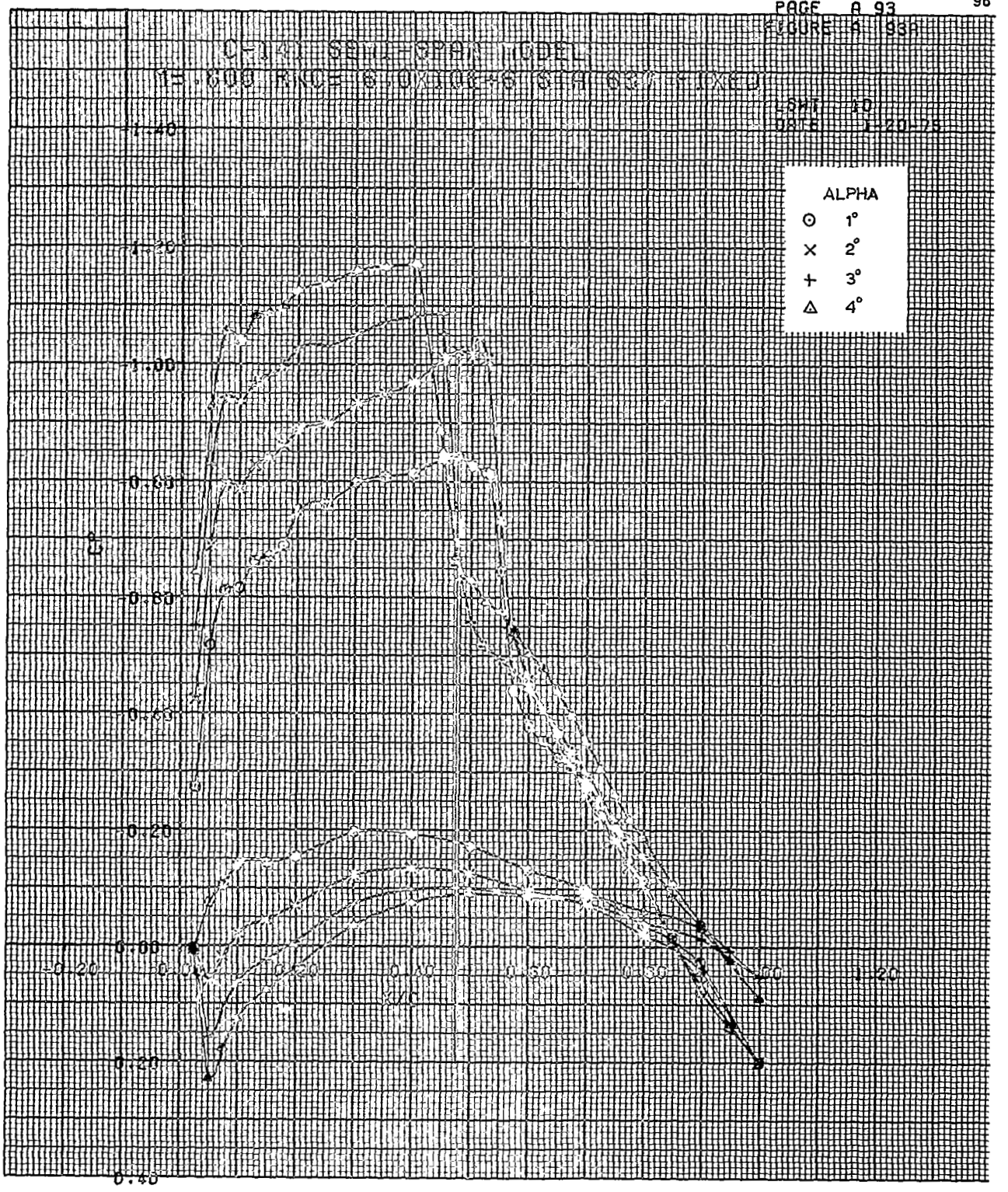
ALPHA
1°
2°
3°
4°
-1.40
-1.00
-0.60
-0.20
0.00
0.20
0.40
-0.20
0.20
0.60
1.00
1.20

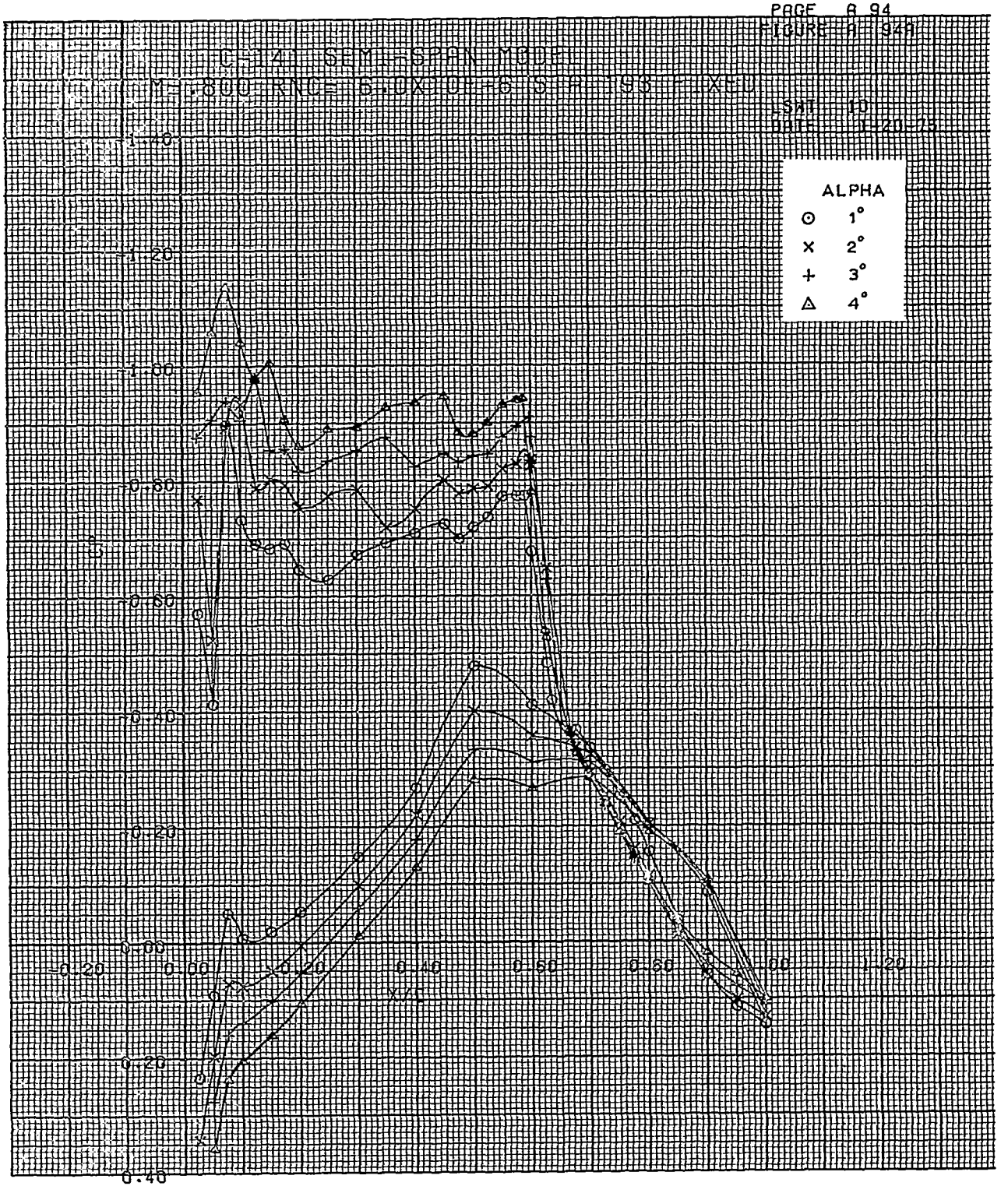
C-141 SEMI-SPAN MODEL
M=.800 RNC= 6.0X10E+6 S A 1976 F XFC 0
SHT 10
DATE 3-20-75
ALPHA
⊙ 1°
× 2°
+ 3°
△ 4°
-1.40
-1.20
-1.00
-0.80
-0.60
-0.40
-0.20
0.00
0.20
0.40
0.60
0.80
1.00
1.20
X/C

C-141 SEMI-SPAN MODEL
M=.800 RNLE 6.0X10E+6 STH 389 FIXED

LSWT 10
DATE 1-20-78

ALPHA
⊙ 1°
× 2°
+ 3°
△ 4°

CP

1.40
1.20
1.00
0.80
0.60
0.40
0.20
0.00
-0.20
-0.40

-0.20 0.00 0.20 0.40 0.60 0.80 1.00 1.20

X/C

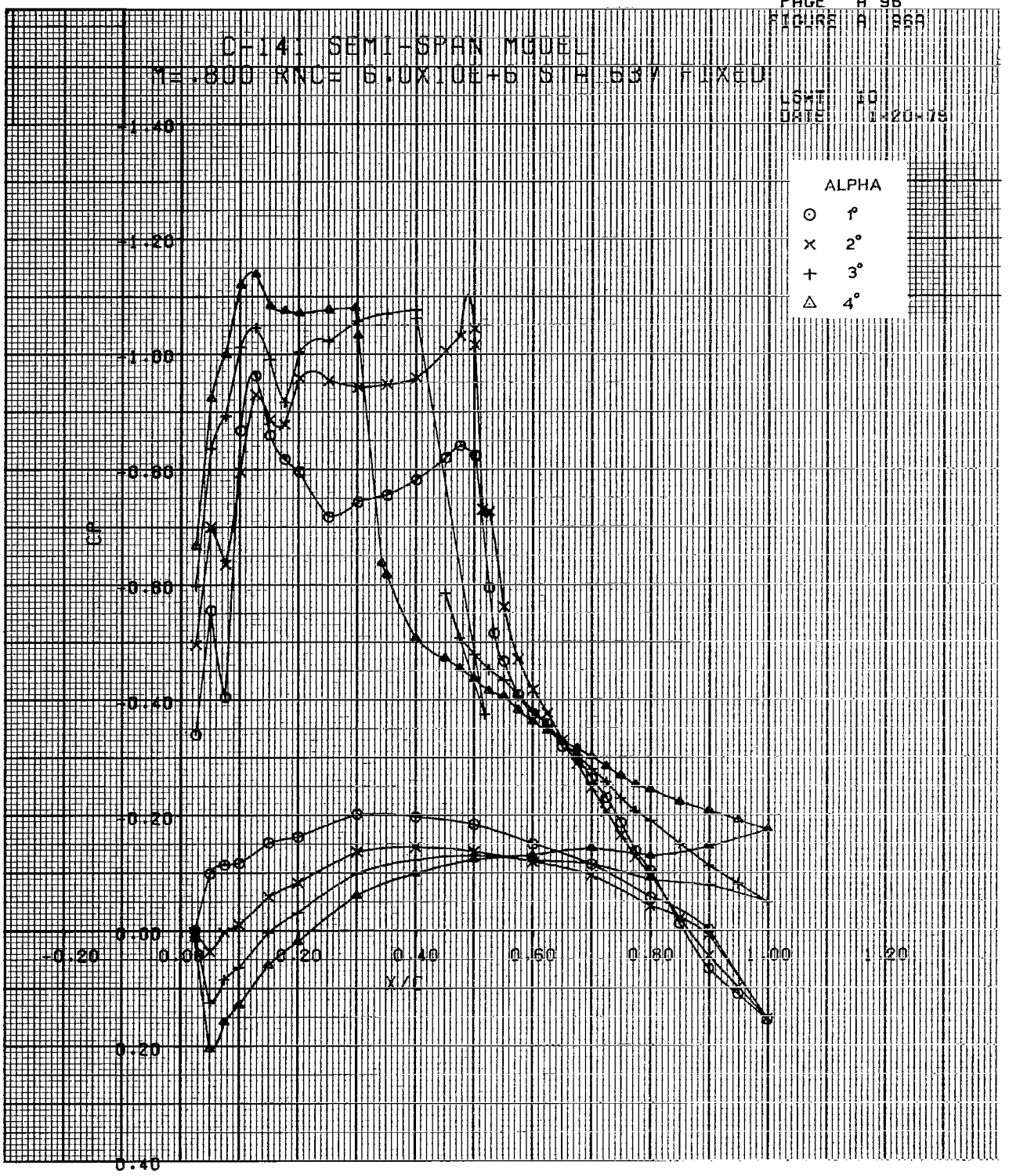
C-141 SEMI-SPAN MODEL
M=.800 RNC= 6.0X10E+6 S.R.63Y FIXED
USER: FD
DATE: 1-20-75
ALPHA
1°
2°
3°
4°
-Cp
+1.40
+1.20
+1.00
+0.80
+0.60
+0.40
+0.20
0.00
-0.20
-0.40
-0.20
0.00
0.20
0.40
0.60
0.80
1.00
1.20
X/C

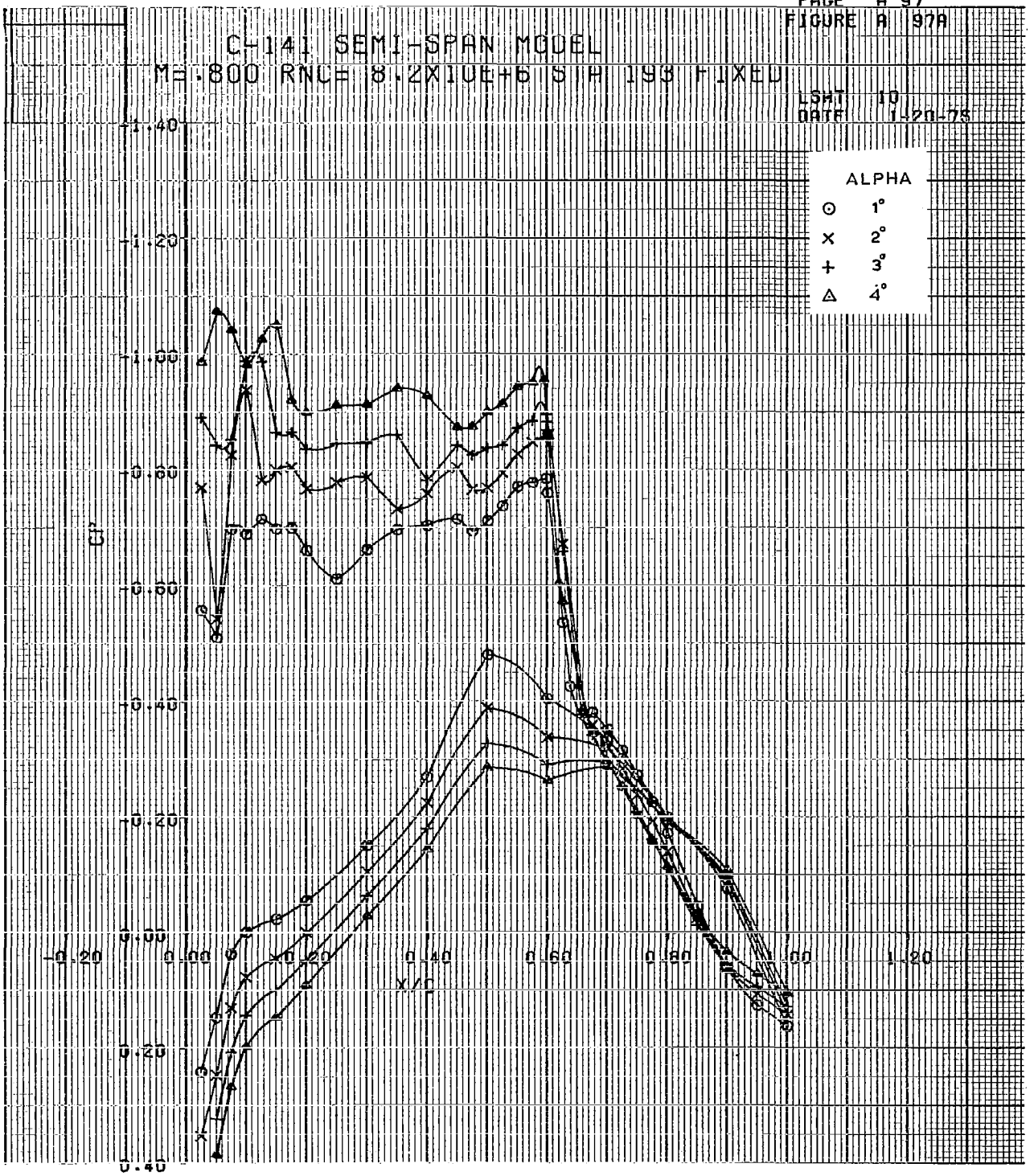
CL-141 SEMI-SPAN MODEL
M=.800 RNL= 8.2X10E+6 S H 193 FIXED
LSHT 10
DATE 1-20-75
ALPHA
⊙ 1°
× 2°
+ 3°
△ 4°
CP
1.40
1.20
1.00
0.80
0.60
0.40
0.20
0.00
-0.20
0.00
0.20
0.40
0.60
0.80
1.00
1.20
X/C

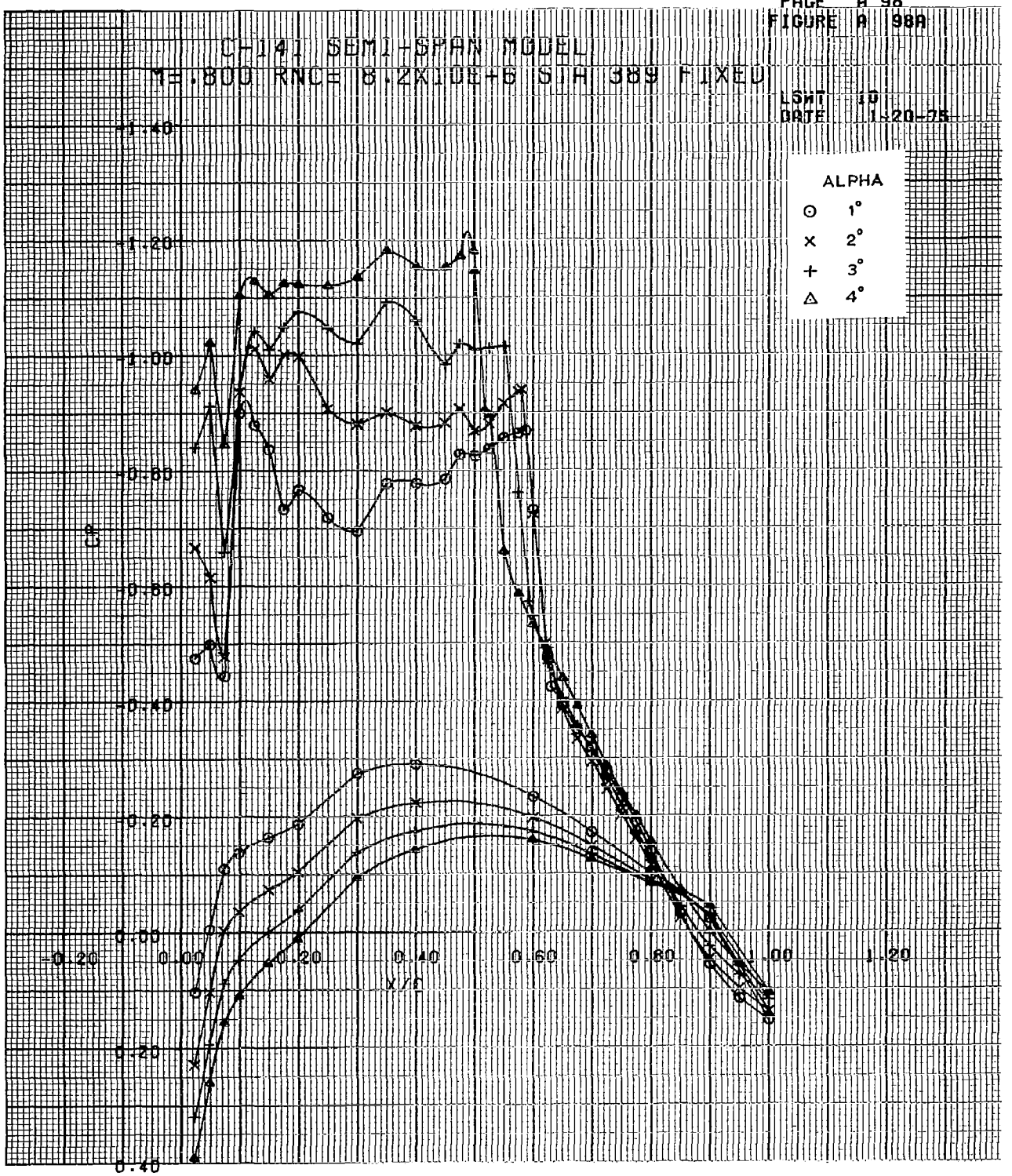
C-141 SEMI-SPAN MODEL
M=.800 RNC= 6.2X10E+6 S/A 389 FIXED
LSHT 10
DATE 1-20-75
ALPHA
1°
2°
3°
4°
-1.40
-1.20
-1.00
-0.80
-0.60
-0.40
-0.20
0.00
0.20
0.40
-0.20
0.00
0.20
0.40
0.60
0.80
1.00
1.20
X/C

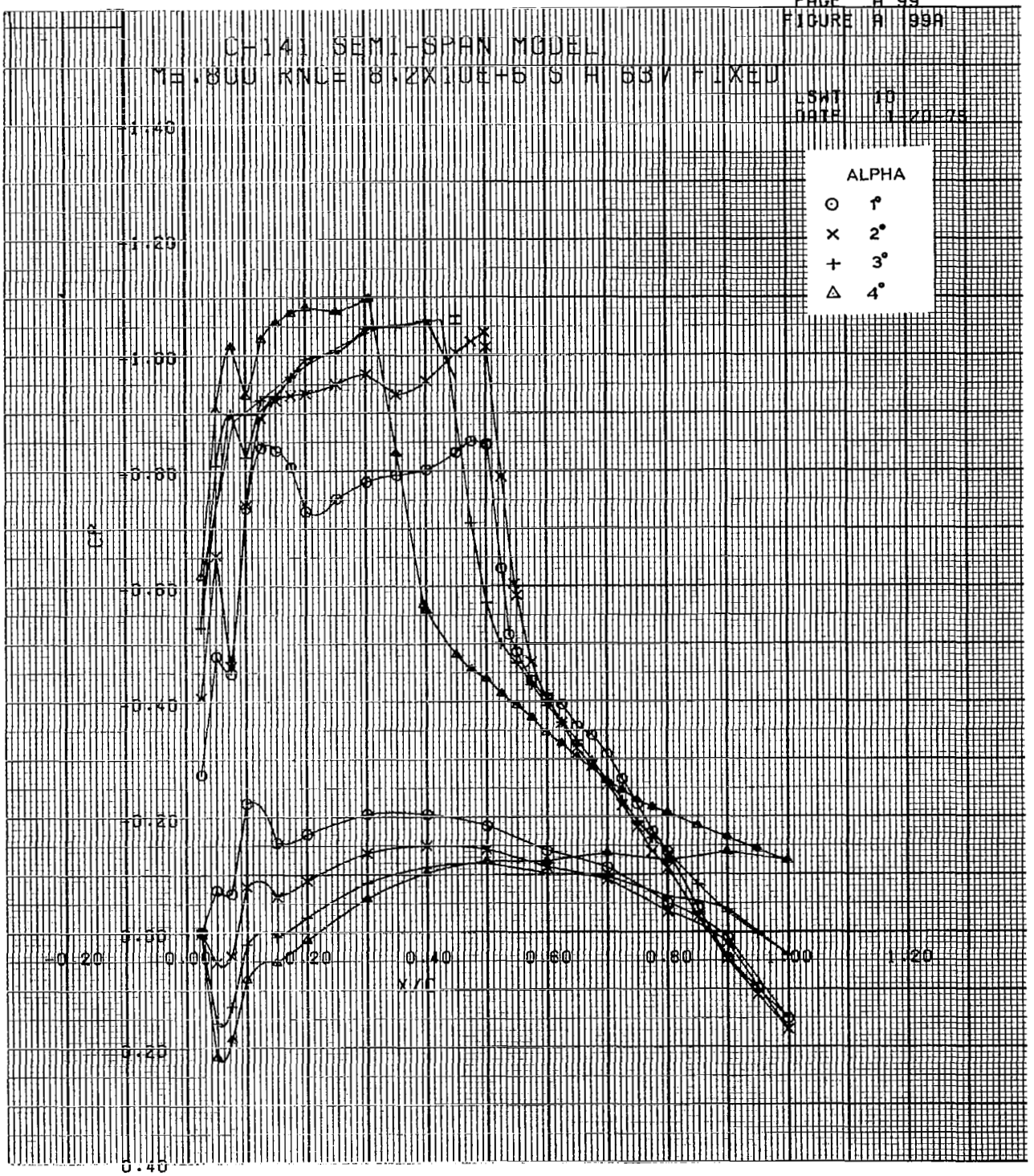
CH141 SEMI-SPAN MODEL
M=.800 RNLE 8.2X10E+6 S A 53Y FIXED
SHT 19
DATE 1-20-75
ALPHA
1°
2°
3°
4°
1.40
1.20
1.00
0.80
0.60
0.40
0.20
0.00
-0.20
-0.40
CP
-0.20
0.00
0.20
0.40
0.60
0.80
1.00
1.20
X/C

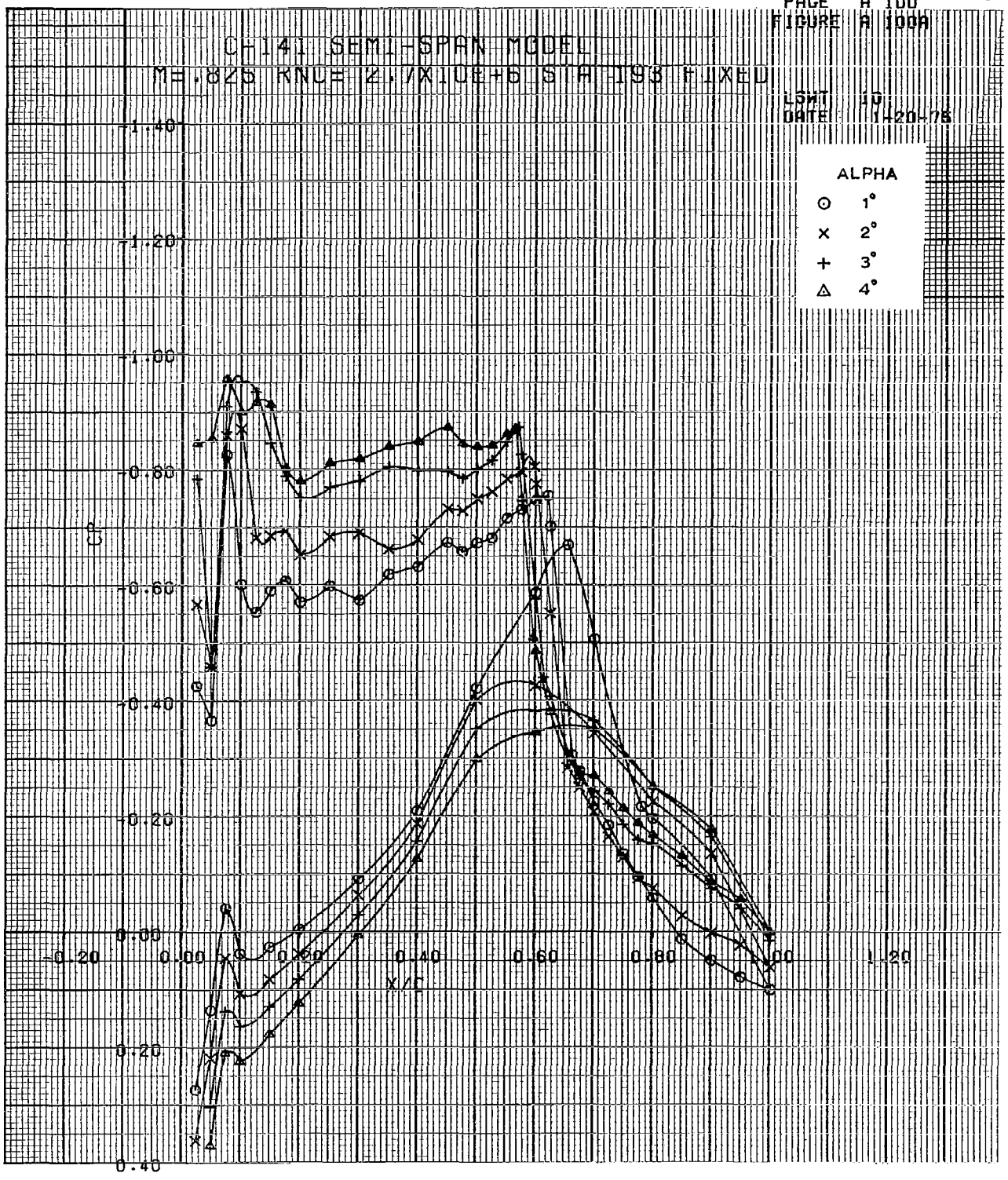
CH141 SEMI-SPAN MODEL
M=.825 KNUE 2.7X10E+6 S A 193 FIXED
LGHT 10
DATE 1-20-78
ALPHA
1°
2°
3°
4°
-1.40
-1.20
-1.00
-0.80
-0.60
-0.40
-0.20
0.00
0.20
0.40
-0.20
0.00
0.20
0.40
0.60
0.80
1.00
1.20
X/C

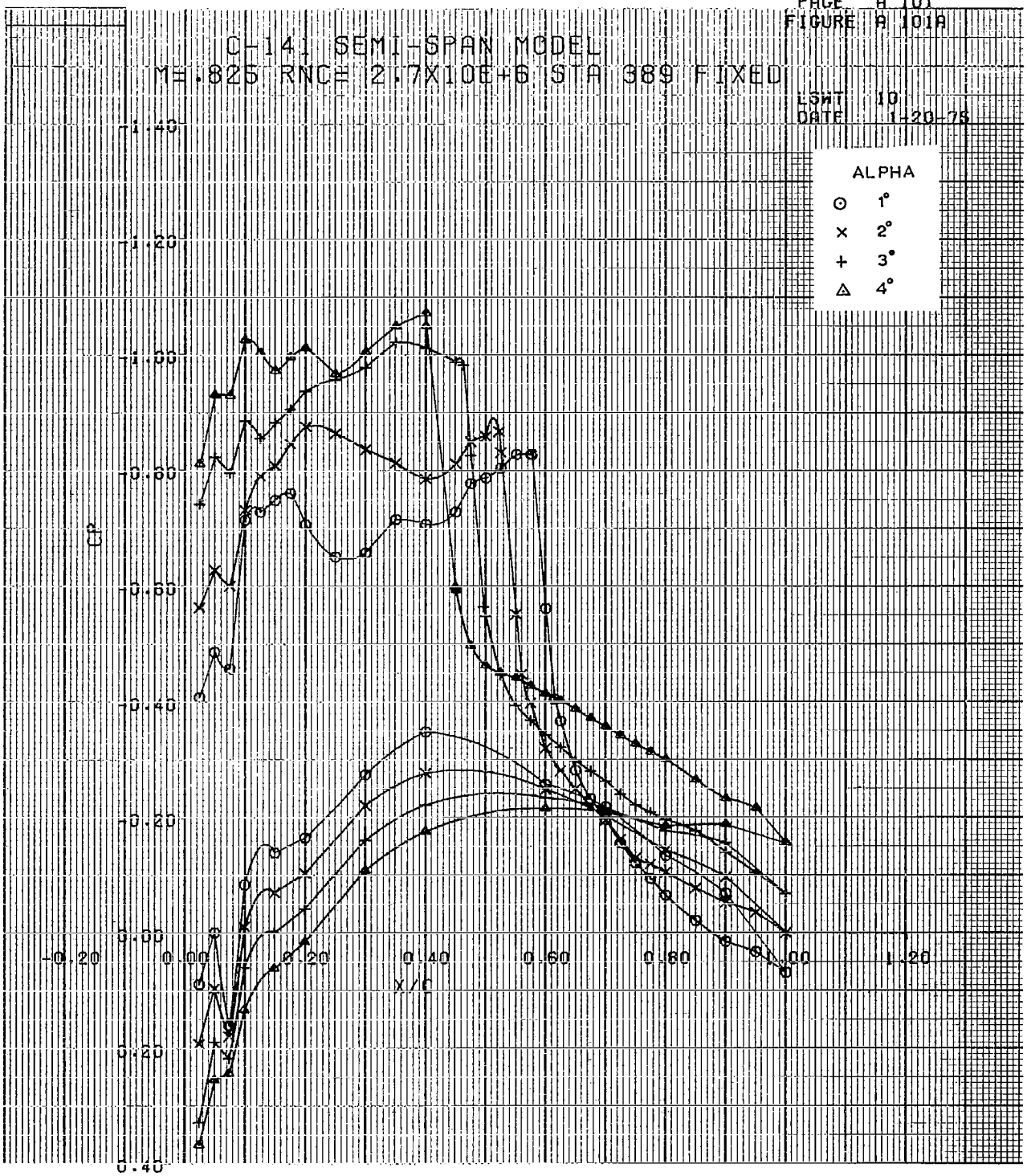
C-141 SEMI-SPAN MODEL
M=.825 RNCF= 2.7X10E+6 STA 389 FIXED
LSHT 10
DATE 1-20-75
ALPHA
⊙ 1°
× 2°
+ 3°
△ 4°
CP
X/C
-0.20
0.00
0.20
0.40
0.60
0.80
1.00
1.20
1.40
1.20
1.00
0.80
0.60
0.40
0.20
0.00
0.20
0.40

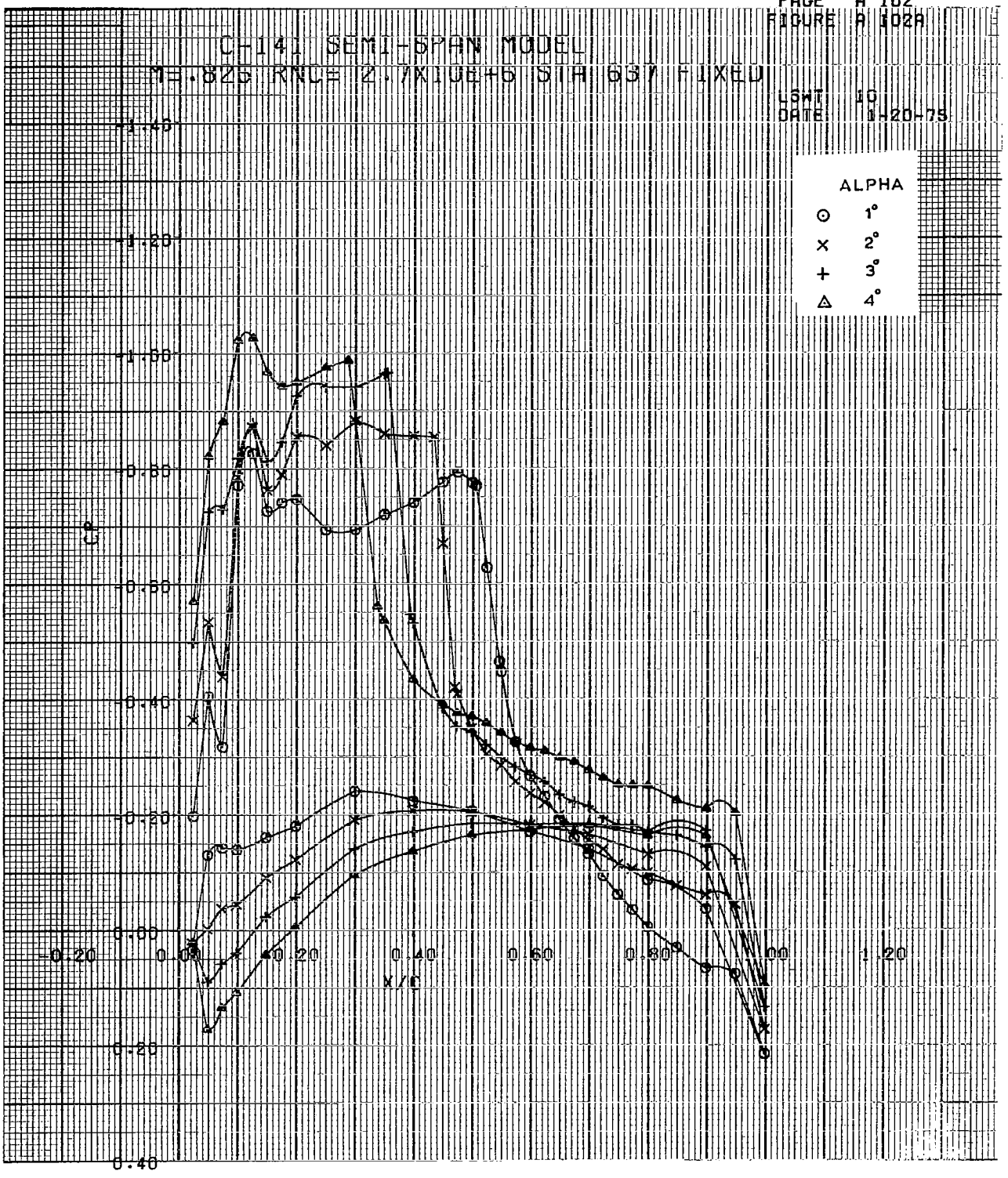
CH141 SEMI-SPAN MODEL
M=.825 RNLE=2.7X10E+6 SIA 637 FIXED
LSWT 10
DATE 1H20-75
ALPHA
1°
2°
3°
4°
-1.40
-1.20
-1.00
-0.80
-0.60
-0.40
-0.20
0.00
0.20
0.40
-0.20
0.00
0.20
0.40
0.60
0.80
1.00
1.20
X/C

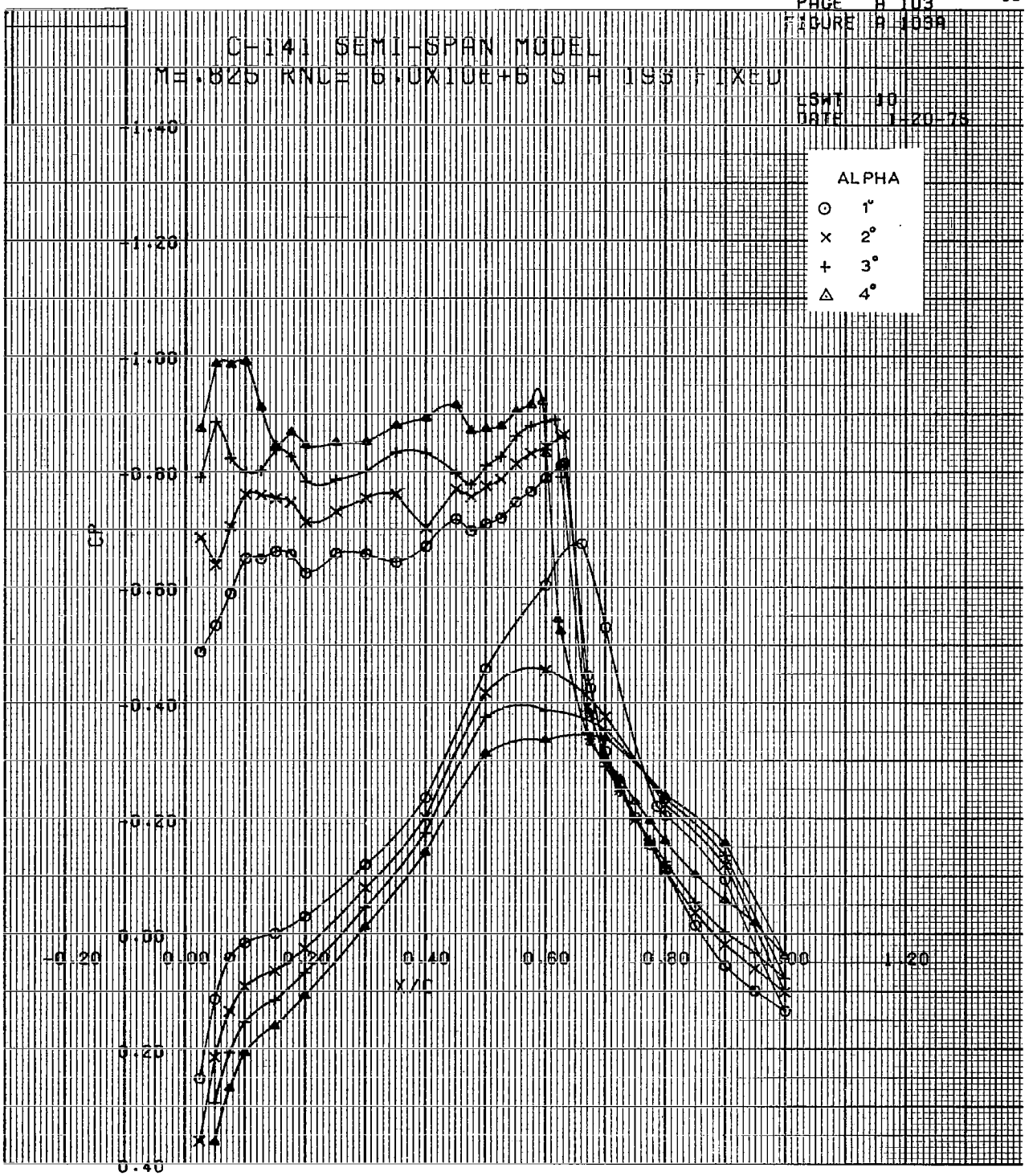
C-141 SEMI-SPAN MODEL
M=.825 RNL=6.0X10E+6 S H 195 - IXED
SHT 10
DATE 1-20-75
ALPHA
1°
2°
3°
4°
-Cp
X/C
1.40
1.20
1.00
0.80
0.60
0.40
0.20
0.00
-0.20
0.00
0.20
0.40
0.60
0.80
1.00
1.20

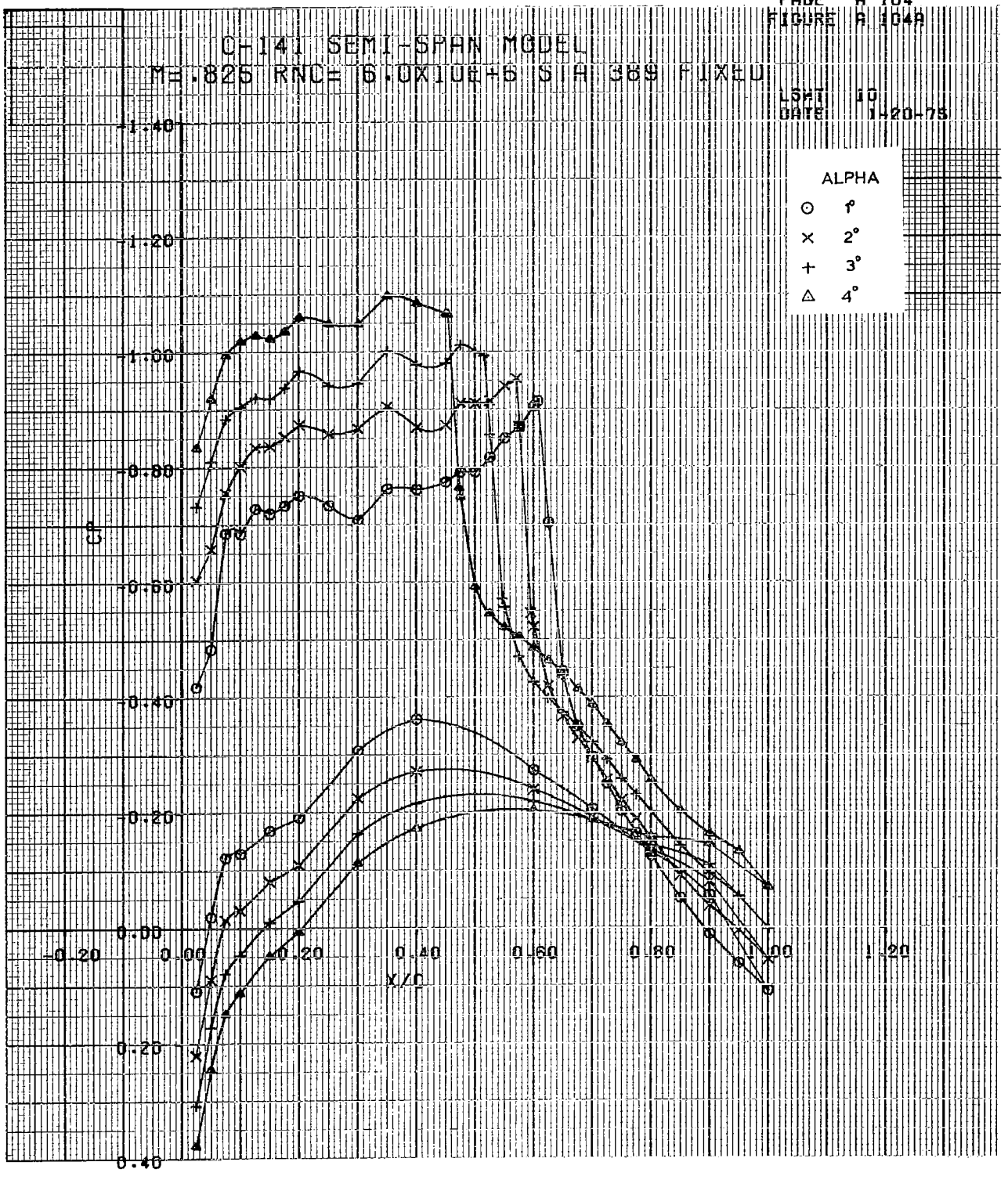
C-141 SEMI-SPAN MODEL
M=.825 RNC= 6.0X10E+6 S/A 369 FIXED
LSRI 10
DATE 1-20-75
ALPHA
1°
2°
3°
4°
-1.40
-1.20
-1.00
-0.80
-0.60
-0.40
-0.20
0.00
0.20
0.40
-0.20
0.00
0.20
0.40
0.60
0.80
1.00
1.20
X/C

C-141 SEMI-SPAN MODEL
MH=.825 RNC= 6.0X10E+6 SIH 637 FIXED

LSWT 10
DATE 1-20-75

ALPHA
⊙ 1°
× 2°
+ 3°
△ 4°

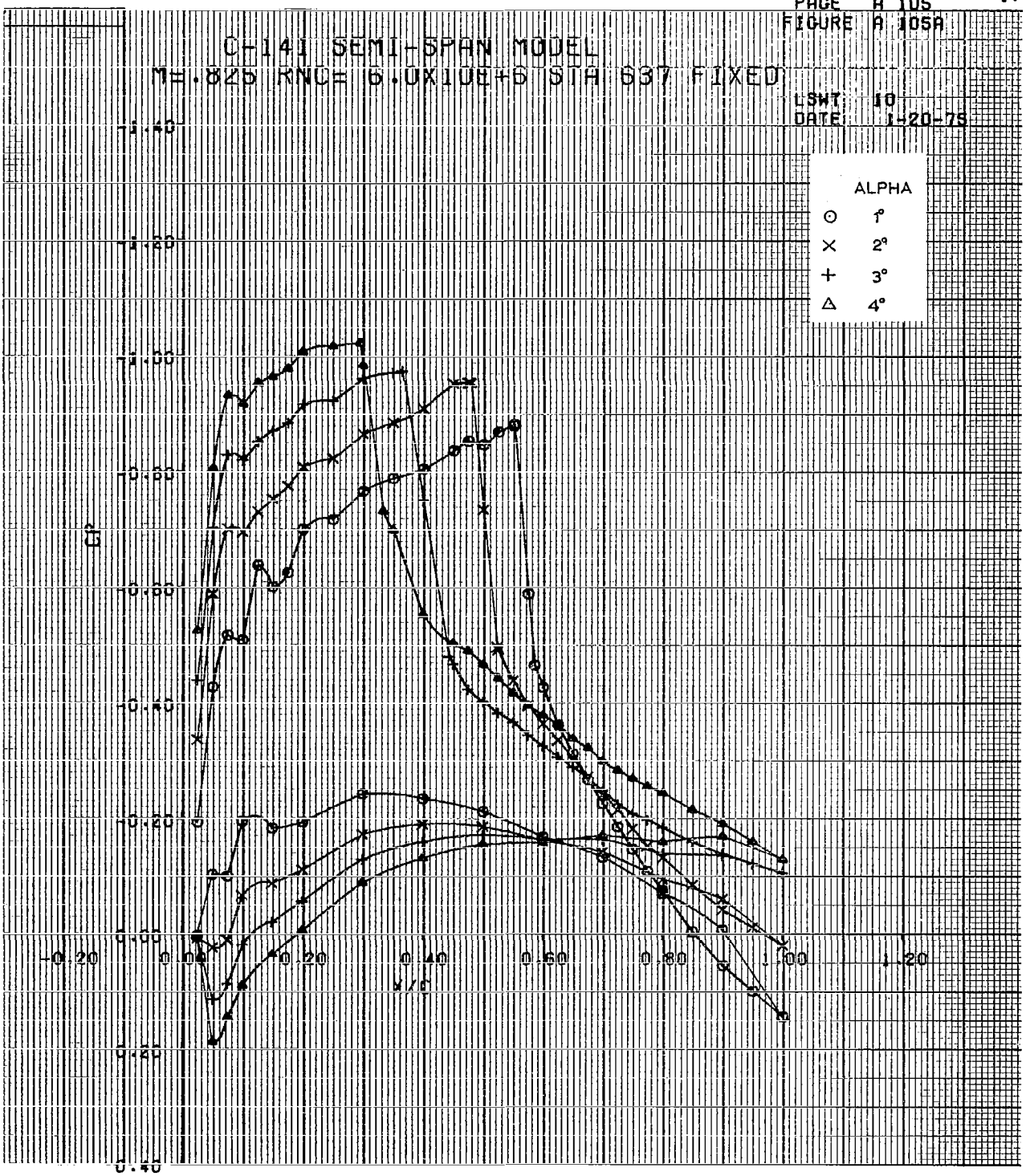

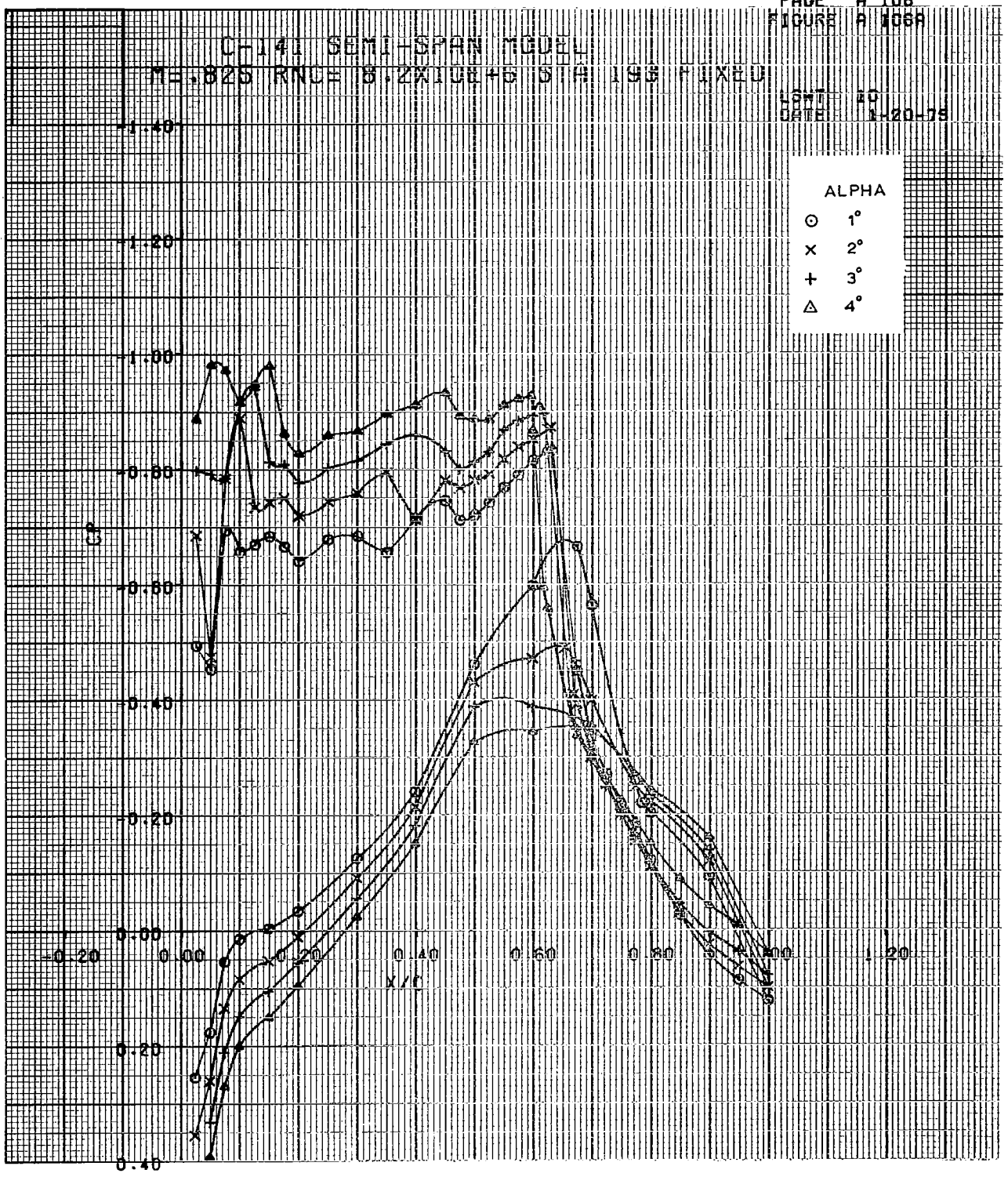
C-141 SEMI-SPAN MODEL
M=.825 RNCE 6.2X10E+6 0 R 155 FLXED
LGMT AD
DATE 1-20-75
ALPHA
⊙ 1°
× 2°
+ 3°
△ 4°
-1.40
-1.20
-1.00
-0.80
-0.60
-0.40
-0.20
0.00
0.20
0.40
-0.20
0.00
0.20
0.40
0.60
0.80
1.00
1.20
X/C

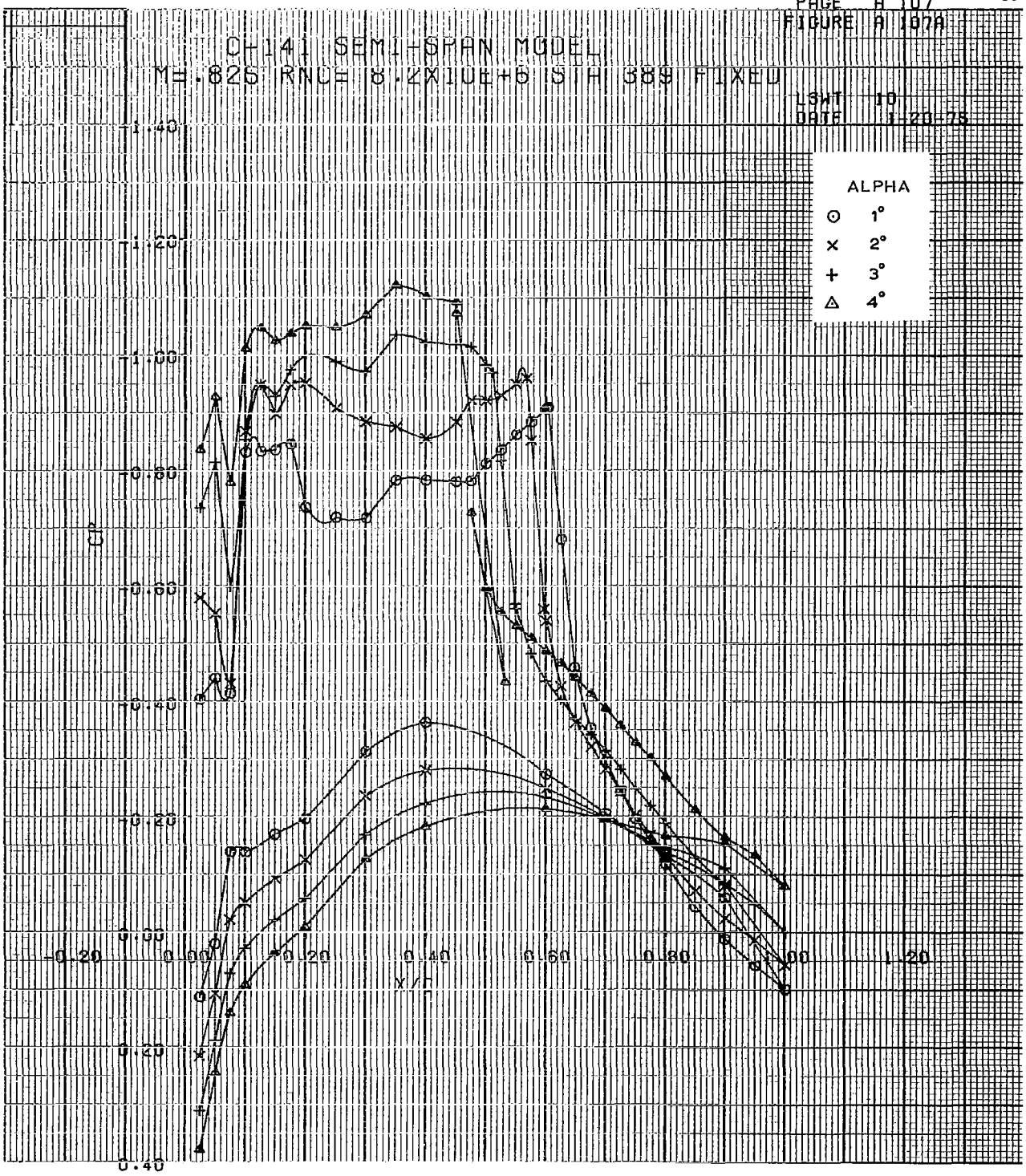
C-141 SEMI-SPAN MODEL
M=.825 RNC= 8.42X10E+6 SHK 38S FIXED
LSHT 10
DATE 1-20-75
ALPHA
⊙ 1°
× 2°
+ 3°
△ 4°
CP
X/C
1.40
1.20
1.00
0.80
0.60
0.40
0.20
0.00
-0.20
0.00
0.20
0.40
0.60
0.80
1.00
1.20

FIGURE A 108A

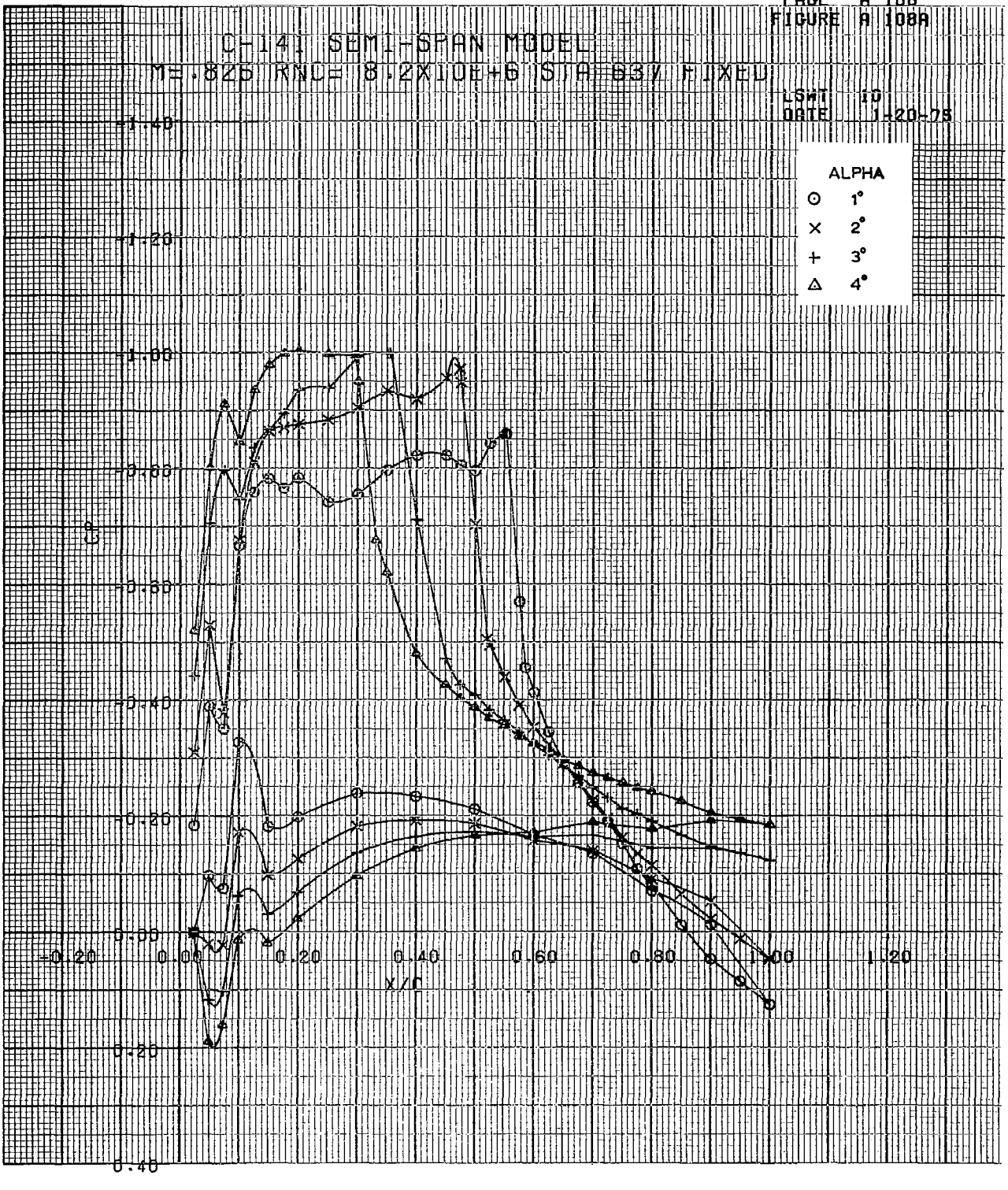

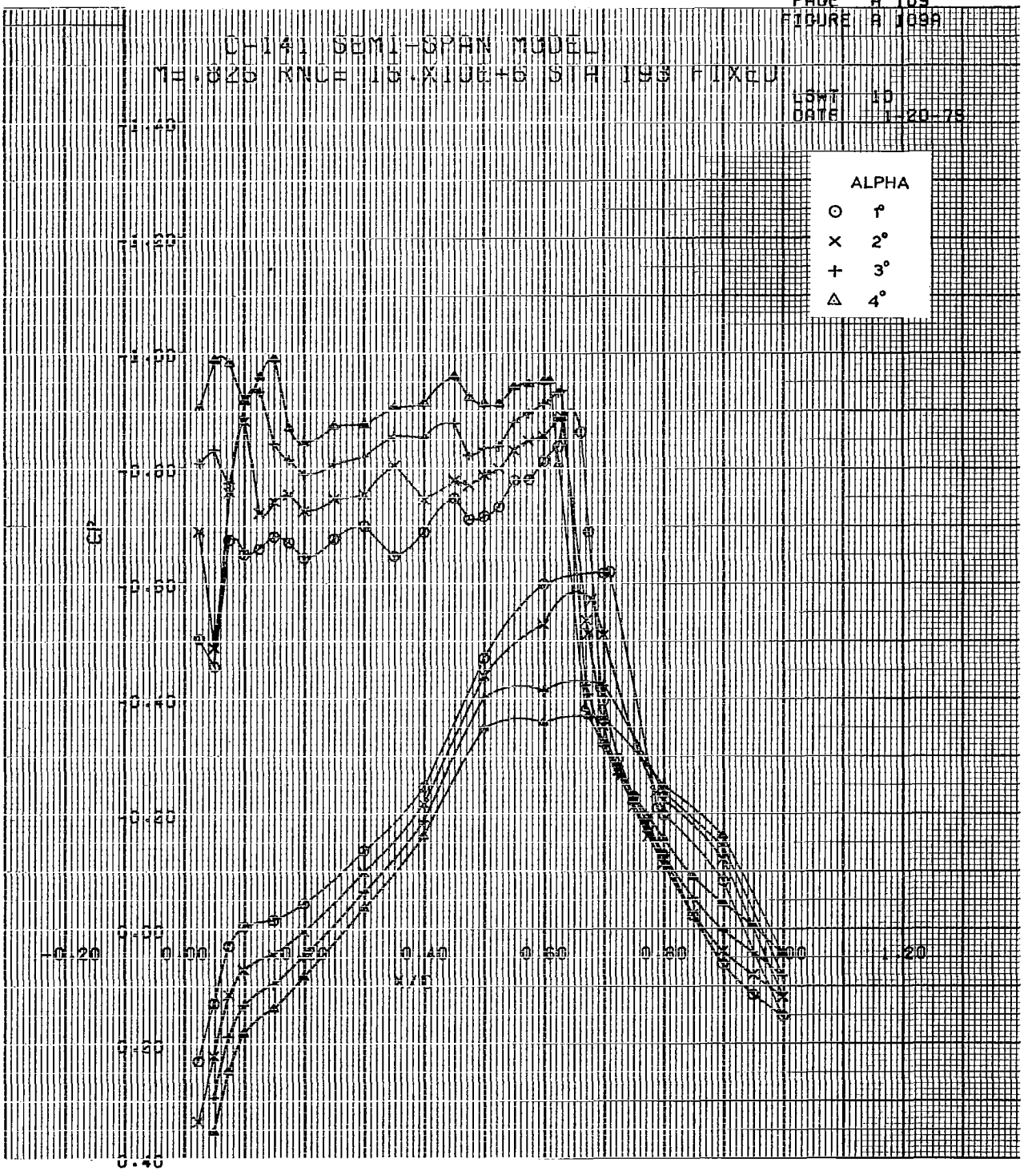
CHINA SEMI-SPAN MODEL
M=.820 RNUM=10.XTUC+6 STR 195 FIXED
SWT 10
DATE 1-20-78
ALPHA
⊙ 1°
× 2°
+ 3°
△ 4°
CL
1.20
0.40

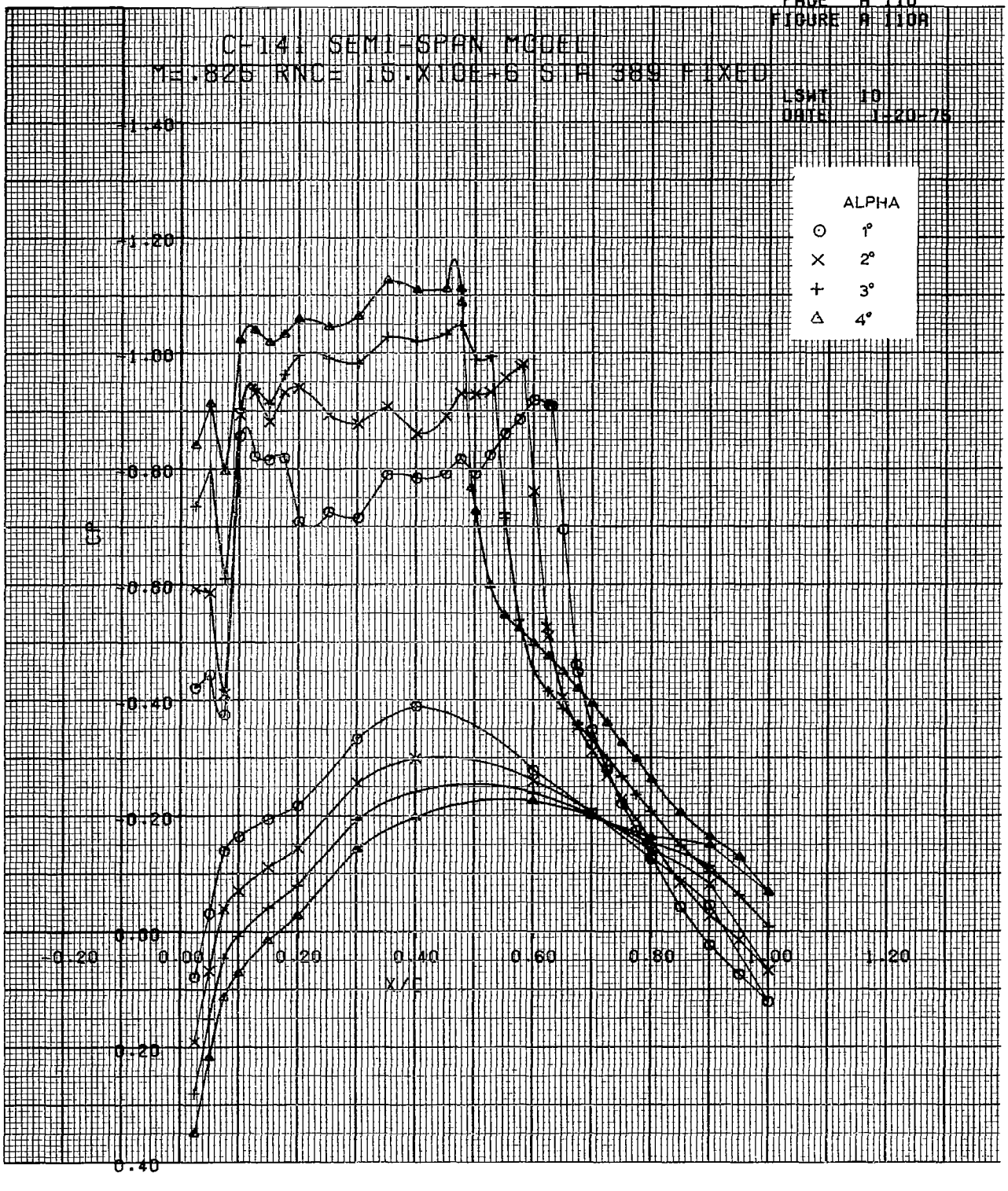
CF-141 SEMI-SPAN MODEL
M=.825 RNDE= 15.X10E+6 STA 389 FIXED
LSHT 10
DATE 1-20-76
ALPHA
1°
2°
3°
4°
-1.40
-1.20
-1.00
-0.80
-0.60
-0.40
-0.20
0.00
0.20
0.40
-0.20
0.00
0.20
0.40
0.60
0.80
1.00
1.20
X/E

C-141 SEMI-SPAN MODEL
M=.825 RNC= 15.X10E+6 STA 637 FIXED

LSHT 10
DATE 1-20-75

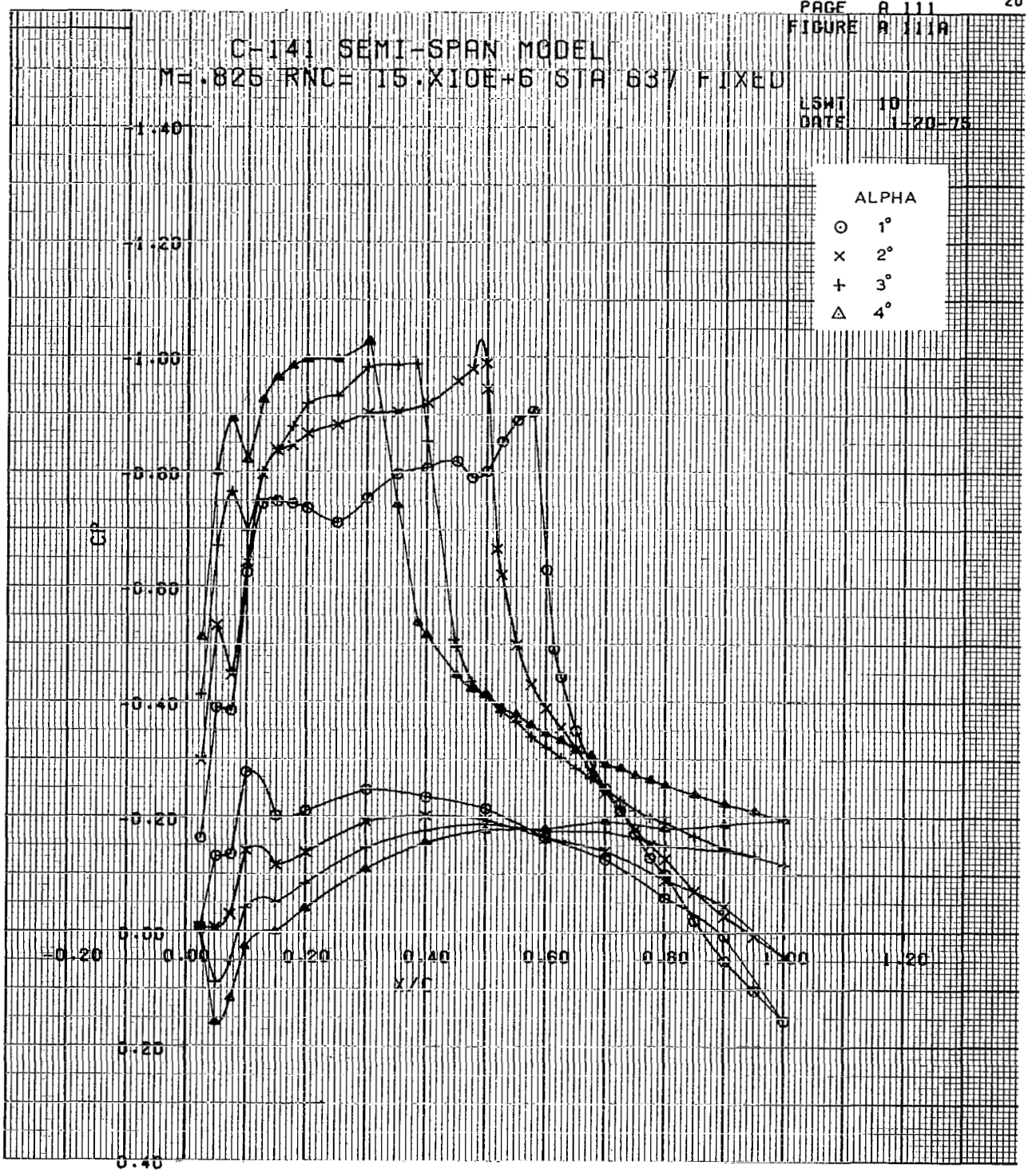

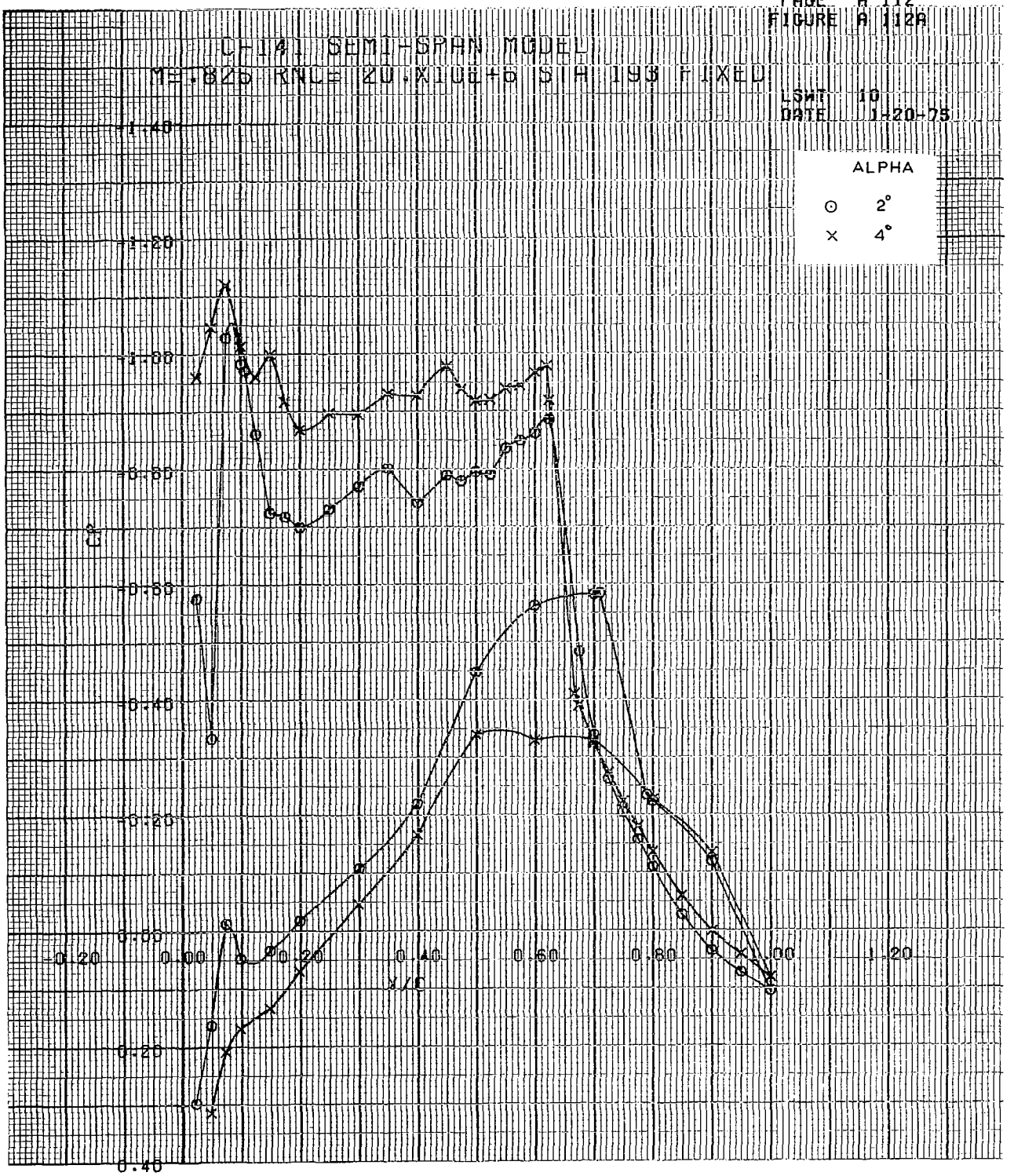
CF14) SEMI-SPAN MODEL
M=.825 RNL= 20.X10E+6 S H 195 F IXED
LSHT 10
DATE 1-20-75
ALPHA
⊙ 2°
× 4°
1.40
1.20
1.00
0.80
0.60
0.40
0.20
0.00
-0.20
-0.40
CL
-0.20
0.00
0.20
0.40
0.60
0.80
1.00
1.20
X/C

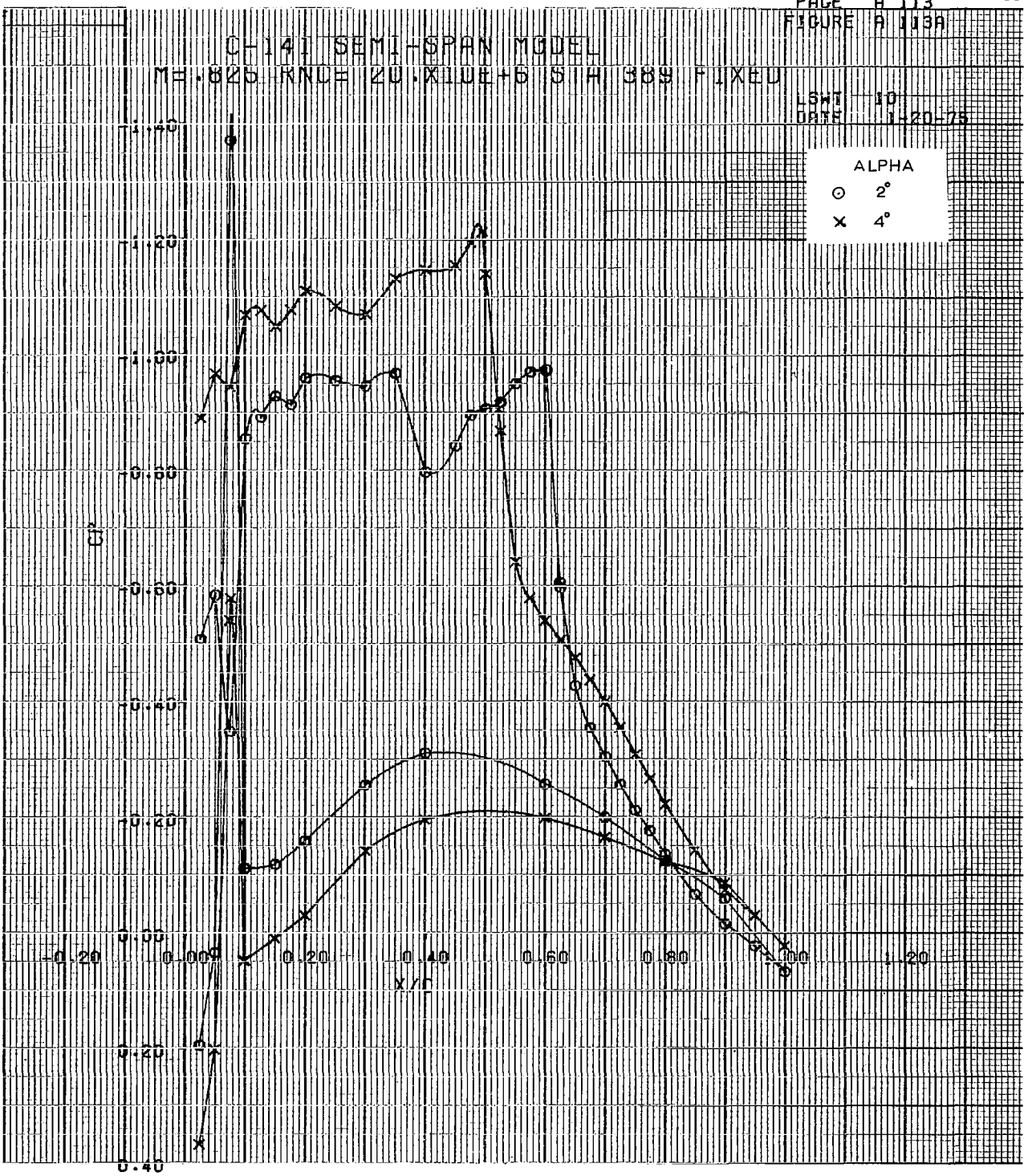
C-141 SEMI-SPAN MODEL
M=.825 KNOB ZERO VALUE +6 SHA 389 FIXED
LSHT 10
DATE 1-20-75
ALPHA
2°
4°
1.40
1.20
1.00
0.80
0.60
0.40
0.20
0.00
-0.20
-0.40
-0.60
-0.80
-1.00
-1.20
-1.40
CP
X/C

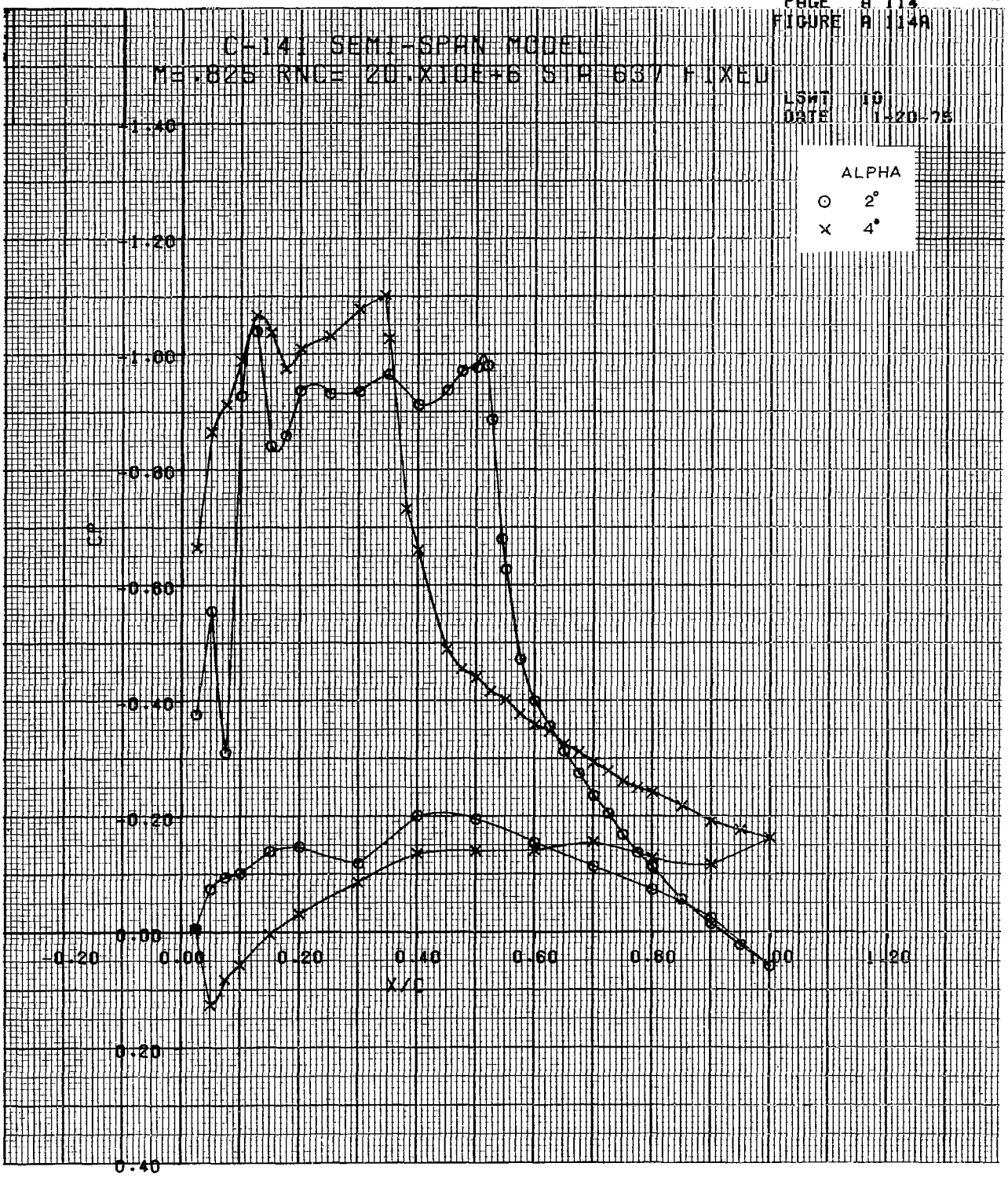
C-141 SEMI-SPAN MODEL
M=.825 RNC= 20.X10E+6 S/B 637 FIXED
LSHT 10
DATE 1-20-75
ALPHA
2°
4°
-1.40
-1.20
-1.00
-0.80
-0.60
-0.40
-0.20
0.00
0.20
0.40
-0.20
0.00
0.20
0.40
0.60
0.80
1.00
1.20
X/C

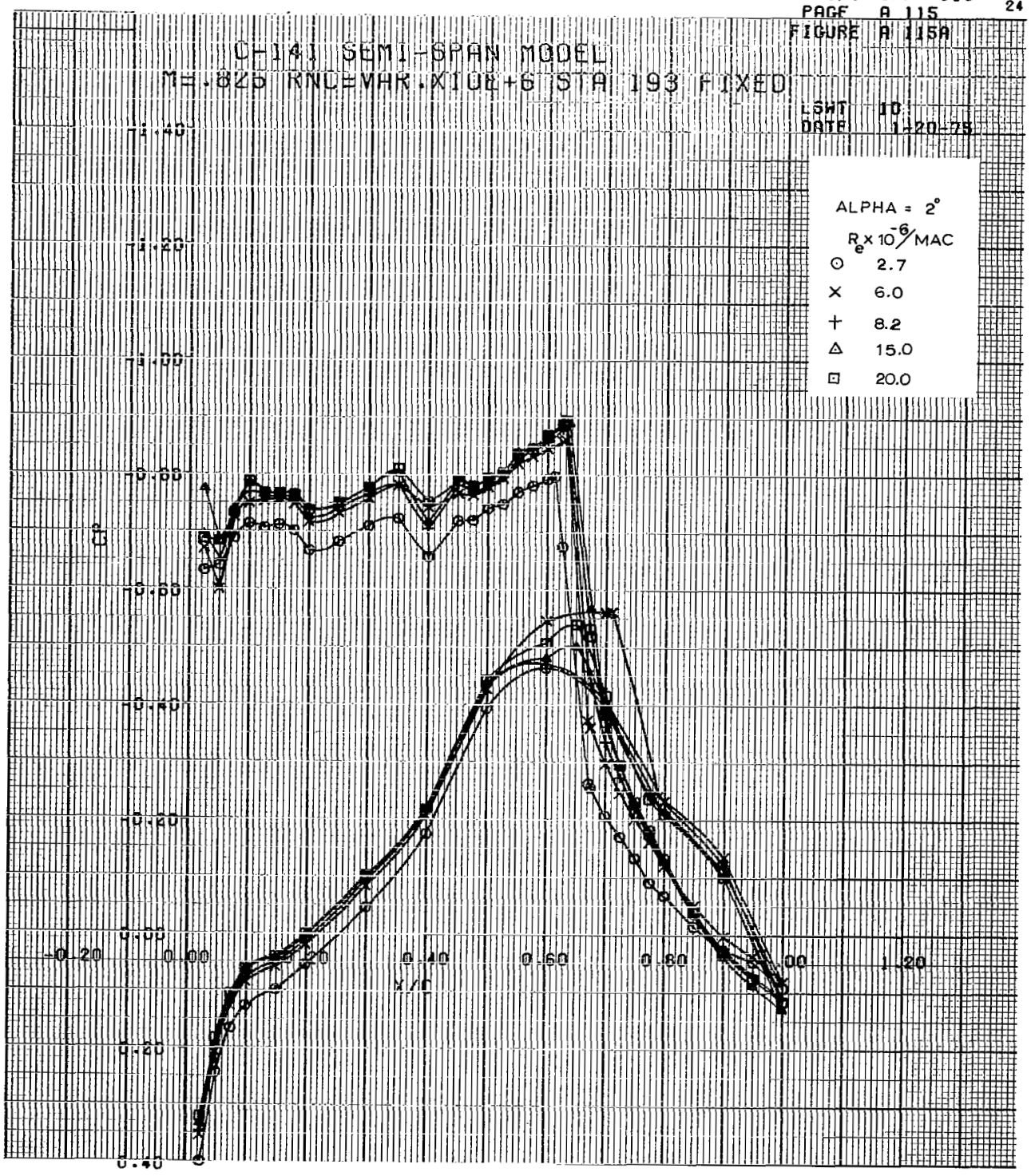
CF141 SEMI-SPAN MODEL
ME.82D RNC=MHR.X10E+6 STA 193 FIXED
LSWT 10
DATE 1-20-75
ALPHA = 2°
Re x 10^-6/MAC
⊙ 2.7
× 6.0
+ 8.2
△ 15.0
⊡ 20.0
CP
X/C
-0.20
0.00
0.40
0.60
0.80
1.00
1.20

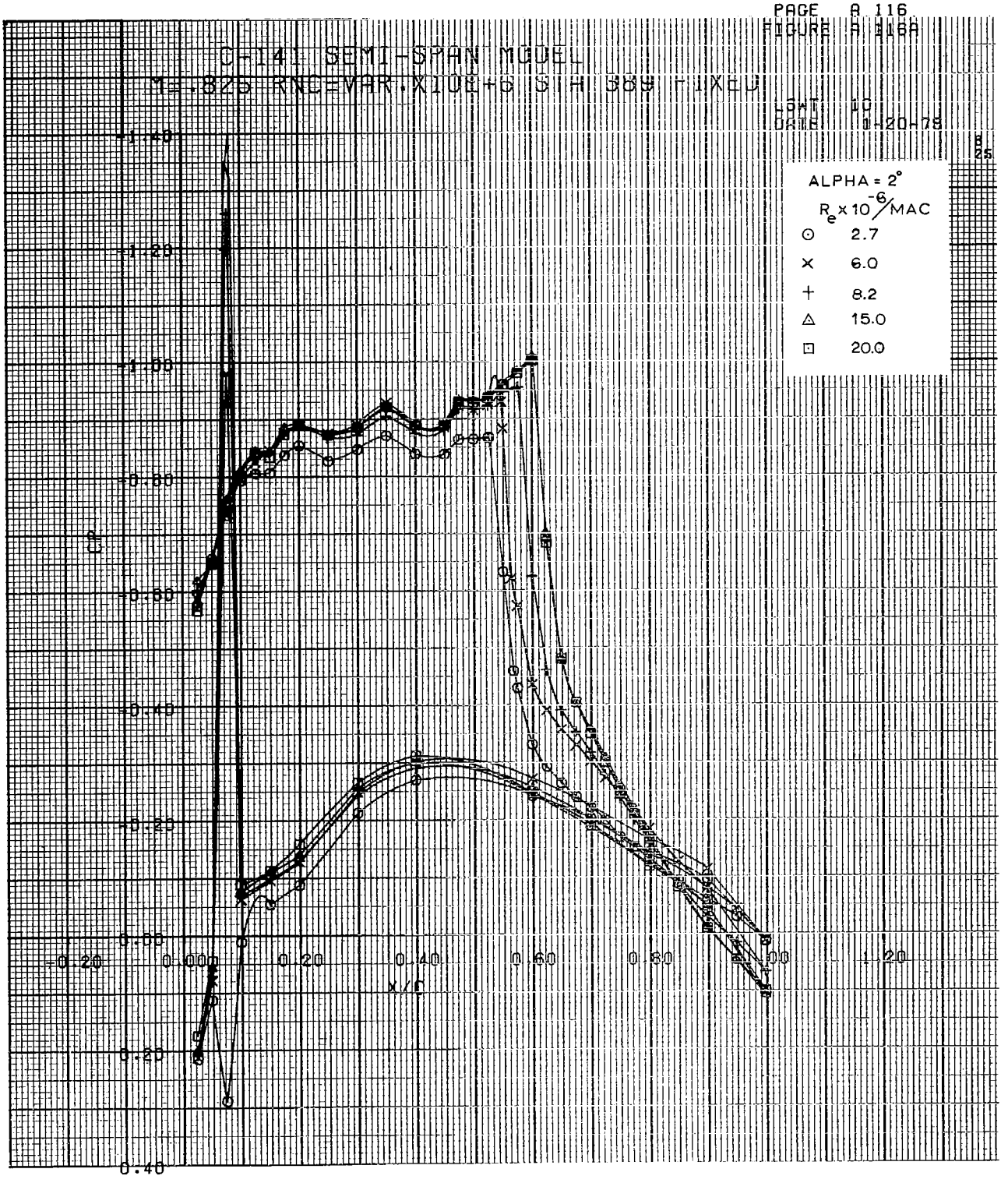
CF-141 SEMI-SPAN MODEL
M=.825 RNCEMAR.X10E+6 S H 365 F 1XEU
CONT FC
DATE 1-20-78
ALPHA = 2°
Re x 10-6/MAC
⊙ 2.7
× 6.0
+ 8.2
△ 15.0
⊡ 20.0
-1.40
-1.20
-1.00
-0.80
-0.60
-0.40
-0.20
0.00
0.20
-0.20
-0.40
-0.20
0.000
0.20
0.40
0.60
0.80
1.00
1.20
X/C

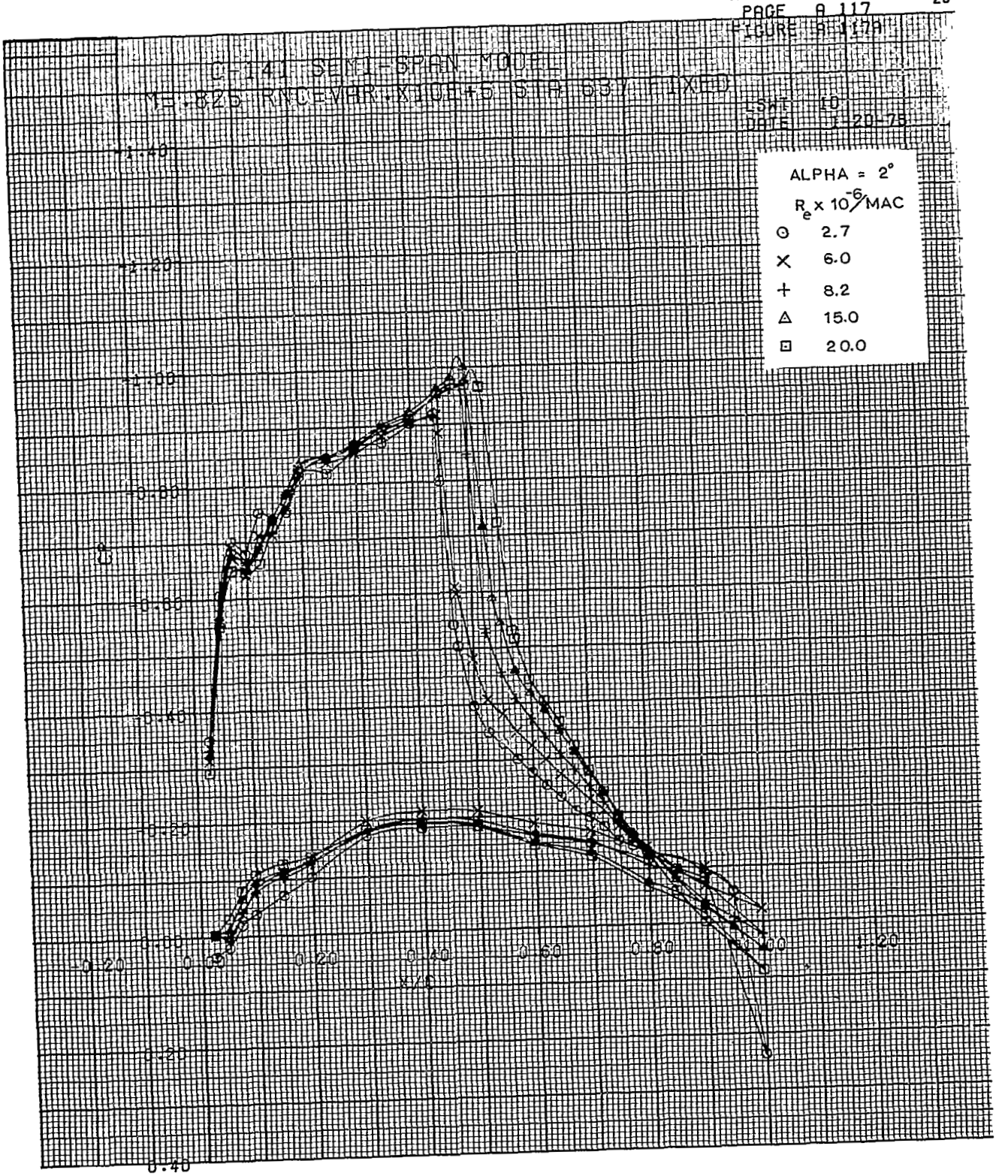
C-141 SEMI-SPAN MODEL
M=.825 RNDEVHR.XTOE+5 STA 537 FIXED
SWT 10
DATE 1-20-75
ALPHA = 2°
$R_e \times 10^{-6}$/MAC
2.7
6.0
8.2
15.0
20.0
-1.40
-1.20
-1.00
-0.80
-0.60
-0.40
-0.20
0.00
0.20
0.40
-0.20
0.00
0.20
0.40
0.60
0.80
1.00
1.20
Y/C
X/C

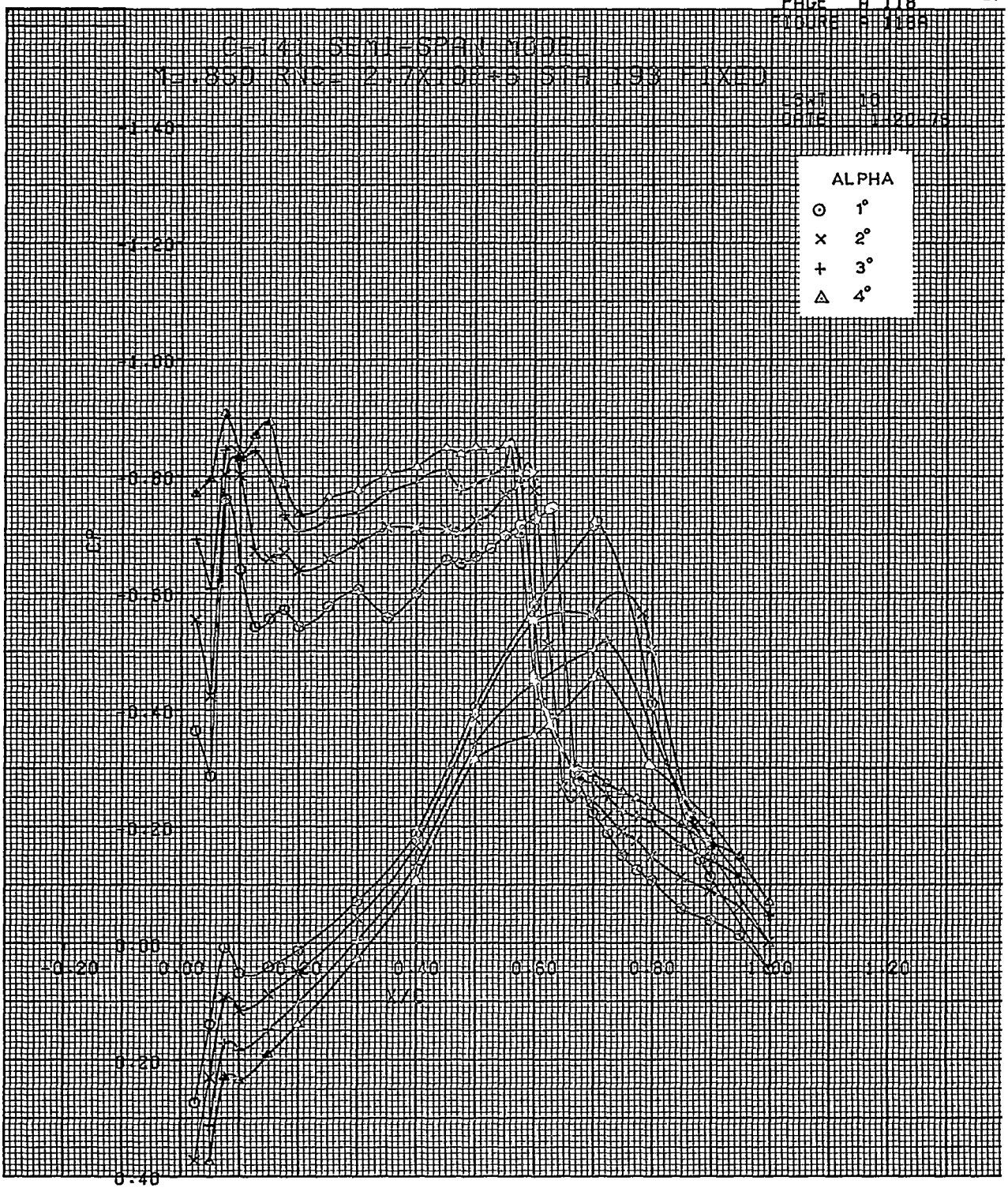
C-141 SEMI-SPAN MODEL
M=.850 RNC= 2.7X10E+6 STB 193 FIXED
CENT 10
DATE 1-20-78
ALPHA
⊙ 1°
× 2°
+ 3°
△ 4°
+1.40
+1.20
+1.00
+0.80
+0.60
+0.40
+0.20
0.00
-0.20
-0.40
-0.20
0.00
0.20
0.40
0.60
0.80
1.00
1.20
X/C

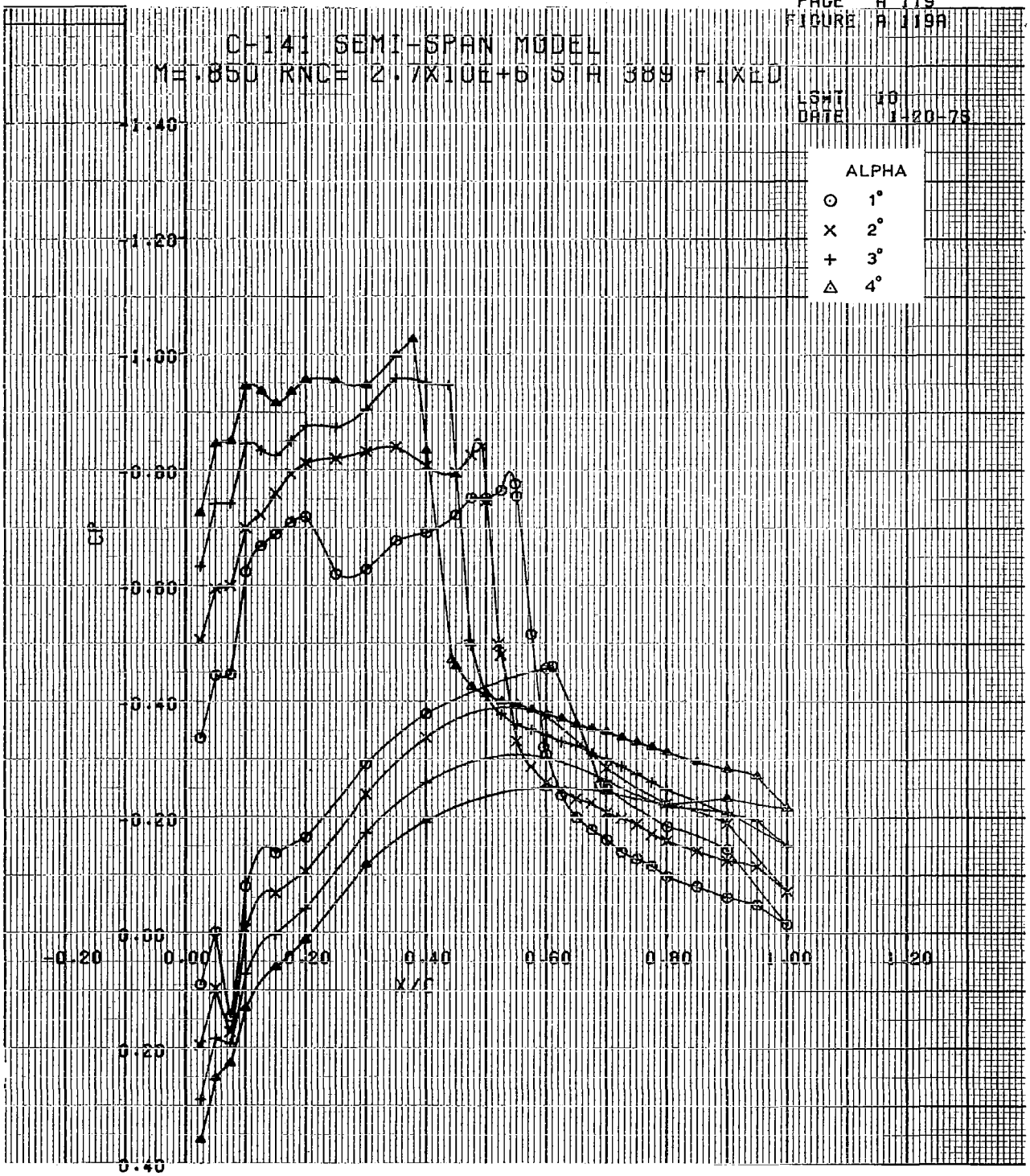
C-141 SEMI-SPAN MODEL
M=.850 RNC= 2.7X10E+6 S/A 389 FLXED
LSHT 10
DATE 1-20-78
ALPHA
1°
2°
3°
4°
CL
1.40
1.20
1.00
0.80
0.60
0.40
0.20
0.00
0.20
-0.20
0.00
0.20
0.40
0.60
0.80
1.00
1.20
X/C

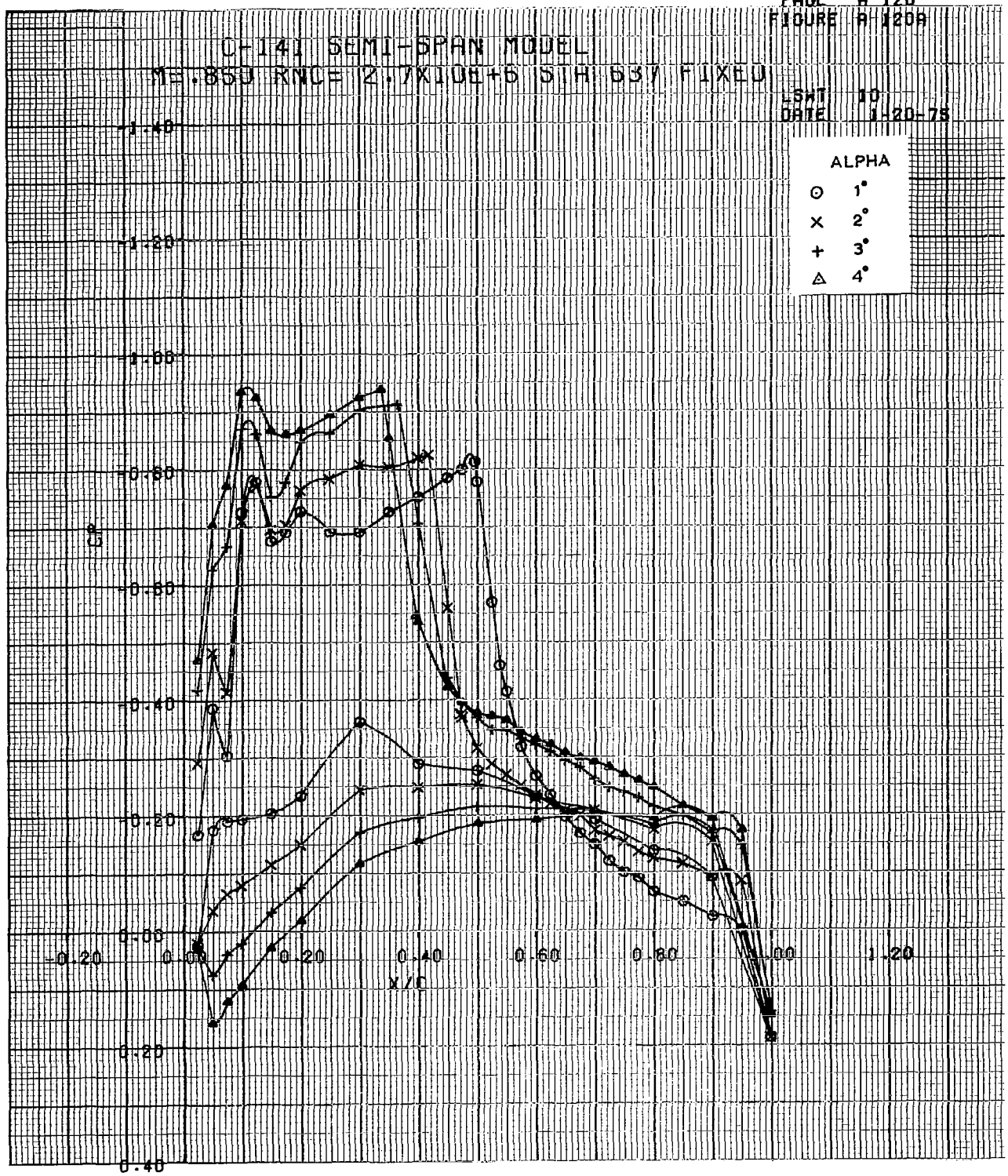
C-141 SEMI-SPAN MODEL
M=.850 RNC= 2.7X10E+6 S.H 537 FIXED
SHT 10
DATE 1-20-75
ALPHA
1°
2°
3°
4°
-1.40
-1.20
-1.00
-0.80
-0.60
-0.40
-0.20
0.00
0.20
-0.20
0.00
0.20
0.40
0.60
0.80
1.00
1.20
X/C
-0.40

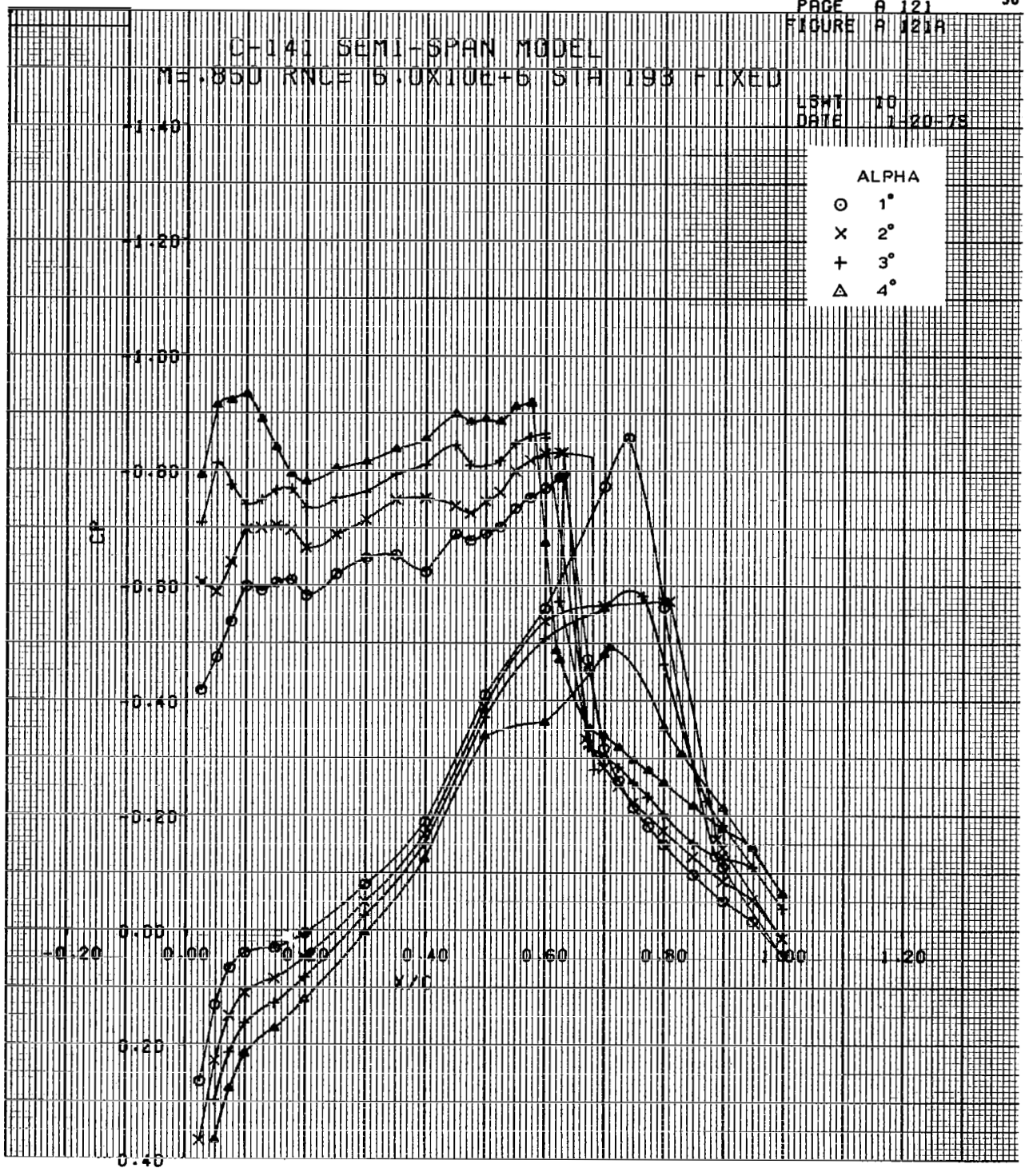
CF-141 SEMI-SPAN MODEL
M=.850 RNCE= 6.0X10E+6 STA 193 FIXED
LSHT 10
DATE 1-20-78
ALPHA
1°
2°
3°
4°
CP
1.40
1.20
1.00
0.80
0.60
0.40
0.20
0.00
-0.20
-0.40
-0.20
0.00
0.40
0.60
0.80
1.00
1.20
Y/C


CH-141 SEMI-SPAN MODEL
ME=.850 RNC= 6.0X10E+6 SIA 389 FIXED
LSWT 10
DATE 1-20-78
ALPHA
1°
2°
3°
4°
CP
X/C
-1.40
-1.20
-1.00
-0.80
-0.60
-0.40
-0.20
0.00
0.20
0.40
-0.20
0.00
0.20
0.40
0.60
0.80
1.00
1.20

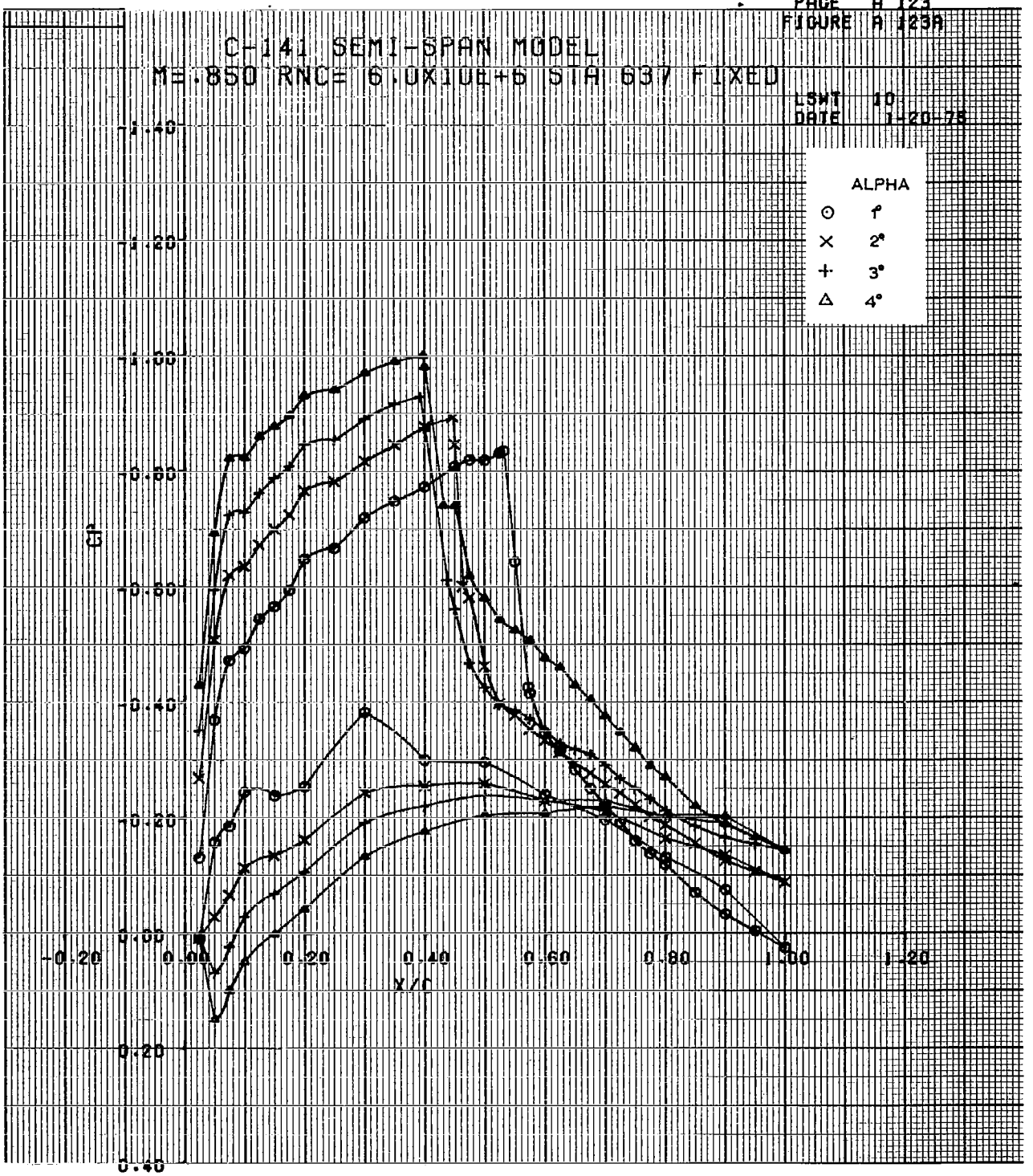
C-141 SEMI-SPAN MODEL
M=.850 RNC= 6.0X10E+6 SIM 63% FIXED
LSWT 10
DATE 1-20-78
ALPHA
1°
2°
3°
4°
CP
X/C
-0.20
0.00
0.20
0.40
0.60
0.80
1.00
1.20
0.20
0.40

C-141 SEMI-SPAN MODEL
M=.850 RNC= 6.0X10E+6 STH 193 FIXED

LSHT 10
DATE 1-20-75

ALPHA
⊙ 1°
× 2°
+ 3°
△ 4°

-1.40
-1.20
-1.00
-0.80
-0.60
-0.40
-0.20
0.00
0.20
0.40

C_p

-0.20 0.00 0.20 0.40 0.60 0.80 1.00 1.20

X/C

C-141 SEMI-SPAN MODEL
MACH NUMBER 0.DUXICE+0 S/A 389 FIXED

LSMT 10
DATE 1-20-76

ALPHA
⊙ 1°
× 2°
+ 3°
△ 4°

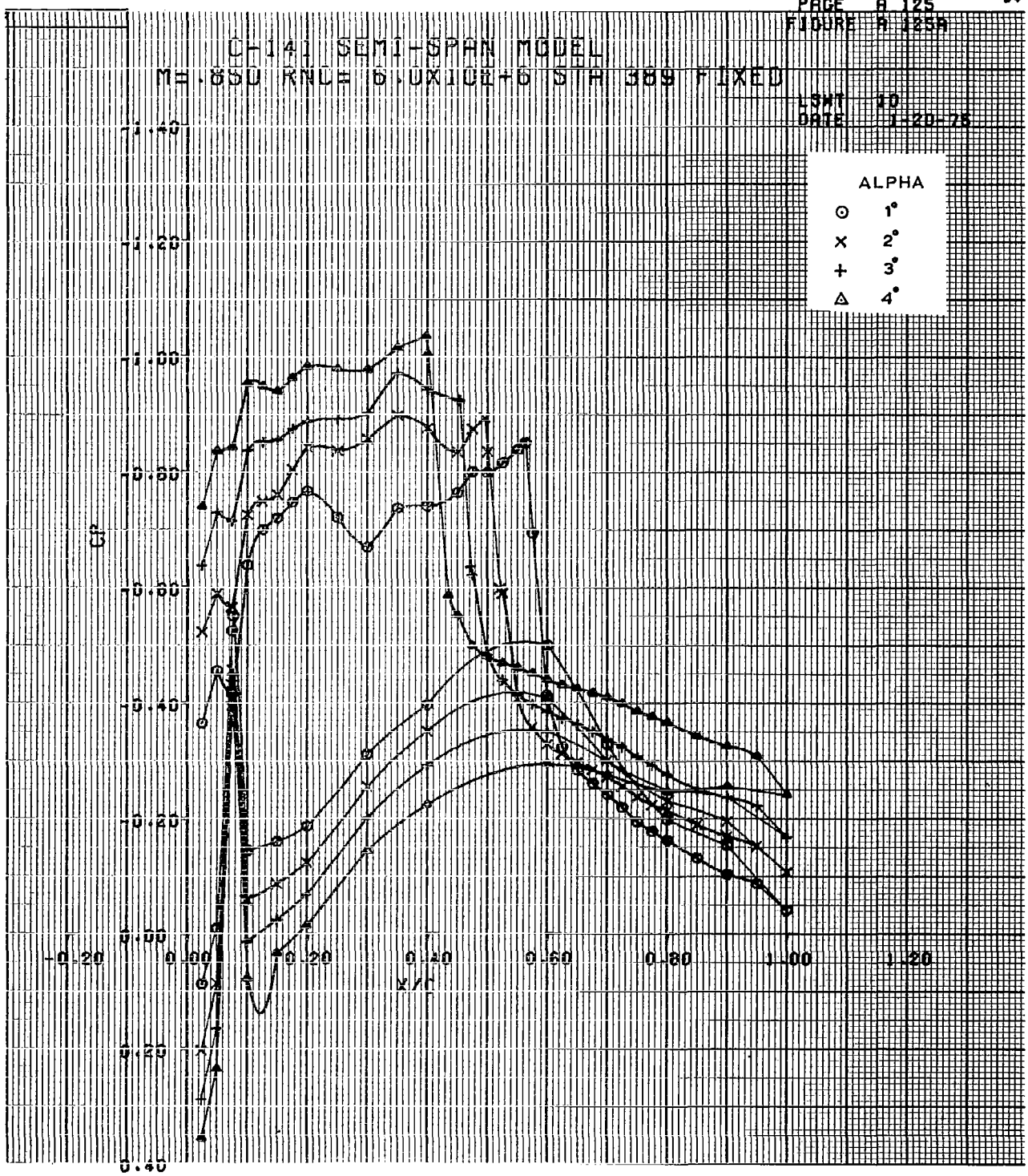

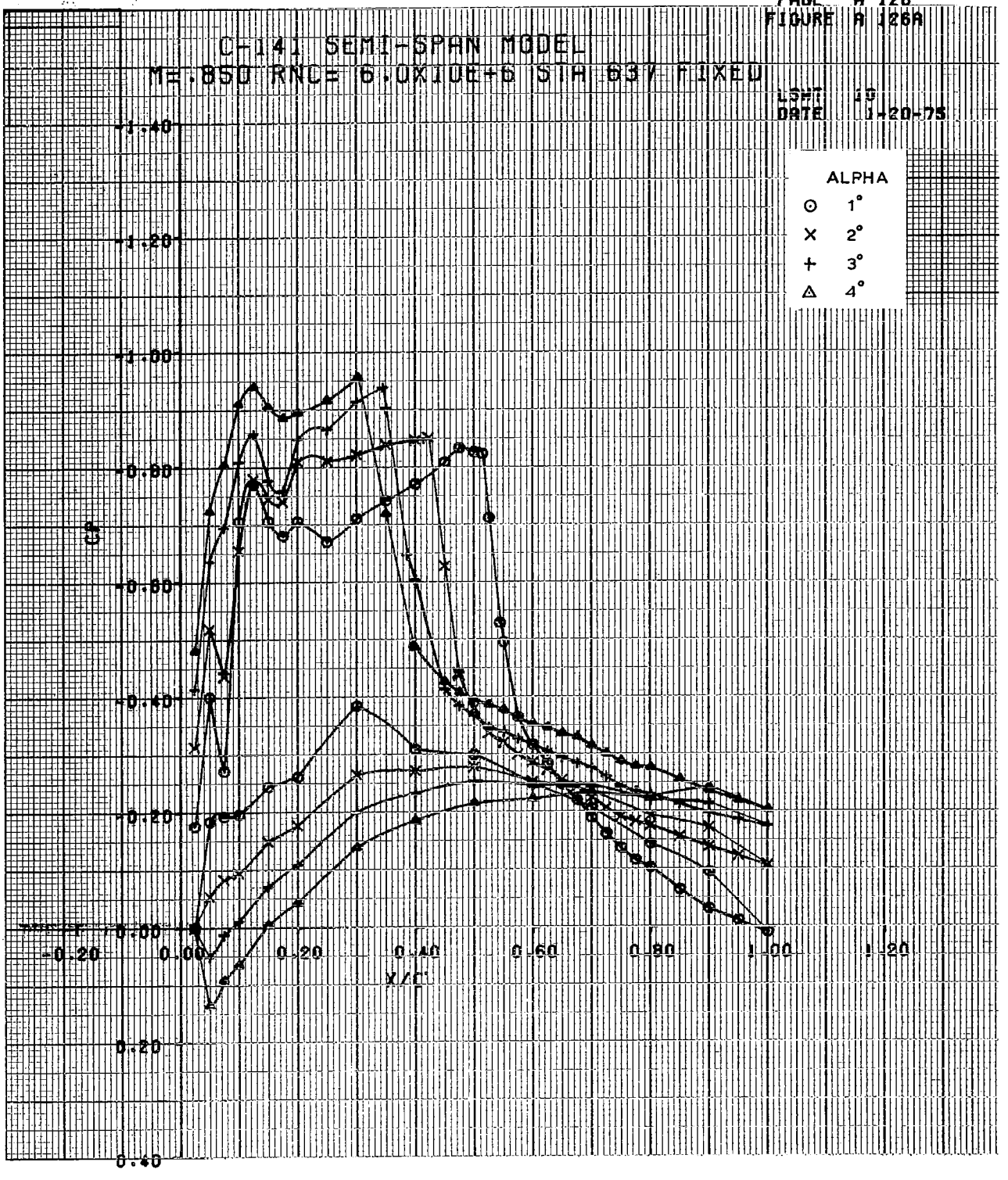
C-141 SEMI-SPAN MODEL
M=.850 RNC= 6.0X10E+6 STH 637 FIXED
LSHT 10
DATE 1-20-75
ALPHA
1°
2°
3°
4°
-1.40
-1.20
-1.00
-0.80
-0.60
-0.40
-0.20
0.00
0.20
0.40
-0.20
0.00
0.20
0.40
0.60
0.80
1.00
1.20
X/C

C-141 SEMI-SPAN MODEL
M=.850 RNC= 8.2X10E+6 STA 193 FIXED

CONT 80
DATE 1-[illegible]-78

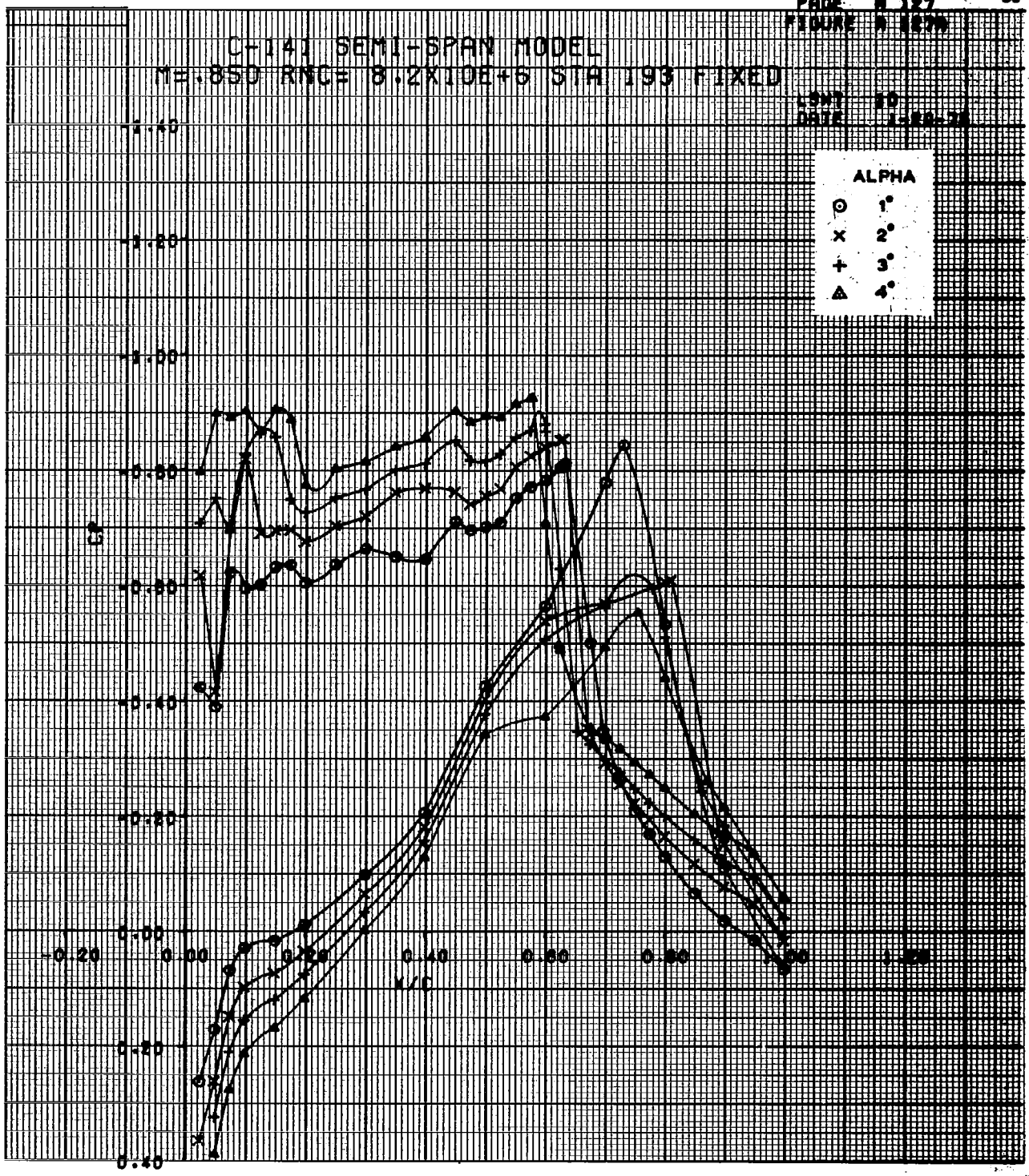

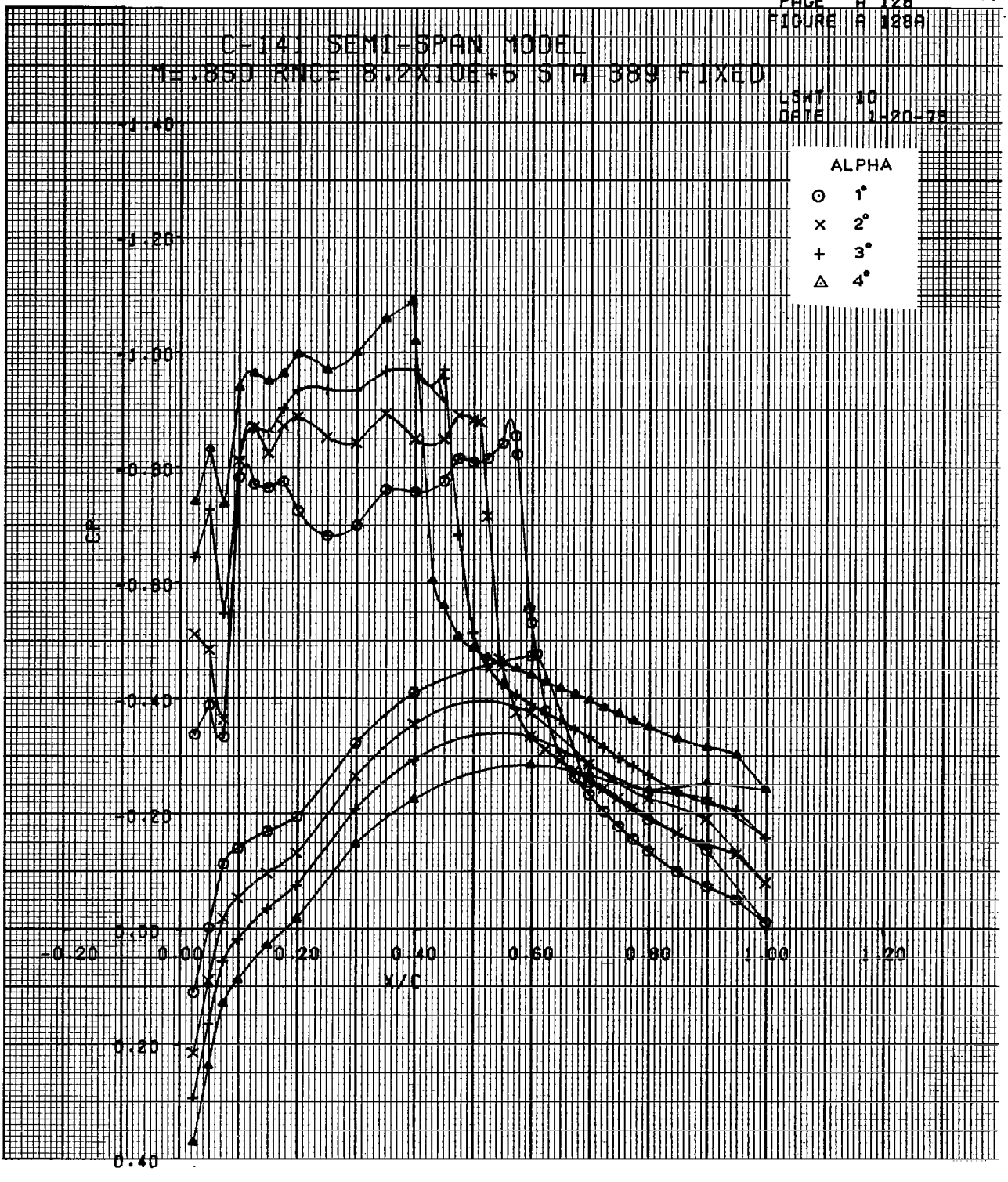
C-141 SEMI-SPAN MODEL
M=.850 RNC= 8.2X10E+6 STA 389 FIXED
SWT 10
DATE 1-20-78
ALPHA
⊙ 1°
× 2°
+ 3°
△ 4°
-1.40
-1.20
-1.00
-0.80
-0.60
-0.40
-0.20
0.00
0.20
0.40
-0.20
0.00
0.20
0.40
0.60
0.80
1.00
1.20
X/C

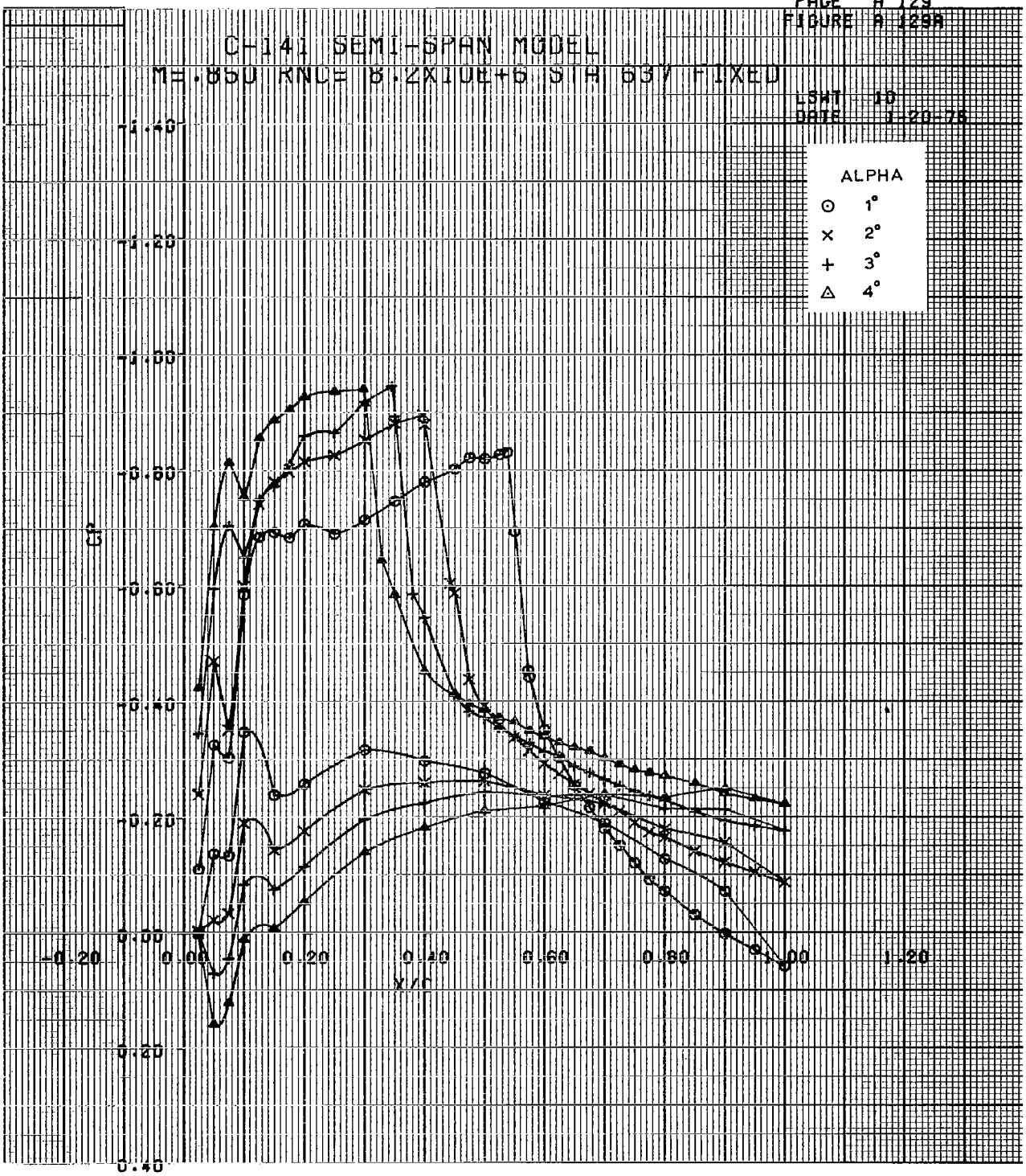
CH-141 SEMI-SPAN MODEL
M=.850 RNCE 8.2X10E+6 STN 63Y FIXED
LSHT 10
DATE 1-20-76
ALPHA
1°
2°
3°
4°
CP
1.40
1.20
1.00
0.80
0.60
0.40
0.20
0.00
-0.20
0.00
0.20
0.40
0.60
0.80
1.00
1.20
X/C

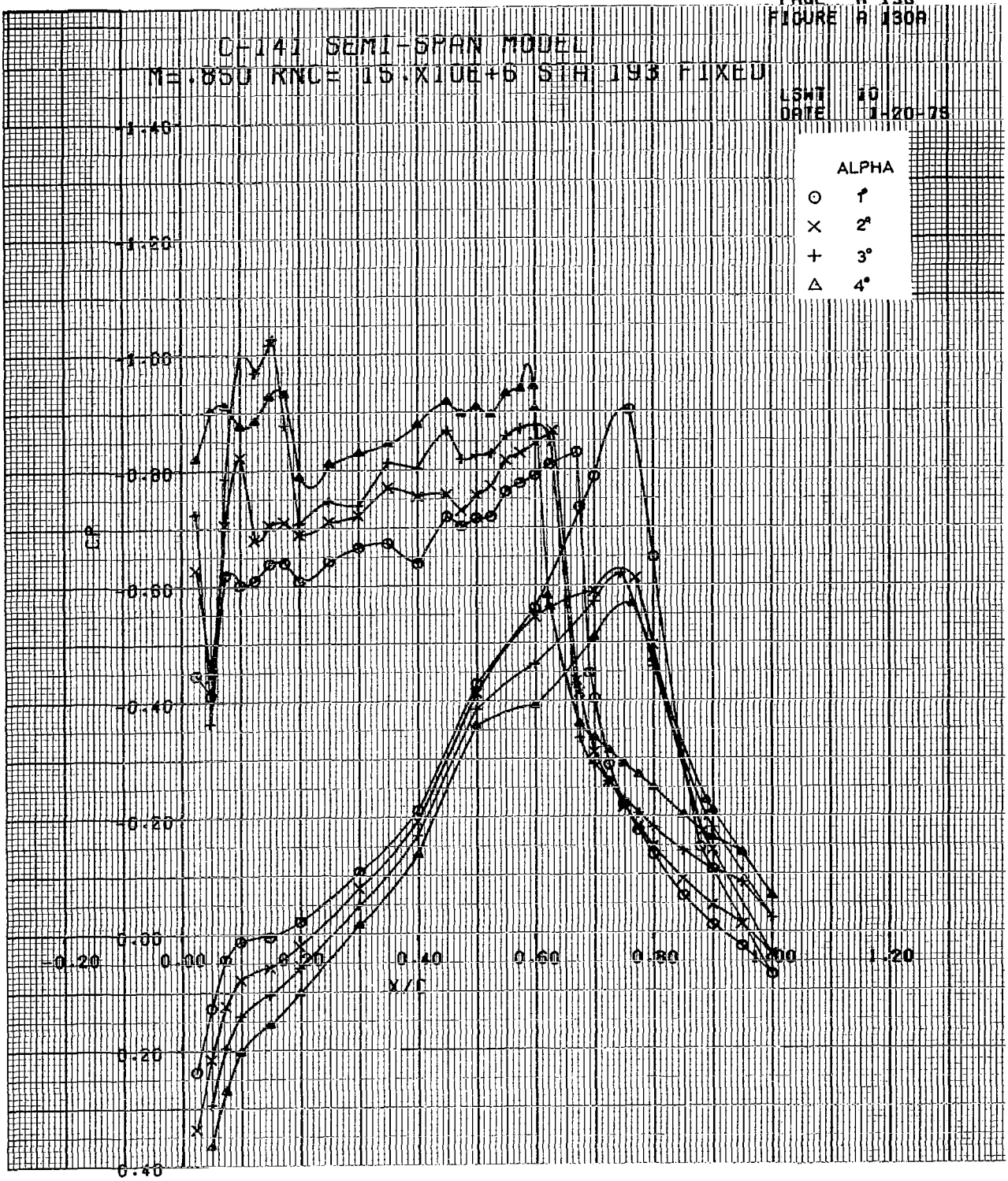
C-141 SEMI-SPAN MODEL
M=.850 RNC= 15.X10E+6 SIH 193 FIXED
LSWT 10
DATE 1-20-78
ALPHA
1°
2°
3°
4°
-1.40
-1.20
-1.00
-0.80
-0.60
-0.40
-0.20
-0.00
0.20
0.40
0.60
0.80
1.00
1.20
-0.20
0.00
0.20
0.40
X/C

C-141 SEMI-SPAN MODEL
M=.850 RNUE= 15.X10E+6 STH 389 FIXED
-SWT 10
DATE 1-20-78

ALPHA
⊙ 1°
× 2°
+ 3°
△ 4°

CL

1.40
1.20
1.00
0.80
0.60
0.40
0.20
0.00
-0.20
-0.40

-0.20 0.00 0.20 0.40 0.60 0.80 1.00 1.20

X/C

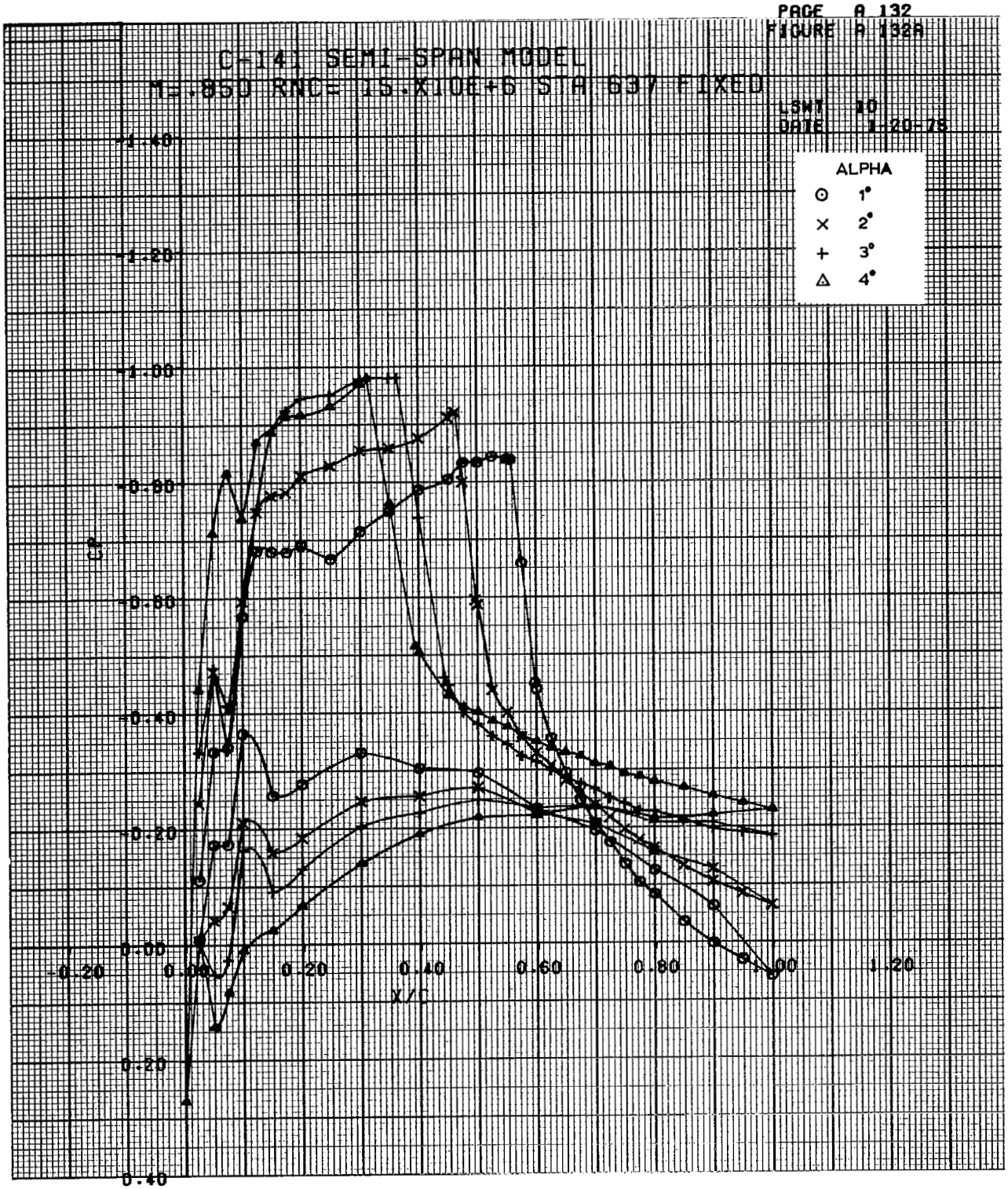

*U.S. GOVERNMENT PRINTING OFFICE: 1975 - 635-275/36